厚生労働科学研究費補助金

難治性疾患等政策研究事業

マイクロアレイ染色体検査でみつかる
染色体微細構造異常症候群の
診療ガイドラインの確立

平成２９年度　総括・分担研究報告書

研究代表者　倉橋　浩樹

平成３０（２０１８）年　３月

目　　次

厚生労働科学研究費補助金（難治性疾患等政策研究事業）
総括研究報告書

マイクロアレイ染色体検査でみつかる染色体微細構造異常症候群の診療ガイドラインの確立

研究代表者　倉橋　浩樹
藤田保健衛生大学・総合医科学研究所・分子遺伝学研究部門・教授

研究要旨
本研究では、マイクロアレイ染色体検査により診断される、多発奇形・発達遅滞を主症状とする染色体微細構造異常症候群の診療ガイドラインの確立を目的として、国内の多施設共同研究により、代表的な 30 疾患に関して、全国調査による国内患者の把握や、臨床診断基準、重症度判定基準の策定を実施する。昨年度に引き続き、実臨床の中での新規患者の掘り起こしに向けたマイクロアレイ染色体検査、ならびに診療情報の収集、整理などを行った。一方で、未診断症例に関しては、第一段階のスクリーニング検査としてのエクソーム解析も平行しておこない、その有用性の検討を行った。その結果、複数の遺伝子が欠失・重複する染色体微細構造異常症候群の場合、XHMM アルゴリズム（エクソーム隠れマルコフモデル法）による定量は検出感度が十分に高く、その有用性が確認された。ただ、確認のための二次検査が必要であり、マイクロアレイ染色体検査は定量性の精度が高く、二次検査として有用であることが確認された。

研究分担者
大橋博文　埼玉県立小児医療センター遺伝科・部長
黒澤健司　地方独立行政法人神奈川県立病院機構神奈川県立こども医療センター・遺伝科・部長
山本俊至　東京女子医科大学・遺伝子医療センター・ゲノム診療科・教授
涌井敬子　信州大学医学部遺伝医学・予防医学教室 講師

A. 研究目的

染色体の欠失や重複のような微細構造異常によるコピー数の変化（copy number variation: CNV）は、器官発生に関わる転写因子や、ヒストン修飾因子、クロマチン因子などの転写調節因子が遺伝子の量的効果の影響を受けやすいため、先天性疾患の原因となることが多い。従来はG分染法による染色体検査やFISH法での診断が行われてきたが、マイクロアレイ染色体検査の普及により、CNVの検出感度が飛躍的に向上した。欧米では、多発奇形・発達遅滞の原因の精査としては従来の染色体検査にかわる第1選択の診断ツールとされてきた。多発奇形・発達遅滞の患者で G 分染法では３％であった異常検出率が、マイクロアレイ染色体検査の導入により、15-20%の患者で責任変異を同定できるとされ、数多くの新規疾患も定義された。日本でも、すでに 5000 以上の患者データが蓄積されている。しかし、網羅的検査に特有の意義不明の CNV の解釈（variation of unknown significance: VUS）、偶発的所見（incidental findings: IF）や二次的所見（secondary findings: SF）への対応などの問題点が未解決であり、一般臨床検査としての提供体制が整っているとはいえない。近年、マイクロアレイ染色体検査が診断に必須な疾患が小児慢性特定疾患や指定難病に追加されるなど、臨床的有用性は高いものの、高コストの問題があり、自費診療の中で一部の患者がその恩恵を被るにとどまる。

一方で、近年は、多発奇形・発達遅滞の患者の原因の精査としては、次世代シーケンサーによるエクソーム解析の台頭もあり、現場での検査適応のための指針が必要である。

研究代表者を含む本研究班員はこれまで、厚労省難治性疾患克服研究事業の支援も受け、多発奇形・発達遅滞の患者の原因の精査としてのマイクロアレイ染色体検査を診療の中でおこなってきた。本研究ではそれを継続する形で、3 年間を通じて、患者サンプルの収集とマイクロアレイ染色体検査を行う。各施設で合計年間 500 例ほどの解析を目標とする。そして、3 年目には、代表的な 30 疾患（1 年目に見直し、2 疾患を加え、合計 32 疾患）に関して、新たな臨床診断基準の作成、そして、個々の構造異常の発生メカニズムの解析を行うことを目標とする。これまでにリストの 30 疾患の多くには診療ガイドラインはなく、本研究は極めて有用な成果を創出する。

また、近年は、多発奇形・発達遅滞の患者の原因へのアプローチとしては、次世代シーケンサーによるエクソーム解析の有用性が確立した。このエクソーム解析はリード数を定量することで CNV を同定することが可能であり、マイクロアレイ染色体検査と同等のデータを創出することができる可能性があるので、多発奇形・発達遅滞の責任変異のスクリーニングにおいて第一選択となりうる。本研究では、多発奇形・発達遅滞の責任変異のスクリーニング法としてのマイクロアレイ染色体検査とエクソームの定量の感度や精度を比較し、その有用性を検討する。

B. 研究方法

日本全国の主な診療施設の小児科もしくは遺伝診療科に連絡を取り、染色体微細構造異常が疑われるような多発奇形・発達遅滞の患者のサーベイランス、患者登録を行う。とくに、リストの 32 疾患（資料１）に関しては診断未確定患者の発掘のために、診断につながる臨床情報を公開する。この調査は、日本小児遺伝学会（小崎健次郎理事長、本研究の研究協力者）との連携のもとに行う。集まった患者情報に基づいて、詳細な臨床情報と末梢血サンプルの収集を行う。末梢血サンプルに対しては、研究代表者を含む各研究分担者が個々の施設でマイクロアレイ染色体検査、必要に応じて FISH 解析を行う。各施設の合計として年間 500 例ほどの解析を目標とする。

研究代表者を含む各研究分担者の研究施設には、すでにマイクロアレイ染色体検査を行う設備が整っており、これまでに臨床検査として行ってきた十分な実績がある。その際、ダウン症候群などの染色体異数性による疾患のような、従来のＧ分染法が有用である疾患や、22q11 欠失症候群などのように疾患特異的 FISH 解析が第 1 選択になるような疾患を、表現型で除外できるように、染色体微細構造異常の診断のためのマイクロアレイ染色体検査の適応を決めるガイドラインを確立する。

多発奇形・発達遅滞の患者の原因の精査としてマイクロアレイ染色体検査による診断を進め、疾患責任 CNV が確定しない場合にはエクソーム解析へと進めた。一方で、症例によってはエクソーム解析を先行させ、その定量により疾患責任 CNV の候補を推定し、二次検査としてマイクロアレイ染色体検査、MLPA 法、qPCR 法により確認した。エクソームのデータはターゲットエクソーム解析、全エクソーム解析ともに、Log2 変換法や隠れマルコフモデル（exome hidden Markov model: XHMM）によるアルゴリズムなどを用いて観察研究として比較検討を行った。

（倫理面への配慮）

本研究は、ヒトゲノム・遺伝子解析研究に関する倫理指針、人を対象とする医学系研究に関する倫理指針を遵守して行った。解析試料の取得は書面でのインフォームドコンセントの上でおこない、研究対象者に対するプライ

バシーの保護など、人権擁護上の問題については十分に配慮したうえで行った。各関連施設から送付される試料は、試料提供機関において連結可能匿名化が行われ、研究代表者や研究分担者の所属機関には匿名化された試料と、予めチェックリストとして作成した臨床データのみが送付されることとした。試料は研究代表者や研究分担者の所属機関にて保管し、研究期間終了後に同意書に基づき破棄を行う予定である。データは研究代表者や研究分担者の所属機関内の鍵のかかるキャビネットに研究期間内、保管する。報告又は発表に際しては、被験者のプライバシー保護に十分配慮する。偶発的所見を含めた、発生しうる諸問題には、各施設の遺伝カウンセリング部門が対応する。マイクロアレイ染色体検査に関する研究は、すでに研究代表者や研究分担者の所属機関のヒトゲノム・遺伝子解析研究倫理審査委員会の承認を得ている（「染色体コピー数異常症に関する研究」藤田保健衛生大学・ヒトゲノム・遺伝子解析研究倫理審査委員会、平成２２年３月１２日承認、5 年後再承認、10 年後再承認、HG13-003。）。

C. 研究結果

（１）マイクロアレイ染色体検査について

研究代表者を含め各班員が、所属施設における実臨床の中での新規患者の発見に向けたマイクロアレイ染色体検査、ならびに診療情報のチェックを行った。本研究の対象疾患である、染色体微細構造異常症 30 疾患の掘り起こしを行った。

（２）染色体微細構造異常症 30 疾患について

昨年度の第 1 回「マイクロアレイ染色体検査でみつかる染色体微細構造異常症候群の診療ガイドラインの確立研究班」班会議で対象疾患の見直しを行い、当初の 30 疾患に 9q34 欠失症候群と 1q 重複症候群の 2 疾患の追加を行い、対象疾患を 32 疾患に拡大した（資料１）。昨年度までに 7 つの疾患（1p36 欠失症候群、4p16 欠失症候群、5p サブテロメア欠失症候群、11p12-p14 欠失症候群、11/22 混合トリソミー、1q 重複症候群、9q34 欠失症候群）に関しては診断基準、重症度判定基準の作成へと進めることができている。

一方、残りの 25 疾患に関して、順次臨床診断基準の作成をおこなうことに関しては、十分な検討を行った。その結果、疾患によっては難病指定を目指すべき疾患と小児慢性特定疾患を目指すべき疾患があり、それらはすでに「先天異常症候群」や「常染色体異常症」という形で認定されている枠組みに紐付けすることを目指すが、個々の疾患の特性は、疾患によって大きく異なるので、診断基準策定は個別に対応する必要があることが確認された。

（３）エクソーム解析との関連性

本年度に未診断の多発奇形・発達遅滞患者 88 例に対して、エクソーム・ファーストでアプローチし、Log2 変換法や XHMM によるアルゴリズムなどの定量的エクソーム解析と、マイクロアレイ染色体検査の比較検討を行った。その結果、36 例（41%）に責任変異としての SNV/indel が同定された。一方、構造異常としての CNV は 4 例(5%)に同定された。欠失が 2 例、重複が 2 例であった。既知の疾患責任遺伝子を含んでいたり、de novo であったりすることにより、患者の症状の責任変異であると確定した。マイクロアレイ染色体検査は確定検査として有用であった。一方で、エクソームデータの定量で見つからなかった症例にマイクロアレイ染色体検査を行い、新たな CNV が同定された症例はなかった。以上により、未診断の多発奇形・発達遅滞患者の診断には、エクソーム・ファーストでアプローチし、定量的エクソーム解析で同定された CNV に対しマイクロアレイ染色体検査でヴァリデーションすることが妥当であると思われた。

D. 考察

近年のエクソームの急速な普及と低価格化とが相俟って、定量的エクソーム解析と、マイクロアレイ染色体検査の位置づけを検討する必要性を認識し、比較検討を開始した。本年度の研究成果により、定量的エクソームを第一段階のスクリーニング検査として使用した場合に、複数の遺伝子が欠失・重複しているような CNV の検出に関しては、XHMM の有用性が確認された。一方で、定量的エクソームのデータには確認作業が必要であり、確定的検査としての二次検査として、マイクロアレイ染色体検査が必要であることを確認した。エクソーム解析により、塩基レベルの遺伝子変化と、複数の遺伝子が欠失・重複しているような CNV の検出とが同時に可能である点で、スクリーニング検査としてのパフォーマンスは、マイクロアレイ染色体検査を完全に凌駕している。今後、次世代シーケンスのさらなる低コスト化が進むと、未診断患者のスクリーニング検査は、エクソーム・ファーストという位置づけとなる可能性が高い。

診断基準､重症度判定基準の作成の作業は実質的には小休止となった。「先天異常症候群」や「常染色体異常症」という大きな枠組みの中でのガイドラインの策定なども考慮されたが、個々の疾患の特性は、疾患によって大きく異なるので､最終的には､診断基準策定は個別に対応する必要があることが確認された。「国際標準に立脚した奇形症候群領域の診療指針に関する学際的・網羅的検討研究班（小崎班）」とも連携をとりながら、個別の疾患単位で進める必要がある。診療ガイドラインなどの研究成果は、ウェブ上で公開してゆく。また、指定難病認定に向けての準備、その後、これらの疾患の診断に必要な遺伝学的検査としてのエクソーム解析やマイクロアレイ染色体検査の保険収載などを視野に入れ、研究を進めていく。本研究の成果は、これらの疾患の患者や家族に対する支援、稀少難病の医療や福祉の向上に貢献することが期待される。

E. 結論

本研究では、マイクロアレイ染色体検査により診断される､多発奇形・発達遅滞を主症状とする染色体微細構造異常症候群の診療ガイドラインの確立を目的として、国内の多施設共同研究により､代表的な 32 疾患に関して､全国調査による国内患者の把握や、臨床診断基準、重症度判定基準の策定を開始し、7 つの疾患に関しては診断基準､重症度判定基準の作成を行うことができたが、定量的エクソーム解析とマイクロアレイ染色体検査の比較研究というタスクができてしまったため、残りの対象疾患に関しては積み残しとなってしまった。今後、新たな研究班を組織し、残りの対象疾患に関して、研究代表者を含めた各班員が実臨床の中での新規患者の掘り起こしに向けたマイクロアレイ染色体検査、ならびに診療情報の収集、チェックなどを行い、同様の検討を進めてゆく。一方で、エクソーム解析の定量とマイクロアレイ染色体検査との比較検討に関しては、スクリーニング検査としてのエクソーム解析の定量の有用性が明らかとなったが、エクソーム解析の定量の二次検査としてマイクロアレイ染色体検査の重要性も再確認された。

F. 健康危険情報

特になし。

G. 研究発表

１．論文発表

(1) Rinaldi VD, Bolcun-Filas E, Kogo H, Kurahashi H, Schimenti JC. The DNA damage checkpoint eliminates mouse oocytes with chromosome synapsis failure. **Mol Cell** 67, 1026-1036.e2, 2017.

(2) Nakae S, Kato T, Murayama K, Sasaki H, Abe M, Kumon M, Kumai T, Yamashiro K, Inamasu J, Hasegawa M, Kurahashi H, Hirose Y. Remote intracranial recurrence of IDH mutant gliomas is associated with TP53 mutations and an 8q gain. **Oncotarget** 8, 84729-84742, 2017.

(3) Azuma Y, Töpf A, Evangelista T, Lorenzoni PJ, Roos A, Viana P, Inagaki H, Kurahashi H, Lochmüller H. Intragenic DOK7 deletion detected by whole-genome sequencing in congenital myasthenic syndromes. **Neurol Genet** 3, e152, 2017.

(4) Nagasaka M, Taniguchi-Ikeda M, Inagaki H, Ouchi Y, Kurokawa D, Yamana K, Harada R, Nozu K, Sakai Y, Mishra SK, Yamaguchi Y, Morikoka I, Toda T, Kurahashi H, Iijima K. Novel missense mutation in DLL4 in a Japanese sporadic case of Adams-Oliver syndrome. **J Hum Genet** 62, 869, 2017.

(5) Kawamura Y, Ohye T, Miura H, Ihira M, Kato Y, Kurahashi H, Yoshikawa T. Analysis of the origin of inherited chromosomally integrated human herpesvirus 6 in the Japanese population. **J Gen Virol** 98, 1823-1830, 2017.

(6) Kato T, Ouchi Y, Inagaki H, Makita Y, Mizuno S, Kajita M, Ikeda T, Takeuchi K, Kurahashi H. Genomic characterization of chromosomal insertions: Implication for mechanism leading to the chromothripsis. **Cytogenet Genome Res** 153, 1-9, 2017.

(7) Kohmoto T, Okamoto N, Naruto T, Murata C, Ouchi Y, Fujita N, Inagaki H, Satomura S, Okamoto N, Saito M, Masuda K, Kurahashi H, Imoto I. A case with concurrent duplication, triplication, and uniparental isodisomy at 1q42.12-qter supporting microhomology-mediated break-induced replication model for replicative rearrangements. **Mol Cytogenet** 10, 15, 2017.

(8) Kato M, Kato T, Hosoba E, Ohashi M, Fujisaki M, Ozaki M, Yamaguchi M, Sameshima H, Kurahashi H. PCS/MVA syndrome caused by an Alu insertion in the BUB1B gene. **Hum Genome Var** 4, 17021, 2017.

(9) Inoue Y, Sakamoto Y, Sugimoto M, Inagaki H, Boda H, Miyata M, Kato H, Kurahashi H, Okumoto T. A family with craniofrontonasal syndrome: the first report of familial cases of craniofrontonasal syndrome with bilateral cleft lip and palate. **Cleft Palate Craniofac J**, 15347, 2018.

(10) Taniguchi-Ikeda M, Morisada N, Inagaki H, Ouchi Y, Takami Y, Tachikawa M, Satake W, Kobayashi K, Tsuneishi S, Takada S, Yamaguchi H, Nagase H, Nozu K, Okamoto N, Nishio H, Toda T, Morioka I, Wada H, Kurahashi H, Iijima K. Two patients with PNKP mutations presenting with microcephaly, seizure, and oculomotor apraxia. **Clin Genet** 93(4), 931-933, 2018.

(11) Ohwaki A, Nishizawa H, Aida N, Kato T, Kambayashi A, Miyazaki J, Ito M, Urano M, Kiriyama Y, Kuroda M, Nakayama M, Sonta SI, Suzumori K, Sekiya T, Kurahashi H, Fujii T. Twin pregnancy with chromosomal abnormalities mimicking a gestational trophoblastic disorder and coexistent foetus on ultrasound. **J Obstet Gynaecol**. 2018 Mar 9:1-3.

(12) Terasawa S, Kato A, Nishizawa H, Kato T, Yoshizawa H, Noda Y, Miyazaki J, Ito M, Sekiya T, Fujii T, Kurahashi H. Multiplex PCR in noninvasive prenatal diagnosis for FGFR3-related disorders. **Congenit Anom (Kyoto)**. 2018 Mar 14.

(13) Kibe M, Ibara S, Inagaki H, Kato T, Kurahashi H, Ikeda T. Lethal persistent pulmonary hypertension of the newborn in Bohring-Opitz syndrome. **Am J Med Genet A**. 2018 May;176(5):1245-1248. Prenatal diagnosis of premature chromatid separation/mosaic variegated aneuploidy (PCS/MVA) syndrome.

(14) Yamaguchi T, Yamaguchi M, Akeno K, Fujisaki M, Sumiyoshi K, Ohashi M, Sameshima H, Ozaki M, Kato M, Kato T, Hosoba E, Kurahashi

H. Prenatal diagnosis of premature chromatid separation/mosaic variegated aneuploidy (PCS/MVA) syndrome. **J Obstet Gynaecol Res**. 2018 Apr 19.

(15) Fukami M, Kurahashi H. Clinical consequences of chromothripsis and other catastrophic cellular events. **Methods Mol Biol.** 2018;1769:21-33.

(16) Yokoi K, Nakajima Y, Ohye T, Inagaki H, Wada Y, Fukuda T, Sugie H, Yuasa I, Ito T, Kurahashi H. Disruption of the responsible Gene in a phosphoglucomutase 1 deficiency patient by homozygous chromosomal inversion. **JIMD Rep**. 2018 May 12.

(17) Tsutsumi M, Fujita N, Suzuki F, Mishima T, Fujieda S, Watari M, Takahashi N, Tonoki H, Moriwaka O, Endo T, Kurahashi H. Constitutional jumping translocation involving the Y and acrocentric chromosomes. **Asian J Androl**, in press.

(18) Sharma R, Gardner A, Homan C, Douglas E, Mefford H, Wieczorek D, Stark Z, Nowak C, Douglas J, Parsons G, Mark P, Loidi L, Mosher TM, Herman G, Gillespie M, Brady L, Madrigal I, Domenech Salgado L, Rabionet R, Ishihara N, Inagaki H, Kurahashi H, Palmer E, Field M, Gecz J. Clinical and functional assessment of novel variation in THOC2, an essential component of nuclear mRNA export machinery. **Hum Mutat**, in press.

(19) 宮﨑純、西澤春紀、倉橋浩樹. 染色体異常発生のメカニズム、産科と婦人科、84(1), 49-54, 2017.

(20) 倉橋浩樹. ゲノム医療の現状と遺伝カウンセリング、日本血栓止血学会誌、28(1), 9-15, 2017.

(21) 加藤武馬、西澤春紀、倉橋浩樹. 出生前診断におけるマイクロアレイ検査と NGS、産婦人科の実際、66(4), 497-502, 2017.

(22) 加藤麻希、倉橋浩樹. 造血器腫瘍のクリニカルシーケンスにおける遺伝診療体制の構築、日本小児血液・がん学会雑誌、印刷中

(23) 加藤武馬、倉橋浩樹. 周産期のゲノムシーケンスの現状、遺伝子医学 MOOK 34 号、印刷中

２．学会発表

(1) Kurahashi H. Screening for Genetic Disease within the Asian context. ASPIRE 3rd Masterclass, Preimplantation Genetic Testing: Screening and Diagnosis, Beijing, China, Oct 12, 2017.

(2) Kurahashi H, Kato T, Kato M, Ouchi Y, Tsutsumi M, Inagaki H. Towards optimization of PGD for recurrent t(11;22) carrier. ESHG2017, Copenhagen, Denmark, May 27-30, 2017.

(3) Inagaki H, Kanyama K, Kato T, Ouchi Y, Yamamoto T, Kurahashi H. Breakpoint analysis of chromosomes having inverted duplication with terminal deletion by NGS. ASHG2017, Orlando, USA, Oct 17-21, 2017.

(4) Ishihara N, Inagaki H, Kawai M, Inuo C, Kurahashi H. Intellectual disability with severe self-injury behavior caused by THOC2 splice site variant. ASHG2017, Orlando, USA, Oct 17-21, 2017.

(5) Taniguchi-Ikeda M, Morisada N, Inagaki H, Okamoto N, Toda T, Morioka I, Kurahashi H, Kazumoto I. Two patients with PNKP mutations presenting microcephaly, seizure, and oculomotor apraxia. ASHG2017, Orlando, USA, Oct 17-21, 2017.

(6) Kato T, Nishiyama S, Nishyama Y, Yoshikai K, Matsuda Y, Sawada T, Yoshizawa H, Furukawa H, Nishizawa H, Kato M, Kanbayashi A, Kurahashi H. Comprehensive chromosomal analysis of blastomeres with developmental arrest. ISPD2017, SanDiego, USA, Jul 9-12, 2017.

(7) Inagaki H, Kanyama K, Kato T, Ouchi Y, Yamamoto T, Kurahashi H. Breakpoint analysis of chromosomes having inverted duplication with

terminal deletion by NGS. 12th International Workshop on Advanced Genomics, Tokyo, Japan, Jun 27-29, 2017.
(8) Ito T, Nakajima Y, Maeda Y, Sakai Y, Gotoh K, Suzuki T, Kurahashi H, Yoshikawa T. Severity and variety of management in 5 patients with methylmalonyl-CoA mutase deficiency. ICIEM2017, Rio de Janeiro, Brazil, Sep 5-8, 2017.
(9) Ishihara N, Inagaki H, Miyake M, Kawamura Y, Yoshikawa T, Kurahashi H. A case of catastrophic early life epilepsy with a novel ATP1A3 mutation. 6th Symposium on ATP1A3 in Disease, Tokyo, Japan, Sep 21-22, 2017.
(10) Ishimaru S, Ishihara N, Mori Y, Miyake M, Hibino H, Kawai M, Inuo C, Tsuge I, Hayakawa M, Kurahashi H. A case of oculoectodermal syndrome with acute transverse myelopathy caused by spinal dural arteriovenous fistula. AOCCN2017, Fukuoka, May 11-14, 2017.
(11) Hattori S, Hagihara H, Takayama Y, Kameyama T, Ouchi Y, Inagaki H, Kurahashi H, Huang FL, Huang KP, Miyakawa T. Neurogranin deficiency causes behavioral and molecular phenotypes related to schizophrenia. Neuroscience 2017, Washington DC, USA, Nov 11-15, 2017.
(12) 倉橋浩樹、造血器腫瘍のクリニカルシーケンスにおける遺伝カウンセリング体制の構築、AMED・臨床ゲノム情報統合データベース整備事業　がん領域における臨床ゲノムデータストレージの整備に関する研究（堀部班）平成 29 年度第 1 回班会議、名古屋、Dec 22, 2017.
(13) 倉橋浩樹、不育症のゲノム医療を目指して、第 1 回 AMED 不育症班会議（齋藤班）、東京、Jul 2, 2017.
(14) 倉橋浩樹、不育症のゲノム医療を目指して、第 2 回 AMED 不育症班会議（齋藤班）、東京、Jan 14, 2017.
(15) 倉橋浩樹、網羅的手法による次世代型 PGD　～PGD の実際とこれから、JISART シンポジウム、名古屋、Jun 11, 2017.
(16) 倉橋浩樹、網羅的手法による次世代型着床前診断、広島生殖医療研究会、広島、Jun 17, 2017.
(17) 倉橋浩樹、次世代型 PGD/PGS の現状と問題点、第 24 回セントルカ・セミナー、大分、Jun 18, 2017.
(18) 倉橋浩樹、網羅的手法による遺伝子染色体診断　～次世代型 PGD の台頭～　大阪大学 IRUD 講演会、大阪、Jul 11, 2017.
(19) 倉橋浩樹、網羅的手法による次世代型 PGD、神和メディカル株式会社創立 15 周年記念学術講演会、神戸、Aug 6, 2017.
(20) 倉橋浩樹、網羅的手法による次世代型着床前診断、第 18 回東北 ART 研究会、仙台、Aug 20, 2017.
(21) 倉橋浩樹、染色体異常の発生メカニズム -男と女-、第 2 回発生遺伝研究会、徳島、Sep 9, 2017.
(22) 倉橋浩樹、家族性腫瘍における遺伝子検査と遺伝カウンセリングの実際 Scientific Exchange Meeting (SEM) 、名古屋、Oct 7, 2017.
(23) 倉橋浩樹、遺伝って何だろう？第２１回 FabryNEXT 交流会 in 名古屋、名古屋、Nov 4, 2017.
(24) 倉橋浩樹、着床前診断の現状と今後の展望、第１９回日本イアンドナルド超音波講座、広島、Nov 5, 2017.
(25) 倉橋浩樹、造血器腫瘍のクリニカルシーケンスにおける遺伝診療体制の構築、第５９回日本小児血液がん学会学術集会、松山、Nov 9, 2017.
(26) 倉橋浩樹、次世代型 PGD/PGS の現状と問題点、第６２回日本生殖医学会学術講演会、下関、Nov 16, 2017.
(27) 倉橋浩樹、Recent advance in our understanding of the molecular nature of chromosomal abnormalities. 日本人類遺伝学会第６２回大会、神戸、Nov 17, 2017.
(28) 倉橋浩樹、がんと遺伝子検査、藤田保健

衛生大学医学部公開講座、豊明、Dec 13, 2017.
(29) 倉橋浩樹、網羅的手法による着床前診断の現状と問題点、大阪大学医学部全国教授の会　第５回総会、Dec 23, 2017.
(30) 倉橋浩樹、染色体の遺伝学、第 9 回遺伝医学セミナー入門コース、名古屋、Feb 17-18, 2018.
(31) 倉橋浩樹、PGD/PGS の現状と問題点、日本生殖発生医学会第１３回学術集会、東京、Mar 18, 2018.
(32) 倉橋浩樹、網羅的手法による PGD/PGS 入門、日本 A-PART 学術講演会 2018、東京、Mar 25, 2018.
(33) 稲垣秀人、加藤武馬、完山和生、大内雄矢、山本俊至、倉橋浩樹、逆位重複・端部欠失の全ゲノムシーケンスによる切断点解析、日本人類遺伝学会第６２回大会、神戸、Nov 17, 2017.
(34) 加藤武馬、加藤麻希、吉貝香里、松田有希野、新井千登勢、浅井菜緒美、中野英子、澤田富夫、倉橋浩樹、初期胚に発生する染色体異常は栄養外胚葉に蓄積する、日本人類遺伝学会第６２回大会、神戸、Nov 17, 2017.
(35) 堤真紀子、藤田尚子、三島隆、藤枝聡子、外木秀文、森若治、遠藤俊明、倉橋浩樹、Y 染色体転座保因者の子に認められた別の染色体への Y の再転座、日本人類遺伝学会第６２回大会、神戸、Nov 17, 2017.
(36)加藤麻希、西澤春紀、森山育実、市原慶和、佐藤労、倉橋浩樹、着床前診断における家系内発端者の遺伝学的情報の重要性、日本人類遺伝学会第６２回大会、神戸、Nov 17, 2017.
(37) 河合美紀、杉本篤哉、平野聡子、石原靖紀、堤真紀子、倉橋浩樹、色素失調症の低頻度モザイク変異解析、日本人類遺伝学会第６２回大会、神戸、Nov 17, 2017.
(38) 藤盛伸美、柘植郁哉、市原慶和、稲垣秀人、堤真紀子、佐藤労、大江瑞恵、倉橋浩樹、デュシェンヌ型筋ジストロフィー双生児の卵性診断、日本人類遺伝学会第６２回大会、神戸、Nov 17, 2017.
(39) 浅井喜美子、倉橋浩樹、大江瑞恵、佐藤労、看護職者が受けた遺伝教育の現状と臨床で求められる遺伝看護実践、日本人類遺伝学会第６２回大会、神戸、Nov 17, 2017.
(40) 障害のある子どもを持つ家族への遺伝カウンセラーとしての支援の在り方、久野千恵子、倉橋浩樹、稲垣秀人、杉本賢政、堤真紀子、大江瑞恵、佐藤労、日本人類遺伝学会第６２回大会、神戸、Nov 17, 2017.
(41) 稲垣秀人、堤真紀子、井上義一、田口佳広、帽田仁子、宮田昌史、奥本隆行、吉川哲史、倉橋浩樹、細胞培養モデルが明らかにした X 連鎖の疾患での女性重症化、第 40 回日本分子生物学会年会、神戸、Dec 6-9, 2017.
(42) 加藤武馬、稲垣秀人、新海保子、堤真紀子、藤田尚子、山本俊至、倉橋浩樹、メイトペアシーケンスによる染色体構造異常の発生メカニズムの解析、第 40 回日本分子生物学会年会、神戸、Dec 6-9, 2017.
(43) 堤真紀子, 加藤武馬、稲垣秀人、倉橋浩樹、均衡型相互転座モデルマウスの精子形成における性染色体不活化異常の発生機構、第 40 回日本分子生物学会年会、神戸、Dec 6-9, 2017.
(44) 加藤武馬、稲垣秀人、藤田尚子、新海保子、蒔田芳男、水野誠司、梶田光晴、池田敏郎、竹内一浩、柘植郁哉、倉橋浩樹、染色体挿入の発生機序、第 40 回日本小児遺伝学会学術集会、東京、Jan 12-13, 2018.
(45) 河合美紀、堤真紀子、鮫島希代子、道和百合、稲垣秀人、倉橋浩樹、失が修復された健常な母親に起因する Jacobsen 症候群の同胞例、第 40 回日本小児遺伝学会学術集会、第 40 回日本小児遺伝学会学術集会、東京、Jan 12-13, 2018.
(46) 堤真紀子, 加藤武馬、稲垣秀人、倉橋浩樹、均衡型相互転座保因者モデルマウスにおける精母細胞の性染色体不活化異常、第 49 回藤田学園医学会、豊明、Oct 12-13, 2017.
(47) 河合美紀、大江瑞恵、佐藤労、倉橋浩樹

「色素失調症患者と家族の集い」開催からの考察、第 49 回藤田学園医学会、豊明、Oct 12-13, 2017.

(48) 加藤麻希、西澤春紀、大江瑞恵、倉橋浩樹、佐藤労、配偶子提供による妊娠および養子縁組に関する意識調査. 第 41 回遺伝カウンセリング学会、大阪、Jun, 22-25, 2017.

(49) 河合美紀、大江瑞恵、佐藤労、倉橋浩樹、「色素失調症患者と家族の集い」開催からの考察、第 41 回遺伝カウンセリング学会、大阪、Jun, 22-25, 2017.

(50) 加藤麻希、加藤武馬、大江瑞恵、市原慶和、佐藤労、倉橋浩樹、25 年前のへその緒で出生前診断を回避できたムコ多糖症Ⅱ型の遺伝カウンセリング、第 20 回中部出生前医療研究会、Mar 4, 2018.

(50) 吉貝香里、加藤武馬、松田有希野、新井千登勢、浅井菜緒美、中野英子、澤田富夫、倉橋浩樹、NGS を用いた TE・ICM 間における核型一致率の比較、第 58 回日本乱視学会学術集会、沖縄、Jun 2-3, 2017.

(51) 松田有希野、加藤武馬、吉貝香里、新井千登勢、中野英子、澤田富夫、倉橋浩樹、5 日目、6 日目の胚盤胞凍結時の細胞のサイズと染色体解析、第 58 回日本乱視学会学術集会、沖縄、Jun 2-3, 2017.

(52) 稲葉美枝, 村松友佳子, 谷合弘子, 野々部典枝, 倉橋浩樹, 水野誠司、エクソームシーケンスで診断し得た VPS13 遺伝子のエクソン欠失とナンセンス変異を認めた Cohen 症候群の一男児例. 第 59 回小児神経学会、大阪、Jun 15-17, 2017.

(53) 日尾野宏美, 石原尚子, 川口将宏, 後藤研誠, 西村直子, 尾崎隆男, 倉橋浩樹、頭部打撲をきっかけとする反復性脳症の 1 家系における遺伝学的検討. 第 59 回小児神経学会、大阪、Jun 15-17, 2017.

(54) 横井摂理, 堤真紀子, 宮冬樹, 宮田昌史, 加藤光広, 岡本伸彦, 角田達彦, 山崎麻美, 金村米博, 小崎健次郎, 齋藤伸治, 倉橋浩樹、Novel compound heterozygous variants in PLK4 cause microcephaly and chorioretinopathy. 第 59 回小児神経学会、大阪、Jun 15-17, 2017.

(55) Ishihara N, Sasaki H, Shima S, Miyake M, Hibino H, Kato T, Shiroki R, Kurahashi H、Correlation between neurological deficits and genotype in patients with tuberous sclerosis complex. 第 59 回小児神経学会、大阪、Jun 15-17, 2017.

(56) 松本祐嗣、池住洋平、宮田昌史、近藤朋実、長谷有紗、川井有里、内田英利、中島葉子、帽田仁子、伊藤哲哉、臨床経過より疑い遺伝子検査により Renal tubular dysgenesis と診断した乳児腎不全例、第 52 回小児腎臓病学会、東京、Jun 1-3, 2017.

(57) 亀井宏一、倉橋浩樹、稲垣秀人、藤丸拓也、蘇原映誠、宍戸清一郎、小椋雅夫、佐藤舞、義岡孝子、緒方謙太郎、石倉健司、ARPKD と同様の臨床像を呈し遺伝子解析で *PKD1* の複合ヘテロ変異が疑われた男児例. 第 39 回日本小児腎不全学会、淡路、Sep 21-22, 2017.

(58) 松本祐嗣、池住洋平、近藤朋実、横井克幸、中島葉子、伊藤哲哉、吉川哲史　倉橋浩樹、ネフローゼ症候群を契機に発症し補体 I 因子変異を認めた aHUS の一乳児例、第 47 回日本腎臓学会西部学術大会、岡山、Oct 13-14, 2017.

(59) 河合美紀、堤真紀子、鮫島希代子、道和百合、稲垣秀人、倉橋浩樹、Jacobsen 症候群の同胞例　―親の解析で見つかった痕跡―、第 12 回東海小児遺伝カンファレンス、名古屋、Sep 15, 2017.

(60) 河合美紀、堤真紀子、稲垣秀人、倉橋浩樹、色素失調症 20 家系の遺伝子解析　～低頻度モザイク変異検出への手がかり～、第 13 回東海小児遺伝カンファレンス、名古屋、Feb 24, 2018.

(61) 大江瑞恵、村松友佳子、水野誠司、秋山秀彦、倉橋浩樹. マイクロアレイ染色体検査によるマーカー染色体の由来検索、第 18 回日本検査血液学会学術集会、札幌、Jul 22-23, 2017.

(62) 加藤麻希、新海保子、加藤武馬、池住洋平、中島葉子、松本祐嗣、稲垣秀人、堤真紀子、倉橋浩樹．Bartter 症候群を例に相同性の高い塩基配列を持つ責任遺伝子における変異解析手法の検討. 第 5 回 NGS 現場の会、仙台、May 22-24, 2017.

H. 知的財産権の出願・登録状況
特になし。

（資料１）

マイクロアレイ染色体検査でみつかる染色体微細構造異常症候群の診療ガイドラインの確立

	対象疾患リスト	担当
1	1p36欠失症候群	山本俊至
2	1q44欠失症候群	大橋博文
3	2p15-p16.1欠失症候群	大橋博文
4	Feingold症候群(2p24.3欠失)	涌井敬子
5	2q23.1欠失症候群(*MBD5*)	涌井敬子
6	2q24.2-q24.3欠失/重複症候群(*SCN1A*)	山本俊至
7	2q32.1-q33.3欠失/重複症候群(*SATB2*)	黒澤健司
8	2q37欠失症候群	大橋博文
9	3p21.31欠失症候群	大橋博文
10	4p16欠失(Wolf-Hirschhorn症候群)	涌井敬子
11	Cri-du-chat症候群(5pサブテロメア欠失)	涌井敬子
12	5q14.3欠失症候群(*MEF2C*)	山本俊至
13	5q31欠失症候群	山本俊至
14	8pサブテロメア欠失	黒澤健司
15	Langer-Giedion症候群(8q24.11欠失)	倉橋浩樹
16	11p12-p14欠失症候群	山本俊至
17	Jacobsen症候群(11qサブテロメア欠失)	倉橋浩樹
18	16p11.2欠失/重複症候群	山本俊至
19	Miller-Dieker症候群(17pサブテロメア欠失)	黒澤健司
20	17p13.1欠失症候群(*GABARAP*)	黒澤健司
21	Smith-Magenis症候群(17p11.2欠失)	黒澤健司
22	Potocki-Lupski症候群(17p11.2重複)	涌井敬子
23	21qサブテロメア欠失症候群	黒澤健司
24	Emanuel症候群(11/22混合トリソミー)	倉橋浩樹
25	22q11.2重複症候群	倉橋浩樹
26	Cat eye症候群(22q11テトラソミー)	倉橋浩樹
27	Phelan-McDermid症候群(22q13欠失)	大橋博文
28	Xp11.3-p11.4欠失(*MAOA*, *MAOB*, *CASK*)	涌井敬子
29	Xq11.1欠失症候群(*ARHGEF9*)	山本俊至
30	MECP2重複症候群(Xq28重複)	倉橋浩樹
31	9q34欠失症候群	黒澤健司
32	1q重複症候群	涌井敬子

（資料２）

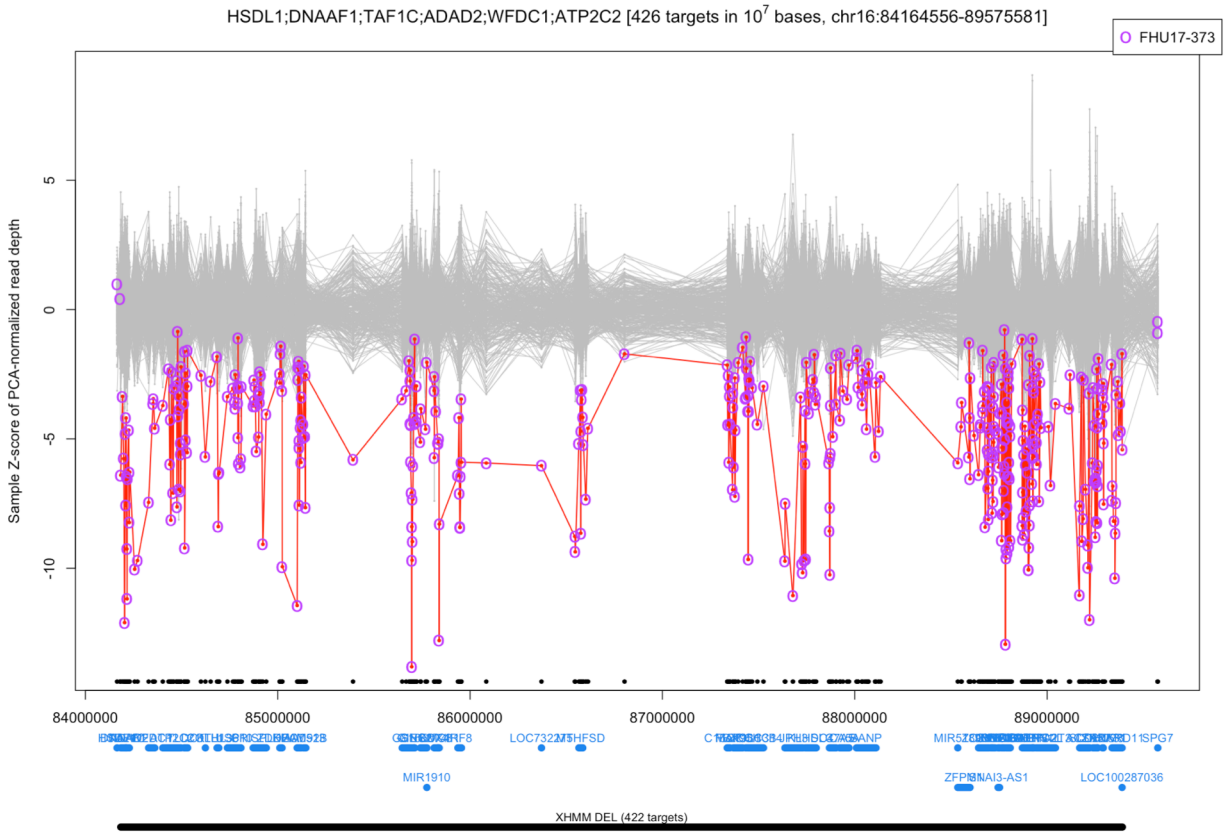

XHMMによる欠失の同定

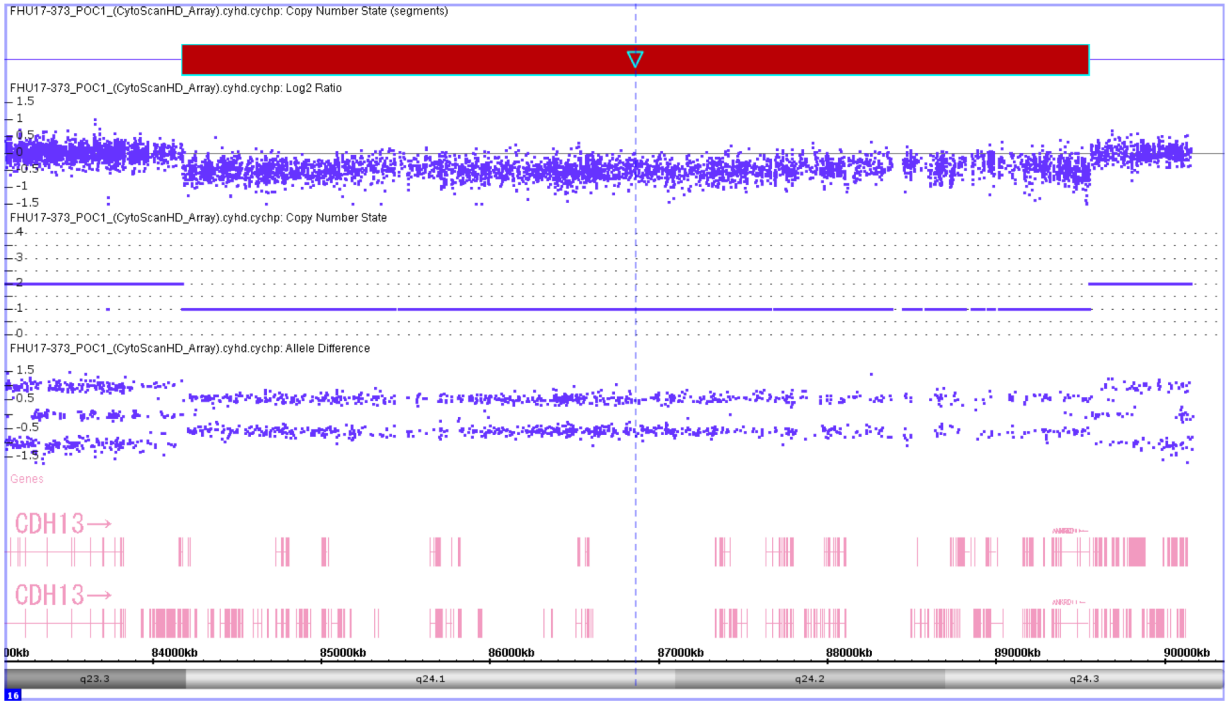

マイクロアレイによる欠失の確認

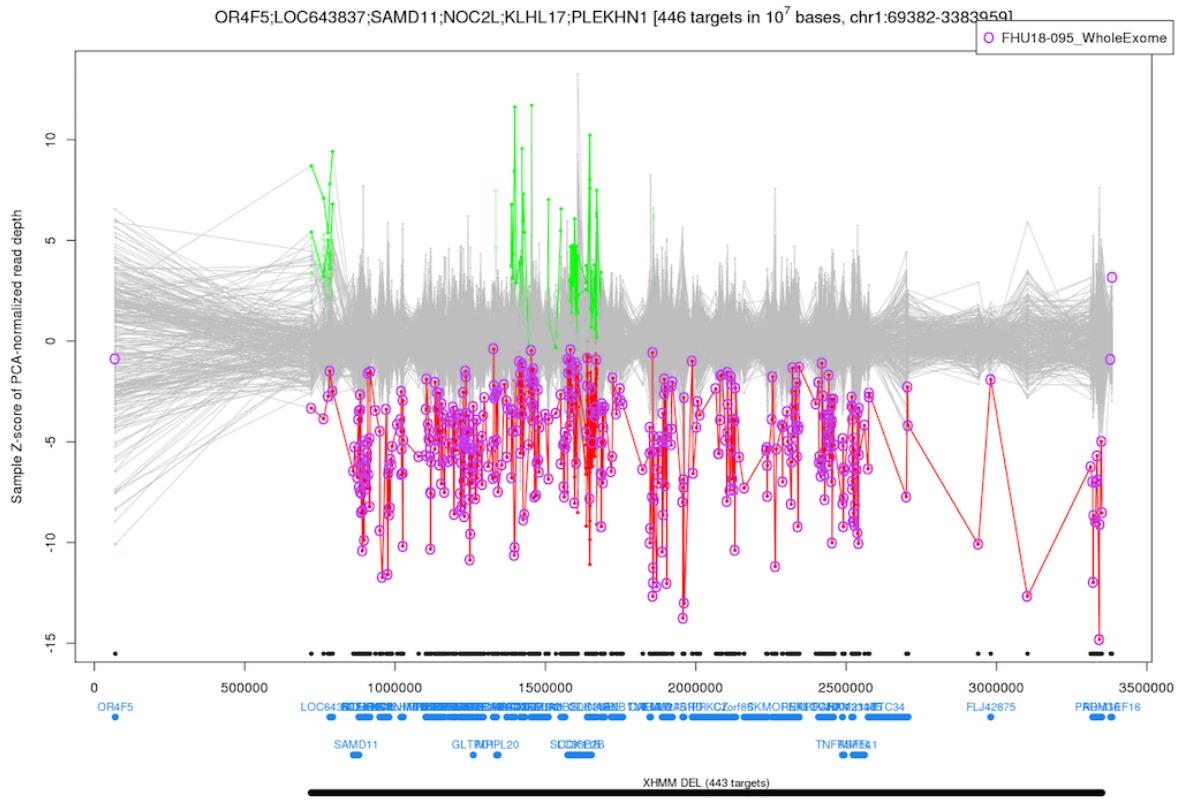

XHMMによる欠失の同定

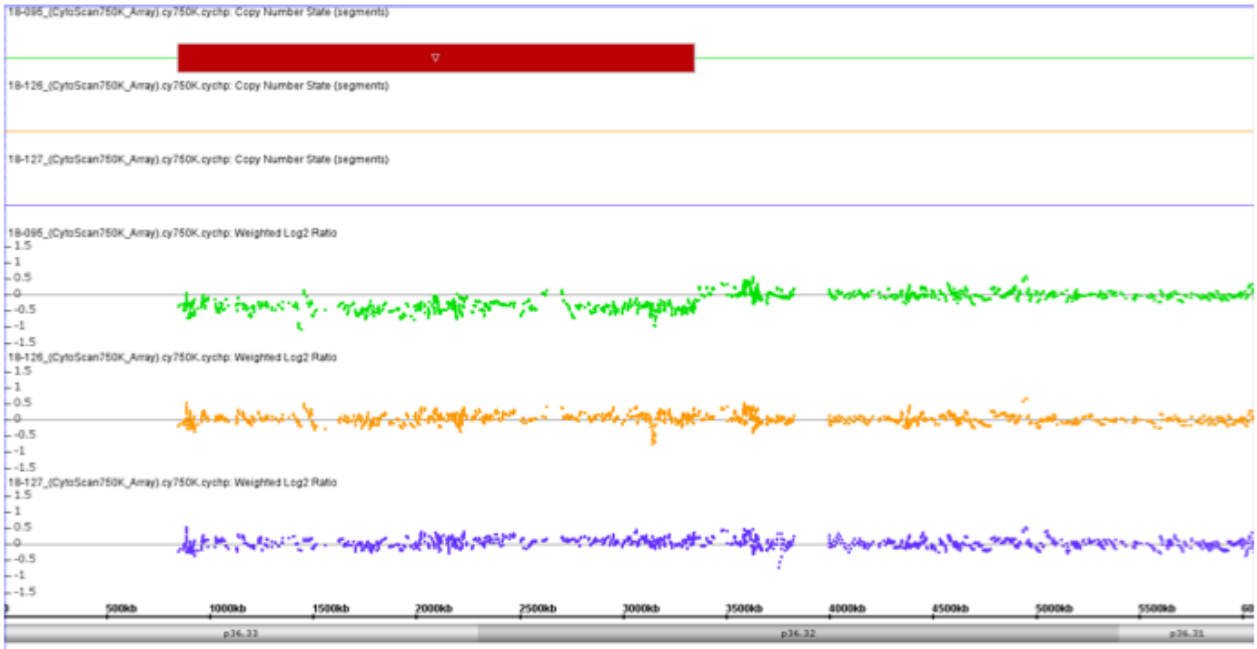

マイクロアレイによるde novo欠失の確認

厚生労働科学研究費補助金（難治性疾患等政策研究事業）

分担研究報告書

マイクロアレイ染色体検査の臨床運用と2q37欠失症候群の診断基準作成について

研究分担者　大橋博文・埼玉県立小児医療センター遺伝科部長

研究要旨

1）本研究班での継続研究として、本年度（平成 29 年度）も診断不明の多発先天異常症例を中心としたマイクロアレイ染色体検査の臨床運用を進めた。平成 29 年 1 月～同年 12 月中旬までの期間でマイクロアレイ染色体検査を施行したのは 125 例（うち両親解析 4 例）であった。このうち G 分染法で既に検出した病原性染色体異常の精密診断は 12 例に施行された。診断不明の先天異常（multiple congenital anomalies; MCA を含む先天異常）の原因診断目的で施行した 109 例中、病原性コピー数異常を 23 例に認め、診断率は 21.1%であった。病原性 CNV 診断例のうち、2 種類の病原性 CNV を認めた 2 例、コピー数不変連続ホモ接合領域（Long Contiguous Stretches of Homozygosity:LCSH）の存在から片親性ダイソミーの診断に至った例、責任遺伝子をシスに調節すると認識されている調節領域の欠失 2 例については詳細に報告し、CGH＋SNP を用いたマイクロアレイ染色体検査の有用性を再認識した。

2）本研究班た対象とするマイクロアレイ染色体検査に関わる疾患として 2q37 欠失症候群の診断基準の策定を試みた。本疾患は軽度から中等度の発達遅滞、低身長、肥満、顔貌所見に加え、特徴的な第 3-5 指趾の中手骨/中足骨の短縮や自閉症スペクトラムを主要症状とする微細欠失症候群である。その診断基準の作成にあたり、既知のレビュー文献とともに、海外の希少染色体疾患のサポートグループである Unique（http://www.rarechromo.org）における疾患ガイドブック情報も参考とした上で疾患概要につきまとめた。また当センターで過去にマイクロアレイ染色体検査で診断した 3 症例の情報も検討した。これらの情報を加味した上で診断基準の作成を試みた。主要症状として①精神運動発達遅滞、②特徴的顔貌、③第 3-5 指（趾）の中手（足）骨短縮（type E brachydactyly）を挙げ、これらのうち①、②を必須症状とし、診断検査として少なくともマイクロアレイ染色体検査を含むコピー数異常解析検査で HDAC4 遺伝子を含む 2q37.3 領域の欠失を同定できたものを診断確定とした。一方、①、②、③を満たす場合は臨床診断が強く示唆されるため、G 分染法、FISH 法を含む従来検査で 2q37 端部（サブテロメア領域）の欠失と判定されれば診断確定とした。

研究協力者

清水　健司　（埼玉県立小児医療センター遺伝科）

大場　大樹　（埼玉県立小児医療センター遺伝科）

Ａ．研究目的

多発先天異常の診断率を 15%前後底上げできる高解像度とゲノム網羅性を併せ持ったマイクロアレイ染色体検査の我が国における認知が拡大する中、当分担研究者の研究として、地域の小児専門医療施設である埼玉県立小児医療センターにおけるマイクロアレイ染色体検査の臨床応用を継続している。これらの成果をもとに本年度は下記 2 点について報告する。１）平成 29 年のマイクロアレイ解析実績の概要と診断に有用であった特記すべき解析結果の報告、２）マイクロアレイ染色体検査で判明する微細欠失症候群の１つである 2q37 欠失症候群について、当センターにおける診断患者、グループ外来開催情報、海外のサポートグループ情報、レビュー文献、等からの情報を基にした診断基準の作成、の２点である。

Ｂ．研究方法

１．マイクロアレイ染色体検査の解析実績

平成 29 年 4 月～同年 12 月までの間に、埼玉県立小児医療センター遺伝科外来を受診した患児のうち、染色体異常症の鑑別を要する先天異常症例や、G 分染法で既に同定された構造異常を有する症例における詳細解析を目的にマイクアレイ染色体検査（SurePrint G3 CGH+SNP 4x180K Microarray Kit :Agilent technologies） を施行し、この中で同定されたコピー数変異（Copy Number Variation: CNV）やコピー数不変連続ホモ接合領域（Long Stretches of Contiguous Homozygosity:LSCH）についての病原性解釈と診断解釈につき、追加解析も含めた網羅的検討と分析を行った。

(倫理面への配慮)

マイクロアレイ染色体検査については、関連ガイドラインを遵守して行う。また、マイクロアレイ染色体検査施行に関しては施設の倫理委員会で承認済みである。

２．2q37 欠失症候群の診断基準作成

マイクロアレイ染色体検査が確定診断に有用な染色体サブテロメア異常症の１つである 2q37 欠失症候群について、GeneReviews®を含む文献情報や、海外におけるサポートグループ Unique（http://www.rarechromo.org）の情報についてレビューを行い、疾患概要をまとめた(下記参考文献参照)。また当センターで現在までにマイクロアレイ染色体検査で診断した 3 症例の情報も検討した。これらの検討事項を総合して診断基準作成を試みた。

[診断基準作成にあたっての参考文献]

1）“2q37 Microdeletion Syndrome” GeneReviews[Internet]. https://www.ncbi.nlm.nih.gov/books/NBK1158/

2) “2q37 deletion syndrome” Unique:understanding chromosome disorders[Internet]. http://www.rarechromo.org/information/Chromosome%20%202/2q37%20deletion%20syndrome%20FTNW.pdf

3) “Chromosome 2q37 deletion:clinical and molecular aspects. Am J Med Genet 2007 145C:357-71
4) “Haploinsufficiency of HDAC4 causes brachydactyly mental retardation syndrome, with brachydactyly type E, developmental delays, and behavioral problems.” Am J Hum Genet 2010 87:219-28
5) “Wilms tumor incidence in children with 2q terminal deletions: a cohort study. Am J Med Gent 2011 155A:2221-3
6) “The 2q37-deletion syndrome: and update of the clinical spectrum including overweight, brachydactyly and behavioural features in 14 new patients.” Eur J Hum Genet 2013 21:602-12.
7) “Deletion 2q37 syndrome: Cognitive-Behavioral Trajectories and Autistic Features Related to Breakpoint and Deletion Size” Am J Med Genet 2016 170A:2282-91

C．研究結果

1．マイクロアレイ染色体検査の解析実績

平成29年１月～同年12月24日までの期間の症例でマイクロアレイ染色体検査を施行したのは125例（うち発端者解析121例、両親解析4例）であり、この間の初診患者382例のうち32%がマイクロアレイ解析の対象となったことになる。その内分けは、診断不明の先天異常（multiple congenital anomalies; MCAを含む先天異常）をもつ児が109例、その他、既に検出した染色体異常の精密診断が12例であった。本研究班がターゲットとする前者の109例中、23例（20.3%）で診断を得た。このうちマイクロアレイ解析の有用性を認識できる特記すべき診断解釈例をとりあげ、その分類と詳細を述べる（表１参照)。

① 2種類の病原性CNV有する診断例

コピー数異常の組み合わせとしてのsecond hitと呼ばれる2種類の病原性CNVを異なるメカニズムで認めた2例を経験した。１例目は先行するG分染法において t(1;3)(p13.3;q12)+t(3;8)(p13;q24.1)の2種類の転座の組み合わせをもつ複雑な均衡型構造異常を認めたが、アレイ解析において、転座に関わる複数の切断点のうち2ヵ所において、切断点より比較的近い領域に、del(1)(p21.1p13.2)の8.8Mb欠失とdel(3)(q13.1q13.13)の3.8Mbの欠失を認めた。ともに認知された既知の症候群領域ではなかったが、欠失サイズやオーバーラップする複数の文献情報から、各々[Pathogenic][Likely Pathogenic]の病原性解釈であり、これらの相加的影響により発端児の表現型を説明しうる診断結果であった。このような複雑な構造異常に伴う欠失はChromothripsis等の機序による１回の独立したイベントに伴い生じるde novo変異の可能性が高いと考えられた。もう１例では、del(1)(p36.32-qter)の2.6Mb端部欠失とdel(17)(q12)の中間部1.6Mb重複の組み合わせが判明した。前者は1p36欠失症候群として病原性が確立しており、浸透率は100%であり発端児の表現型を満たしていた。一方で、17q12微細重複はLow Copy Repeatに惹起される共通領域の重複であり、病原性感受性領域とし

て認知されており、発達遅滞が主たる表現型であるが、浸透率は21%とされている。このことから、前者はde novo、後者は片親由来である可能性が高いと考えられた。

② マーカー染色体を有し、コピー数不変連続ホモ接合領域(Long Contiguous Stretches of Homozogosity:LCSH)を契機とした診断例

成長障害を主とする症例において先行するG分染で47,XX,+mar[11]/46,XX[9]が判明し、詳細解析としてマイクロアレイ施行したところ、SNP解析にて7番染色体全域にわたり数十Mbの断続的なLCSHが判明した。表現型と合わせmaternal UPD7（Russell-Silver症候群）が考えられたため、同領域のメチル化特異的MLPA法による追加解析施行し、母由来パターンと判明し診断確定した。またマーカー染色体は非常に小さく、CEP7プローブFISHでは予想通り7番染色体由来と判明したが、アレイ解析では7番染色体上に有意なコピー数上昇としては認識されず、重複としての病原性は否定的であった。発生メカニズムとしては、LCSHがセントロメア周囲を含んでいたことから、母由来第２減数分裂時の不分離に起因すると考えられた。SNP解析を有することによる診断の有用性を再認識する結果であった。

③ 調節領域欠失による診断例

ハプロ不全でおこる疾患の責任遺伝子を含む病原性欠失と関連して、時に原因遺伝子を含まない隣接領域の欠失が同様の表現型を有することを契機に、当該領域が責任遺伝子の調節領域（エンハンサーもしくはサイレンサー領域）と判明することがある。今年度はこのような調節領域のCNV同定を2例で認めた。

1例目は特有の舞踏様運動を伴う神経疾患であるBrain-lung-thyroid syndrome(MIM#610978)の診断が強く疑われる児において、原因遺伝子NKX2-1遺伝子を含まず、その近位のエンハンサー領域と認識されている14q13.2-q13.34領域の約1.6Mbの中間部欠失を認めた。本欠失領域は過去複数の文献において特異的表現型とともに報告されている調節領域のcritical regionを含んでおり、Pathogenicと判断した。

もう1例は、重度の筋緊張低下を伴う発達遅滞症例において、Rett症候群バリアント（MIM#613454）の原因遺伝子FOXG1を含まず、隣接するPRKD1遺伝子を含む14q12-q13.1領域の4.1Mbの欠失を認めた。複数論文の複数例でPRKD1遺伝子を含む欠失がFOXG1遺伝子の発現を変化させること、FOXG1欠失と同様の表現型を呈することが判明しており、本症例においても特異的顔貌所見を含む共通の表現型を有しており、病原性と判断した。

２．2q37 欠失症候群の診断基準作成

① 疾患のレビュー

[概要]

2q37 欠失症候群は、主として 2 番染色体長腕端部 2q37.3 領域の微細欠失に起因する染色体サブテロメア異常症であり、軽度から中等度の発達遅滞・知的障害、低身長、肥満、顔貌所見に加え、特徴的な第 3-5 指趾の中手骨/中足骨の短縮（type E brachydactyly）や自閉症スペクトラムを主要症状とする。

[原因]

2q37.3 領域に座位するヒストン脱アセチル化酵素をコードし、骨・軟骨発生、神経細胞維

持に関わる HDAC4 遺伝子が本症候群の主たる骨格・神経症状に寄与する主要な候補遺伝子とされる。単一遺伝子病として HDAC4 ハプロ不全を引き起こす遺伝子内変異による類似表現型の報告を契機に判明した。その他、隣接領域に座位する PRLH, TWIST2、KIF1A, FARP2, PER2, AGAP1 等も主要臨床所見の候補遺伝子として報告されている。

[疫学]

発症頻度を明らかにした報告はないが、少なくとも世界で 115 例を超える診断例の報告がある。また 2013 年におけるサポートグループ Unique への登録患者家族は 88 家族であり、新生児～44 歳までの年齢幅であった。欠失範囲は 3Mb 前後から 10Mb 程度の幅である。大部分が新生変異であるが、約 5%が片親の均衡型転座に起因する不均衡型転座である。性差はやや女性に多い。

[臨床症状]

・発達遅滞（100%）
軽度から中等度の発達遅滞をほぼ全例に有する。独歩開始は 15 ヶ月-4 歳。

・自閉症スペクトラム（30%前後）
症状の幅は広いが有意な頻度で認める。特定の者や行動に対するこだわりは過半数に認める。

・中手骨・中足骨の短縮（>50%）
第 3-5 指趾、時に第 4 指趾のみに認める本症候群の特徴的骨格所見である。Type E brachydactyly とも称される。機能的に問題ないことが多く、また小児期早期には臨床的に明らかでないことも多い。

・特徴的顔貌（ほぼ 100%）
目立つ前頭部、狭い眼瞼裂、眼瞼裂斜上、深い眼窩、小さい鼻、上向き鼻孔、目立つ鼻柱、平坦な人中、ふくよかな頬部、薄い上口唇、小さな口などの特徴所見の組み合わせをもつ

・低身長 / 肥満（50%前後）
肥満の報告は多く、年齢とともに目立つ

・Wilms 腫瘍（過去 3 例）
2q37.1 領域を含む欠失例において過去 3 例報告があり、いずれも 2 歳以下で発症

・その他合併症（多岐にわたる）
筋緊張低下（50%）、摂食障害、けいれん（20-25%）、関節可動域亢進、脱臼、偏平足、脊椎側彎、骨密度低下、胃食道逆流、湿疹、腎嚢胞、口蓋裂、先天性心疾患、先天性難聴、中枢神経奇形（脳梁形成異常、水頭症）、鼠径ヘルニア、臍ヘルニア

[健康管理]

上記身体合併症の評価を行い、判明した合併症に応じた関連科でのフォローを行う（循環器科、整形外科、耳鼻科、腎臓科、神経科等）。発達遅滞においては、発達のマイルストーンにおける適切な評価と程度に応じた療育サポート（理学療法、作業療法、言語療法）を行う。肥満に対しては適切な栄養管理と活動的なライフスタイルを推奨。Wilms 腫瘍のリスクにおいては、2q37.1 領域まで含む欠失がある場合は腹部エコースクリーニングのフォローアップを検討するなどより注意した経過観察を行う。また 2q37.1 に座位し腫瘍抑制の働きを有する DIS3L2 遺伝子欠失の有無にも留意する。

[鑑別診断]

Smith-Magenis 症候群は、17p11.2 領域の RAI１遺伝子を含む critical region の欠失でおこることが大多数で、一般に染色体検査で鑑別可能である。HDAC4 のハプロ不全が RAI 1 の発現に影響することが報告されており、臨床症状の類似性を遺伝学的にも説明可能であり、留意すべき鑑別診断である。

また、Albright 遺伝性骨異栄養症（Albright hereditary osteodystrophy:AHO）は、促進型 G 蛋白質共役型受容体をコードする GNAS 遺伝子の機能喪失変異によるおこる。2q37 欠失症候群は、別名 AHO-like 症候群とも呼ばれ、肥満、低身長、短指などの臨床所見が類似するが、Ca、P、副甲状腺、甲状腺ホルモンなどの内分泌学的検査で鑑別する。

その他、type E brachydactyly を共有する Turner 症候群は顔貌所見が異なることや異なる染色体異常症であるため鑑別は比較的容易である。

[予後]

一般に生命予後が短いという報告はないが、先天性の合併症の重症度に依存すると考えられる。

②　当センター診断例の検討

当センターで現在までマイクロアレイ染色体検査により本症候群と診断した 3 症例の情報も検討した。

[症例 1]　8 歳女児

arr[hg18]2q37.1q37.3(233,781,112-242,717,069)x1

HDAC4 遺伝子含む 8.9Mb の端部欠失

＊合併所見

・知的障害（軽度：IQ65）支援学級在籍
・特徴的顔貌
・足趾の第４中手骨短縮
・心室中隔欠損症（Ope 既往 s）
・膀胱尿管逆流（VUR）IV 度
・左内斜視
・腰椎側弯、頚椎亜脱臼（軽度）

明らかな自閉傾向なく、愛嬌がありにこやかであるが他人とのコミュニケーションは困難な面があり。顔貌所見は典型的であり、2q37.1 を含む端部欠失であるが、DIS3L2 遺伝子は欠失内に存在せず、現在まで腎に嚢胞や Wilms 腫瘍の指摘なし。

[症例 2]　7 歳男児

arr[hg18]
2q37.1q37.3(232,657,119-242,654,701)x1

HDAC4 遺伝子含む 10.0Mb の端部欠失

＊合併所見

・中等度発達遅滞：支援学校在籍
・低身長（-2.4SD）、肥満なし
・特徴的顔貌
・短指趾あるも詳細評価未
・中耳炎
・外反偏平足
・心房中隔欠損
・粘膜下口蓋裂
・臍ヘルニア

自閉傾向やこだわりがあり、知的障害も症例１よりは重度である。にこにこと愛嬌があることは症例 1 と共通している。同様に 2q37.1 領域を含む端部欠失であるが、DIS3L2 遺伝子は外れており、Wilms 腫瘍や腎嚢胞などは指摘されていない。

[症例 3]　11 歳男児
arr[hg19]
2q37.2q37.3(235,859,197-243,068,396)x1,
21q22.3(43,592,014-48,090,317)x3
2q 側 7.2Mb の端部欠失（HDAC4 遺伝子含む）と 21q 側 4.5Mb の端部重複
＊合併所見
・知的障害（重度）
・低身長（-3.6SD）、肥満なし
・特徴的顔貌
・手指の第４-5 中手骨短縮
・ファロー四徴症（Ope 既往）
・胃食道逆流（Ope 既往）
・尿道下裂（Ope 既往）
・周期性嘔吐症
自閉症スペクトラムの詳細な評価は未。顔貌所見は症例１や２に比べるとやや非典型である。21q 重複の病原性解釈については Down 症候群の責任領域を外れており uncertain の評価。不均衡転座の可能性あり。

[検討]
すべての症例で HDAC4 遺伝子を含む 2q37.3 領域の欠失を証明できており、発達遅滞、特徴的顔貌の所見を共有していたため、確定診断となった。文献報告の通り、合併症を含む表現型の幅が症例間で大きかった。不均衡転座の症例では他の重複領域が発達遅滞や顔貌所見に影響を与え、より重度の発達遅滞とやや非典型的な顔貌所見につながっていると考えられた。

症例１と症例２においては当センターで過去にグループ外来を開催しており（当時症例１は 3y0m、症例２は 1y11m）、同じ希少疾患をもつ家族同士のピアカウンセリングにつながり、類似した顔貌所見や親しみやすい行動面についても共有した。一方で個々での合併症の幅があることもお互いの感想として述べられた。

③ <u>診断基準の作成</u>
①と②の情報検討から暫定的に下記診断基準を作成した。
a.【主要症状】
必須症状もしくは診断特異性の高い症状
I.　精神運動発達遅滞
II. 特徴的顔貌所見（狭い眼瞼裂、眼瞼裂斜上、深い眼窩、ふくよかな頬、目立つ平坦な人中、目立つ鼻柱、薄い上口唇、小口）
III.　第3-5指（趾）中手（足）骨の短縮（第4指趾のみの場合も可）
注）IとIIは感度100％の所見であるが、Iは診断特異性が低く、IIは評価者により精度が異なる。IIIの感度はI, IIより低い(>50%)が、診断特異性が高い客観所見であるためI-IIIをすべて認めた場合は2q37欠失の臨床診断を強く疑う。年長児での肥満や自閉症スペクトラムなども参考にすべき補助所見である。
b.【検査所見】
I.　マイクロアレイ染色体検査等のコピー数解析で、少なくともHDAC4遺伝子を含む2q37.3領域の欠失の同定

II. G分染法で2q37領域の欠失と判定

III. 2qサブテロメアプローブを用いたFISH法で欠失を同定

注）最も確実な診断検査はIであるが、日本の遺伝学的検査の現状からIIやIIIのみもカテゴリーに入れた。しかしIIやIIIにおいては、欠失と判定されても、critical regionであるHDAC4遺伝子が欠失範囲から外れている可能性を否定できない。一方でIIやIIIは染色体構造を同定できるため、診断後に家族検査等遺伝カウンセリングにつながる情報となる検査であり、診断後の臨床遺伝学的フォローにおいて必要な検査であることに留意する。一方で、HDAC4遺伝子内変異や、当該遺伝子に近接する切断点を有する転座例において同様の表現型を伴う報告があるが、2q37欠失症候群という名称とは異なる原因となるため、本検査基準からは除外した。

c.【診断のカテゴリー】

〈Definite〉

I. AのI,II,IIIすべてを満たしかつBのI,II,IIIのどれかを満たす

II. AのI,IIを満たしかつBのIを満たす

〈Possible〉

I. aのI, IIを満たしかつbのIIもしくはIIIを満たす

注) 主要症状をすべて満たす場合は、臨床診断が強く疑われるため遺伝学的検査の精度が100%でないIIもしくはIIIを満たす場合もdefiniteの診断カテゴリーとした。

d.【除外診断】

I. Smith-Magenis症候群

II. Albright 遺伝性骨異栄養症（偽性副甲状腺機能低下症Ia型）

D．考察

マイクロアレイ染色体検査（SNP解析含む）の臨床応用において、今年度取り上げたタイプの診断解釈例（CNVのセカンドヒット、LCSHからUPD疾患の同定、調節領域に関連する病原性CNVの同定）は、とりわけ本検査における診断有用性が高いケースと考えられたため抽出して報告した。特に責任遺伝子の外にある調節領域の新たな発見は、遺伝型-表現型の新たな相関に資する情報ともなる。

この有用性を十分生かすためにも、データの解釈を行う際には、当該CNV内に含まれる情報のみならず、染色体バンドから類推できる重要遺伝子や当該CNVに隣接する領域の重要遺伝子の存在に留意するとともに、詳細な臨床情報の把握と合わせて最終的な診断解釈をすることが求められる。

一方、2q37欠失症候群の診断基準作成にあたっては、既知の文献や海外サポートグループ、自施設診断例における臨床情報や遺伝学的検査の情報を参考に、最も感度が高い臨床所見（発達遅滞と特徴的顔貌）と最も本疾患をrule-inしやすい臨床所見（type E brachydactyly）を主要症状として抽出した。一方で、検査所見では、最も確実な遺伝学的診断としてマイクロアレイ染色体検査等によるコピー数解析によりHDAC4遺伝子を含む欠失を同定することとしたが、HDAC4遺伝子

欠失による浸透率は必ずしも完全ではないとの報告もあり、議論の余地があるかもしれない。また必ずしもHDAC4遺伝子を含む欠失を直接的に確定できないG分染法やサブテロメアプローブによるFISH法も選択肢に分類したが、主要症状と検査選択における組み合わせのバランスにより、診断の確からしさのカテゴリー分類を試みた。

Ｆ．研究発表

（発表誌名巻号・頁・発行年等も記入）

1. 論文発表

1) Shiohama T, Ohashi H, Shimizu K, Fujii K, Oba D, Takatani T, Kato M, Shimojo N. l-Thyroxine-responsive drop attacks in childhood benign hereditary chorea: A case report. Brain Dev. 2018 40:353-356

2) Nakane T, Sawanobori E, Ohashi H, Sugita K. Hyperechoic renal medullary pyramids in a boy with Simpson-Golabi-Behmel syndrome. Clin Dysmorphol. 2018 27:25-26

3) Miyamoto T, Akutsu SN, Fukumitsu A, Morino H, Masatsuna Y, Hosoba K, Kawakami H, Yamamoto T, Shimizu K, Ohashi H, Matsuura S. PLK1-mediated phosphorylation of WDR62/MCPH2 ensures proper mitotic spindle orientation. Hum Mol Genet. 2017 26:4429-4440

4) Shiohama T, Fujii K, Shimizu K, Ohashi H, Takatani T, Okamoto N, Nishimura G, Kato M, Shimojo N. Progressive subglottic stenosis in a child with Pallister-Killian syndrome. Congenit Anom (Kyoto). 2017 doi: 10.1111/cga.12240. [Epub ahead of print]

2. 学会発表

１）渡辺　聡、土屋美智子、伊達木澄人、森内浩幸、松本　正、森藤香奈子、清水健司、大橋博文、道和百合、知念安紹、水野誠司、皆川京子、神谷素子、近藤達郎。1q 部分重複症候群患者の自然歴についての検討−18 例のアンケート調査より−。第 40 回日本小児遺伝学会 2018.1.12-13, 東京

Ｇ．知的財産権の出願・登録状況（予定を含む。）

1. 特許取得

該当なし

2. 実用新案登録

該当なし

3. その他

特に

厚生労働科学研究費補助金（難治性疾患等政策研究事業（難治性疾患政策研究事業））
分担研究報告書

SATB2 異常症の診療ガイドライン

研究分担者　黒澤健司
地方独立行政法人神奈川県立病院機構神奈川県立こども医療センター　遺伝科部長

研究要旨

先天異常は、一般集団の約 2－3%に及ぶ遺伝的異質性の高い疾患で、医療においてその正確な診断は不可欠である。この集団に対してマイクロアレイ染色体検査で検出できる疾患は 12%程度とされている。今回、重度精神遅滞、特徴的顔貌を特徴とする SATB2 異常症の頻度について検討し、医療管理の内容をまとめた。自験症例である診断未確定 1000 例中に同疾患症例は検出しなかった。治療は対症療法が中心となり、早期のリハビリテーションや療育の対応は極めて重要である。摂食指導や言語指導も重要である。斜視や屈折異常などに対しては眼科精査も適応となる。口蓋奇形に由来する耳鼻咽喉科疾患にも早期からの対応が重要である。てんかん発作に対して、疾患特異的抗てんかん薬は認めない。睡眠障害も目立つことがある。ほかに側彎なども注意する必要がある。診断の手掛かりにもなる歯牙の異常に対しては、定期的歯科受診が重要である。

A．研究目的

先天異常は、一般集団の約 2－3%に及ぶ遺伝的異質性の高い疾患で、その発生頻度からも病因解析研究は常に医学の大きな課題である。医療においてその正確な診断は不可欠である。しかし、遺伝的異質性が高いが故に、原因解明は膨大な労力を要する。一般に中等度以上の精神遅滞の病因における遺伝的背景の占める割合は、染色体検査で検出可能な疾患は 3%、マイクロアレイ染色体検査で検出できる疾患は 12%程度とされている。本研究では、次世代シーケンス技術やマイクロアレイ染色体検査を用いて、正確な診断を行い、診療ガイドラインを確立することを目的とする。

SATB2 関連症候群（SAS）は、言語発達の遅れ、行動異常および特徴的顔貌を合併し、重度の精神遅滞を特徴とする多臓器にわたる先天異常症候群の一つである。現在まで報告された症例の多くは発達遅滞/知的障害を認めている。幼児期からの筋緊張低下や摂食障害を有することが多い。行動の問題には、自閉症、多動などが含まれる。顔面口腔の異常（口蓋裂、高口蓋、および二分口蓋垂）、歯列異常、上部中央切歯の異常な形状または大きさが含まれる。ほかに骨格異常、成長障害、斜視や屈折異常、先天性心疾患、泌尿生殖器異常、てんかんがある。原因は SATB2 遺伝子異常で、SATB2 遺伝子ヘテロ接合異常（61%）。SATB2（22%）を含む 2q33.1 染色体でのヘテロ接合欠失、SATB2 の遺伝子内欠失または重複（9%）

が原因としてあげられ、さらに SATB2 を破壊する 2q33.1 を切断点とする染色体転座（8%）などがある。

今回、診断未確定症例約 1000 例に置いてマイクロアレイスクリーニングを行い、症例の有無を検討、さらに文献的考察を行った。

B．研究方法

施設内スクリーニングの対象は、神奈川県立こども医療センター受診歴のある診断未確定症例約 1000 例で、染色体検査などなど一般的遺伝学的検査がなされて染色体異常症は臨床的に否定されている。マイクロアレイ CGH は、Agilent 社製マイクロアレイシステムを用い、アレイは SurePrint G3 Human CGHMicroarray kit 8x60K を用いた。解析手順は、Agilent 社による標準プロトコールに準じて進めた。得られたデータの解析は Agilent Genomic Workbench ソフトウェアを用いた。データは DLR spread 値< 0.30 を採用した。比較対照 DNA は、Promega 社製 Female および Male genomic DNA を用いた。解析したゲノム DNA は、QIAamp DNA Blood Mini kit を用いて自動抽出機で末梢血液から抽出した。アレイ CGH で検出されたゲノムコピー数異常は、ISCN2009 に準じて記載した。参照ゲノムマップとして UCSC Genome Browser on Human Feb. 2009 (hg19) Assembly を用いた。

SATB2 を含む 2q32.1-q33.3 欠失/重複症候群の疾患概要および診療ガイドライン作成を試みた。文献的考察を中心にまとめた。先天異常症候群を含む遺伝病の疾患概要ならびに遺伝カウンセリング、診療ガイドラインをまとめた GeneReviews（https://www.ncbi.nlm.nih.gov/）や OMIM（https://www.ncbi.nlm.nih.gov/omim）を中心に、さらに個別症例報告も参照して、まとめた。

（倫理面への配慮）

マイクロアレイ CGH による解析は、こども医療センター倫理審査において、研究課題「原因不明多発奇形精神遅滞症候群のゲノムワイドな病因解析」として平成 22 年 7 月 22 日に承認を得たものである。検査前に十分な説明を行い、文書により同意のもとで解析を行った。解析にあたっては、全ての個人情報を潜在化した。

C、D．研究結果と考察

施設内診断未確定 1000 症例中には、CNV による SATB2 異常症は検出されなかった。一般に発生頻度は、診断未確定精神遅滞症例の 0.25-0.3%と推定されている。実際には、さらに頻度は低い可能性がある。

文献的考察による診療の指針：治療は対症療法が中心となる。発達遅滞に対しては早期のリハビリテーションや療育の対応は極めて重要である。この中には摂食指導や言語指導なども含まれることもある。斜視や屈折異常などに対しては眼科精査も適応となる。口蓋奇形に由来する耳鼻咽喉科疾患にも早期からの対応が重要である。てんかん発作に対して、疾患特異的抗てんかん薬は認めない。睡眠障害も目立つことがある。ほかに側彎なども注意する必要がある。診断の手掛かりにもなる歯牙の異常に対しては、定期的歯科受診が重要である。

Ｅ．結論

重度精神遅滞、特徴的顔貌を特徴とするSATB2 異常症の頻度について検討し、医療管理の内容をまとめた。自験症例である診断未確定 1000 例中に同疾患症例は検出せず、マイクロアレイ染色体検査では解析の限界があり、次世代シーケンサーなどによる網羅的解析が期待される。

Ｆ．研究発表

１．論文発表

Shimbo H, Yokoi T, Aida N, Mizuno S, Suzumura H, Nagai J, IdaK, Enomoto Y, HatanoC, Kurosawa K. Haploinsufficiency of BCL11A associated with cerebellar abnormalities in 2p15p16.1 deletion syndrome. Molecular Genetics & Genomic Medicine 2017;5(4):429-437.

Hori I, Kawamura R, Nakabayashi K, Watanabe H, Higashimoto K, Tomikawa J, Ieda D, Ohashi K, Negishi Y, Hattori A, Sugio Y, Wakui K, Hata K, Soejima H, Kurosawa K, Saitoh S.CTCF deletion syndrome: clinical features and epigenetic delineation. J Med Genet. 2017 Aug 28. pii: jmedgenet-2017-104854. doi: 10.1136/jmedgenet-2017-104854. [Epub ahead of print]

黒澤健司　マイクロアレイ染色体検査　小児臨床検査のポイント 2017　小児内科　2017;49（増刊号）:687-690.

２．学会発表

榎本友美、黒澤健司　CNV 検出手法 XHMM と log2ratio 変換法の比較－実際の解析例について－　第 169 回染色体研究会　2017.4.8. 東京慈恵医大

Kurosawa K, Minatogawa M, Yokoi T, Enomoto Y, Ida K, Harada N, Nagai J, Tsurusaki Y. Microdeletion of 17q21.31 causes a novel malformation syndrome. American Society of Human Genetics 2017, 2017.10.17-21. Orlando.

Ｇ．知的財産権の出願・登録状況

なし

平成 29 年度厚生労働科学研究費補助金(難治性疾患政策研究事業)
分担研究報告書

染色体微細欠失・重複症候群の診断システムについて

研究分担者　山本　俊至　東京女子医科大学附属遺伝子医療センター・教授

研究要旨

研究目的:
染色体の微細欠失や重複は、いわゆるゲノムコピー数変化(copy number variation; CNV)としてよく知られている。微細な染色体欠失や重複などの CNV を効率的に調べる方法として、欧米ではマイクロアレイ染色体検査が普及している。この方法によって、multiple congenital anomalies/ intellectual disability (MCA/ID)患者のうち、およそ 17%程度で何らかの疾患関連 CNV が認められる。ただ、MCA/ID の原因の内訳としては、CNV より、一塩基変化(single nucleotide variant; SNV)が占める割合の方が高く、次世代シーケンサーが普及してきた現在、マイクロアレイ染色体検査による CNV 解析より、次世代シーケンサーによる SNV 解析を優先させる傾向がある。次世代シーケンサーを用いた CNV 解析も一部では行われているため、次世代シーケンサーfirst の解析による CNV 同定について検討した。
研究方法:
次世代シーケンサーによる SNV 解析で得られた BAM file を eXome Hidden Markov Model (XHMM)によって解析し、得られたデータをマイクロアレイ染色体検査で確認した。
結果と考察:
発達の遅れと自閉症症状を示す患者において、次世代シーケンサーによる SNV 解析を行ったが有力な病的バリアントを見出すことができなかった。そこで XHMM 解析を行ったところ、15q14 領域の欠失を示唆する所見が得られた。この所見はマイクロアレイ染色体検査で確認できたが、両親には認められず、de novo 変異であった。欠失範囲には *MEIS* 遺伝子が含まれており、この遺伝子が発達遅滞と自閉症の原因となったことが明らかとなった。
結論:
次世代シーケンサーfirst による解析によっても CNV を着実に検出できるようになった。そのため、費用を別に考慮すれば、マイクロアレイ染色体検査による CNV 解析より、次世代シーケンサーfirst による解析の方が効率的と考えられる。ただし、XHMM では CNV 範囲の正確な同定や、コピー数の同定を確実に行うことができないため、XHMM で CNV を検出した場合、マイクロアレイ染色体検査による確認が必要である。

A. 研究目的

染色体の微細欠失や重複は、いわゆるゲノムコピー数変化(copy number variation; CNV)としてよく知られている。微細な染色体欠失や重複などの CNV を効率的に調べる方法として、欧米ではマイクロアレイ染色体検査が普及している。この方法によって、multiple congenital anomalies/ intellectual disability (MCA/ID)患者のうち、およそ 17%程度で何らかの疾患関連 CNV が認められる。ただ、MCA/ID の原因の内訳としては、CNV より、一塩基変化(single nucleotide variant; SNV)が占める割合の方が高く、次

世代シーケンサーが普及してきた現在、マイクロアレイ染色体検査による CNV 解析より、次世代シーケンサーによる SNV 解析を優先させる傾向がある。次世代シーケンサーを用いた CNV 解析も一部では行われているため、次世代シーケンサーfirst の解析による CNV 同定について検討した。

B. 研究方法

次世代シーケンサーによる SNV 解析で得られた BAM file を eXome Hidden Markov Model (XHMM)によって解析し、得られたデータをマイクロアレイ染色体検査で確認した。

なお、本研究は東京女子医科大学における「遺伝子解析研究に関する倫理審査委員会」で認められた研究の一部として行い、患者あるいはその家族から書面による同意を得て行った。

C. 研究結果

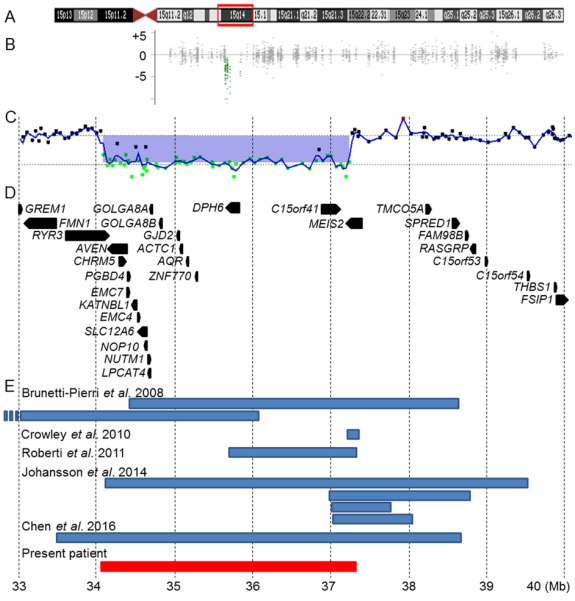

症例は 9 歳男児。心室中隔欠損による心雑音を示したが、自然閉鎖した。浸出性中耳炎を繰り返している。20 ヵ月で始歩が見られるなど、発達の遅れが認められた。発達指数は 63 と軽度の知的障害を認める。粘膜下口蓋裂のため構音障害を示す。オーム返しが多く、読字困難あり。思い通りにならない場合、しばしば癇癪を起す。コミュニケーションに問題があり、友人関係を構築できない。これらの症状は自閉症を示唆するものであった。

発達の遅れと自閉症症状の原因を明らかにするために、TruSight One (Illumina)を用いた次世代シーケンスによる SNV 解析を行ったが有力な病的バリアントを見出すことができなかった。そこで得られた BAM ファイルを用いて XHMM 解析を行ったところ、15q14 領域の欠失を示唆する所見が得られた。この所見はマイクロアレイ染色体検査で確認できたが、両親には認められず、de novo 変異であった。欠失範囲には *MEIS* 遺伝子が含まれており、この遺伝子が発達遅滞と自閉症の原因となったことが明らかとなった。

D. 考察

15q14 微細欠失を示す症例は過去に数例報告があり、共通して欠失する領域に MEIS2 が存在している。近年の次世代シーケンスによる解析で、MEIS2 の SNV によって発症した自閉症患者の報告があり、当該遺伝子は原因であることが明らかになっており、本症例は報告と矛盾しない。

E. 結論

次世代シーケンサーfirst による解析によっても 15q14 微細欠失を同定することができた。このことは、次世代シーケンスデータ

の応用によってCNVを着実に検出できることを示唆している。解析費用を別に考慮すれば、マイクロアレイ染色体検査によるCNV解析より、次世代シーケンサーfirstによる解析の方が効率的と考えられる。ただし、XHMMではCNV範囲の正確な同定や、コピー数の同定を確実に行うことができないため、XHMMでCNVを検出した場合、マイクロアレイ染色体検査による確認が必要であると考える。

F. 研究発表

1. 論文発表

1. Yamamoto T, Lu Y, Nakamura R, Shimojima K, Kira R. Novel A178P mutation in *SLC16A2* in a patient with Allan-Herndon-Dudley syndrome. Congenit Anom (in press)
2. Shimojima K, Okamoto N, Ohmura K, Nagase H, Yamamoto T. Infantile spasms related to a 5q31.2-q31.3 microdeletion including *PURA*. Hum Genome Var 5; 18007, 2018
3. Shimojima K, Okamoto N, Yamamoto T, A 10q21.3q22.2 microdeletion identified in a patient with severe developmental delay and multiple congenital anomalies including congenital heart defects. Congenit Anom 58; 36-38, 2018
4. 福島 茂樹, 瀬戸 俊之, 藤田 賢司, 麻生 和良, 百瀬 有里, 山下 加奈子, 保科 隆男, 佐久間 悟, 新宅 治夫, 東山 滋明, 河邉 譲治, 山本 俊至. 強直間代発作と労作時脱力を繰り返した *PRRT2* 遺伝子異常症の 1 例. 小児科臨床 71; 41-46, 2018
5. Seto T, Hamazaki T, Nishigaki S, Kudo S, Shintaku H, Ondo Y, Shimojima K, Yamamoto T. A novel *CASK* mutation identified in siblings exhibiting developmental disorders with/without microcephaly. Intractable Rare Dis Res 6; 177-182, 2017
6. Shimojima K, Okamoto N, Goel H, Ondo Y, Yamamoto T. Familial 9q33q34 microduplication in siblings with developmental disorders and acrocephaly. Eur J Med Genet 60; 650-654, 2017
7. Hanafusa H, Morisada N, Ishida Y, Sakata R, Morita K, Miura S, Ye M-Y, Yamamoto T, Okamoto N, Nozu K, Iijima K. A girl with the smallest de novo microdeletion of 20q11.2; intellectual disability and dysmorphic features. Hum Genome Var 4; 17050, 2017
8. Okamoto K, Tsuchiya Y, Kuki I, Yamamoto T, Saitsu H, Kitagawa D, Matsumoto N. Disturbed chromosome segregation and multipolar spindle formation in a patient with *CHAMP1* mutation. Mol Genet Genomic Med 5; 585-591, 2017
9. Matsumaru S, Oguni H, Ogura H, Shimojima k, Nagata S, Kanno H, Yamamoto T. A novel *PGK1* mutation associated with neurological dysfunction and the absence of episodes of hemolytic anemia or myoglobinuria. Intractable Rare Dis Res 6: 132-136,

2017.

10. Lu YP, Ondo Y, Shimojima K, Osaka H, Yamamoto T. A novel *TUBB4A* mutation G96R identified in a patient with hypomyelinating leukodystrophy onset beyond adolescence. Hum Genome Var 4: 17035, 2017.
11. Shimojima K, Yamamoto T. Characteristics of rare and private deletions identified in phenotypically normal individuals. Hum Genome Var 4; 17037, 2017.
12. Shimojima K, Ondo Y, Okamoto N, Yamamoto T. A 15q14 microdeletion involving *MEIS2* identified in a patient with autism spectrum disorder. Hum Genome Var 4; 17029, 2017.
13. Baba S, Sugawara Y, Moriyama K, Inaji M, Maehara T, Yamamoto T, Morio T. Amelioration of intractable epilepsy by adjunct vagus nerve stimulation therapy in a girl with a *CDKL5* mutation. Brain Dev 39: 341-344, 2017.
14. Yamamoto T, Shimojima K, Ondo Y, Shimakawa S, Okamoto N. *MED13L* haploinsufficiency syndrome: A de novo frameshift and recurrent intragenic deletions due to parental mosaicism. Am J Med Genet A. 173A; 1264-1269, 2017.
15. Okamoto N, Shimojima K, Yamamoto T. Neurological Manifestations of 2q31 Microdeletion Syndrome. Congenit Anom 57; 197-200, 2017
16. Shimojima K, Higashiguchi T, Kishimoto K, Miyatake S, Miyake N, Takanashi J, Matsumoto N, Yamamoto T. A novel *DARS2* mutation in a Japanese patient with leukoencephalopathy with brainstem and spinal cord involvement but no lactate elevation. Hum Genome Var 4; 1705, 2017
17. Iwama K, Mizuguchi T, Takanashi J, Shibayama H, Shichiji M, Ito S, Oguni H, Yamamoto T, Sekine A, Nagamine S, Ikeda Y, Nishida H, Kumada S, Yoshida T, Awaya T, Tanaka R, Chikuchi R, Niwa H, Oka Y, Miyatake S, Nakashima M, Takata A, Miyake N, Ito S, Saitsu H, Matsumoto N. Identification of novel *SNORD118* mutations in seven patients with leukoencephalopathy with brain calcifications and cysts. Clin Genet 92; 180-187, 2017
18. Lu YP, Chong P-F, Kira R, Seto T, Ondo Y, Shimojima K, Yamamoto T. Mutations in *NSD1* and *NFIX* in three patients with clinical features of Sotos syndrome and Malan syndrome. J Pediatr Genet 6; 234-237, 2017
19. Shimojima K, Okamoto N, Yamamoto T. Possible genes responsible for developmental delay observed in patients with rare 2q23q24 microdeletion syndrome: literature review and description of an additional patient. Congenit Anom 57; 109-113, 2017
20. Alber M, Kalscheuer VM, Marco E, Sherr EH, Lesca G, Till M, Gradek G, Wiesener A, Korenke CG, Mecier S,

Becker F, Yamamoto T, Scherer SW, Marshall C, Walker S, Dutta U, Dalal A, Suckow V, Jamali P, Kahrizi K, Najmabadi H, Minassian BA. The *ARHGEF9* Disease: Phenotype Clarification and Genotype-Phenotype Correlation. Neurol Genet 3: e148, 2017

21. Shirai K, Higashi Y, Shimojima K, Yamamoto T. An Xq22.1q22.2 nullisomy in a male patient with severe neurological impairment. Am J Med Genet A 173A; 1124-1127, 2017.
22. Sangu N, Shimojima K, Takahashi Y, Ohashi T, Tohyama J, Yamamoto T. A 7q31.33q32.1 microdeletion including *LRRC4* and *GRM8* is associated with severe intellectual disability and characteristics of autism. Hum Genome Var 4; 17001, 2017.
23. Murakoshi M, Takasawa K, Nishioka M, Asakawa M, Kashimada K, Yoshimoto T, Yamamoto T, Takekoshi K, Ogawa Y, Shimohira M. Abdominal paraganglioma in a young woman with 1p36 deletion syndrome. Am J Med Genet A 173A; 495-500, 2017.
24. Matsuo M, Yamauchi A, Ito Y, Sakauchi M, Yamamoto T, Okamoto N, Tsurusaki Y, Miyake N, Matsumoto N, Saito K. Mandibulofacial dysostosis with microcephaly: A case presenting with seizures. Brain Dev 39; 177-181, 2017.
25. Yamamoto T, Shimojima K, Matsufuji M, Mashima R, Sakai E, Okuyama T. Aspartylglucosaminuria caused by a novel homozygous mutation in the *AGA* gene was identified by an exome-first approach in a patient from Japan. Brain Dev 39; 422–425, 2017.
26. 四家達彦, 高橋幸利, 木村暢佑, 今井克美, 山下行雄, 山本俊至, 高橋孝雄. 治療戦略の変更により ADL を改善し得た *CDKL5* 異常症による難治性てんかんの女児例. 脳と発達 49; 28-31, 2017.

2. 著書

1. 山本俊至. がんゲノム医療. 東京女子医科大学雑誌. 88(1); 1-5, 2018
2. 山本俊至. 進行性白質脳症の特徴と診断の実際. 新薬と臨床 67; 271-276, 2018
3. 山本俊至.【ニューロジェネティクス新時代 次世代シークエンサーが拓く新しい世界】筋疾患・神経疾患のジェネティクス てんかん. Clinical Neuroscience 36; 233-235, 2018.
4. 山本俊至. マイクロアレイ染色体検査. 水口雅・岡明・尾内一信［編］. 小児臨床検査ガイド 第 2 版. 文光堂, 東京, pp668-672, 2017.

3. 学会発表

1. 松尾真理, 山本俊至, 洲鎌倫子, 齋藤加代子. 1q43-44 部分トリソミーの１例. 第４０回日本小児遺伝学会学術集会, 2018/01/13,東京
2. 渡辺基子, 金子実基子, 山本俊至. X 染色体を含む転座による 3:1 分離で生じた過剰マーカー染色体を示す重度発達遅滞症例. 第４０回日本小児遺伝学会学術集会, 2018/01/13, 東京

3. 瀬戸俊之，山本俊至，新宅治夫. Zinc-Finger469 遺伝子異常が認められた複数の脱臼歴と骨密度定価を呈する一例. 第４０回日本小児遺伝学会学術集会, 2018/01/13, 東京
4. 高野梢，下島圭子，岡本伸彦，山本俊至. Proximal 22q13 欠失；SHANK3 のハプロ不全だけでは症状を説明できない症例について. 第４０回日本小児遺伝学会学術集会，2018/01/12, 東京
5. 下島圭子, 岡本伸彦, 山本俊至. PURA を含む 5q31 微細欠失の新規例. 第４０回日本小児遺伝学会学術集会, 2018/01/12, 東京
6. 柳下友映，下島圭子，中野さやか，今井克美，山本俊至. WDR26 ハプロ不全によるてんかん症候群；新規 1q41q42 微細欠失からの考察. 第４０回日本小児遺伝学会学術集会, 2018/01/12, 東京
7. 今泉太一，渡辺基子，下島圭子，熊倉啓，山本俊至. １番染色体 UPD による SZT2 ホモ接合変異によって生じたと考えられる重度知的障害症例. 第４０回日本小児遺伝学会学術集会, 2018/01/12, 東京
8. 山内泰輔, 白井謙太朗, 永吉友香子, 神保教広，南洋輔，堀哲夫，今村公俊, 渡辺章充, 山本俊至. 上気道狭窄とてんかん発作の対応に苦慮しクリニカルエクソーム解析で診断が確定した Schinzel-Giedion 症候群の乳児例. 第４０回日本小児遺伝学会学術集会, 2018/01/12, 東京
9. Sekiguchi H, Sato K, Abe T, Yamamoto E, Sakai A, Yamamoto T, Hagiwara N. Insight into Polygenetic Abnormalities in Japanese Heterozygous Familial Hypercholesterolemia. BCVR The 1st JCS Council Forum on Basic CardioVascular Research, 2018/01/06, Tokyo, Japan
10. 二宮伸介，久保田真通，萩野佳代，山本俊至. 16q11.2q12.2 の微細欠失をきたした１例. 日本人類遺伝学会第 62 回大会, 2017/11/17, 神戸
11. 下島圭子, 白井謙太朗, 岡本伸彦, 山本俊至. X 染色体上のゲノムコピー数異常を認めた症例の考察. 日本人類遺伝学会第 62 回大会, 2017/11/17, 神戸
12. 菊池規子，関口治樹，佐藤加代子，菅野仁, 山本俊至, 萩原誠久. ヘテロ家族性高コレステロール血症：日本人における多遺伝子異常とその特徴. 日本人類遺伝学会第 62 回大会, 2017/11/17, 神戸
13. 森島靖行，沼部博直，若井未央，森地振一郎，石田悠，稲垣夏子，柏木保代, 山本俊至, 河島尚志. モザイク 13q ヘキサソミーの一例. 日本人類遺伝学会第 62 回大会, 2017/11/17, 神戸
14. 山本俊至，下島圭子，恩藤由美子，岡本伸彦. 自閉症スペクトラム患者に認められた MEIS2 を含む 15q14 微細欠失. 日本人類遺伝学会第 62 回大会, 2017/11/17, 神戸
15. 山本俊至. [シンポジウム]染色体微細構造異常による小児神経疾患とその発症メカニズム. 日本人類遺伝学会

第 62 回大会, 2017/11/17, 神戸

16. 結城奏、白井謙太朗、高瀬千尋、山内健、神保教広、堀哲夫、榎本啓典、渡辺章充、山本俊至. RAD21 を含む 8 番染色体長腕の微細欠失による Cornelia de Lange syndrome-like phenotype の 1 例. 日本人類遺伝学会第 62 回大会, 2017/11/16, 神戸
17. 秋澤叔香, 浦野真理, 大木岳志, 大森鉄平, 松尾真理, 佐藤裕子, 川上和之, 山本俊至, 冨田尚裕, 徳重克年, 山本雅一, 松井英雄, 齋藤加代子. 遺伝性腫瘍を疑い小腸がんから診断した Lynch 症候群の 1 家系. 日本人類遺伝学会第 62 回大会, 2017/11/16, 神戸
18. 稲垣秀人, 完山和生, 加藤武馬, 大内雄矢, 山本俊至, 倉橋浩樹. 逆位重複・端部欠失の全ゲノムシーケンスによる切断点解析. 日本人類遺伝学会第 62 回大会, 2017/11/16, 神戸
19. 松尾真理、山本俊至、齋藤加代子. [シンポジウム]網羅的ゲノム解析における遺伝カウンセリングと遺伝カウンセラーの役割. 日本人類遺伝学会第 62 回大会, 2017/11/16, 神戸
20. Yamamoto T, Shimojima K . [シンポジウム] Neuro-functional analysis using disease-specific iPS cells. Bulletin of the Japanese Sciety for Neurochemistry, 2017/09/08, Sendai
21. 下島圭子, 岡本伸彦, 山本俊至. 2q23q24 微細欠失症候群の患者に認められる発達遅滞の候補遺伝子絞り込み. 第５７回日本先天異常学会学術集会, 2017/08/26, 東京
22. 山本俊至, 下島圭子, 岡本伸彦, 齋藤加代子. CTNNA3 変異の表現型との関係についての考察. 第２４回日本遺伝子診療学会大会, 2017/07/15, 東京
23. 山本俊至, 下島圭子, 岡本伸彦. 網羅的ゲノム解析により発達障害患者に認められた de novo 遺伝子変異. 第 59 回日本小児神経学会学術集会, 2017/06/15, 大阪
24. 島田姿野, 小國弘量, 大谷ゆい, 西川愛, 伊藤進, 衛藤薫, 中澤友幸, 永田智, 山本俊至. 発達遅滞を呈し感染を契機に急性脳症を来した HNRNPU 遺伝子変異の 1 男児例. 第 59 回日本小児神経学会学術集会, 2017/06/16, 大阪
25. 小坂仁, 井上健, 久保田雅也, 黒澤健司, 才津浩智, 佐々木征行, 髙梨潤一, 松井大, 三重野牧子, 山本俊至, 吉田誠克. 遺伝性白質疾患の診断・治療・研究システムの構築. 第 59 回日本小児神経学会学術集会, 2017/06/16, 大阪
26. 林仁美, 鶴澤礼実, 小川厚, 山本俊至. マイクロアレイ CGH 検査で診断した Rubinstein-Taybi 症候群の 3 歳男児例. 第 59 回日本小児神経学会学術集会, 2017/06/16, 大阪
27. 松岡剛司, 比屋根真彦, 大府正治, 山本俊至, 小坂仁, 高梨潤一, 才津浩智, 井上健. 急性散在性脳脊髄炎(ADEM)を発症した PolIII 関連白質ジストロフィーの一例. 第 59 回日本小児神経学会学術集会, 2017/06/15, 大阪
28. 兵頭勇紀, 秋山麻里, 小林勝弘, 山本

俊至. GABRG2 de novo 変異を有し難治てんかんと四肢麻痺を示す 1 女子例. 第 28 回日本小児神経学会中国・四国地方会、2017/7/15, 岡山

29. 高野梢, 浦野真理, 松尾真理, 荒川玲子, 岩崎直子, 山内あけみ, 近藤恵里, 秋澤叔香, 佐藤裕子, 金子実基子, 渡辺基子, 山本俊至, 小川正樹, 斎藤加代子. 東京女子医科大学における無侵襲的出生前遺伝学的検査の遺伝カウンセリングの検討. 第 41 回日本遺伝カウンセリング学会学術集会, 2017.6.22-25, 東大阪市
30. 山本俊至, 下島圭子, 岡本伸彦, 斎藤加代子. 同胞間で反復して認められた染色体微細構造異常　親世代の低頻度モザイク CNV. 第 41 回日本遺伝カウンセリング学会学術集会, 2017.6.22-25, 東大阪市

H. 知的所有権の取得状況

1. 特許取得

なし

2. 実用新案登録

なし

3. その他

厚生労働科学研究費補助金（難治性疾患政策研究事業）
分担研究報告書

マイクロアレイ染色体検査の結果解釈の留意点と活用
～劣性遺伝性疾患，片親性ヘテロダイソミー診断への応用～

研究分担者　涌井 敬子　信州大学医学部遺伝医学・予防医学教室 講師

研究要旨:マイクロアレイ染色体検査で検出されるゲノムコピー数バリアントの臨床的評価は必ずしも容易でないが,解析症例の蓄積により国際的に臨床的評価の検討が進んでいる．また，コピー数バリアントの検索は，主に優性遺伝形式で発症する疾患を対象としているが，劣性遺伝性疾患の診断に有用だった症例，SNP アレイの genotype 確認により片親性ヘテロダイソミーの診断に到った症例なども経験したので,それらの結果もふまえ，結果解釈のための留意点等について改めて検討した．

Ａ．研究目的

マイクロアレイ染色体検査による染色体微細構造異常症候群の診断の現状把握と実施に際しての課題を検討するとともに，検出されるゲノムコピー数バリアント（CNVs）の結果解釈に有用となる留意点・工夫等について検討する．

Ｂ．研究方法

１．諸外国におけるCNVs解析の実態とわが国の課題

次世代シーケンス（NGS）解析技術を用いたターゲットエクソーム解析・全エクソーム解析が原因不明の先天異常症の診断の主流となりつつあり，NGS解析により得たシーケンスデータからCNVsを検出することも可能となってきたが，解析方法に関わらずCNVsの結果解釈の重要性は変わらない．諸外国で進められている臨床的評価の検討についてweb検索した．

２．マイクロアレイ染色体検査による劣性遺伝性疾患,片親性ヘテロダイソミー診断への応用

CNVsの臨床的評価は,主に優性遺伝形式で発症する疾患を対象としている．また，SNP アレイでcall されるのは，ホモとなっている領域すなわち片親性のアイソダイソミーであり,片親性でもヘテロダイソミーはcallされない．

これまでに劣性遺伝性疾患の診断に有用だった症例，片親性ヘテロダイソミーの診断に到った症例など，病的ゲノムバリアントの確認に通常のドライ解析に工夫が必要だった症例を経験したので，結果解釈での留意点とともに紹介する．

解析は，CGX^{TM} SNPアレイ（180K），解析ソフトはGenoglyphix（共にパーキンエルマー）のプラットフォームで実施した．

（倫理面への配慮）

本研究の実施に際しては，倫理指針等を遵守し，関係する多発奇形・発達遅滞を有する患者やその家族が不利益を被ることの無いよう，個人情報の保護に留意する．

Ｃ．研究結果

１．諸外国におけるCNVs解析の実態とわが国の課題

諸外国では，検出されたゲノムバリアントに対する結果解釈のワーキンググループが組織され，蓄積されたデータからの評価を情報公開している．従来，シーケンスバリアントとコピー数バリアントは別々に検討されていたが，遺伝子のゲノムバリアントとしてDosage Sensitivity の検討がすすんでいる．米国ではClinGen，英国ではDECIPHER におけるデータの更新が顕著である．さらに，両組織は情報共有も進めている．そしてClinGenでは，既知の染色体微細構造異常を含め，評価したPathogenic CNV regionsも公開を開始した．その情報を,一部改変して別表として示した．

＊ ClinGen < https://www.clinicalgenome.org/ >
＊ DECIPHER < https://decipher.sanger.ac.uk/ >

２．マイクロアレイ染色体検査による劣性遺伝性疾患,片親性ヘテロダイソミー診断への応用

【症例１】２才女児．プラダーウイリー症候群（PWS）が疑われたが，*SNRPN*メチレー

ションPCR解析は正常パターン，同時に実施されたマイクロアレイ染色体検査にて，2p21に約150kbのCNVs lossを認めたが，その欠失パターンは通常の欠失のパターンでなく，セントロメア寄りの約80kbはlog2 ratioの平均（AV）は約−0.9であり通常のヘテロ欠失と考えられたが，端部寄りの約70kbの領域はAV：−4以下とホモの欠失となっていることが示唆された．両親の同領域のCNVを確認したところ，父親は児に認めた約150kbがAV：約−0.9のCNVs loss，母親はその端部寄り約70kbが AV：約−0.9のCNVs lossと，それぞれヘテロの欠失を有しており，児は父と母の欠失の共通領域がホモの欠失となった，常染色体劣性遺伝形式（AR）で発症する，homozygous2p21 deletion 症候群としても知られるhypotonia-cystinuria 症候群と診断された．

【症例２】2才男児．腎機能障害と自閉スペクトラム症を伴っていた．マイクロアレイ染色体検査にて病的CNVsは検出されなかったが，SNPアレイで２番染色体の約4/5にabsence of heterozygosity（AOH）がcallされた．その後のTruSight One Sequencing Panel解析にて2番染色体に座位する常染色体劣性遺伝性の多臓器障害の関連遺伝子であるX遺伝子のフレームシフトバリアントがホモ接合体で検出され，２番染色体片親性アイソダイソミーにより顕在化したことによるものと評価された．

【症例３】2才男児．発達遅滞，低身長，両側停留精巣，低緊張等を認めた．他院で実施したG分染法，PWS領域および22q11.2欠失症候群領域のFISH法では異常を認めなかった．当院初診時，典型的なPWSの所見に乏しいと評価されたため，まずマイクロアレイ染色体検査を実施し，病的CNVsは検出されなかったが，15q11.2-q12と15q22.31-q23に各約4MbのAOHがcallされた．両親のgenotype を追加解析し児と比較したところ，15番染色体のAOH callされた２領域は母由来アイソダイソミー，AOH callがなかった領域も母由来のアイソorヘテロダイソミーとして矛盾ないことが確認された．その後追加解析した*SNRPN*メチレーションPCR解析でもPWSパターンを示し，PWSと診断された．

D．考察

ゲノム解析により検出されるCNVsは多岐にわたり，その臨床的評価は容易でない．解析方法が代わっても，臨床的評価には関係ない．諸外国で構築しているような，ゲノムバリアント解析技術の標準化，検出されたゲノムバリアントに対する結果解釈のワーキンググループの組織化，国立研究開発法人日本医療研究開発機構（AMED）等で取り組まれているが，CNVsを含む日本人ゲノムバリアントデータベースの構築，wetおよびdry解析担当者の人材育成等，課題は多い．

また，CNVsの臨床的評価は，主に優性遺伝形式で発症する疾患を対象としているため，一般成人に確認されたCNVsのデータベースであるDGV < dgv.tcag.ca/ >などで確認し，登録が多ければそのCNVsはbenignである可能性が高いと考えるが，劣性遺伝性疾患の場合，同領域の欠失を有している一般成人のデータが含まれていることになるので，CNVsの評価に際しては，AVを確認し，ホモ欠失の可能性がないか，その領域に劣性遺伝形式の疾患関連遺伝子が含まれていないかに留意することにより，劣性遺伝性疾患の診断に繋げることができる可能性がある．

E．結論

マイクロアレイ染色体検査で検出されるCNVsの臨床的評価は必ずしも容易でないが，解析症例の蓄積により国際的に染色体微細構造異常症候群を含む病的ゲノムバリアントの診断に有用な，Dosage Sensitivity の検討がすすんでいる．

また，病的ゲノムバリアントの検索は主に優性遺伝形式で発症する疾患を対象としているが，劣性遺伝性疾患の検出も視野に，CNVs解析に際してはAVの確認が考慮される．さらにSNPアレイでcall されるのは，ホモとなっている領域すなわち片親性のアイソダイソミーであり，片親性でもヘテロダイソミーはcallされないことを認識する必要がある．片親性ヘテロダイソミーを検出するアルゴリズムの開発も期待される．

ゲノム解析技術は改良されても，CNVsを含むゲノムバリアントデータの臨床的評価は変わらない．ゲノム医療の充実のため，日本人のゲノムバリアントデータベース，ゲノムバリアントのwetおよびdry解析担当者の人材育成等を含む体制構築が望まれる．

G．研究発表

1. 論文発表

Takano K, Goto K, Motobayashi M, Wakui K, Kawamura R, Yamaguchi T, Fukushima Y, Kosho T. Early manifestations of epileptic encephalopathy, brain atrophy, and elevation of serum neuron specific enolase in a boy with beta-propeller protein-associated neurodegeneration. Eur J Med Genet. 60:521-6, 2017

2. 学会発表

マイクロアレイ染色体検査データ解釈の応用～劣性遺伝性疾患領域のホモ欠失バリアントと片親性ヘテロダイソミーの同定～. 涌井敬子，髙野亨子，山口智美，高橋有希，河村理恵，三宅康之，福山哲広，古庄知己，福嶋義光．日本人類遺伝学会第62回大会，2017.11.16-18，神戸

想定より複雑な染色体(ゲノム)再構成が起きている―Metaphase解析により同定できた複雑染色体構造異常例―．涌井敬子．日本人類遺伝学会第62回大会，2017.11.16-18，神戸

マイクロアレイ染色体検査にて派生染色体に端部欠失が検出されなかった不均衡型転座症例．河村理恵，神谷素子，松田和之，重藤翔平，古庄知己，福嶋義光，涌井敬子．日本人類遺伝学会第62回大会，2017.11.16-18，神戸

信大病院遺伝子医療研究センター知的障害(ID)外来におけるマイクロアレイおよび次世代シークエンサー用いた遺伝学的診断．高野亨子，古庄知己，涌井敬子，西恵理子，運崎愛，石川真澄，黄瀬恵美子，山口智美，河村理恵，本林光雄，福山哲広，笛木昇，平林伸一，稲葉雄二，要匡，秦健一郎，松原洋一，福嶋義光．日本人類遺伝学会第62回大会，2017.11.16-18，神戸

マイクロアレイ染色体検査のSNP genotypeデータを用いた構造異常染色体の親由来検討．涌井敬子，松本直通，古庄知己，福嶋義光．第40回日本小児遺伝学会学術集会，2018.1.12-13，東京

20番染色体母性片親性ダイソミー5例の臨床像の検討．川嶋明香，中村明枝，井上毅信，堀川玲子，涌井敬子，髙野亨子，水野誠司，椿淳子，緒方勤，深見真紀，鏡雅代．第40回日本小児遺伝学会学術集会，2018.1.12-13，東京

なし

H．知的財産権の出願・登録状況
（予定を含む．）

1. 特許取得
なし

2. 実用新案登録
なし

3.その他

表．Pathogenic CNV regions

Region name	Location on GRCh37	size (bp)	Haploinsufficiency score	Triplosensitivity score
1p36 terminal region (includes GABRD)	chr1:834083-6289973	5,455,890	3	2
1q21.1 recurrent region (BP3-BP4, distal) (includes GJA5)	chr1:146577486-147394506	817,020	3	3
1q43q44 terminal region (includes AKT3)	chr1:243287730-245318287	2,030,557	3	0
2p15p16.1 region (includes BCL11A)	chr2:59139200-62488871	3,349,671	3	1
2q13 recurrent region (includes NPHP1)	chr2:110879906-110962594	82,688	30: Gene associated with autosomal recessive phenotype	0
2q37.3 terminal region (includes HDAC4)	chr2:239954693-242930600	2,975,907	3	0
3q29 recurrent region (includes DLG1)	chr3:195756054-197344665	1,588,611	3	2
4p16.3 terminal (Wolf-Hirshhorn syndrome) region	chr4:331568-2010962	1,679,394	3	2
5p15 terminal (Cri du chat syndrome) region	chr5:37693-11347262	11,309,569	3	2
5q35 recurrent (Sotos syndrome) region (includes NSD1)	chr5:175728978-177013961	1,284,983	3	3
6q24 region (includes PLAGL1)	chr6:144243292-144416561	173,269	1	3
7q11.23 recurrent (Williams-Beuren syndrome) region (includes ELN)	chr7:72744454-74142513	1,398,059	3	3
7q21.2q21.3 region (includes SHFM1)	chr7:95533860-96779486	1,245,626	Not yet evaluated	Not yet evaluated
7q36.3 ZRS (SHH cis-regulatory) duplication region (within LMBR1 intron 5)	chr7:156583796-156584568	772	0	3
8p23.1 recurrent region (includes GATA4)	chr8:8119295-11765719	3,646,424	3	3
9q34.3 telomere region (includes EHMT1)	chr9:140513444-140730578	217,134	3	0
10q22.3q23.2 recurrent region (LCR-3/4-flanked) (includes BMPR1A)	chr10:81683648-88743240	7,059,592	3	1
11p15 region (includes H19, KCNQ1)	chr11:2016406-2906995	890,589	0	3
11p15.5 region (Imprinting Control Region 1)	chr11:2019075-2024375	5,300	3	0
11p13 (WAGR syndrome) region	chr11:31803509-32510988	707,479	3	1
11p11.2 (Potocki-Shaffer syndrome) region (includes ALX4, EXT2)	chr11:43894800-46152450	2,257,650	3	0
12q14 region (includes GRIP1 and HMGA2)	chr12:65071919-68645525	3,573,606	Not yet evaluated	Not yet evaluated
15q11q13 recurrent (PWS/AS) region (BP1-BP3, Class 1)	chr15:22876632-28557186	5,680,554	3	3
15q11q13 recurrent (PWS/AS) region (BP2-BP3, Class 2)	chr15:23758390-28557186	4,798,796	3	3
15q13.3 recurrent region (BP4-BP5) (includes CHRNA7)	chr15:31137104-32445408	1,308,304	3	1
15q24 recurrent region (LCR15q24A to D) (includes STRA6 and CSPG4)	chr15:72963541-75912944	2,949,403	3	1
15q25.2 recurrent region (LCR B-C, proximal)	chr15:83213988-84714734	1,500,746	3	0
16p13.3 region (includes CREBBP)	chr16:3775056-3930121	155,065	3	1
16p13.11 recurrent region (includes MYH11)	chr16:15504454-16292268	787,814	3	2
16p11.2 recurrent region (includes SH2B1) (distal region) (BP2-BP3)	chr16:28822634-29046502	223,868	3	1
16p11.2 recurrent region (includes TBX6) (proximal region) (BP4-BP5)	chr16:29649996-30199855	549,859	3	3
17p13.3 (Miller-Dieker syndrome) region (includes YWHAE and PAFAH1B1)	chr17:1247833-2588909	1,341,076	3	3
17p12 recurrent (HNPP/CMT1A) region (includes PMP22)	chr17:14097915-15470901	1,372,986	3	3
17p11.2 recurrent (SMS/PLS) region (includes RAI1)	chr17:16757111-20219651	3,462,540	3	3
17q11.2 recurrent region (includes NF1)	chr17:29162822-30218667	1,055,845	3	3
17q12 recurrent (RCAD syndrome) region (includes HNF1B)	chr17:34815072-36192492	1,377,420	3	3
17q21.3 recurrent region (includes KANSL1)	chr17:43686245-44164876	478,631	3	2
22q11.21 recurrent (Cat eye syndrome) region (includes CECR2)	chr22:17392953-18591860	1,198,907	0	3
22q11.2 recurrent (DGS/VCFS) region (proximal region, LCR22-A to -B)	chr22:18661725-20311904	1,650,179	3	3
22q11.2 recurrent (DGS/VCFS) region (proximal region, LCR22-A to -D)	chr22:18661725-21561514	2,899,789	3	3
22q11.2 recurrent region (distal region, LCR22-D to LCR22-E or -F)	chr22:21797378-23649113	1,851,735	3	3
22q13 region (includes SHANK3)	chr22:51045516-51178945	133,429	3	0
Xp22.31 recurrent region (includes STS)	chrX:6455811-8133196	1,677,385	3	40: Dosage sensitivity unlikely
Xp11.23 region (includes MAOA and MAOB)	chrX:43514154-43741720	227,566	3	0
Xq28 recurrent region (includes GDI1)	chrX:153564626-153889019	324,393	0	3
Xq28 recurrent region (int22h1/int22h2-flanked) (includes RAB39B)	chrX:154124111-154564398	440,287	3	3

**ClinGen Dosage Sensitivity Curation Page <https://www.ncbi.nlm.nih.gov/projects/dbvar/clingen/pathogenic_region.shtml> より一部改変引用*

別紙４

研究成果の刊行に関する一覧表レイアウト

書籍

著者氏名	論文タイトル名	書籍全体の編集者名	書　籍　名	出版社名	出版地	出版年	ページ
Fukami M, Kurahashi H	Clinical consequences of chromothripsis and other catastrophic cellular event	Franck Pellestor	Methods Mol Biol.	Springer	UK	2017	21-34

雑誌

発表者氏名	論文タイトル名	発表誌名	巻号	ページ	出版年
Rinaldi VD, Bolcun-Filas E, Kogo H, Kurahashi H, Schimenti JC.	The DNA damage checkpoint eliminates mouse oocytes with chromosome synapsis failure.	**Mol Cell**	67	1026-1036.e2	2017
Nakae S, Kato T, Murayama K, Sasaki H, Abe M, Kumon M, Kumai T, Yamashiro K, Inamasu J, Hasegawa M, Kurahashi H, Hirose Y.	Remote intracranial recurrence of IDH mutant gliomas is associated with TP53 mutations and an 8q gain.	**Oncotarget**	8	84729-84742	2017
Azuma Y, Töpf A, Evangelista T, Lorenzoni PJ, Roos A, Viana P, Inagaki H, Kurahashi H, Lochmüller H.	Intragenic DOK7 deletion detected by whole-genome sequencing in congenital myasthenic syndromes.	**Neurol Genet**	3	e152	2017
Nagasaka M, Taniguchi-Ikeda M, Inagaki H, Ouchi Y, Kurokawa D, Yamana K, Harada R, Nozu K, Sakai Y, Mishra SK, Yamaguchi Y, Morikoka I, Toda T, Kurahashi H, Iijima K.	Novel missense mutation in DLL4 in a Japanese sporadic case of Adams-Oliver syndrome.	J Hum Genet	62	869	2017
Kawamura Y, Ohye T, Miura H, Ihira M, Kato Y, Kurahashi H, Yoshikawa T.	Analysis of the origin of inherited chromosomally integrated human herpesvirus 6 in the Japanese population.	**J Gen Virol**	98	1823-1830	2017
Kato T, Ouchi Y, Inagaki H, Makita Y, Mizuno S, Kajita M, Ikeda T, Takeuchi K, Kurahashi H.	Genomic characterization of chromosomal insertions: Implication for mechanism leading to the chromothripsis.	**Cytogenet Genome Res**	153	1-9	2017

Kohmoto T, Okamoto N, Naruto T, Murata C, Ouchi Y, Fujita N, Inagaki H, Satomura S, Okamoto N, Saito M, Masuda K, Kurahashi H, Imoto I.	A case with concurrent duplication, triplication, and uniparental isodisomy at 1q42.12-qter supporting microhomology-mediated break-induced replication model for replicative rearrangements.	**Mol Cytogenet**	10	15	2017
Kato M, Kato T, Hosoba E, Ohashi M, Fujisaki M, Ozaki M, Yamaguchi M, Sameshima H, Kurahashi H.	PCS/MVA syndrome caused by an Alu insertion in the BUB1B gene.	**Hum Genome Var**	4	17021	2017
Inoue Y, Sakamoto Y, Sugimoto M, Inagaki H, Boda H, Miyata M, Kato H, Kurahashi H, Okumoto T.	A family with craniofrontonasal syndrome: the first report of familial cases of craniofrontonasal syndrome with bilateral cleft lip and palate.	**Cleft Palate Craniofac J**	1	15347	2018
Taniguchi-Ikeda M, Morisada N, Inagaki H, Ouchi Y, Takami Y, Tachikawa M, Satake W, Kobayashi K, Tsuneishi S, Takada S, Yamaguchi H, Nagase H, Nozu K, Okamoto N, Nishio H, Toda T, Morioka I, Wada H, Kurahashi H, Iijima K.	Two patients with PNKP mutations presenting with microcephaly, seizure, and oculomotor apraxia.	**Clin Genet**	93(4)	931-933	2018
Ohwaki A, Nishizawa H, Aida N, Kato T, Kambayashi A, Miyazaki J, Ito M, Urano M, Kiriyama Y, Kuroda M, Nakayama M, Sonta SI, Suzumori K, Sekiya T, Kurahashi H, Fujii T..	Twin pregnancy with chromosomal abnormalities mimicking a gestational trophoblastic disorder and coexistent foetus on ultrasound.	**J Obstet Gynaecol**.	In press	In press	2018
Terasawa S, Kato A, Nishizawa H, Kato T, Yoshizawa H, Noda Y, Miyazaki J, Ito M, Sekiya T, Fujii T, Kurahashi H.	Multiplex PCR in noninvasive prenatal diagnosis for FGFR3-related disorders.	**Congenit Anom (Kyoto)**	In press	In press	2018
Kibe M, Ibara S, Inagaki H, Kato T, Kurahashi H, Ikeda T.	Lethal persistent pulmonary hypertension of the newborn in Bohring-Opitz syndrome.	**Am J Med Genet A**	176(5)	1245-1248	2018

Yamaguchi T, Yamaguchi M, Akeno K, Fujisaki M, Sumiyoshi K, Ohashi M, Sameshima H, Ozaki M, Kato M, Kato T, Hosoba E, Kurahashi H.	Prenatal diagnosis of premature chromatid separation/mosaic variegated aneuploidy (PCS/MVA) syndrome.	**J Obstet Gynaecol Res**	In press	In press	2018
Yokoi K, Nakajima Y, Ohye T, Inagaki H, Wada Y, Fukuda T, Sugie H, Yuasa I, Ito T, Kurahashi H.	Disruption of the responsible Gene in a phosphoglucomutase 1 deficiency patient by homozygous chromosomal inversion.	**JIMD Rep**	In press.	In press.	2018
Tsutsumi M, Fujita N, Suzuki F, Mishima T, Fujieda S, Watari M, Takahashi N, Tonoki H, Moriwaka O, Endo T, Kurahashi H.	Constitutional jumping translocation involving the Y and acrocentric chromosomes.	**Asian J Androl**	In press.	In press.	2018
Sharma R, Gardner A, Homan C, Douglas E, Mefford H, Wieczorek D, Stark Z, Nowak C, Douglas J, Parsons G,	Clinical and functional assessment of novel variation in THOC2, an essential component of nuclear mRNA export machine	**Hum Mutat**	In press.	In press.	2018

Article

Molecular Cell

The DNA Damage Checkpoint Eliminates Mouse Oocytes with Chromosome Synapsis Failure

Graphical Abstract

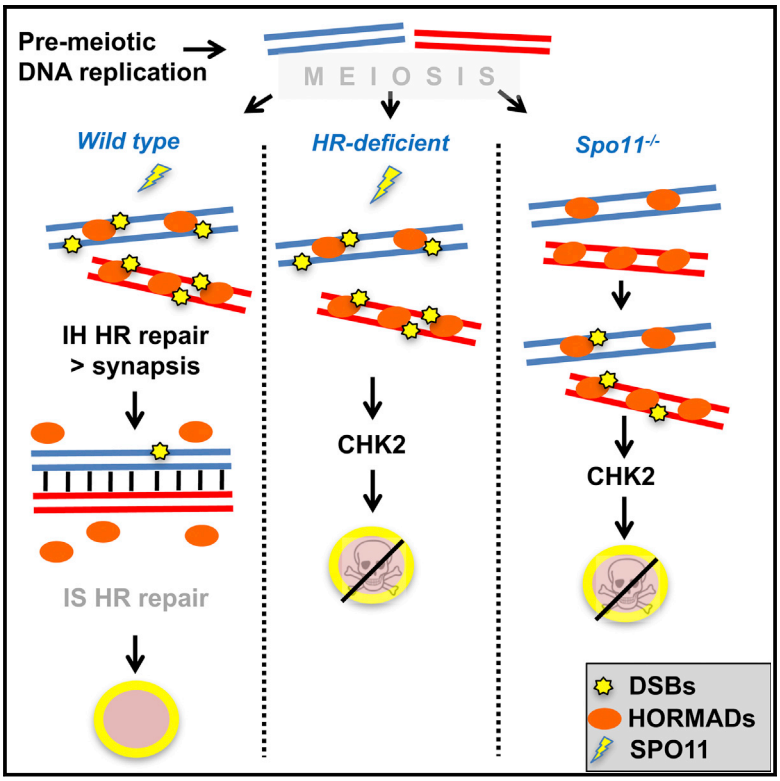

Highlights

- Late meiosis I oocytes bearing more than 10 DSBs are killed by the DNA damage checkpoint
- CHK2 is responsible for eliminating many asynaptic, SPO11-deficient mouse oocytes
- *Spo11*$^{-/-}$ oocytes acquire spontaneous DSBs that often exceed the 10-DSB threshold
- HORMAD2 on pachytene chromosomes prevents DSB repair via intersister recombination

Authors

Vera D. Rinaldi, Ewelina Bolcun-Filas, Hiroshi Kogo, Hiroki Kurahashi, John C. Schimenti

Correspondence

jcs92@cornell.edu

In Brief

Proper chromosome segregation during meiosis requires recombination repair of programmed DNA breaks to drive homolog pairing. Gametes with potentially devastating unsynapsed chromosomes or unrepaired breaks are killed. Surprisingly, Rinaldi et al. find that the CHK2 DNA damage checkpoint is important for eliminating mutant oocytes with either type of defect.

Rinaldi et al., 2017, Molecular Cell 67, 1026–1036
September 21, 2017
http://dx.doi.org/10.1016/j.molcel.2017.07.027

CellPress

Molecular Cell
Article

The DNA Damage Checkpoint Eliminates Mouse Oocytes with Chromosome Synapsis Failure

Vera D. Rinaldi,[1] Ewelina Bolcun-Filas,[1,2] Hiroshi Kogo,[4] Hiroki Kurahashi,[3] and John C. Schimenti[1,5,*]
[1]Cornell University, Departments of Biomedical Sciences and Molecular Biology and Genetics, Ithaca, NY 14850, USA
[2]The Jackson Laboratory, Bar Harbor, ME 14850, USA
[3]Fujita Health University, Institute of Comprehensive Molecular Science, Toyoake, Aichi 470-1192, Japan
[4]Gunma University, Department of Anatomy and Cell Biology, Maebashi, Gunma 371-8511, Japan
[5]Lead Contact
*Correspondence: jcs92@cornell.edu
http://dx.doi.org/10.1016/j.molcel.2017.07.027

SUMMARY

Pairing and synapsis of homologous chromosomes during meiosis is crucial for producing genetically normal gametes and is dependent upon repair of SPO11-induced double-strand breaks (DSBs) by homologous recombination. To prevent transmission of genetic defects, diverse organisms have evolved mechanisms to eliminate meiocytes containing unrepaired DSBs or unsynapsed chromosomes. Here we show that the CHK2 (CHEK2)-dependent DNA damage checkpoint culls not only recombination-defective mouse oocytes but also SPO11-deficient oocytes that are severely defective in homolog synapsis. The checkpoint is triggered in oocytes that accumulate a threshold level of spontaneous DSBs (~10) in late prophase I, the repair of which is inhibited by the presence of HORMAD1/2 on unsynapsed chromosome axes. Furthermore, *Hormad2* deletion rescued the fertility of oocytes containing a synapsis-proficient, DSB repair-defective mutation in a gene (*Trip13*) required for removal of HORMADs from synapsed chromosomes, suggesting that many meiotic DSBs are normally repaired by intersister recombination in mice.

INTRODUCTION

Genome maintenance in germ cells is critical for fertility, prevention of birth defects, and the genetic stability of species. Throughout mammalian germline development, from primordial germ cells (PGCs) through completion of meiosis, there are mechanisms that prevent the transmission of gametes with genetic defects. Indeed, mutation rates in germ cells are far lower than in somatic cells (Conrad et al., 2011; Murphey et al., 2013; Stambrook and Tichy, 2010). This is reflected by the exquisite sensitivity of PGCs to mutations in certain DNA repair genes (Agoulnik et al., 2002; Luo et al., 2014; Nadler and Braun, 2000) (Watanabe et al., 2013), sensitivity of resting oocytes to clastogens such as radiation and chemotherapeutics (Maltaris et al., 2007; Perez et al., 1997; Suh et al., 2006), and sensitivity of developing prophase I meiocytes to genetic anomalies, including a modicum of DNA damage (Meirow and Nugent, 2001; Suh et al., 2006) or the presence of a single asynapsed chromosome or even a chromosomal subregion (Burgoyne and Baker, 1985; Homolka et al., 2012).

Genetic and developmental analyses of mouse mutants have suggested that there are at least two distinct checkpoints during meiotic prophase I in oocytes, one that monitors double-strand break (DSB) repair and another that monitors synapsis. Oocytes defective for either synapsis or DSB repair are eliminated with different dynamics and severity. Females with mutations causing pervasive asynapsis alone (e.g., *Spo11*$^{-/-}$) are born with a grossly reduced oocyte pool. The surviving oocytes undergo folliculogenesis but are reproductively inviable, becoming exhausted within a few weeks by atresia and ovulation (Di Giacomo et al., 2005). Oocytes defective in DSB repair alone (*Trip13*$^{Gt/Gt}$) or defective in both synapsis and meiotic DSB repair (e.g., *Dmc1*$^{-/-}$; *Msh5*$^{-/-}$) are virtually completely eliminated between late gestation and wean age by the action of a DNA damage checkpoint (Di Giacomo et al., 2005; Li and Schimenti, 2007). Furthermore, genetic ablation of meiotic DSB formation confers a *Spo11*$^{-/-}$-like phenotype to such DSB repair mutants, consistent with the existence of separate DNA damage and synapsis checkpoints (Di Giacomo et al., 2005; Finsterbusch et al., 2016; Li and Schimenti, 2007; Reinholdt and Schimenti, 2005). For DSB repair, CHK2 (checkpoint kinase 2) signaling to TRP53/TAp63 is crucial for eliminating *Trip13*$^{Gt/Gt}$ mutant oocytes that exhibit full chromosome synapsis but have unrepaired SPO11-induced DSBs (Bolcun-Filas et al., 2014). Interestingly, *Chk2* deficiency imparted a *Spo11* null-like phenotype upon *Dmc1*$^{-/-}$ ovaries, consistent with separate, sequentially acting checkpoints (Bolcun-Filas et al., 2014). Genetic evidence for a distinct synapsis checkpoint came from studies of mice lacking HORMAD1 or HORMAD2, proteins that load onto axes of meiotic chromosomes throughout early prophase I but are removed upon synapsis (Wojtasz et al., 2009). Ablation of either in mice prevented loss of SPO11-deficient oocytes, resulting in the persistence of a nonfertile primordial follicle reserve in adults (Daniel et al., 2011; Kogo et al., 2012a; Wojtasz et al., 2012). These data suggest that the HORMADs are components of a synapsis checkpoint pathway. Another mechanism for elimination of oocytes is related to the phenomenon of MSUC (meiotic

silencing of unsynapsed chromatin). Although not formally a checkpoint, the transcriptional inactivation of a chromosome containing genes essential for oocyte survival and development can block progression past diplonema (Cloutier et al., 2015).

Although these lines of evidence support the existence of separate checkpoints monitoring DNA damage and synapsis, studies in non-mammalian organisms indicate that the "pachytene checkpoint"—a term referring to delayed progression of meiosis or death of meiocytes triggered by genetic aberrations present in late pachynema—is more complex, consisting of both distinct and overlapping signaling pathways that also affect DNA repair modalities such as choice of recombination partner for the repair of meiotic DSBs (e.g., sister chromatid versus homolog) (Joshi et al., 2015; MacQueen and Hochwagen, 2011; Roeder and Bailis, 2000; Subramanian and Hochwagen, 2014). Here we report the results of a series of experiments designed to discriminate whether the pachytene checkpoint in mouse oocytes indeed consists of distinct pathways responding to different signals or whether the responses are integrated into a single checkpoint pathway. Using a variety of mouse mutants, we show that most oocytes that are highly defective for chromosome synapsis accumulate spontaneous DSBs at a level that can trigger the CHK2-dependent DNA damage signaling pathway, leading to their elimination. Additionally, we present evidence that the reason why asynaptic *Spo11*$^{-/-}$ oocytes can be rescued by HORMAD1/2 deficiency is that their absence disrupts the so-called barrier to sister chromatid recombination (BSCR), enabling intersister (IS) repair of those spontaneous DSBs. Taken together, we propose that the pachytene checkpoint consists primarily of a canonical DNA damage signaling pathway and that extensive asynapsis leads to oocyte loss by inhibiting homologous recombination (HR) repair rather than triggering a distinct "synapsis checkpoint."

RESULTS

CHK2 Is Involved in the Elimination of *Spo11*$^{-/-}$ Oocytes

To investigate potential overlap of the meiotic DSB repair and synapsis checkpoint pathways in mice, we tested whether CHK2, a well-defined DSB signal transducer, contributes to the elimination of *Spo11*$^{-/-}$ oocytes that are asynaptic because of lack of programmed meiotic DSBs needed for recombination-driven homolog pairing. Consistent with prior reports (Baudat et al., 2000; Di Giacomo et al., 2005), we observed a greatly reduced number of total follicles in 3-week-postpartum (pp) *Spo11*$^{-/-}$ ovaries compared with the WT, and, in particular, the oocyte reserve (the pool of primordial resting follicles) was almost completely exhausted by 8 weeks of age (Figure 1). Surprisingly, *Chk2* deletion rescued the oocyte reserve (Figures 1A and 1B), albeit not to WT levels. The rescued follicles in double-mutant females persisted robustly at least until 6 months pp (in one case, 554 total in a single ovary).

HORMAD2 Deficiency Prevents Elimination of *Trip13* Mutant Oocytes that Have Complete Synapsis but Unrepaired Meiotic DSBs, Restoring Female Fertility

Taken alone, the rescue of *Spo11*$^{-/-}$ oocytes by *Chk2* deletion suggests that severe asynapsis leads to CHK2 activation and signaling to mediate oocyte elimination. This led us to postulate that either CHK2 is a common component of otherwise distinct synapsis and DNA damage checkpoints or that there is a single linear checkpoint pathway that responds to both asynapsis and DNA damage and that DNA damage activates the checkpoint pathway more robustly or sooner in prophase I (thus accounting for the different patterns of oocyte elimination in asynaptic versus DSB repair-deficient oocytes mentioned above; Di Giacomo et al., 2005).

We reasoned that if there is a single linear checkpoint pathway, then putative synapsis checkpoint genes required to eliminate *Spo11*$^{-/-}$ oocytes would also be required to eliminate *Trip13*$^{Gt/Gt}$ oocytes. *Trip13*$^{Gt/Gt}$ meiocytes have synapsed chromosomes and persistent SPO11-dependent DSBs, which leads to neonatal depletion of follicles in a CHK2 > TRP53/TAp63 pathway-dependent manner (Figure 2A; Bolcun-Filas et al., 2014; Li and Schimenti, 2007). To test this, we determined whether deficiency of HORMAD2, a putative synapsis checkpoint protein, could rescue *Trip13*$^{Gt/Gt}$ oocytes. HORMAD2 and its paralog HORMAD1 are HORMA (Hop1, Rev7, and Mad2) domain-containing proteins orthologous to the *Saccharomyces cerevisiae* synaptonemal complex (SC) axial element protein Hop1p, and deletion of either prevents elimination of *Spo11*$^{-/-}$ oocytes (Daniel et al., 2011; Kogo et al., 2012a; Wojtasz et al., 2012). We used a mutant of *Hormad2* rather than *Hormad1* because deletion of the latter disrupts recombination and homolog synapsis (Daniel et al., 2011; Kogo et al., 2012b; Shin et al., 2010). Remarkably, not only did ovaries of 2-month-old *Trip13*$^{Gt/Gt}$ *Hormad2*$^{-/-}$ mice retain a substantial primordial follicle pool (Figures 2A and 2B), but these females were also fertile (Figure 2C). The rescued fertility of these oocytes suggests either that these DSBs were compatible with further oocyte maturation or that they were eventually repaired, as in the case of *Trip13*$^{Gt/Gt}$ females, whose fertility was restored by *Chk2* ablation (Bolcun-Filas et al., 2014). The dynamics of DSB repair are addressed below.

Because TRIP13 is required for removal of the HORMADs from chromosome axes upon synapsis (Wojtasz et al., 2009), and persistence of HORMADs on unsynapsed chromosomes correlates with MSUC-mediated silencing of essential genes (Cloutier et al., 2015; Wojtasz et al., 2012), the question arises of whether *Trip13*$^{Gt/Gt}$ oocytes are eliminated not because of unrepaired DSBs but, rather, by transcriptional silencing. However, this is unlikely for the following reasons. First, *Trip13*$^{Gt/Gt}$ oocytes are depleted with a temporal pattern and degree consistent with mutants defective in DSB repair, not asynapsis (Di Giacomo et al., 2005; Li and Schimenti, 2007). Second, *Spo11* is epistatic to *Trip13* in that *Trip13*$^{Gt/Gt}$ *Spo11*$^{-/-}$ ovaries resemble *Spo11* single mutants in their pattern of oocyte elimination (Li and Schimenti, 2007), demonstrating that unrepaired meiotic DSBs drive early culling of *Trip13* mutant oocytes. Third, HORMAD persistence on synapsed *Trip13*$^{Gt/Gt}$ or unsynapsed *Spo11*$^{-/-}$ meiotic chromosome axes is not affected by *Chk2* deletion (Figure S1), which might be predicted if CHK2 was rescuing either mutant class by disrupting the ability of HORMADs to signal asynapsis. The latter is further supported by the fact that CHK2 depletion does not interfere with MSCI (meiotic sex chromosome inactivation), which is mechanistically similar or identical to MSUC, in

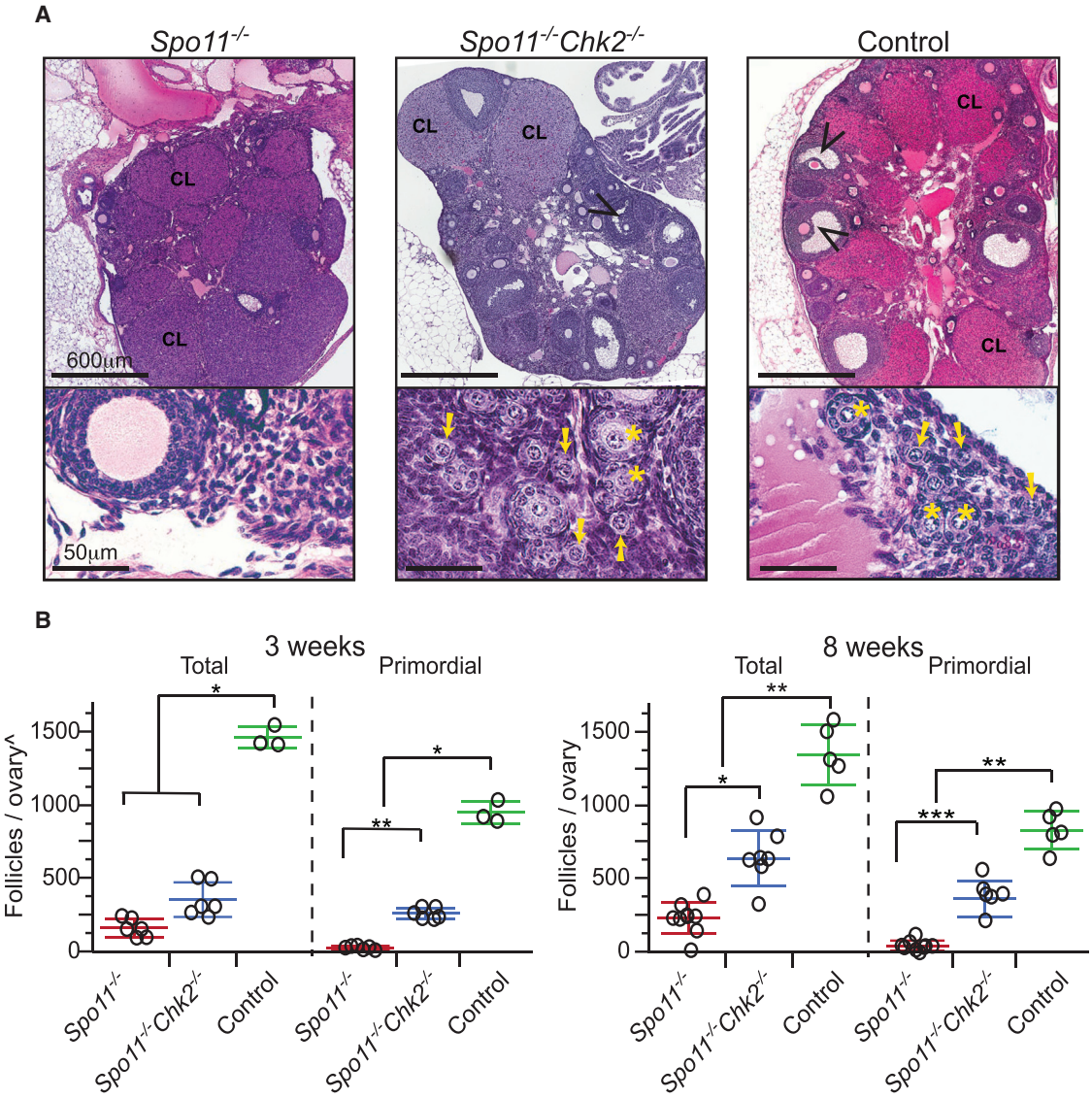

Figure 1. CHK2 Is Required for Efficient Elimination of Asynaptic *Spo11*$^{-/-}$ Mouse Oocytes

(A) H&E-stained histological sections of 8-week-old ovaries. Black arrowheads indicate antral follicles. The presence of corpora lutea (CL) is indicative of prior rounds of ovulation. Shown at the bottom are higher-magnification images of an ovarian cortical region, where primordial follicles reside. Yellow arrows and asterisks indicate primordial and primary follicles, respectively.

(B) Follicle counts from ovaries of the indicated genotypes at 3 and 8 weeks pp, respectively. Each data point is from a single ovary, each from a different animal. Total, all follicle types. Horizontal hashes denote mean and SD. Littermate controls included animals with the following genotypes: *Spo11*$^{+/+}$*Chk2*$^{+/+}$, *Spo11*$^{+/-}$ *Chk2*$^{+/-}$, and *Spo11*$^{+/+}$*Chk2*$^{+/-}$. ^, the values obtained for the 3-week follicles/ovaries counts are not comparable with the 8-week ones (see STAR Methods). *p = 0.005–0.05, **p = 0.001–0.005 and *** p $\leq$ 0.001 derived from a non-parametric, one-way ANOVA test (Kruskal-Wallis).

males (Pacheco et al., 2015) and that *Chk2*$^{-/-}$ mice are fertile, unlike *Hormad1*$^{-/-}$ animals (Daniel et al., 2011; Kogo et al., 2012b; Shin et al., 2013).

HORMAD2 Inhibits DSB Repair in Prophase I Oocytes

That HORMAD2 deficiency could rescue both *Trip13*$^{Gt/Gt}$ and *Spo11*$^{-/-}$ oocytes is consistent with a single checkpoint capable of detecting both damaged DNA and asynapsed chromosomes. If there is indeed a single checkpoint pathway, then combined deficiency for CHK2 and HORMAD2 should rescue asynaptic and DSB repair-defective *Dmc1*$^{-/-}$ oocytes to the same degree as deficiency for either one alone. However, *Dmc1*$^{-/-}$ *Chk2*$^{-/-}$ *Hormad2*$^{-/-}$ females had $\geq$3-fold increase in primordial and total follicles compared with *Dmc1*$^{-/-}$ *Hormad2*$^{-/-}$ or *Dmc1*$^{-/-}$ *Chk2*$^{-/-}$ ovaries (Figures 3A and 3B; Figure S2). This lack of epistasis indicates that HORMAD2 and CHK2 are not functioning solely as members of a single linear checkpoint pathway sensing either or both asynapsis and DNA damage.

We therefore considered two alternative explanations for why *Hormad2* deficiency rescues *Trip13*$^{Gt/Gt}$ oocytes: it reduces the

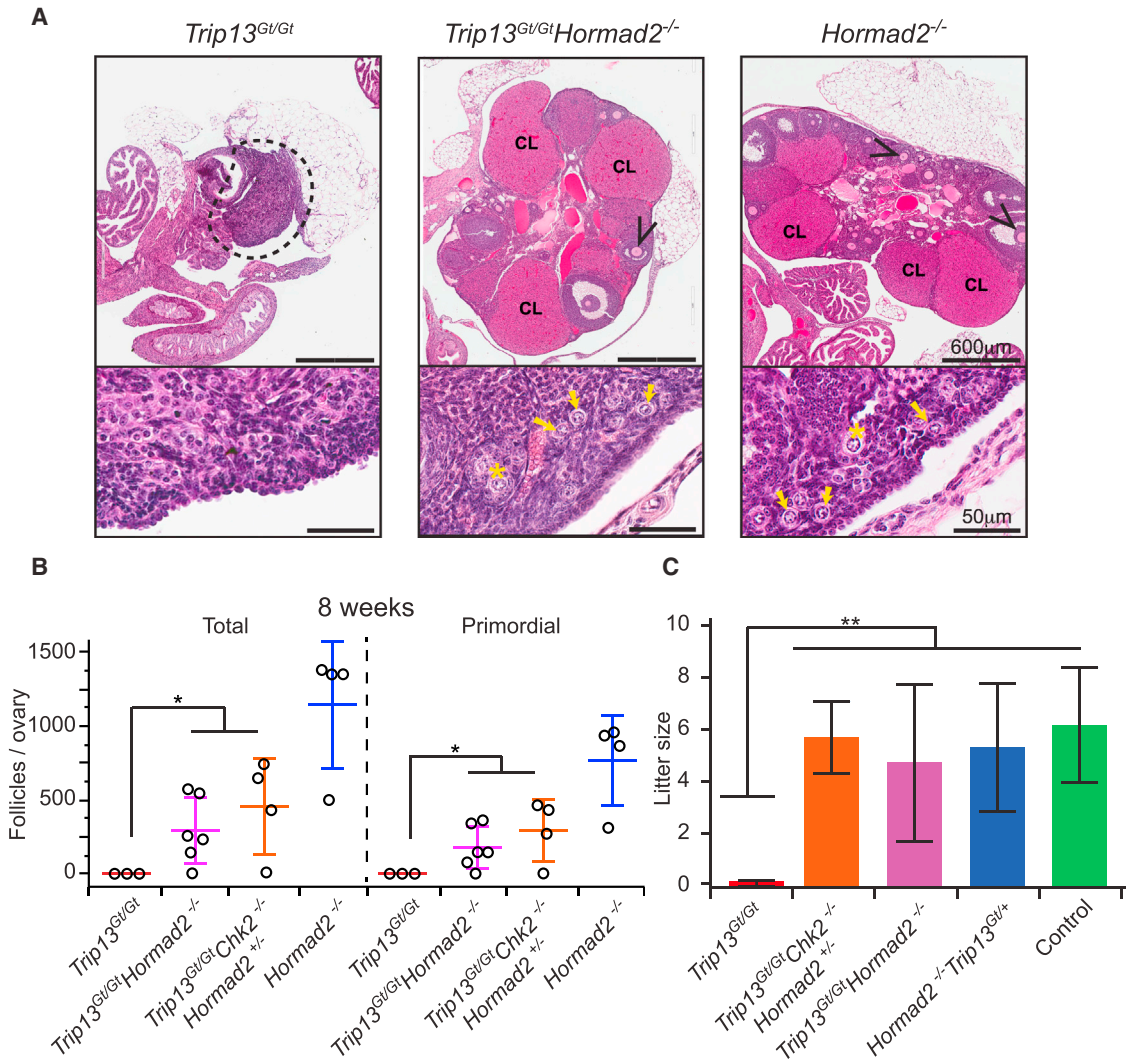

Figure 2. Synapsis-Competent *Trip13*$^{Gt/Gt}$ Oocytes Are Eliminated in a HORMAD2-Dependent Manner

(A) H&E-stained histological sections of 8-week-old ovaries of the indicated genotypes. Black arrowheads indicate antral follicles. Shown at the bottom are higher-magnification images of cortical regions of ovaries. Yellow arrows and asterisks indicate primordial and primary follicles, respectively.

(B) Follicle quantification of 8-week-old ovaries. Each data point is from a single ovary, each from a different animal. Total, all follicle types. Horizontal hashes denote mean and SD. The statistic used was a Kruskal-Wallis test. *p = 0.002.

(C) Graphed are mean litter sizes. n $\geq$ 3 females tested for fertility per genotypic group. Control matings were between mice with the genotypes *Trip13*$^{Gt/+}$ and *Trip13*$^{Gt/+}$ *Hormad2*$^{+/-}$. Error bars represent SD, and **p $\leq$ 0.005, derived from the Kruskal-Wallis test.

number of SPO11-induced DSBs to a level sufficient for synapsis but below the threshold for checkpoint activation, and/or it facilitates DSB repair. Studies of related proteins support both explanations. Absence of the budding yeast ortholog Hop1p not only decreases meiotic DSB formation but also increases use of the sister chromatid as a template for HR repair (Carballo et al., 2008; Lam and Keeney, 2014; Latypov et al., 2010; Mao-Draayer et al., 1996; Niu et al., 2005; Schwacha and Kleckner, 1997). Mouse HORMAD1 is required for loading HORMAD2 onto unsynapsed axes, proper SC formation (Daniel et al., 2011), and normal levels of meiotic DSBs (Daniel et al., 2011; Stanzione et al., 2016). Although *Dmc1*$^{-/-}$ *Hormad1*$^{-/-}$ or irradiated *Hormad1*$^{-/-}$ oocytes exhibit fewer DSB markers than oocytes containing HORMAD1 (Daniel et al., 2011; Shin et al., 2010), this can be attributable largely to enhanced repair (Shin et al., 2013). IS HR repair of DSBs in *S. cerevisiae* is substantial, and it increases in *hop1* mutants (Goldfarb and Lichten, 2010). Moreover, disruption of SC axes in mice (deletion of *Sycp2* or *Sycp3*) appears to alter recombination partner choice in favor of the sister chromatid, decreasing persistent DSBs in *Trip13*$^{Gt/Gt}$ oocytes to a degree that diminishes their elimination in a RAD54-dependent manner (Li et al., 2011). These data led us to hypothesize that the rescue of *Trip13* mutant oocytes by *Hormad2* deficiency was due to increased DSB repair, possibly by diminishing the BSCR.

To test this, we quantified the levels and rates of meiotic DSB repair in various genotypes of prophase I oocytes. Although the

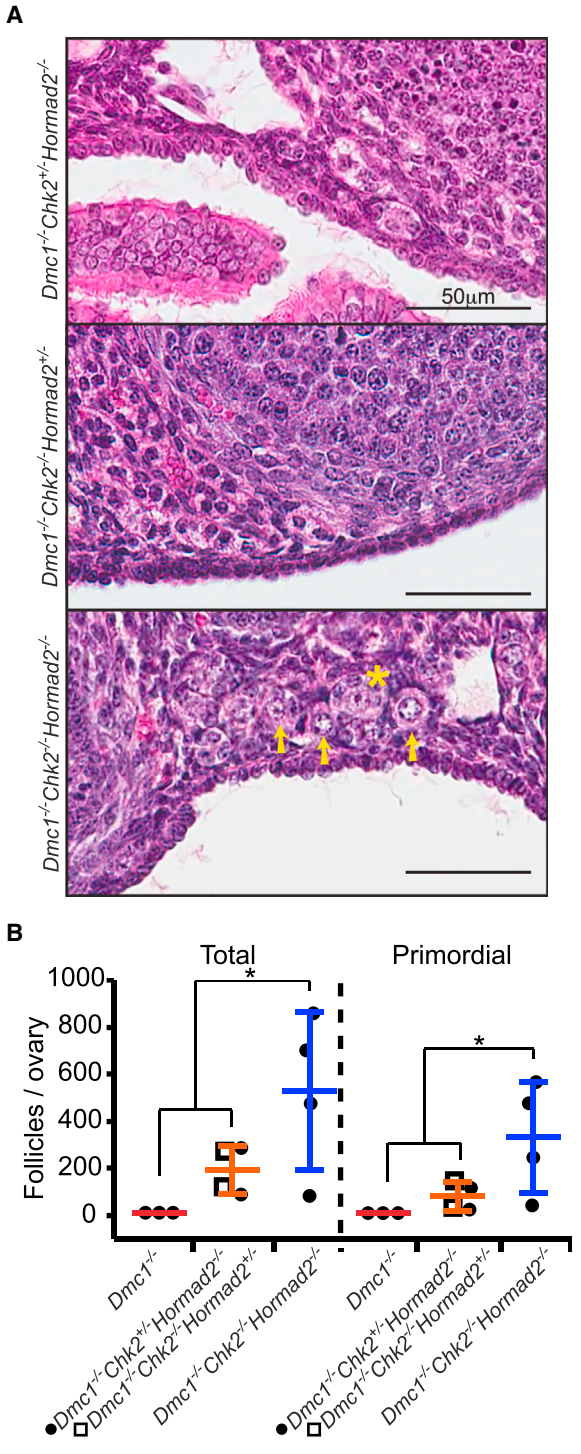

Figure 3. HORMAD2 and CHK2 Are Not in the Same Checkpoint Pathway

(A) H&E-stained histological sections of cortical regions of 8-week-old mutant mouse ovaries, where primordial follicles are concentrated. Histologies of whole ovaries of these genotypes are presented in Figure S2. Primordial follicles, which constitute the oocyte reserve, are indicated by yellow arrows, and a primary follicle by an asterisk. Residual *Dmc1*$^{-/-}$ ovaries are not represented because they are completely devoid of oocytes (Pittman et al., 1998).

(B) Follicle counts from ovaries of the indicated genotypes at 8 weeks of age. Total, all types of follicles. Data points represent follicle counts derived from one ovary, each ovary originating from a different animal. *p $\leq$ 0.05 (Kruskal-Wallis test).

number of leptotene- and zygotene-stage RAD51 foci was not significantly different in *Trip13*$^{Gt/Gt}$ *Hormad2*$^{-/-}$ oocytes compared with *Trip13*$^{Gt/Gt}$ or other control and mutant genotypes (Figures 4A and 4B; Table S1), there were significantly fewer compared with *Trip13*$^{Gt/Gt}$ by pachynema and diplonema ($p = 0.02$ and 0.03, respectively, using Tukey honest significant difference (HSD) in a mixed model). RAD51 levels in *Trip13*$^{Gt/Gt}$ and *Trip13*$^{Gt/Gt}$ *Chk2*$^{-/-}$ newborn oocytes remained high in diplonema compared with all other genotypes (Figures 4A and 4B; Table S1), presumably reflecting a relative deficiency in DSB repair. Furthermore, we found that RAD51 foci induced by 2 Gy of ionizing radiation (IR) disappeared more rapidly in *Spo11*$^{-/-}$ *Hormad2*$^{-/-}$ oocytes than in either *Spo11*$^{-/-}$ or *Spo11*$^{-/-}$ *Chk2*$^{-/-}$ oocytes, as assessed 8 hr after treatment (Figure 5; Table S2). Overall, the data suggest that HORMAD2 on the axes of either asynapsed (*Spo11*$^{-/-}$) or synapsed (*Trip13*$^{Gt/Gt}$) (Wojtasz et al., 2009) meiotic chromosomes inhibits IS recombination-mediated DSB repair.

Evidence that CHK2-Mediated Elimination of Asynaptic Oocytes Is Driven by Accumulation of SPO11-Independent DSBs

If indeed *Hormad2* deletion rescues DSB-containing oocytes by weakening or eliminating the BSCR, then this raises the question of why HORMAD2 deficiency rescues *Spo11*$^{-/-}$ oocytes that do not make meiotic DSBs. A clue comes from the surprising observation that *Spo11*$^{-/-}$ oocytes sustain DSBs of unknown origin (but possibly from LINE-1 retrotransposon activation) during early pachynema (Malki et al., 2014; Carofiglio et al., 2013). We hypothesized that these DSBs occur at levels sufficient to trigger the CHK2-dependent checkpoint in *Spo11*$^{-/-}$ oocytes but that, in the absence of SC axis-bound HORMAD2, there is sufficient DSB repair to prevent checkpoint activation. To test this, we determined the threshold number of DSBs that kills WT and *Chk2*$^{-/-}$ oocytes by exposing explanted newborn ovaries to a range of IR. RAD51 foci on chromosome axes accumulated roughly linearly in oocytes exposed to 0.5–9 Gy (Figure 6A; Figure S5), and *Chk2*$^{-/-}$ oocytes withstood up to 7 Gy (Figure 6B), a dosage that induces 73.3 RAD51 foci (Figure 6A). In contrast, as little as 0.3 Gy (10.3 foci by linear regression) abolished the entire primordial follicle pool of wild-type (WT) ovaries. Consistent with our hypothesis that HORMAD2 prevents DSB repair, the SC axes of *Spo11*$^{-/-}$ zygotene/pachytene-like chromosomes in newborn oocytes contained far more discrete RAD51 foci (raw average of 39.8; likely an underestimate; see Figure S3) than in *Spo11*$^{-/-}$ *Hormad2*$^{-/-}$ oocytes (average of 7.3 foci), the latter being almost identical to WT or *Chk2*$^{-/-}$ oocytes (7.5 and 7.3, respectively; Figure 6C; Table S3), in which HORMAD2 has been removed from synapsed chromosomes. These data indicate that the majority of *Spo11*$^{-/-}$ oocytes (60.8%) bear a level of DSBs (>10.3 foci) sufficient to trigger their elimination by the CHK2-dependent DNA damage checkpoint, whereas most WT oocytes (71%) are below this threshold (Table S3).

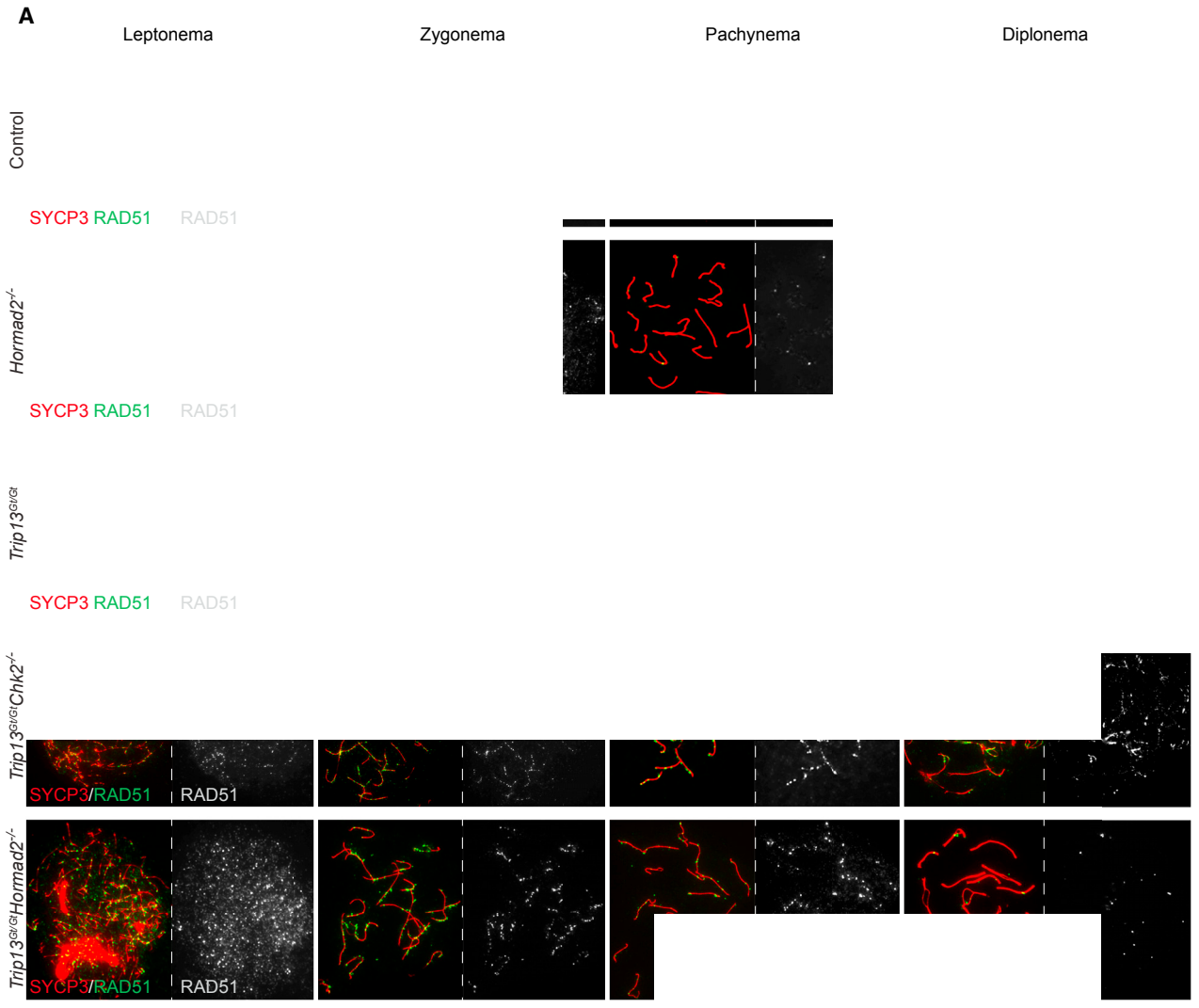

(legend on next page)

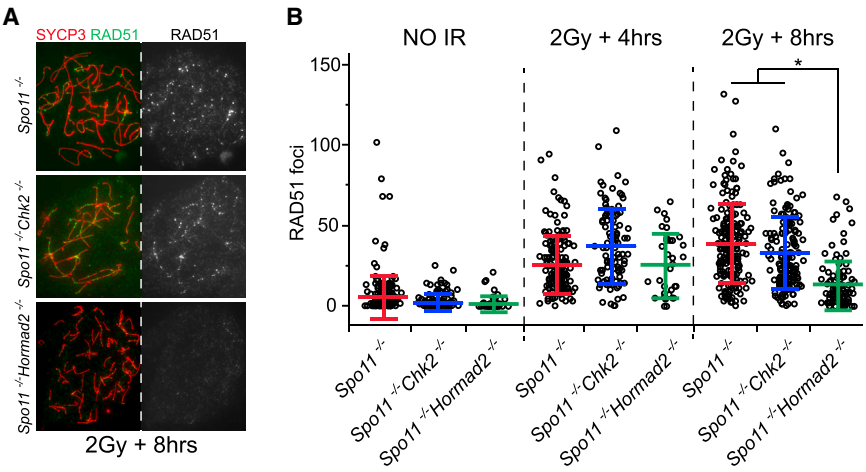

Figure 5. Depletion of HORMAD2 Accelerates Repair of Induced DSBs in Oocytes

(A) Immunolabeling of surface-spread chromosomes from oocytes after exposure to ionizing radiation (IR). Fetal ovaries were collected at 15.5 DPC, cultured for 24 hr, exposed to 2 Gy of IR, and then cultured for an additional 4-8 hr. Shown are those recovered 8 hr after IR. See Figure S4 for single *Hormad2*$^{-/-}$ single-mutant results.

(B) Quantification of RAD51 foci. Each data point represents one oocyte. The graphs include mean and SD and are color-coded according to genotypic group. The 4- and 8-hr unirradiated samples were combined. Data were derived from at least two different animals per condition. See Table S2 for associated raw data and statistical calculations.

DISCUSSION

Meiocytes have genetic quality control mechanisms that respond to their unique developmental circumstances, chromosome biology, and cell cycle. For example, the pachytene/prophase I checkpoint is active only at a point in prophase I at which DSBs have normally been repaired but not during the time between programmed DSB formation and HR repair. Although the oocyte pachytene checkpoint is distinct with respect to its cell cycle timing and its ability to monitor an event (chromosome synapsis) unique to meiosis, our current and prior (Bolcun-Filas et al., 2014) work indicate that, for circumstances involving extensive asynapsis and DNA damage, this checkpoint in oocytes involves a DNA damage response (DDR) common to somatic cells. Our surprising finding that the DDR is involved in culling of *Spo11*$^{-/-}$ oocytes raises the question of how SPO11-independent DSBs, first reported by Carofiglio et al. (2013) and confirmed here, arise on unsynapsed chromosomes. One possible source is LINE-1 retrotransposon activation, which has been correlated with natural oocyte attrition (Malki et al., 2014). However, transposon expression normally occurs only transiently at the onset of meiosis before epigenetic silencing (van der Heijden and Bortvin, 2009). It is possible that the extensive asynapsis in *Spo11*$^{-/-}$ oocytes per se or disruption of the meiotic program, including the normal course of DSB induction and repair, interferes with transposon silencing. Another possibility is that unsynapsed chromosomes are more susceptible to spontaneous breakage. These outcomes could be exacerbated by extended retention of HORMADs on unsynapsed axes, inhibiting repair of these breaks. An intriguing question is whether the production of these SPO11-independent DSBs, whatever their origin, evolved as a contributory mechanism for genetic quality control. It is also conceivable that the extended presence of HORMADs themselves contributes to spontaneous DSB formation, possibly as a "last ditch" mechanism to drive pairing or synapsis in chromosomes devoid of sufficient interhomolog recombination events.

The late appearance and highly variable number (Figure 6C) of SPO11-independent DSBs in *Spo11*$^{-/-}$ oocytes may explain the differences in timing and extent of oocyte elimination in exclusively asynaptic versus DSB repair-deficient (e.g., *Dmc1*, *Trip13*) mutants. As reported by Di Giacomo et al. (2005), although *Dmc1*$^{-/-}$ oocytes were completely eliminated before dictyate arrest and follicle formation, *Spo11*$^{-/-}$ ovaries contained ~15%–20% of the WT number of follicles (including 27-fold fewer primordial follicles by 4 days pp); this reduced oocyte reserve was depleted by 2–3 months of age by subsequent cycles of recruitment and maturation. Additionally, *Dmc1*$^{-/-}$ oocytes degenerate before *Spo11*$^{-/-}$ oocytes, suggesting that an earlier-acting mechanism was triggering *Dmc1*$^{-/-}$ oocyte death. These distinctions, in conjunction with epistasis analysis of mutants doubly deficient for *Spo11* and DSB repair mutations, led to the conclusion that there are DSB-dependent and -independent mechanisms to eliminate defective oocytes. We suggest that the difference in timing of oocyte elimination, at least in part, may be related to the DSB load. The abundant SPO11 DSBs formed early in prophase I may trigger the checkpoint sooner and more uniformly in recombination mutants that fail to reduce DSB levels in a timely manner. According to this scenario, spontaneous DSBs that do

Figure 4. Depletion of HORMAD2 Accelerates DSB Repair during Early Stages of Meiotic Prophase I

(A) Representative images of meiotic chromosome spreads from oocytes at different substages of meiotic prophase I, probed with antibodies for SYCP3 (SC axis protein) and the DSB marker RAD51. Oocytes were isolated from female embryos ranging from 15.5 DPC to newborns. See Figure S1 for HORMAD2 localization in meiotic mutants.

(B) Numbers of RAD51 foci in the specified meiotic prophase I substage of the indicated mutants. Only RAD51 foci present on SYCP3-stained axes were scored. Each data point represents one cell. In each genotypic group, at each stage, the counts are derived from at least three animals. Horizontal hashes in summary statistic plots denote mean and SD. Values of the mixed-model calculation can be found in Table S1. Colors correspond to genotypes. Asterisks indicate statistical significant differences between groups in terms of the least square means of RAD51 foci: ***p ≤ 0.001, **p ≤ 0.005, *p ≤ 0.05 (Tukey HSD). See Table S1 for associated raw data and statistical calculations.

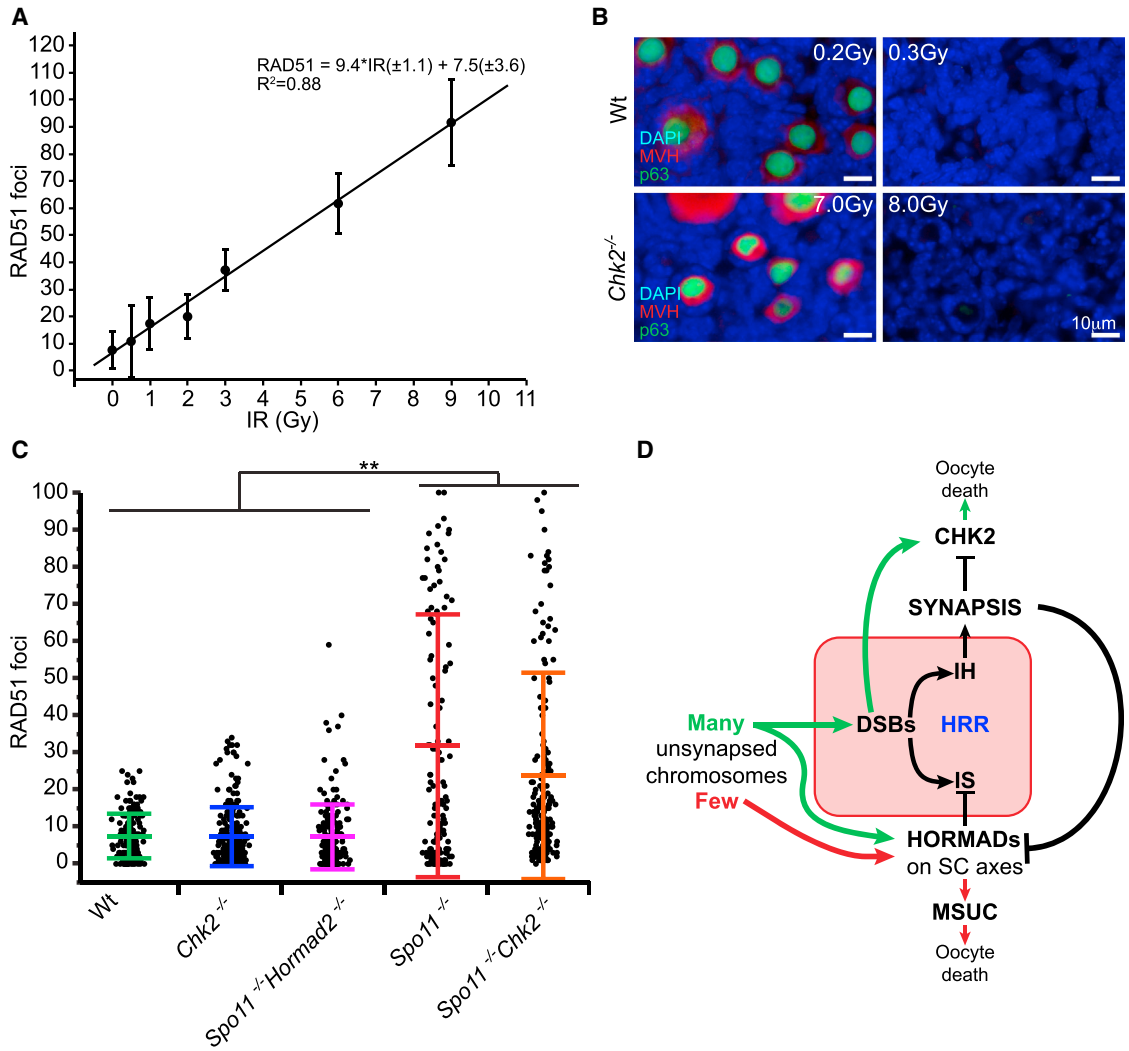

Figure 6. DNA Damage Threshold Required to Trigger Oocyte Death and Evidence for HORMAD-Mediated Inhibition of IS Repair

(A) Linear regression for conversion of radiation dosages to RAD51 focus counts. Meiotic surface spreads were made from WT neonatal ovaries 2.5 hr after IR. Plotted are means with SD. Each IR dose has focus counts from ~25 pachytene oocytes derived from a total of 18 animals. See Figure S5 for single-cell focus counts and numerical values.

(B) *Chk2*$^{-/-}$ oocytes are highly IR-resistant. Shown are immunofluorescence images of ovarian sections labeled with nuclear and cytoplasmic germ cell markers (p63 and MVH, respectively).

(C) RAD51 focus counts from newborn oocyte spreads. Only oocytes with discrete patterns of RAD51 foci were scored, as defined in Figure S3. Data points represent individual oocytes, derived from at least five different animals from each genotypic group. Horizontal hashes denote means and SD calculated using a mixed model (see STAR Methods). Asterisks indicate statistically significant differences between groups: ***p ≤ 0.001, **p ≤ 0.005, *p ≤ 0.05 (Tukey HSD). See Table S3 for raw data and statistical calculations.

(D) Model for pachytene checkpoint activation in mouse oocytes. Oocytes with many unsynapsed chromosomes (green) ultimately accumulate DSBs, which cannot be repaired because of block to IS recombination imposed by HORMADs on asynapsed axes. Failure of DSB repair leads to activation of CHK2 and downstream effector proteins (p53/TAp63) that trigger apoptosis. Few asynapsed chromosomes (red) lead to inactivation of essential genes by MSUC, thereby causing oocyte death.

not arise until latter stages of prophase I in *Spo11*$^{-/-}$ oocytes would trigger the DNA damage checkpoint at a later point. Based on our data (Figure 6A; Figure S5), we suggest that oocytes with below-threshold DSB levels escape the DNA damage checkpoint and are either eliminated by other mechanisms (see below) or survive to constitute the reduced follicular reserve in *Spo11* mutants.

Although the CHK2-dependent checkpoint is of central importance to genetic quality control in oocytes, our observations that *Chk2* deletion does not fully restore oocyte numbers to WT levels in mutants indicates that it is not absolutely required for eliminating all oocytes with unrepaired DSBs. Rather, the fraction of oocytes rescued is inversely related to the burden of unrepaired meiotic DSBs. For example, although *Chk2* deficiency rescued

nearly one-third of *Trip13*$^{Gt/Gt}$ oocytes (which are partially proficient for DSB repair and harbor 35 ± 4 and 63 ± 4.7 persistent RAD51 foci in diplonema and pachynema, respectively; Figure 4B), it rescued only a small fraction (~5%) of profoundly recombination-deficient *Dmc1*$^{-/-}$ oocytes (harboring an average of ~150 RAD51 foci; Li et al., 2011). We posit that the oocytes that fail to be rescued in these mutants are eliminated either by a separate or a complementary checkpoint pathway (for example, ATR-CHK1; Smith et al., 2010) or succumb to catastrophic levels of DNA damage. It is informative that deletion of *Hormad1*, but not *Hormad2*, rescues *Dmc1*$^{-/-}$ oocytes to a greater extent than *Chk2* deletion. As discussed earlier, the rescued *Dmc1*$^{-/-}$ *Hormad1*$^{-/-}$ oocytes had a marked reduction in DSBs (Bolcun-Filas et al., 2014; Shin et al., 2013; Wojtasz et al., 2012). Because HORMAD1 is needed to load HORMAD2 onto unsynapsed chromosome axes (not vice versa), the effect of *Hormad1* deletion upon IS recombination constitutes the combined roles of both HORMAD proteins. However, when *Hormad2* alone is deleted, the continued presence of chromosomally bound HORMAD1 may provide a less effective but still substantive BSCR. The lower level of residual DSBs in *Spo11* and *Trip13* mutant oocytes (compared with *Dmc1*$^{-/-}$) may render them responsive to a weaker BSCR, such as when *Hormad2* is deleted. We postulate that, because of its involvement in stimulating SPO11 activity (Daniel et al., 2011), *Hormad1* deletion is very effective in rescuing a DSB repair mutant like *Dmc1* because not only are fewer DSBs formed, but IS recombination is also more active.

Our results add to increasing evidence that IS recombination is important in mammalian meiosis. As discussed in the text, the HORMADs and SC axial element structure appear to inhibit IS repair of meiotic DSBs preferentially, thus allowing interhomolog (IH) recombination to drive homolog pairing and synapsis. However, as synapsis progresses and the SC is formed, the HORMADs are removed and, presumably, both IS and IH recombination can occur readily, as in yeast (Subramanian et al., 2016). Because not all RAD51 foci disappear by pachynema when synapsis is complete (for example, see Figure 4B), it is possible that a substantial fraction of these DSBs is normally repaired by IS recombination. We speculate that the persistent unrepaired DSBs on synapsed chromosomes of *Trip13* mutants, which retain HORMADs on their SCs, may actually constitute a substantial fraction of SPO11-induced DSBs (an average of ~65/oocyte nucleus of the 200–300 induced; Figure 4) that would normally be repaired by IS recombination. However, we cannot rule out the possibility that the "persistent" DSBs on synapsed *Trip13*$^{Gt/Gt}$ chromosomes actually arise from continued SPO11 cleavage signaled by continued presence of SC-bound HORMADs (Kauppi et al., 2013).

When trying to decipher the quality control mechanisms functioning during meiosis, it is important to recognize that experimental studies such as those performed here employ mutants with pervasive, non-physiological levels of defects. Meiocytes in WT individuals would have less extreme genetic defects. In oocytes bearing a small number (1–3) of unsynapsed chromosomes, the unsynapsed chromosomes undergo transcriptional silencing (MSUC) during pachynema, causing elimination at the diplotene stage (Cloutier et al., 2015; Kouznetsova et al., 2009) from lack of essential gene products encoded by these chromosomes (Cloutier et al., 2015). However, oocytes with more than 2–3 unsynapsed chromosomes impair MSUC, presumably because of a limiting amount of BRCA1 (Kouznetsova et al., 2009). Nevertheless, *Spo11*$^{-/-}$ meiocytes typically exhibit "pseudo sex bodies," named as such because they resemble the XY (sex) body involving a small number of asynapsed autosomes (Bellani et al., 2005). Formation of pseudo sex bodies in *Spo11*$^{-/-}$ oocytes is dependent on HORMADs (Daniel et al., 2011; Kogo et al., 2012b), leading to the proposal that these are responsible for oocyte elimination (Kogo et al., 2012a). This may be the case in a subset of oocytes where the pseudo sex body affects either a chromosomal region containing haploinsufficient loci or both alleles of a locus needed for meiotic progression or oocyte survival. Because CHK2 deficiency can rescue *Spo11*$^{-/-}$ oocytes while not abolishing HORMAD localization (Figure S1) or pseudo sex body formation (data not shown) but does not rescue all *Spo11* oocytes, it is likely that neither MSUC nor CHK2 alone is entirely responsible for elimination of all oocytes with pervasive asynapsis. Finally, because MSUC involves many components of the DNA damage response (Fernandez-Capetillo et al., 2003; Ichijima et al., 2011; Turner et al., 2004), it is conceivable that asynapsis leading to MSUC would activate effector elements of the DNA damage checkpoint pathway, including CHK2. However, this does not appear to be the case because silenced supernumerary chromosomes do not eliminate oocytes (Cloutier et al., 2015), MSCI does not kill spermatocytes, and asynaptic oocytes are not eliminated in a pattern typical of DNA repair mutants.

The pachytene checkpoint has commonly been thought to consist of separate DNA damage and synapsis checkpoints in multiple organisms. However, the finding that MSUC can cause the death of oocytes led to the suggestion that there is only 1 formal cell cycle checkpoint in mouse oocytes, the DNA damage checkpoint (Cloutier et al., 2015), - and our data provide mechanistic evidence consistent with this idea. Current information supports a model (Figure 6D) for two major mechanisms by which oocytes with synapsis defects are eliminated: 1) MSUC, for oocytes with a small number of asynapsed chromosomes that do not accumulate unrepaired DSBs above a threshold and in which both homologs bear essential genes for meiotic progression are silenced (Cloutier et al., 2015), and the DNA damage checkpoint, for oocytes with multiple asynapsed chromosomes that accumulate a sufficient number of DSBs to trigger the DNA damage checkpoint (Figure 6D). These disparate mechanisms may have distinct purposes. Because oocytes with only 1 or 2 unsynapsed chromosomes may not efficiently trigger the spindle assembly checkpoint (SAC) (LeMaire-Adkins et al., 1997), the MSUC pathway would safeguard against aneuploidy. Superficially, it would seem that, because oocytes with extensive asynapsis would effectively trigger the SAC, the DNA damage checkpoint mechanism is redundant. However, it is likely advantageous reproductively to eliminate such defective oocytes before they enter dictyate as constituents of the ovarian reserve, otherwise the fraction of unproductive ovulations (those terminated by the SAC) would increase, compromising fecundity.

STAR★METHODS

Detailed methods are provided in the online version of this paper and include the following:

- KEY RESOURCES TABLE
- CONTACT FOR REAGENT AND RESOURCE SHARING
- EXPERIMENTAL MODEL AND SUBJECT DETAILS
- METHOD DETAILS
  - Organ Culture and Irradiation
  - Histology and Immunostaining
  - Immunofluorescence of meiotic chromosome surface spreads
  - Focus Quantification
  - Fertility Test
- QUANTIFICATION AND STATISTICAL ANALYSIS
  - Statistical analysis
- DATA AND SOFTWARE AVAILABILITY

SUPPLEMENTAL INFORMATION

Supplemental Information includes five figures and three tables and can be found with this article online at http://dx.doi.org/10.1016/j.molcel.2017.07.027.

AUTHOR CONTRIBUTIONS

V.D.R. and E.B.F. performed the experiments and contributed to the writing of the paper. H Kogo and H. Kurahashi provided the *Hormad2* mutant ESCs and provided feedback on the manuscript. J.C.S. supervised the work and wrote most of the paper.

ACKNOWLEDGMENTS

This work was supported by a grant from the NIH (R01 GM45415 to J.C.S.) and contract CO29155 from the New York State Stem Cell Program (NYSTEM). The authors would like to thank R. Munroe and C. Abratte for generating chimeric mice, Stephen Parry from the Cornell Statistical Consulting Unit for help with statistical analysis, Dr. Atilla Toth for the HORMAD2 antibody, and M.A. Handel for feedback on the manuscript.

Received: April 3, 2017
Revised: June 14, 2017
Accepted: July 28, 2017
Published: August 24, 2017

REFERENCES

Agoulnik, A.I., Lu, B., Zhu, Q., Truong, C., Ty, M.T., Arango, N., Chada, K.K., and Bishop, C.E. (2002). A novel gene, *Pog*, is necessary for primordial germ cell proliferation in the mouse and underlies the germ cell deficient mutation, gcd. Hum. Mol. Genet. *11*, 3047–3053.

Baudat, F., Manova, K., Yuen, J.P., Jasin, M., and Keeney, S. (2000). Chromosome synapsis defects and sexually dimorphic meiotic progression in mice lacking *Spo11*. Mol. Cell *6*, 989–998.

Bellani, M.A., Romanienko, P.J., Cairatti, D.A., and Camerini-Otero, R.D. (2005). SPO11 is required for sex-body formation, and *Spo11* heterozygosity rescues the prophase arrest of *Atm*-/- spermatocytes. J. Cell Sci. *118*, 3233–3245.

Bolcun-Filas, E., Rinaldi, V.D., White, M.E., and Schimenti, J.C. (2014). Reversal of female infertility by Chk2 ablation reveals the oocyte DNA damage checkpoint pathway. Science *343*, 533–536.

Burgoyne, P.S., and Baker, T.G. (1985). Perinatal oocyte loss in XO mice and its implications for the aetiology of gonadal dysgenesis in XO women. J. Reprod. Fertil. *75*, 633–645.

Carballo, J.A., Johnson, A.L., Sedgwick, S.G., and Cha, R.S. (2008). Phosphorylation of the axial element protein Hop1 by Mec1/Tel1 ensures meiotic interhomolog recombination. Cell *132*, 758–770.

Carofiglio, F., Inagaki, A., de Vries, S., Wassenaar, E., Schoenmakers, S., Vermeulen, C., van Cappellen, W.A., Sleddens-Linkels, E., Grootegoed, J.A., Te Riele, H.P., et al. (2013). SPO11-independent DNA repair foci and their role in meiotic silencing. PLoS Genet. *9*, e1003538.

Cloutier, J.M., Mahadevaiah, S.K., Ellnati, E., Nussenzweig, A., Tóth, A., and Turner, J.M. (2015). Histone H2AFX links meiotic chromosome asynapsis to prophase I oocyte loss in mammals. PLoS Genet. *11*, e1005462.

Conrad, D.F., Keebler, J.E., DePristo, M.A., Lindsay, S.J., Zhang, Y., Casals, F., Idaghdour, Y., Hartl, C.L., Torroja, C., Garimella, K.V., et al.; 1000 Genomes Project (2011). Variation in genome-wide mutation rates within and between human families. Nat. Genet. *43*, 712–714.

Daniel, K., Lange, J., Hached, K., Fu, J., Anastassiadis, K., Roig, I., Cooke, H.J., Stewart, A.F., Wassmann, K., Jasin, M., et al. (2011). Meiotic homologue alignment and its quality surveillance are controlled by mouse HORMAD1. Nat. Cell Biol. *13*, 599–610.

Di Giacomo, M., Barchi, M., Baudat, F., Edelmann, W., Keeney, S., and Jasin, M. (2005). Distinct DNA-damage-dependent and -independent responses drive the loss of oocytes in recombination-defective mouse mutants. Proc. Natl. Acad. Sci. USA *102*, 737–742.

Fernandez-Capetillo, O., Celeste, A., and Nussenzweig, A. (2003). Focusing on foci: H2AX and the recruitment of DNA-damage response factors. Cell Cycle *2*, 426–427.

Finsterbusch, F., Ravindranathan, R., Dereli, I., Stanzione, M., Tränkner, D., and Tóth, A. (2016). Alignment of homologous chromosomes and effective repair of programmed DNA double-strand breaks during mouse meiosis require the minichromosome maintenance domain containing 2 (MCMDC2) protein. PLoS Genet. *12*, e1006393.

Goldfarb, T., and Lichten, M. (2010). Frequent and efficient use of the sister chromatid for DNA double-strand break repair during budding yeast meiosis. PLoS Biol. *8*, e1000520.

Gray, S., and Cohen, P.E. (2016). Control of meiotic crossovers: from double-strand break formation to designation. Annu. Rev. Genet. *50*, 175–210.

Hirao, A., Cheung, A., Duncan, G., Girard, P.M., Elia, A.J., Wakeham, A., Okada, H., Sarkissian, T., Wong, J.A., Sakai, T., et al. (2002). Chk2 is a tumor suppressor that regulates apoptosis in both an ataxia telangiectasia mutated (ATM)-dependent and an ATM-independent manner. Mol. Cell. Biol. *22*, 6521–6532.

Homolka, D., Jansa, P., and Forejt, J. (2012). Genetically enhanced asynapsis of autosomal chromatin promotes transcriptional dysregulation and meiotic failure. Chromosoma *121*, 91–104.

Ichijima, Y., Ichijima, M., Lou, Z., Nussenzweig, A., Camerini-Otero, R.D., Chen, J., Andreassen, P.R., and Namekawa, S.H. (2011). MDC1 directs chromosome-wide silencing of the sex chromosomes in male germ cells. Genes Dev. *25*, 959–971.

Joshi, N., Brown, M.S., Bishop, D.K., and Börner, G.V. (2015). Gradual implementation of the meiotic recombination program via checkpoint pathways controlled by global DSB levels. Mol. Cell *57*, 797–811.

Kauppi, L., Barchi, M., Lange, J., Baudat, F., Jasin, M., and Keeney, S. (2013). Numerical constraints and feedback control of double-strand breaks in mouse meiosis. Genes Dev. *27*, 873–886.

Kogo, H., Tsutsumi, M., Inagaki, H., Ohye, T., Kiyonari, H., and Kurahashi, H. (2012a). HORMAD2 is essential for synapsis surveillance during meiotic prophase via the recruitment of ATR activity. Genes Cells *17*, 897–912.

Kogo, H., Tsutsumi, M., Ohye, T., Inagaki, H., Abe, T., and Kurahashi, H. (2012b). HORMAD1-dependent checkpoint/surveillance mechanism eliminates asynaptic oocytes. Genes Cells *17*, 439–454.

Kouznetsova, A., Wang, H., Bellani, M., Camerini-Otero, R.D., Jessberger, R., and Höög, C. (2009). BRCA1-mediated chromatin silencing is limited to oocytes with a small number of asynapsed chromosomes. J. Cell Sci. *122*, 2446–2452.

Lam, I., and Keeney, S. (2014). Mechanism and regulation of meiotic recombination initiation. Cold Spring Harb. Perspect. Biol. *7*, a016634.

Latypov, V., Rothenberg, M., Lorenz, A., Octobre, G., Csutak, O., Lehmann, E., Loidl, J., and Kohli, J. (2010). Roles of Hop1 and Mek1 in meiotic chromosome pairing and recombination partner choice in *Schizosaccharomyces pombe*. Mol. Cell. Biol. *30*, 1570–1581.

LeMaire-Adkins, R., Radke, K., and Hunt, P.A. (1997). Lack of checkpoint control at the metaphase/anaphase transition: a mechanism of meiotic nondisjunction in mammalian females. J. Cell Biol. *139*, 1611–1619.

Li, X.C., and Schimenti, J.C. (2007). Mouse pachytene checkpoint 2 (*trip13*) is required for completing meiotic recombination but not synapsis. PLoS Genet. *3*, e130.

Li, X.C., Bolcun-Filas, E., and Schimenti, J.C. (2011). Genetic evidence that synaptonemal complex axial elements govern recombination pathway choice in mice. Genetics *189*, 71–82.

Luo, Y., Hartford, S.A., Zeng, R., Southard, T.L., Shima, N., and Schimenti, J.C. (2014). Hypersensitivity of primordial germ cells to compromised replication-associated DNA repair involves ATM-p53-p21 signaling. PLoS Genet. *10*, e1004471.

MacQueen, A.J., and Hochwagen, A. (2011). Checkpoint mechanisms: the puppet masters of meiotic prophase. Trends Cell Biol. *21*, 393–400.

Malki, S., van der Heijden, G.W., O'Donnell, K.A., Martin, S.L., and Bortvin, A. (2014). A role for retrotransposon LINE-1 in fetal oocyte attrition in mice. Dev. Cell *29*, 521–533.

Maltaris, T., Seufert, R., Fischl, F., Schaffrath, M., Pollow, K., Koelbl, H., and Dittrich, R. (2007). The effect of cancer treatment on female fertility and strategies for preserving fertility. Eur. J. Obstet. Gynecol. Reprod. Biol. *130*, 148–155.

Mao-Draayer, Y., Galbraith, A.M., Pittman, D.L., Cool, M., and Malone, R.E. (1996). Analysis of meiotic recombination pathways in the yeast Saccharomyces cerevisiae. Genetics *144*, 71–86.

Meirow, D., and Nugent, D. (2001). The effects of radiotherapy and chemotherapy on female reproduction. Hum. Reprod. Update *7*, 535–543.

Murphey, P., McLean, D.J., McMahan, C.A., Walter, C.A., and McCarrey, J.R. (2013). Enhanced genetic integrity in mouse germ cells. Biol. Reprod. *88*, 6.

Nadler, J.J., and Braun, R.E. (2000). Fanconi anemia complementation group C is required for proliferation of murine primordial germ cells. Genesis *27*, 117–123.

Niu, H., Wan, L., Baumgartner, B., Schaefer, D., Loidl, J., and Hollingsworth, N.M. (2005). Partner choice during meiosis is regulated by Hop1-promoted dimerization of Mek1. Mol. Biol. Cell *16*, 5804–5818.

Pacheco, S., Marcet-Ortega, M., Lange, J., Jasin, M., Keeney, S., and Roig, I. (2015). The ATM signaling cascade promotes recombination-dependent pachytene arrest in mouse spermatocytes. PLoS Genet. *11*, e1005017.

Perez, G.I., Knudson, C.M., Leykin, L., Korsmeyer, S.J., and Tilly, J.L. (1997). Apoptosis-associated signaling pathways are required for chemotherapy-mediated female germ cell destruction. Nat. Med. *3*, 1228–1232.

Peters, A.H., Plug, A.W., van Vugt, M.J., and de Boer, P. (1997). A drying-down technique for the spreading of mammalian meiocytes from the male and female germline. Chromosome Res. *5*, 66–68.

Pittman, D.L., Cobb, J., Schimenti, K.J., Wilson, L.A., Cooper, D.M., Brignull, E., Handel, M.A., and Schimenti, J.C. (1998). Meiotic prophase arrest with failure of chromosome synapsis in mice deficient for Dmc1, a germline-specific RecA homolog. Mol. Cell *1*, 697–705.

Reinholdt, L.G., and Schimenti, J.C. (2005). *Mei1* is epistatic to *Dmc1* during mouse meiosis. Chromosoma *114*, 127–134.

Reinholdt, L., Ashley, T., Schimenti, J., and Shima, N. (2004). Forward genetic screens for meiotic and mitotic recombination-defective mutants in mice. Methods Mol. Biol. *262*, 87–107.

Rinaldi, V.D., Hsieh, K., Munroe, R., Bolcun-Filas, E.M., and Schimenti, J.C. (2017). Pharmacological inhibition of the DNA damage checkpoint prevents radiation-induced oocyte death. Genetics. Published online June 2, 2017. http://dx.doi.org/10.1534/genetics.117.203455.

Roeder, G.S., and Bailis, J.M. (2000). The pachytene checkpoint. Trends Genet. *16*, 395–403.

Schindelin, J., Arganda-Carreras, I., Frise, E., Kaynig, V., Longair, M., Pietzsch, T., Preibisch, S., Rueden, C., Saalfeld, S., Schmid, B., et al. (2012). Fiji: an open-source platform for biological-image analysis. Nat. Methods *9*, 676–682.

Schwacha, A., and Kleckner, N. (1997). Interhomolog bias during meiotic recombination: meiotic functions promote a highly differentiated interhomolog-only pathway. Cell *90*, 1123–1135.

Shin, Y.H., Choi, Y., Erdin, S.U., Yatsenko, S.A., Kloc, M., Yang, F., Wang, P.J., Meistrich, M.L., and Rajkovic, A. (2010). *Hormad1* mutation disrupts synaptonemal complex formation, recombination, and chromosome segregation in mammalian meiosis. PLoS Genet. *6*, e1001190.

Shin, Y.H., McGuire, M.M., and Rajkovic, A. (2013). Mouse HORMAD1 is a meiosis i checkpoint protein that modulates DNA double- strand break repair during female meiosis. Biol. Reprod. *89*, 29.

Smith, J., Tho, L.M., Xu, N., and Gillespie, D.A. (2010). The ATM-Chk2 and ATR-Chk1 pathways in DNA damage signaling and cancer. Adv. Cancer Res. *108*, 73–112.

Stambrook, P.J., and Tichy, E.D. (2010). Preservation of genomic integrity in mouse embryonic stem cells. Adv. Exp. Med. Biol. *695*, 59–75.

Stanzione, M., Baumann, M., Papanikos, F., Dereli, I., Lange, J., Ramlal, A., Tränkner, D., Shibuya, H., de Massy, B., Watanabe, Y., et al. (2016). Meiotic DNA break formation requires the unsynapsed chromosome axis-binding protein IHO1 (CCDC36) in mice. Nat. Cell Biol. *18*, 1208–1220.

Subramanian, V.V., and Hochwagen, A. (2014). The meiotic checkpoint network: step-by-step through meiotic prophase. Cold Spring Harb. Perspect. Biol. *6*, a016675.

Subramanian, V.V., MacQueen, A.J., Vader, G., Shinohara, M., Sanchez, A., Borde, V., Shinohara, A., and Hochwagen, A. (2016). Chromosome synapsis alleviates Mek1-dependent suppression of meiotic DNA repair. PLoS Biol. *14*, e1002369.

Suh, E.K., Yang, A., Kettenbach, A., Bamberger, C., Michaelis, A.H., Zhu, Z., Elvin, J.A., Bronson, R.T., Crum, C.P., and McKeon, F. (2006). p63 protects the female germ line during meiotic arrest. Nature *444*, 624–628.

Turner, J.M., Aprelikova, O., Xu, X., Wang, R., Kim, S., Chandramouli, G.V., Barrett, J.C., Burgoyne, P.S., and Deng, C.X. (2004). BRCA1, histone H2AX phosphorylation, and male meiotic sex chromosome inactivation. Curr. Biol. *14*, 2135–2142.

van der Heijden, G.W., and Bortvin, A. (2009). Transient relaxation of transposon silencing at the onset of mammalian meiosis. Epigenetics *4*, 76–79.

Watanabe, N., Mii, S., Asai, N., Asai, M., Niimi, K., Ushida, K., Kato, T., Enomoto, A., Ishii, H., Takahashi, M., and Murakumo, Y. (2013). The REV7 subunit of DNA polymerase ζ is essential for primordial germ cell maintenance in the mouse. J. Biol. Chem. *288*, 10459–10471.

Wojtasz, L., Daniel, K., Roig, I., Bolcun-Filas, E., Xu, H., Boonsanay, V., Eckmann, C.R., Cooke, H.J., Jasin, M., Keeney, S., et al. (2009). Mouse HORMAD1 and HORMAD2, two conserved meiotic chromosomal proteins, are depleted from synapsed chromosome axes with the help of TRIP13 AAA-ATPase. PLoS Genet. *5*, e1000702.

Wojtasz, L., Cloutier, J.M., Baumann, M., Daniel, K., Varga, J., Fu, J., Anastassiadis, K., Stewart, A.F., Reményi, A., Turner, J.M., and Tóth, A. (2012). Meiotic DNA double-strand breaks and chromosome asynapsis in mice are monitored by distinct HORMAD2-independent and -dependent mechanisms. Genes Dev. *26*, 958–973.

STAR★METHODS

KEY RESOURCES TABLE

REAGENT or RESOURCE	SOURCE	IDENTIFIER
Antibodies		
mouse anti-p63	Novus Biologicals	Novus Cat# NB 100-691; RRID: AB_525968
rabbit anti-MVH	Abcam	Abcam Cat# ab13840; RRID: AB_443012
rabbit anti-RAD51 Chip-Grade	Abcam	Abcam Cat# ab176458; RRID: AB_2665405
mouse anti-SYCP3	Abcam	Abcam Cat# ab97672; RRID: AB_10678841
guinea pig anti-HORMAD2	Wojtasz et al., 2012	gift from Dr. Attila Toth
Deposited Data		
Raw images	This paper; Mendeley Data	http://dx.doi.org/10.17632/3n2yfpk4vh.1
Experimental Models: Organisms/Strains		
Mouse: *Trip13*$^{Gt/Gt}$: *Trip13*$^{Gt(RRB047)Byg}$	Li and Schimenti, 2007	RRID:MGI:372059
Mouse: *Dmc1*$^{-/-}$: *Dmc1*^{tm1Jcs}	Pittman et al., 1998	RRID:MGI:3768914
Mouse: *Chk2*$^{-/-}$: *Chk2*^{tm1Mak}	Tak Mak; Hirao et al., 2002	RRID:MGI:2662578
Mouse: *Spo11*$^{-/-}$: *Spo11*^{tm1Mjn}	Maria Jasin; Baudat et al., 2000	RRID:MGI:4358251
Mouse: *Hormad2*$^{-/-}$: *Hormad2*	Kogo et al., 2012a	RRID:MGI:5466572
Software and Algorithms		
JMP Pro12 software v.12.0.1	SAS Inc., Cary, NC-USA	RRID:SCR_014242
Fiji-ImageJ	Schindelin et al., 2012	RRID:SCR_002285

CONTACT FOR REAGENT AND RESOURCE SHARING

Further information and requests for reagents may be directed to and will be fulfilled by the Lead Contact, John Schimenti (jcs92@cornell.edu).

EXPERIMENTAL MODEL AND SUBJECT DETAILS

Experiments were performed on female mice, and of course male mice were used for matings to produce desired genotypes. Samples for histological analysis were from eight week old animals. The alleles used have been previously described and were the following: *Trip13*$^{Gt(RRB047)Byg}$ (referred to as *Trip13*^{Gt} in the manuscript) (Li and Schimenti, 2007); *Dmc1*^{tm1Jcs} (Pittman et al., 1998); *Chk2*^{tm1Mak} (Hirao et al., 2002); *Spo11*^{tm1Mjn} (Baudat et al., 2000); and *Hormad2* (Kogo et al., 2012a). All mice were in a mixed genetic background of strains C57BL/6J and C3H/HeJ. The Cornell's Animal Care and Use Committee approved all animal usage, under protocol 2004-0038 to JCS.

The embryonic age of pre-term animals was counted using the morning in which copulation plug was detected as being the 0.5 days post coitus (dpc).

METHOD DETAILS

Organ Culture and Irradiation

Embryonic and pp explanted ovaries were cultured under conditions as we previously detailed (Rinaldi et al., 2017). Ovaries were irradiated in a ^{137}cesium irradiator with a rotating turntable. Immediately after irradiation, the media was replaced, and ovaries were cultured for indicated periods of time prior to tissue processing.

Histology and Immunostaining

Ovaries were dissected and incubated in Bouin's fixative overnight at room temperature. Afterward, tissues were washed in 70% ethanol prior to being embedded in paraffin for serial sectioning at 6 μm thickness. Ovaries were stained with Harris Hematoxylin and Eosin (H&E) and follicles counted in every fifth section except for the three-week counts reported in Figure 1B, in which every 12th section was counted. There was no correction factor applied to the values reported. Only one ovary per animal was used.

Cultured ovaries, used for histological sections followed by immunostaining, were fixed in 4% paraformaldehyde/PBS over night at 4°C. After 70% ethanol washes, ovaries were embedded in paraffin and serially sectioned at 5 μm. These ovaries were immunostained using standard methods. Briefly, slides were deparaffinized and re-hydrated prior to antigen retrieval using sodium citrate buffer. Slides were blocked with 5% goat serum (PBS/Tween 20) and incubated at 4°C overnight with primary antibodies: mouse anti-p63 (1:500, 4A4, Novus Biologicals); and rabbit anti-MVH (1:1000, Abcam). Afterward, sections were incubated with Alexa Fluor® secondary antibodies for one hour and Hoechst dye for 5 min. Slides were mounted with ProLong Anti-fade (Thermo-Fisher) and imaged.

Histological images were obtained from slides digitized using a Leica Scanscope CS2.

Immunofluorescence of meiotic chromosome surface spreads

Meiotic surface spreads of prophase I female meiocytes were prepared using an adaptation (Reinholdt et al., 2004) of a drying-down technique (Peters et al., 1997) that was described in great detail in the former reference. Meiotic stages (leptonema-diakinesis) were determined based on SYCP3 staining patterns (Gray and Cohen, 2016). Slides were stored at −80°C until immunostained. For staining, slides were brought to room temperature (RT) and washed once with PBS+0.1% Tween-20 (PBS-T). Slides were blocked for 40 min at RT with PBS-T containing 5% normal goat serum (5%GS-PBS-T). Primary antibodies were diluted into 5%GS-PBS-T and incubated overnight at RT in a humidified chamber. Antibodies and dilutions used included: rabbit anti-RAD51 (1:250 Abcam 176458), mouse anti-SYCP3 (1:600 Abcam) and guinea pig anti-HORMAD2 antibody (1:1000, kind gift from Attila Toth). Secondary antibodies used were diluted 1:1000 in in 5%GS-PBS-T and included goat anti-rabbit Alexa 488/594, goat anti-mouse Alexa 488/594 and goat anti-guinea pig Alexa 488/594. Images were taken using an Olympus microscope with 40X lens or 100X immersion oil lens and CCD camera.

Focus Quantification

Foci were quantified both manually, through the visualization and annotation of individual foci, and also semi-automatically using Fiji-ImageJ (Schindelin et al., 2012). Semi-automated counts were performed using binary images obtained from the RAD51-labeled channel, with the threshold set above background level. The count was obtained after performing "Watershed," by the "Analyze Particles" functionality with size set for 1.5 to infinity. Cell counts that displayed discrepancy of more than 20% between manual and semi-automated counts were discarded.

Fertility Test

To test if HORMAD2 deficiency was able to rescue the *Trip13*$^{Gt/Gt}$ sterility phenotype, three double mutant females were mated to WT C3H/HeJ males proven to be fertile through previous matings. Each female provided more than 4 consecutive litters up to the time of preparation of this manuscript. All three females originated from different litters. *Trip13*$^{Gt/Gt}$ littermates were housed with fertile males and used as negative controls.

QUANTIFICATION AND STATISTICAL ANALYSIS

Statistical analysis

Comparisons between compound mutants and controls were done using littermates or related animals. Unless otherwise noted, all experiments used at least three mice per experimental group. All statistical analyses were done using JMP Pro12 software (SAS Inc., Cary, NC-USA, version 12.0.1). Comparisons of fertility and follicle counts between genotypic groups were tested using both the Tukey honest significance different (HSD) and the non-parametric, one-way ANOVA test (Kruskal -Wallis). Both tests provided concordant results. RAD51 focus counts were analyzed using a mixed model with animal ID as random effect and genotype as fixed effect. Least square means (LSMeans) differences were tested using Tukey HSD. The residuals from the mixed model were normally distributed.

DATA AND SOFTWARE AVAILABILITY

Raw data of RAD51 foci counts are in supplementary tables (Table S1, Table S2, and Table S3). The raw image files can be downloaded at Mendeley data: http://dx.doi.org/10.17632/3n2yfpk4vh.1.

Original Article

Cytogenetic and Genome Research

Cytogenet Genome Res
DOI: 10.1159/000481586

Accepted: August 22, 2017
by M. Schmid
Published online: October 27, 2017

Genomic Characterization of Chromosomal Insertions: Insights into the Mechanisms Underlying Chromothripsis

Takema Kato[a] Yuya Ouchi[a, b] Hidehito Inagaki[a, b] Yoshio Makita[g] Seiji Mizuno[c] Mitsuharu Kajita[d] Toshiro Ikeda[e] Kazuhiro Takeuchi[f] Hiroki Kurahashi[a, b]

[a]Division of Molecular Genetics, Institute for Comprehensive Medical Science (ICMS), and [b]Genome and Transcriptome Analysis Center, Fujita Health University, Toyoake, [c]Department of Pediatrics, Central Hospital, Aichi Human Service Center, Kasugai, [d]Department of Pediatrics, Toyota Kosei Hospital, Toyota, [e]Department of Obstetrics and Gynecology, Faculty of Medicine, Kagoshima University, and [f]Takeuchi Ladies Clinic/Infertility Center, Kagoshima, and [g]Education Center, Asahikawa Medical University, Hokkaido, Japan

Keywords
Chromothripsis · Insertion · Trisomy rescue

Abstract
Chromosomal insertions are rare structural rearrangements, and the molecular mechanisms underlying their origin are unknown. In this study, we used whole genome sequencing to analyze breakpoints and junction sequences in 4 patients with chromosomal insertions. Our analysis revealed that none of the 4 cases involved a simple insertion mediated by a 3-chromosomal breakage and rejoining events. The inserted fragments consisted of multiple pieces derived from a localized genomic region, which were shuffled and rejoined in a disorderly fashion with variable copy number alterations. The junctions were blunt ended or with short microhomologies or short microinsertions, suggesting the involvement of nonhomologous end-joining. In one case, analysis of the parental origin of the chromosomes using nucleotide variations within the insertion revealed that maternal chromosomal segments were inserted into the paternal chromosome. This patient also carried both maternal alleles, suggesting the presence of zygotic trisomy. These data indicate that chromosomal shattering may occur in association with trisomy rescue in the early postzygotic stage.

Chromosomal structural rearrangements (CSRs), also known as gross chromosomal rearrangements, are generated by 2 double-strand DNA breaks (DSBs) followed by aberrant DNA repair [Shaffer and Lupski, 2000; Kurahashi et al., 2009]. The DSBs are generally processed by an error-free pathway, called homologous recombination, and repaired properly. However, recurrent CSRs are

T.K. and Y.O. contributed equally to this work.

KARGER

E-Mail karger@karger.com
www.karger.com/cgr

Hiroki Kurahashi, MD, PhD
Division of Molecular Genetics, ICMS
Fujita Health University, 1–98 Dengakugakubo
Toyoake, Aichi 470-1192 (Japan)
E-Mail kura@fujita-hu.ac.jp

caused by genomic instability induced by 2 specific sequences that exist as DSB hotspots [Kato et al., 2012]. Alternatively, DSBs at the segmental duplications are often repaired aberrantly by nonallelic homologous recombination (NAHR), leading to recurrent CSRs [Ou et al., 2011; Hermetz et al., 2012]. In contrast, DSBs that arise randomly are often repaired by an error-prone pathway, nonhomologous end-joining (NHEJ), which leads to nonrecurrent CSRs [Gu et al., 2008]

Recent advances in genomic analysis have provided detailed information on the breakpoints and junction sequences of CSRs and have helped us to understand their origin and mechanism. We now know that replication-based pathways such as fork-stalling and template-switching as well as microhomology-mediated break-induced replication are the major pathways leading to CSRs [Zhang et al., 2009]. The products of these pathways occasionally manifest complex junction structures that include duplication or triplication of the breakpoint proximity. In addition, recent high-resolution microarray and next-generation sequencing studies have found that large numbers of complex chromosomal rearrangements occur in one or a few chromosomes [Holland and Cleveland, 2012]. This catastrophic rearrangement is called chromothripsis. Unfortunately, the precise mechanism that induces the chromosome shattering is still unknown [Kloosterman et al., 2011; Stephens et al., 2011].

Chromosomal insertion, also called insertional translocation, is one of several gross interchromosomal structural rearrangements [Van Hemel and Eussen, 2000]. Insertions involve a translocation of a segment from one chromosome and its insertion as an interstitial region into another nonhomologous chromosome [Weckselblatt and Rudd, 2015]. Balanced carriers are healthy but occasionally have reproductive problems such as infertility, recurrent pregnancy loss, or offspring with multiple congenital anomalies due to an unbalanced insertion. Unbalanced insertions also arise de novo. They are relatively rare CSRs, with an estimated incidence of about 1: 80,000 according to conventional cytogenetic techniques [Van Hemel and Eussen, 2000]. However, 3 recent cohort studies using high-resolution aCGH in conjunction with FISH found a higher incidence than previously estimated [Kang et al., 2010; Neill et al., 2011; Nowakowska et al., 2012].

Little is known about the mechanism of the insertion. It requires at least 3 breaks followed by aberrant repair, but information on the breakpoints and junctions is scarce. One previous study using microarray analysis showed that a small subset of insertions may involve the NAHR pathway, but the etiology of most nonrecurrent insertions is unclear [Neill et al., 2011]. A recent large-scale study using next-generation sequencing of 6 cases with an insertion identified the underlying mechanism leading to the insertion to be a chromothripsis-like replication-related pathway [Gu et al., 2016]. In the present study, we characterized 4 insertion cases via a combination of cytogenetic and genomic techniques such as whole genome sequencing and mate-pair sequencing for the detection of rearrangement breakpoints. We subsequently genotyped the polymorphisms on the relevant chromosomes and determined their parental origin, thereby shedding light on the mechanisms underlying the origin of the insertion.

Case Reports and Results

Case 1

This patient was referred to our facility because of developmental delay. Initial G-banding revealed a 46,XX,add(14)(q32.1) karyotype. We performed cytogenetic microarray analysis and detected a duplication in chromosome 4q and a deletion in 14q. Detailed copy number analysis revealed complex chromosomal rearrangements that included duplications encompassing a 13.1-Mb region at 4q32.1q32.3 and a 0.3-Mb region in 4q35.2, some parts of which appeared to be triplicated, while a 2.7-Mb deletion was found in 14q32.33 (Fig. 1a). Subsequently, using FISH, we found that these copy number variations were due to a chromosomal insertion of 4q32.1q32.3 into 14q32.33 (Fig. 1b). This insertion was not identified in either of the parents and was found to have occurred de novo in the index case.

Next, we performed whole genome sequencing to determine the breakpoints and junctions. LUMPY, a probabilistic structural variant caller, revealed the presence of 6 discordant reads, possibly including the junctions of the rearrangements. To characterize breakpoints at a nucleotide resolution, breakpoint-spanning PCR followed by Sanger sequencing was performed. According to the sequence information of the 6 junctions, the original fragments were shuffled and rejoined in a disorderly manner (Fig. 1c). Some regions were lost, while some appeared twice among the inserted fragments, resulting in triplication. Of the junction sequences identified, 1 involved simple end-joining (junction 1), 2 had microhomology of a few nucleotides (junctions 3 and 6), and 1 had a 4-nucleotide microinsertion (junction 1). The remaining 2 junctions carried insertions consisting of small pieces of a segment derived from the vicinity of the breakpoint region in chromosome 4 (Fig. 1d; junctions 4 and 5). The likely structure is shown in Figure 1d, e.

To determine the parental origin of the chromosomal insertion, we genotyped common SNPs in the related regions of chromosomes 4 and 14 using DNA from the proband and his parents. When we compared the SNP data of the 14q32.33 region deleted in the proband, the proband carried only the maternal allele, supposedly reflecting the normal homolog of chromosome 14. This suggests that the original chromosome 14 of der(14) with the insertion was of paternal origin (Fig. 1f). Following, we genotyped

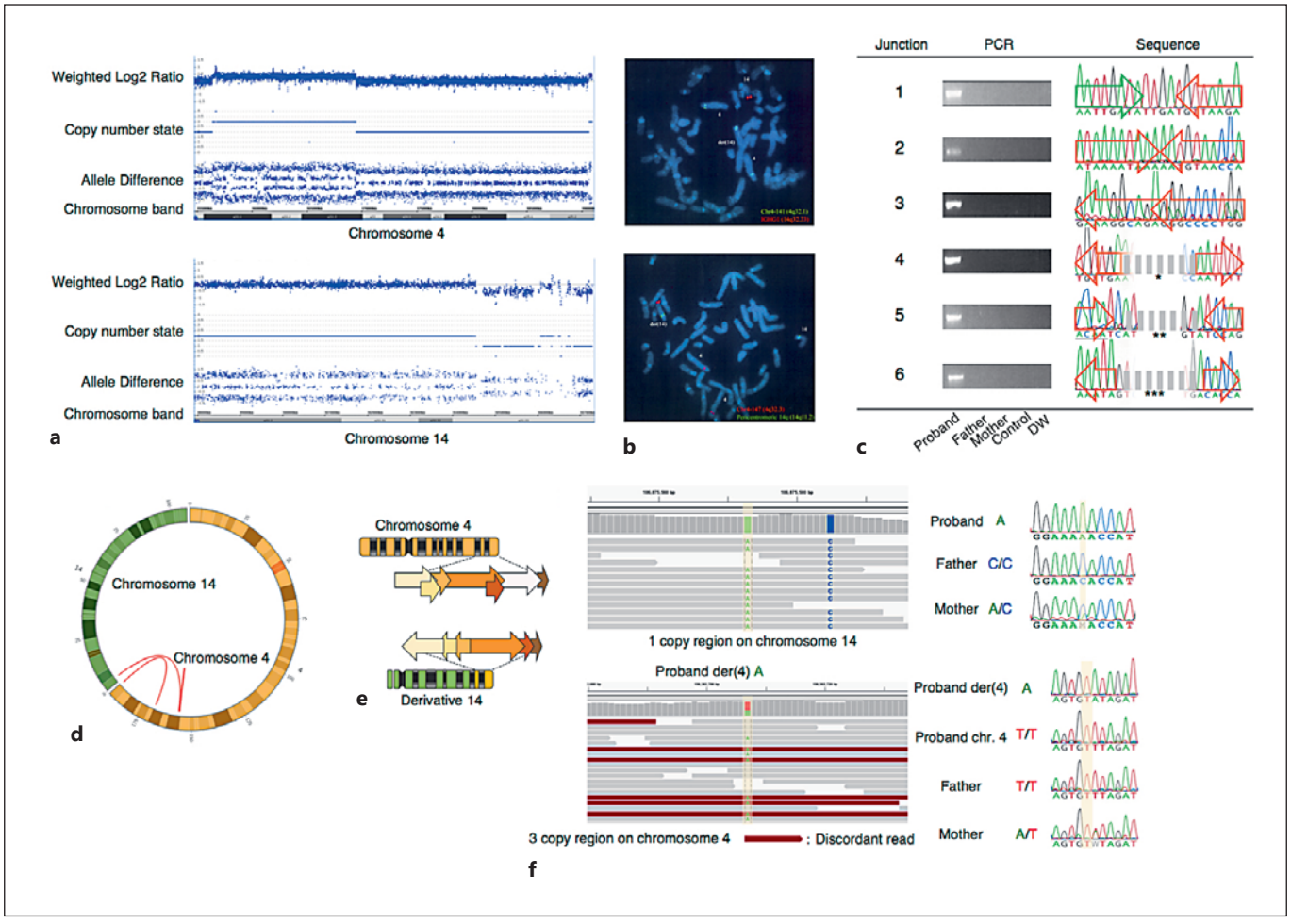

Fig. 1. Analysis of the chromosomal insertion in case 1. **a** Chromosome Analysis Suite (ChAS) graphic results for chromosomes 4 and 14 showing copy number gain and loss, respectively. The results are designated as arr[hg19] 4q32.1q32.3(156,376,846–169,441,822)×3 ~ 4,4q35.2(190,659,209–190,957,473)×3,14q32.33(104,549,511–107,285,437)×1. Although ChAS showed a normal copy number region within the deletion in chromosome 14, FISH analysis did not identify it as a diploid region (data not shown). **b** FISH confirming the deletion in 14q32.33 (red) shown at the top and the insertion of 4q32.3 (red) into the long arm of chromosome 14 (green) shown at the bottom. **c** Breakpoint-specific PCR and its sequence. Green and orange arrows indicate chromosomes 14 and 4, respectively. The distance between the arrows correlates with microhomology or microinsertion. Asterisks indicate the insertion of a few dozen nucleotides. * The gray-dashed line encompasses a 35-nt sequence at position 156,671,582–156,671,616 in chromosome 4 and a 37-nt sequence of unknown origin. ** The gray-dashed line encompasses a 24-nt sequence of unknown origin, a 21-nt sequence at position 156,711,369–156,711,389 in chromosome 4 with inverted orientation, and a 34-nt sequence of unknown origin. *** The gray-dashed line encompasses a 25-nt sequence of unknown origin. **d** The detected chromosomal rearrangements are visualized by a Circos plot using ClicO FS. **e** Multiple segments in chromosome 4 were shuffled and inserted into chromosome 14. Some of the segments were missing or duplicated during the rearrangements. **f** An example of a parent-of-origin analysis. The top shows the vicinity of the breakpoint, and the bottom shows a deleted region in chromosome 14. Discordant reads (dark red) and SNPs (light green and blue) are visualized by different colors. SNP genotyping was conducted by Sanger sequencing. SNPs are superimposed on the yellow background.

the SNPs within the insertional region in chromosome 4. The inserted segments were found to originate from the maternal chromosome. This indicates a postzygotic origin of the insertion. Furthermore, the proband was found to have 2 normal chromosomes 4, one paternal and the other maternal, and this normal maternal chromosome 4 was revealed to be a different allele from the inserted segments of maternal origin. Thus, it is suggested that 2 normal chromosomes 4 were transmitted from the mother and one from the father and that one of the maternal chromosomes 4 was then shattered and integrated into the paternal chromosome 14 in the early postzygotic stage in the trisomic zygote (Fig. 5a).

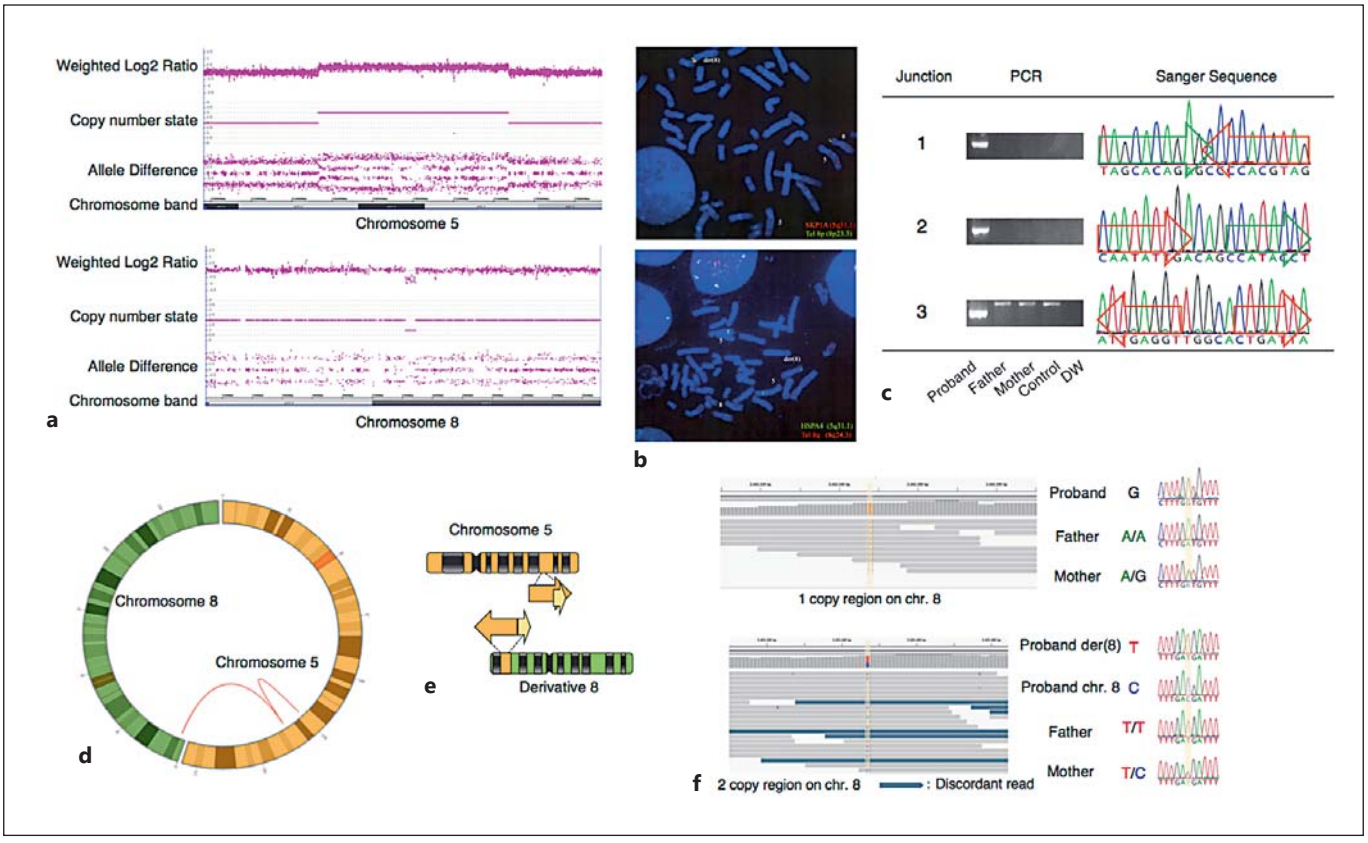

Fig. 2. Analysis of the chromosomal insertion in case 2. **a** Copy number abnormalities in chromosomes 5 and 8 are graphically displayed using ChAS. Positional information on the copy number change is designated as arr[hg19] 5q23.2q31.1(125,311,267–134,731,795)×3,8p23.2(2,421,059–2,488,315)×1. **b** FISH analysis confirming the insertion of 5q31.1 (red) into the vicinity of 8p23.3. **c** Breakpoint-specific PCR and its sequence. The analysis was performed as described in Figure 1. Orange and green arrows indicate chromosomes 5 and 8, respectively. The distance between the arrows corresponds to microhomology or microinsertion. **d** The detected chromosomal rearrangements are visualized by a Circos plot using ClicO FS. **e** Two segments in chromosome 5 were shuffled and translocated into chromosome 8. One segment completely overlaps another segment. **f** SNP-based parental origin determination. The top shows the 1-copy region in chromosome 8, whereas the bottom shows the 2-copy region in chromosome 8. The details are the same as those provided in Figure 1. Discordant reads are shown in dark blue. SNPs used for analysis are presented on a yellow background.

Case 2

This case was referred to our facility for the examination of postnatal short stature. Initial G-banding revealed a 46,XX,add(8)(p22) karyotype. Cytogenetic microarray data showed that the patient had both a duplication at 5q23.2q31.1 and a deletion in chromosome 8p23.2 (Fig. 2a). FISH analysis showed that the interstitial chromosome 8p23.2 deletion was due to an insertion at chromosome 5q23.2q31.1 (Fig. 2b). This insertion was not identified in either of the parents and was thus determined to have occurred de novo in the index case.

To identify the deletion and insertion breakpoints, we applied LUMPY to the whole genome sequencing data. Three breakpoints were found and validated by PCR and Sanger sequencing. One breakpoint was between the 5q regions, while the others were rejoined between chromosomes 5 and 8 but with different orientations. The inserted 5q chromosome comprised 2 segments in chromosome 5, one large segment spanning from 125,317,703 to 134,732,368 and the other spanning from 134,730,551 to 134,731,048. This suggests that smaller 497-bp fragments were triplicated and inserted adjacent to the larger insertion in an inverted orientation. Similar to case 1, one junction had a 2-nucleotide microhomology (junction 1), whereas 2 junctions had microinsertions of an unknown origin (Fig. 2c; junctions 2 and 3). The likely structure is shown in Figure 2d, e.

SNP genotyping of the deleted region in chromosome 8 showed that the paternal chromosome 8p23.2 was deleted and that the normal chromosome 8 was of maternal origin. In addition, the inserted 5q segments originated from the paternal chromosome, suggesting that the paternal fragment from chromosome 5 was integrated into the paternal chromosome 8 (Fig. 2f). However, the inserted 5q segments were different from the normal paternal homologue chromosome, indicating the presence of 2 paternal 5q chromosomes. This suggests that one of the paternal chromosomes 5 was shattered and integrated into the paternal chromo-

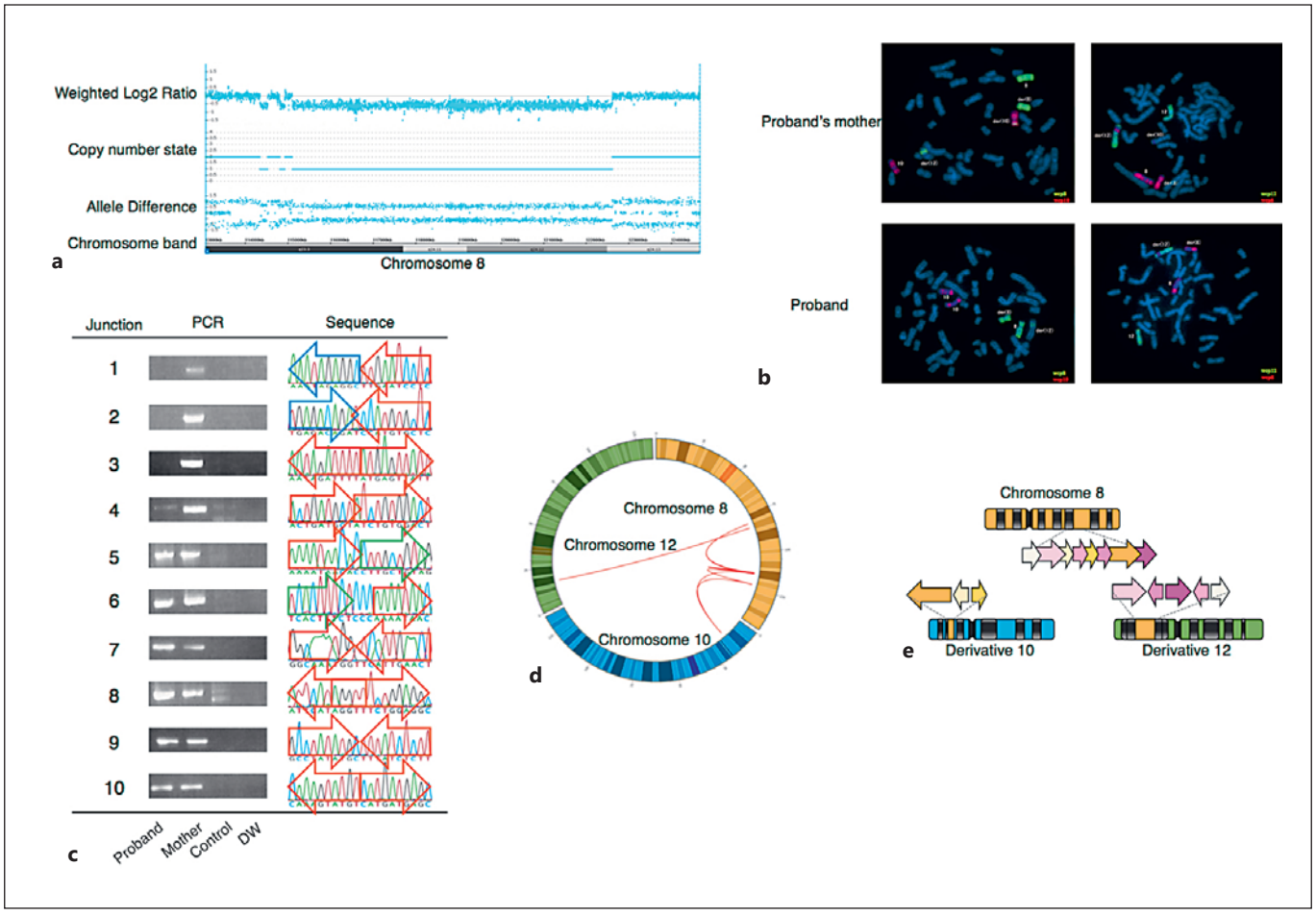

Fig. 3. Analysis of the chromosomal insertion in case 3. **a** Analysis of copy number state using ChAS software revealed that the proband had 3 distinct deletions in chromosome 10. The copy number change was designated as arr[hg19] 8q23.3(114,340,065–114,527,620)×1, arr[hg19] 8q23.3(114,806,300–114,925,879)×1, arr[hg19] 8q23.3q24.13(115,101,169–122,616,401)×1. **b** FISH analysis of the proband's mother with whole chromosome painting of chromosomes 8, 10, and 12 confirms the insertion of chromosome 8 into chromosomes 10 and 12. FISH analysis of the proband confirming the insertion of chromosome 8 into chromosome 12. **c** PCR validation of a discordant read. The details are the same as those provided in Figure 1. Orange arrows show chromosome 8, blue arrows show chromosome 10, and green arrows show chromosome 12. The distance between the arrows corresponds to microhomology or microinsertion. **d** The detected chromosomal rearrangements are visualized by a Circos plot using ClicO FS. **e** A number of segments in chromosome 8 were shuffled and translocated into chromosomes 10 and 12. There may be uncharacterized breakpoints in the region of chromosome 8 of the derivative chromosome 12.

some 8p in the premeiotic stage, during MII, or in the postzygotic stage in the trisomic zygote (Fig. 5b).

Case 3

This patient was referred to our facility for the diagnosis of Langer-Giedion syndrome. Initial G-banding revealed a 46,XY,der(12)ins(12;8)(p12;q21q23) karyotype. CytoScan HD array analysis showed that the proband had a deletion at chromosome 8q23.3q24.13 (Fig. 3a). The mother of the proband was 46,XX (data not shown). FISH with whole chromosome painting probe analysis revealed that she had a balanced insertion that involved chromosomes 8, 10, and 12. The long arm of chromosome 8 was found to be inserted into chromosomes 10 and 12. The proband inherited only der(8) and der(12), not der(10), resulting in the deletion of chromosome bands 8q23.3q24.13 and causing Langer-Giedion syndrome (Fig. 3b).

Breakpoint analysis of the chromosomal rearrangements allowed us to identify 10 discordant reads. Of these, 6 junctions were detected in both proband and maternal DNA (junctions 5–10), whereas the remaining 4 were not detected in the proband (junctions 1–4), suggesting that 6 junctions are in der(8) and der(12), and 4 are in der(10) (Fig. 3c). The inserted chromosome 8 regions consisted of pieces of segments, which were shuffled, rejoined in direct or inverted orientation, and inserted into either chromosome 10 or 12. Six junctions of rearrangements involved simple end-joining (junctions 1, 3, 5, 7, 9, and 10), and the remaining 4

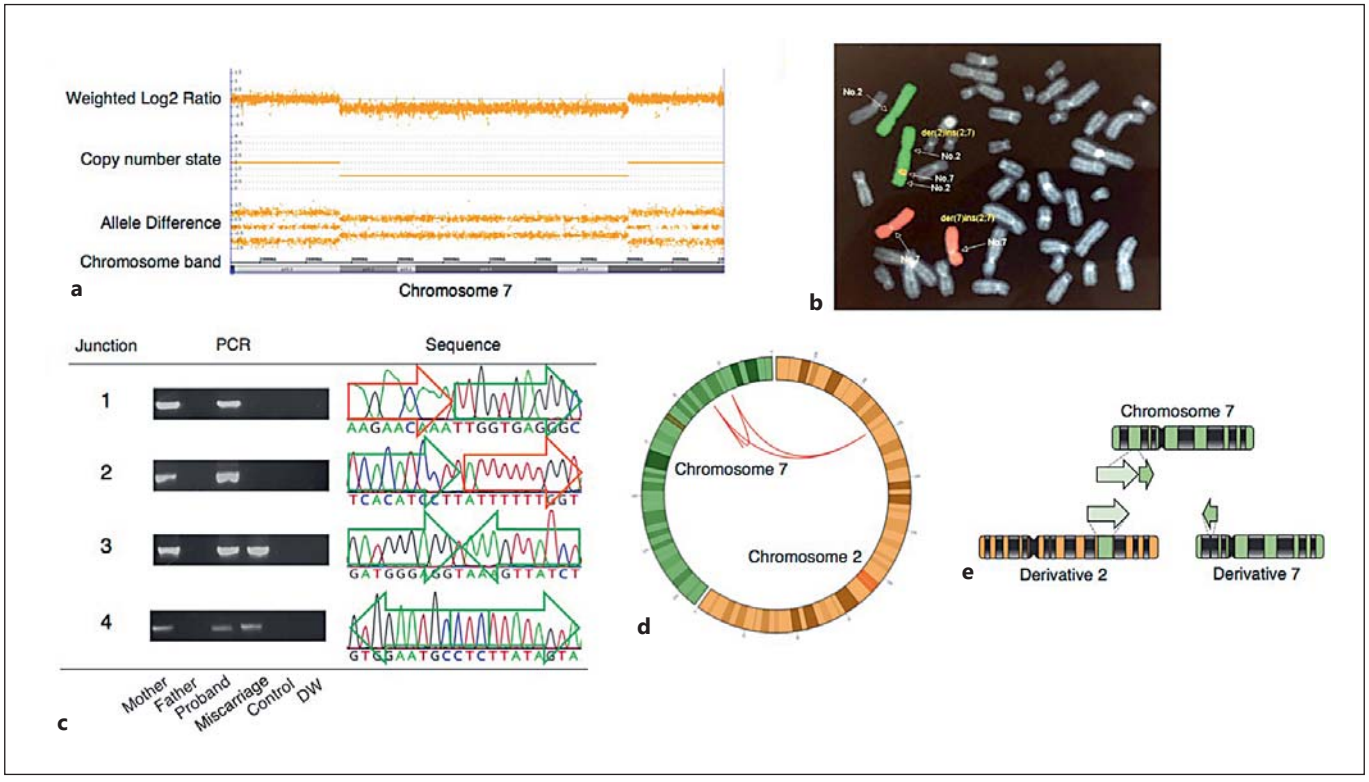

Fig. 4. Analysis of the chromosomal insertion in case 4. **a** The fetus has a copy number loss in chromosome 7. The genomic position of the copy number change is arr[hg19] 7p15.3p14.1 (25,471,046–38,067,611)×1. **b** Whole chromosome painting of chromosomes 2 (green) and 7 (red) showing the insertion from chromosome 7 into band 2q. **c** PCR confirmation of a discordant read. The details are the same as those provided in Figure 1. Orange and green arrows indicate chromosomes 2 and 7, respectively. The distance between the arrows corresponds to microhomology or microinsertion. **d** The detected chromosomal rearrangements are visualized by a Circos plot using ClicO FS. **e** Two pieces of segments in chromosome 7 were inserted into chromosomes 2 and 7.

junctions had either microhomology (junctions 2 and 4) or microinsertion (junction 6). The likely structure is shown in Figure 3d, e.

Because we did not obtain the parental sample of the mother, who was a carrier of a balanced insertion, we could not analyze the origin of the insertion.

Case 4

This patient was referred to our facility because of recurrent pregnancy loss. The initial G-banded karyotype was 46,XY,ins(2;7)(q31;p11.2p13). We confirmed the balanced insertion of the proband by whole chromosome painting (Fig. 4b). Cytogenetic microarray analysis revealed that the aborted fetus of the proband had a deletion at 7p15.3p14.1 (Fig. 4a).

Breakpoint analysis of chromosomal rearrangements allowed us to identify discordant reads. Four discordant reads were discovered by LUMPY and validated by junction-specific PCR and Sanger sequencing. Two junctions formed by rejoining between chromosomes 2q and 7p were identified only in the proband, not in the fetus (junctions 1 and 2), whereas the remaining 2 junctions composed of 7p rejoined in an inverted orientation were identified in both the proband and fetus (Fig. 4c; junctions 3 and 4). These results suggest that the fragments of 7p were divided into 2 pieces, one inserted into 2q and the other inserted into the same 7p region but in the opposite direction (Fig. 4d). Three were blunt-end rejoined junctions (junctions 1–3) and 1 had a 3-nucleotide microhomology (junction 4). The likely structure is shown in Figure 4d, e.

Junction-spanning PCR showed that the proband's mother also had a balanced insertion. Because we did not obtain samples from the grandparents, we could not analyze the origin of the insertion.

Materials and Methods

We obtained blood from the patients and their family members. Genomic DNA was extracted using standard procedures. We analyzed 4 patients with an unbalanced chromosomal insertion and their relatives in this study.

Cytogenetic Analyses of Chromosomal Insertions

Individuals with a chromosomal insertion were identified by FISH and SNP array analysis. FISH analysis was performed on metaphase spreads or interphase nuclei from the patients and their

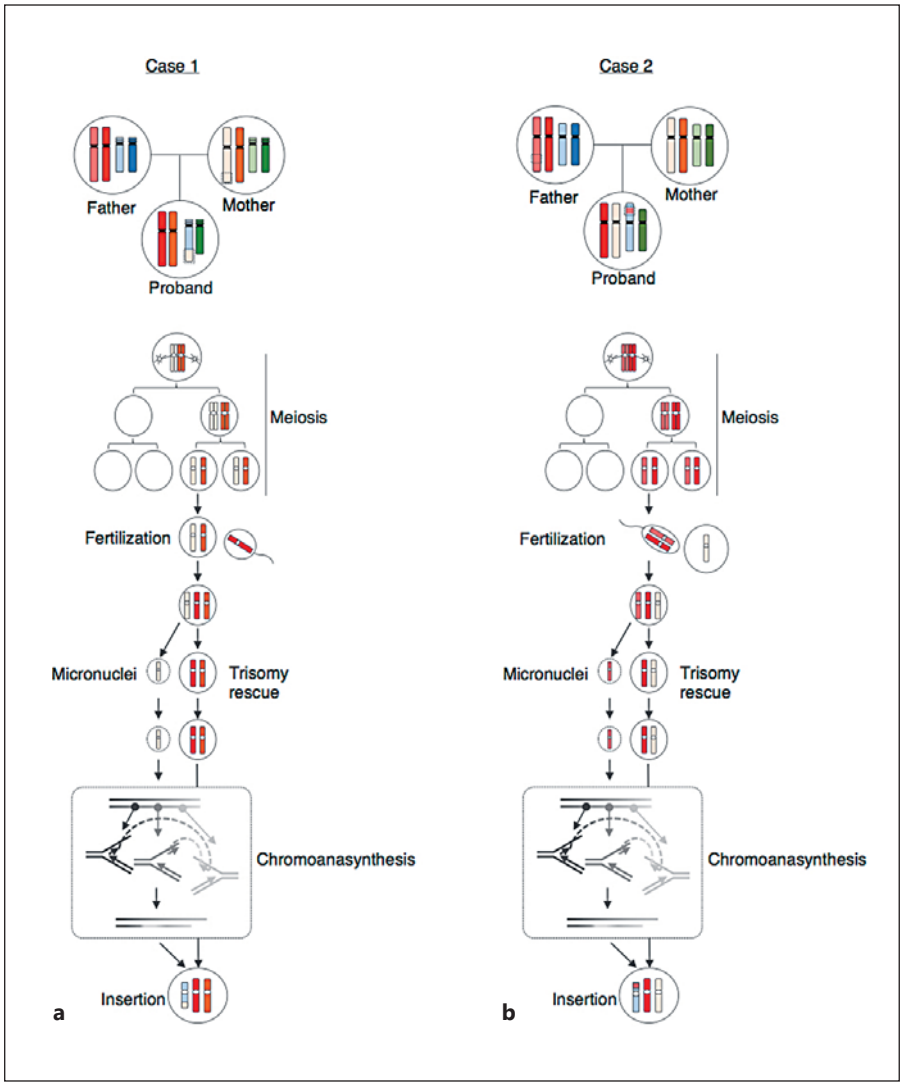

Fig. 5. The parental origin of chromosomal rearrangements reveals the mechanism of chromosomal insertion. Parent-of-origin analysis diagrams are shown at the top. Each chromosome is shown in a different color. A trisomic chromosome resulting from malsegregation in meiosis was corrected by subsequent anaphase lagging during an early embryonic stage.

parents, obtained by standard protocols using appropriate region-specific probes and whole chromosome painting probes. SNP array was performed using a CytoScan HD Array Kit (Affymetrix, Santa Clara, CA, USA) for high-resolution analysis of copy number variations and determination of the genotypes of derivative chromosomes. The genome coordinates were based on hg19 in this manuscript.

Breakpoint Characteristics of Chromosomal Insertions by Next-Generation Sequencing

Mate-pair or paired-end whole genome sequencing was performed to detect the breakpoints of chromosomal rearrangements. Libraries were prepared using a Nextera Mate Pair Library Preparation Kit or TruSeq DNA PCR-Free Library Preparation Kit (Illumina, San Diego, CA, USA) according to the manufacturer's protocol. For preparation of the mate-pair library, fragments of 9 kb in length were extracted. Libraries for next-generation sequencing analysis were then subjected to 2 × 100-bp paired-end sequencing on a HiSeq 1500 platform (Illumina). Sequence data were demultiplexed using bcl2fastq-1.8.4 (Illumina). In the mate-pair sequence case, duplex reads were trimmed using NxTrim [O'Connell et al., 2015]. Sequence reads were then mapped onto the human reference hg19 using BWA 0.7.10 [Li and Durbin, 2010]. Sorting and recalibration of the mapped reads were done using SAMtools 0.1.19 and GATK 3.3-0 [Li et al., 2009; McKenna et al., 2010]. LUMPY was used to identify putative breakpoints of chromosomal rearrangements [Layer et al., 2014]. We focused on discordant reads in the vicinity of the breakpoint junction from FISH and SNP array information. All putative breakpoints were confirmed by visual inspection using the Integrative Genomics Viewer and breakpoint-spanning PCR [Thorvaldsdóttir et al., 2013]. The detected structural variants were visualized by a Circos plot using ClicO FS [Cheong et al., 2015]. PCR was performed with appropriate primer sets and conditions using TaKaRa Ex Taq DNA polymerase (Takara Bio, Otsu, Japan). Sanger sequencing of breakpoint-spanning PCR fragments was carried out using an ABI3130xl sequencer (Life Technologies, Foster City, CA, USA).

SNP-Based Parental Origin Determination

To determine the parental origin of the chromosomal rearrangement, genotype information from derivative chromosome-specific PCR, SNP array, or whole genome sequencing was compared with that of the parental genotype.

Discussion

In this study, we analyzed chromosomal insertions in 4 individuals. We found that the chromosomal insertions in all 4 cases were not generated by simple inaccurate repair of 3 DSBs, but showed structural complexity. Many pieces of genomic fragments derived from a highly localized chromosomal region were reconstructed in a disorderly array associated with copy number alterations. A recent study of 6 insertion cases also showed similar results [Gu et al., 2016]. The insertion of similar highly shuffled chromosomal segments was also documented in another subset of CSRs, namely, unbalanced translocations [Weckselblatt et al., 2015]. Thus, CSRs, even when observed as a simple rearrangement in conventional karyotyping, are actually more complex than we thought.

Such localized complex CSRs have been termed chromoanagenesis [Holland and Cleveland, 2012; Zhang et al., 2013]. Chromoanagenesis includes 2 different concepts, chromothripsis and chromoanasynthesis. Chromothripsis is a local chromosome shattering and restitching by NHEJ, whereas chromoanasynthesis is a replication-based complex rearrangement that involves fork-stalling and template-switching as well as microhomology-mediated break-induced replication [Zhang et al., 2009; Kloosterman et al., 2011; Stephens et al., 2011]. Our data show that chromosomal insertions include regions of more than 4 copies in diploid cells, which is not compatible with the definition of chromothripsis (an alteration of 2 copy number states), but rather implies the involvement of a replication-mediated complex rearrangement mechanism. On the other hand, junction analysis showed that the junctions were blunt ended or with short microhomologies or short microinsertions in junction sequences. This conversely implicates the involvement of NHEJ, which is a characteristic of chromothripsis. Given that micronucleus-related chromosome shattering is a mechanism for the origin of chromothripsis, chromosome replication in the micronucleus is not synchronous with that in the nucleus, suggesting that a variable copy number is acceptable in chromothripsis [Crasta et al., 2012; Ly et al., 2017]. Thus, this micronucleus-related chromothripsis pathway may possibly be the mechanism that leads to chromosomal insertion.

Determination of the parental origin of a de novo insertion can shed light on the timing and mechanisms of its formation. In general, de novo constitutional structural rearrangements are predominantly of paternal origin [Thomas et al., 2010]. However, we showed compound paternal and maternal rearrangements in case 1, suggesting a postzygotic origin of the insertion. Such postzygotic CSRs of both parental chromosomes are also observed in de novo unbalanced translocations [Robberecht et al., 2013]. Furthermore, surprisingly, case 1 may have undergone trisomy rescue in the postzygotic stage as evidenced by the presence of 2 maternal and 1 paternal chromosomes. Even in case 2, the presence of 2 paternal chromosomes suggested that the insertion may have arisen in the premeiotic stage or, possibly, in the postzygotic stage in the trisomic zygote. These data imply that the trisomic fertilization may precede the chromothripsis event and be followed by trisomy rescue in the early postzygotic stage, resulting in insertion. [Conlin et al., 2010; Taylor et al., 2014]. Micronuclei formed from anaphase-lagging chromosomes may predispose a pulverized insertion due to low stringency at the spindle checkpoint in this embryonic stage [Mertzanidou et al., 2013]. To conclude, further studies involving higher sample numbers may elucidate a more precise understanding of the mechanisms underlying the etiology of chromosomal insertions.

Acknowledgments

We thank the patients and their families who participated in this study. We also thank Drs. Kazuhiro Matsuda and Masanobu Ito for providing samples as well as Ms. Makiko Tsutsumi, Naoko Fujita, and Asami Kuno for technical assistance. This study was supported by a Grant-in-Aid for Scientific Research from the Ministry of Education, Culture, Sports, Science, and Technology of Japan (15K19042 to T.K., 15H04710 and 24390085 to H.K.) and from the Ministry of Health, Welfare and Labor (16ek0109067h0003 to H.K.).

Statement of Ethics

This study was approved by the Ethical Review Board for Human Genome Studies at the Fujita Health University. Written informed consent was obtained from the patients. All experiments were carried out in accordance with the relevant guidelines and regulations.

Disclosure Statement

The authors have no conflicts of interest to declare.

References

Cheong WH, Tan YC, Yap SJ, Ng KP: ClicO FS: an interactive web-based service of Circos. Bioinformatics 31:3685–3687 (2015).

Conlin LK, Thiel BD, Bonnemann CG, Medne L, Ernst LM, et al: Mechanisms of mosaicism, chimerism and uniparental disomy identified by single nucleotide polymorphism array analysis. Hum Mol Genet 19:1263–1275 (2010).

Crasta K, Ganem NJ, Dagher R, Lantermann AB, Ivanova EV, et al: DNA breaks and chromosome pulverization from errors in mitosis. Nature 482:53–58 (2012).

Gu S, Szafranski P, Akdemir ZC, Yuan B, Cooper ML, et al: Mechanisms for complex chromosomal insertions. PLoS Genet 12:e1006446 (2016).

Gu W, Zhang F, Lupski JR: Mechanisms for human genomic rearrangements. Pathogenetics 1:4 (2008).

Hermetz KE, Surti U, Cody JD, Rudd MK: A recurrent translocation is mediated by homologous recombination between HERV-H elements. Mol Cytogenet 5:6 (2012).

Holland AJ, Cleveland DW: Chromoanagenesis and cancer: mechanisms and consequences of localized, complex chromosomal rearrangements. Nat Med 18:1630–1638 (2012).

Kang SH, Shaw C, Ou Z, Eng PA, Cooper ML, et al: Insertional translocation detected using FISH confirmation of array-comparative genomic hybridization (aCGH) results. Am J Med Genet A 152A:1111–1126 (2010).

Kato T, Kurahashi H, Emanuel BS: Chromosomal translocations and palindromic AT-rich repeats. Curr Opin Genet Dev 22:221–228 (2012).

Kloosterman WP, Guryev V, van Roosmalen M, Duran KJ, de Bruijn E, et al: Chromothripsis as a mechanism driving complex de novo structural rearrangements in the germline. Hum Mol Genet 20:1916–1924 (2011).

Kurahashi H, Bolor H, Kato T, Kogo H, Tsutsumi M, et al: Recent advance in our understanding of the molecular nature of chromosomal abnormalities. J Hum Genet 54:253–260 (2009).

Layer RM, Chiang C, Quinlan AR, Hall IM: LUMPY: a probabilistic framework for structural variant discovery. Genome Biol 15:R84 (2014).

Li H, Durbin R: Fast and accurate long-read alignment with Burrows-Wheeler transform. Bioinformatics 26:589–595 (2010).

Li H, Handsaker B, Wysoker A, Fennell T, Ruan J, et al: The sequence alignment/map format and SAMtools. Bioinformatics 25:2078–2079 (2009).

Ly P, Teitz LS, Kim DH, Shoshani O, Skaletsky H, et al: Selective Y centromere inactivation triggers chromosome shattering in micronuclei and repair by non-homologous end joining. Nat Cell Biol 19:68–75 (2017).

McKenna A, Hanna M, Banks E, Sivachenko A, Cibulskis K, et al: The Genome Analysis Toolkit: a MapReduce framework for analyzing next-generation DNA sequencing data. Genome Res 20:1297–1303 (2010).

Mertzanidou A, Spits C, Nguyen HT, Van de Velde H, Sermon K: Evolution of aneuploidy up to Day 4 of human preimplantation development. Hum Reprod 28:1716–1724 (2013).

Neill NJ, Ballif BC, Lamb AN, Parikh S, Ravnan JB, et al: Recurrence, submicroscopic complexity, and potential clinical relevance of copy gains detected by array CGH that are shown to be unbalanced insertions by FISH. Genome Res 21:535–544 (2011).

Nowakowska BA, de Leeuw N, Ruivenkamp CA, Sikkema-Raddatz B, Crolla JA, et al: Parental insertional balanced translocations are an important cause of apparently de novo CNVs in patients with developmental anomalies. Eur J Hum Genet 20:166–170 (2012).

O'Connell J, Schulz-Trieglaff O, Carlson E, Hims MM, Gormley NA, Cox AJ: NxTrim: optimized trimming of Illumina mate pair reads. Bioinformatics 31:2035–2037 (2015).

Ou Z, Stankiewicz P, Xia Z, Breman AM, Dawson B, et al: Observation and prediction of recurrent human translocations mediated by NAHR between nonhomologous chromosomes. Genome Res 21:33–46 (2011).

Robberecht C, Voet T, Zamani Esteki M, Nowakowska BA, Vermeesch JR: Nonallelic homologous recombination between retrotransposable elements is a driver of de novo unbalanced translocations. Genome Res 23:411–418 (2013).

Shaffer LG, Lupski JR: Molecular mechanisms for constitutional chromosomal rearrangements in humans. Annu Rev Genet 34:297–329 (2000).

Stephens PJ, Greenman CD, Fu B, Yang F, Bignell GR, et al: Massive genomic rearrangement acquired in a single catastrophic event during cancer development. Cell 144:27–40 (2011).

Taylor TH, Gitlin SA, Patrick JL, Crain JL, Wilson JM, Griffin DK: The origin, mechanisms, incidence and clinical consequences of chromosomal mosaicism in humans. Hum Reprod Update 20:571–581 (2014).

Thomas NS, Morris JK, Baptista J, Ng BL, Crolla JA, Jacobs PA: De novo apparently balanced translocations in man are predominantly paternal in origin and associated with a significant increase in paternal age. J Med Genet 47:112–115 (2010).

Thorvaldsdóttir H, Robinson JT, Mesirov JP: Integrative Genomics Viewer (IGV): high-performance genomics data visualization and exploration. Brief Bioinform 14:178–192 (2013).

Van Hemel JO, Eussen HJ: Interchromosomal insertions. Hum Genet 107:415–432 (2000).

Weckselblatt B, Rudd MK: Human structural variation: mechanisms of chromosome rearrangements. Trends Genet 31:587–599 (2015).

Weckselblatt B, Hermetz KE, Rudd MK: Unbalanced translocations arise from diverse mutational mechanisms including chromothripsis. Genome Res 25:937–947 (2015).

Zhang CZ, Leibowitz ML, Pellman D: Chromothripsis and beyond: rapid genome evolution from complex chromosomal rearrangements. Genes Dev 27:2513–2530 (2013).

Zhang F, Carvalho CMB, Lupski JR: Complex human chromosomal and genomic rearrangements. Trends Genet 25:298–307 (2009).

Original Article

Cytogenetic and Genome Research

Cytogenet Genome Res
DOI: 10.1159/000455026

Accepted: August 16, 2016
by M. Schmid
Published online: January 19, 2017

Complex X-Chromosomal Rearrangements in Two Women with Ovarian Dysfunction: Implications of Chromothripsis/Chromoanasynthesis-Dependent and -Independent Origins of Complex Genomic Alterations

Erina Suzuki[a] Hirohito Shima[a] Machiko Toki[b] Kunihiko Hanew[c] Keiko Matsubara[a] Hiroki Kurahashi[d] Satoshi Narumi[a] Tsutomu Ogata[a, e] Tsutomu Kamimaki[b, f] Maki Fukami[a]

[a]Department of Molecular Endocrinology, National Research Institute for Child Health and Development, Tokyo, [b]Department of Pediatrics, Hiratsuka City Hospital, Hiratsuka, [c]Hanew Endocrine Clinic, Sendai, [d]Division of Molecular Genetics, Institute for Comprehensive Medical Science, Fujita Health University, Toyoake, [e]Department of Pediatrics, Hamamatsu University School of Medicine, Hamamatsu, and [f]Department of Pediatrics, Shizuoka City Shimizu Hospital, Shizuoka, Japan

Keywords

Chromothripsis · Genomic rearrangement · Isochromosome · Turner syndrome · X inactivation

Abstract

Our current understanding of the phenotypic consequences and the molecular basis of germline complex chromosomal rearrangements remains fragmentary. Here, we report the clinical and molecular characteristics of 2 women with germline complex X-chromosomal rearrangements. Patient 1 presented with nonsyndromic ovarian dysfunction and hyperthyroidism; patient 2 exhibited various Turner syndrome-associated symptoms including ovarian dysfunction, short stature, and autoimmune hypothyroidism. The genomic abnormalities of the patients were characterized by array-based comparative genomic hybridization, high-resolution karyotyping, microsatellite genotyping, X-inactivation analysis, and bisulfite sequencing. Patient 1 carried a rearrangement of unknown parental origin with a 46,X,der(X)(pter→p22.1::p11.23→q24::q21.3→q24::p11.4→pter) karyotype, indicative of a catastrophic chromosomal reconstruction due to chromothripsis/chromoanasynthesis. Patient 2 had a paternally derived isochromosome with a 46,X,der(X)(pter→p22.31::q22.1→q10::q10→q22.1::p22.31→pter) karyotype, which likely resulted from 2 independent, sequential events. Both patients showed completely skewed X inactivation. CpG sites at Xp22.3 were hypermethylated in patient 2. The results indicate that germline complex X-chromosomal rearrangements underlie nonsyndromic ovarian dysfunction and Turner syndrome. Disease-causative mechanisms of these rearrangements likely include aberrant DNA methylation, in addition to X-chromosomal mispairing and haplo-

E.S., H.S., and M.T. contributed equally to this study.

1424–8581/17/0000–0000$39.50/0

E-Mail karger@karger.com
www.karger.com/cgr

Maki Fukami
National Research Institute for Child Health and Development
2-10-1 Okura, Setagaya
Tokyo 157-8535 (Japan)
E-Mail fukami-m@ncchd.go.jp

insufficiency of genes escaping X inactivation. Notably, our data imply that germline complex X-chromosomal rearrangements are created through both chromothripsis/chromoanasynthesis-dependent and -independent processes.

Complex chromosomal rearrangements are common in cancer genomes and can also appear in the germline [Liu et al., 2011; Kloosterman and Cuppen, 2013]. To date, germline complex rearrangements have been identified in a small number of individuals [Liu et al., 2011; Ochalski et al., 2011; Auger et al., 2013; Kloosterman and Cuppen, 2013; Plaisancié et al., 2014]. Of these, complex autosomal rearrangements were often associated with congenital malformations and mental retardation, which probably reflect dysfunction or dysregulation of multiple genes on the affected chromosome [Liu et al., 2011; Kloosterman and Cuppen, 2013; Plaisancié et al., 2014]. In contrast, complex X-chromosomal rearrangements were detected primarily in women with nonsyndromic ovarian dysfunction and were occasionally associated with other clinical features such as short stature, muscular hypotonia, and an unmasked X-linked recessive disorder [Ochalski et al., 2011; Auger et al., 2013]. The lack of severe developmental defects in women with complex X-chromosomal rearrangements is consistent with prior observations that structurally abnormal X chromosomes, except for X;autosome translocations, frequently undergo selective X inactivation [Heard et al., 1997]. The clinical features of these women, such as ovarian dysfunction and short stature, are ascribable to X-chromosomal mispairing and haploinsufficiency of genes that escape X inactivation [Zhong and Layman, 2012]. Mutations in *BMP15* at Xp11.22, *POF1B* at Xq21.1, *DIAPH2* at Xq21.33, or *PGRMC1* at Xq24 have been shown to lead to ovarian dysfunction, while mutations in *SHOX* at Xp22.33 impair skeletal growth [Bione et al., 1998; Bione and Toniolo, 2000; Mansouri et al., 2008; Zhong and Layman, 2012]. However, considering the limited number of reported cases, further studies are necessary to clarify the phenotypic characteristics of germline complex X-chromosomal rearrangements. Furthermore, it remains uncertain whether such rearrangements perturb DNA methylation of the affected X chromosomes.

Recent studies revealed that complex genomic rearrangements are caused by catastrophic cellular events referred to as chromothripsis and chromoanasynthesis [Liu et al., 2011; Pellestor, 2014; Leibowitz et al., 2015; Zhang et al., 2015]. Chromothripsis is characterized by massive DNA breaks in a single or a few chromosomes followed by random reassembly of the DNA fragments [Liu et al., 2011; Pellestor, 2014; Zhang et al., 2015]. Chromothripsis is predicted to arise from micronucleus-mediated DNA breakage of mis-segregated chromosomes, although several other mechanisms such as telomere erosion, p53 inactivation, and abortive apoptosis have also been implicated [Liu et al., 2011; Pellestor, 2014; Zhang et al., 2015]. Chromothripsis typically results in copy-number-neutral translocations/inversions or rearrangements with copy number loss; however, in some cases, genomic rearrangements with copy number gain have also been linked to chromothripsis [Liu et al., 2011; Pellestor, 2014]. Copy number gains in these cases are ascribed to replication-based errors during chromosomal reassembly [Liu et al., 2011]. Chromoanasynthesis is proposed to arise from serial template switching during DNA replication [Leibowitz et al., 2015]. Chromoanasynthesis has been reported as a cause of complex rearrangements with duplications and triplications [Leibowitz et al., 2015]. To date, the clinical significance of germline chromothripsis/chromoanasynthesis has not been fully determined. In particular, it remains unknown whether these catastrophic events account for all cases of complex rearrangements in the germline. Here, we report the clinical and molecular characteristics of 2 women with complex X-chromosomal rearrangements.

Patients and Methods

Patients

Patients 1 and 2 were unrelated Japanese women. Patient 1 was hitherto unreported, while patient 2 was previously reported as a female with Turner syndrome [Uehara et al., 2001]. Both patients underwent G-banding analysis in endocrine clinics and were found to have X-chromosomal rearrangements. Thus, they were referred to our institute for further investigation.

Molecular Analysis

Copy number alterations in the genomes were analyzed by comparative genomic hybridization using catalog human arrays (2x400K or 4x180K formats; Agilent Technologies, Palo Alto, CA, USA). We referred to the Database of Genomic Variants (http://dgv.tcag.ca/dgv/app/home) to exclude benign copy number polymorphisms. Then, we genotyped 15 microsatellite loci on the X chromosome. Each locus was PCR-amplified using fluorescently labeled forward primers and unlabeled reverse primers. Primer sequences are available from the authors upon request. We also examined the X inactivation status by performing methylation analysis of CpG sites and microsatellite assays of a polymorphic CAG repeat tract in the androgen receptor (*AR*) gene. The methods were described previously [Muroya et al., 1999]. Furthermore, to clarify whether the genomic rearrangements in the patients affect the

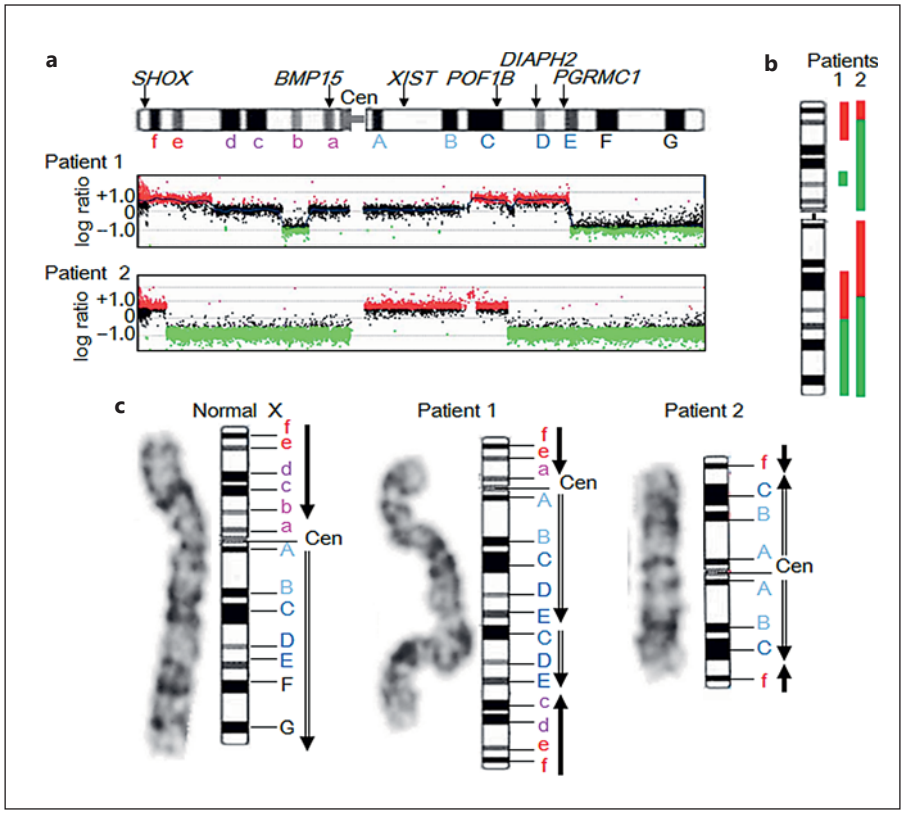

Fig. 1. a Array-based comparative genomic hybridization of the patients' X chromosomes. The black, red, and green dots denote normal, increased (log ratio higher than +0.4), and decreased (log ratio lower than –0.8) copy numbers, respectively. The upper panel shows the structure of the X chromosome and the positions of *SHOX*, *BMP15*, *XIST*, *POF1B*, *DIAPH2*, and *PGRMC1*. Cen, centromere. **b** Summary of copy number alterations in patients 1 and 2. The red and green lines depict duplicated and deleted regions, respectively. **c** High-resolution banding of a normal and the rearranged X chromosomes. The black and double-line arrows indicate the orientation of the X chromosome segments (from pter to the centromere and from the centromere to qter, respectively).

DNA methylation of X-chromosomal genes, we performed bisulfite sequencing for CpG sites in the upstream region of *SHOX*. In this experiment, genomic DNA samples were treated with bisulfite using the EZ DNA Methylation Kit (Zymo Research, Irvine, CA, USA). A DNA fragment (chrX:580,597–580,771, hg19, build 37) containing 12 *SHOX*-flanking CpG sites was PCR-amplified using a primer set that hybridizes with both the methylated and unmethylated clones. The PCR products were subcloned with the TOPO TA Cloning Kit (Life Technologies, Carlsbad, CA, USA) and subjected to direct sequencing.

Results

Clinical Manifestations of Patients 1 and 2

Patient 1 was born to phenotypically normal nonconsanguineous parents. This patient showed normal growth during childhood. At 12 years of age, she developed goiter. She was diagnosed with hyperthyroidism and was treated with propylthiouracil for 13 years. This patient exhibited age-appropriate sexual development and experienced menarche at 12 years of age (mean menarcheal age in the Japanese population: 12.3 years). However, her menstrual cycles were irregular and ceased at 15 years of age. Blood examinations at 26 years of age revealed markedly increased gonadotropin levels. She received estrogen and progesterone supplementation and had periodic withdrawal bleeding. She was otherwise healthy and had no Turner stigmata. Her mental development was normal. Her adult height was within the normal range (151.0 cm, –1.3 SD).

Patient 2 was previously reported as a female with Turner syndrome [Uehara et al., 2001]. At 16 years of age, she presented with short neck, shield chest, and cubitus valgus. She also exhibited hypertension, diabetes mellitus, and autoimmune hypothyroidism. In addition, she showed severe short stature (138 cm, –3.8 SD) despite being treated with growth hormone from 8 years of age. She lacked spontaneous pubertal development and was diagnosed with hypogonadism. Her mental development was normal.

Characterization of Genomic Rearrangements

Patient 1 had a 46,X,der(X)(pter→p22.1::p11.23→q24::q21.3→q24::p11.4→pter) karyotype (Fig. 1). The rearranged X chromosome involved at least 5 breakpoints and showed copy number gain of ~20-Mb and ~27-Mb regions at Xp and Xq, respectively, and copy number loss of ~7-Mb and ~36-Mb regions at Xp and Xq, respective-

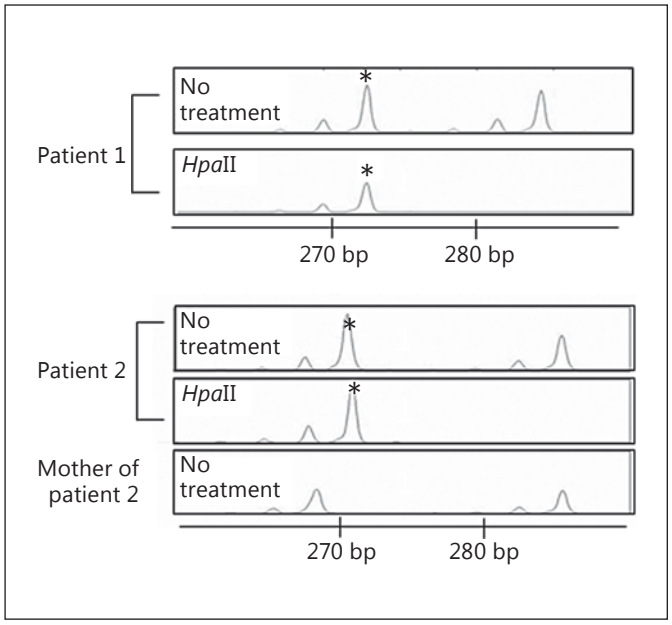

Fig. 2. X-inactivation analysis of *AR*. Microsatellite analysis was performed for polymorphic dinucleotide repeats before and after digestion with the methylation-sensitive enzyme *Hpa*II. In patient 1, the 274-bp peak (indicated by an asterisk) represents the PCR products amplified from the inactive X chromosome, while the 283-bp peak indicates the products amplified from the active X chromosome. In patient 2, the 271-bp peak (asterisk) represents the PCR products amplified from the inactive rearranged X chromosome, while the 286-bp peak depicts the products amplified from the maternally transmitted normal X chromosome. These data suggest that the rearranged X chromosome of patient 2 was of paternal origin.

Table 1. Representative results of the microsatellite analysis in patient 2 and her mother

Locus	Chromosomal position[a]	Copy number in the genome of patient 2	PCR products, bp	
			patient 2	mother
SHOX (CA)	Xp22.33	3	142/150	132/142
DXYS233	Xp22.33	3	277	277
DXYS85	Xp22.33	3	200/204	204
DXS1449	Xp22.33	3	116	116
DXS85	Xp22.2	3	174/232	174/232
DXS8025	Xp11.4	1	186	180/186
DXS1069	Xp11.4	1	256	256
DXS1068	Xp11.4	1	254	250/254
ALAS2	Xp11.21	1	155	155/157
AR	Xq12	3	271/286	268/286
DXS8020	Xq22.1	3	194/196	194/196
HPRT1	Xq26.2–26.3	1	290	282/290
DXS8377	Xq28	1	233	229/233
DXS7423	Xq28	1	187	183/187
DXS15	Xq28	1	148	146/148

[a] Based on Ensembl Genome Browser (http://www.ensembl.org).

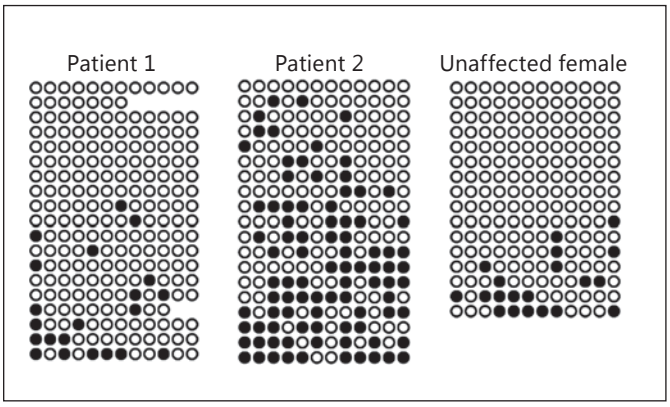

Fig. 3. Methylation analysis of *SHOX*-flanking CpG sites. Each horizontal line indicates the results of 1 clone. Filled and open circles indicate methylated and unmethylated cytosines in the CpG dinucleotides, respectively.

ly. This rearrangement caused overdosage of *SHOX*, *POF1B*, *DIAPH2*, and *PGRMC1* but did not affect the copy number of *BMP15* or *XIST* (X inactive specific transcript). X-inactivation analysis confirmed completely skewed inactivation (Fig. 2). *SHOX*-flanking CpG sites were barely methylated both in patient 1 and in an unaffected control individual (Fig. 3).

Patient 2 had a 46,X,der(X)(pter→p22.31::q22.1→q10::q10→q22.1::p22.31→pter) karyotype (Fig. 1). The rearranged X chromosome comprised at least 3 breakpoints and showed copy number gain of an ~8-Mb region at Xp and an ~40-Mb region at Xq and copy number loss of an ~53-Mb region at Xp and an ~54-Mb region at Xq. *SHOX*, *XIST*, and *POF1B* were duplicated, while *BMP15*, *DIAPH2*, and *PGRMC1* were deleted. There were no copy-number-neutral regions on this X chromosome. Microsatellite analysis suggested that this chromosome consisted of 2 identical arms ("isochromosome") of paternal origin (Table 1). The rearranged X chromosome was selectively inactivated (Fig. 2). *SHOX*-flanking CpG islands in patient 2 were hypermethylated (Fig. 3).

Discussion

We characterized complex germline X-chromosomal rearrangements in 2 patients. The clinical manifestations of the patients are consistent with the genomic structure. First, both patients manifested ovarian dysfunction. This feature is attributable to X-chromosomal mispairing, as suggested in cases of Turner syndrome due to X mono-

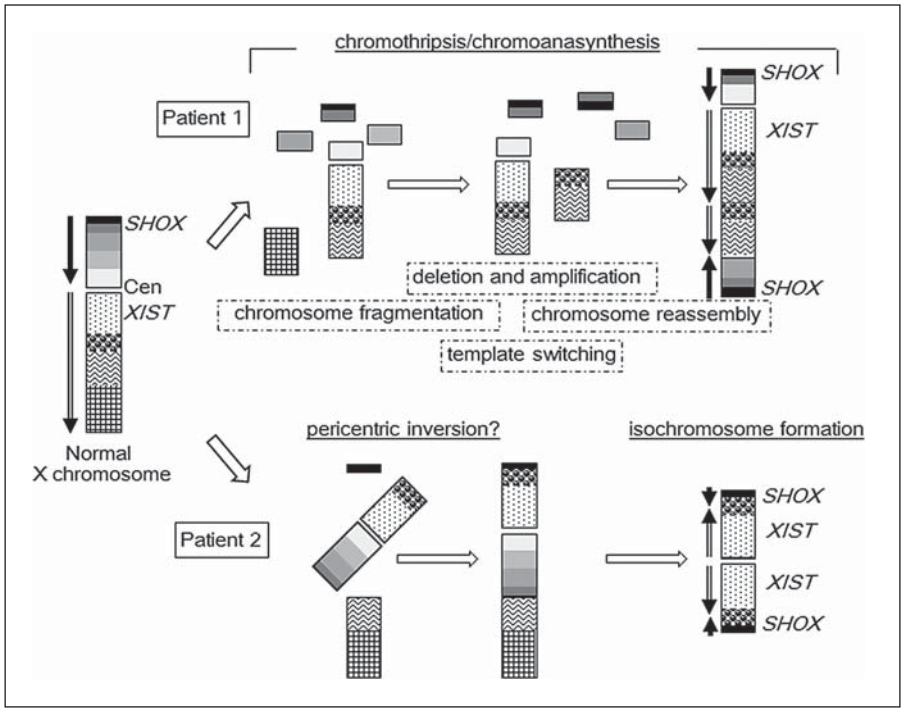

Fig. 4. Predicted mechanisms of the chromosomal rearrangements. The black and double-line arrows indicate the orientation of X chromosome segments (from pter to the centromere and from the centromere to qter, respectively). The rearranged X in patient 1 is consistent with a catastrophic reconstruction due to chromothripsis/chromoanasynthesis, while that in patient 2 likely results from 2 independent sequential events. It remains to be clarified whether the father of patient 2 carries a pericentric inversion.

somy [Ogata and Matsuo, 1995]. Furthermore, patient 2 lacked *BMP15*, *DIAPH2*, and *PGRMC1*, which have been implicated in ovarian function [Bione et al., 1998; Bione and Toniolo, 2000; Mansouri et al., 2008]. Copy number changes of other genes might also have contributed to the ovarian dysfunction in patients 1 and 2, because multiple X-chromosomal loci have been linked to this phenotype [Zhong and Layman, 2012]. Second, Turner stigmata such as short neck, shield chest, and cubitus valgus were observed in patient 2 but not in patient 1. These results support the previously proposed notion that a lymphogenic gene responsible for Turner stigmata resides at Xp11.2 [Ogata et al., 2001a], a genomic region deleted in patient 2 and preserved in patient 1. Third, both patients manifested thyroid disorders. Notably, isochromosome Xq is known to be associated with a high risk of autoimmune thyroid disorders [Elsheikh et al., 2001]. Indeed, the hypothyroidism of patient 2 may have resulted from copy number gain of *GPR174* at Xq21.1, because increased expression of *GPR174* has been linked to the risk of an autoimmune thyroid disorder [Chu et al., 2013]. However, the copy number of *GPR174* remained intact in patient 1. Thus, the genomic interval at Xq21.32q22.1> Xq21.32-q22.1, duplicated in both patients, may contain a hitherto uncharacterized gene associated with autoimmune thyroid disorders. Lastly, patient 1 had a normal stature, and patient 2 showed severe short stature, although both patients carried 3 copies of *SHOX*. This is inconsistent with previous findings that trisomy of the Xp22.3 region encompassing *SHOX* leads to tall stature [Ogata et al., 2001b]. In patients 1 and 2, positive effects of *SHOX* overdosage on skeletal growth may be balanced by negative effects of X-chromosomal mispairing and copy number alterations of minor growth genes on the X chromosome. Furthermore, short stature in patient 2 may be associated with *SHOX* dysregulation, because *SHOX*-flanking CpG islands were hypermethylated in this individual. These sites were barely methylated in the control individual, which is in agreement with the fact that *SHOX* escapes X inactivation [Rao et al., 1997]. It has been shown that in patients with X;autosome translocations, aberrant DNA methylation can spread to regions larger than 1 Mb of the autosomal segments [Cotton et al., 2014]. Hypermethylation of the *SHOX*-flanking CpG sites in patient 2 may reflect decreased physical distance between *SHOX* and *XIST* and/or copy number gain of *XIST*.

The genomic rearrangements in patients 1 and 2 appear to have been formed through different mechanisms (Fig. 4). The rearrangement in patient 1 is consistent with catastrophic reconstruction due to chromothripsis/chromoanasynthesis [Liu et al., 2011; Leibowitz et al., 2015].

This case provides further evidence that X-chromosomal chromothripsis/chromoanasynthesis accounts for a small portion of cases with nonsyndromic ovarian dysfunction. In contrast, the rearrangement in patient 2 is inconsistent with the "all-at-once" nature of chromothripsis/chromoanasynthesis [Liu et al., 2011; Hatch and Hetzer, 2015]. The rearranged chromosome of this patient had 2 identical arms consisting of Xp and Xq material, indicating that this chromosome arose by 2 independent sequential events, namely, a fusion between the Xp22.31 and Xq22.1 segments followed by isochromosome formation. Notably, the rearrangement occurred in the paternally inherited X chromosome. Thus, although the Xp22.31;Xq22.1 translocation is the simplest explanation of this rearrangement, it is implausible in this case, because X;X translocation rarely occurs during male meiosis. The results of patient 2 can be explained by assuming that the phenotypically normal father carried a pericentric inversion, inv(X)(p22.31q22.1), which was subjected to meiotic or postzygotic isochromosome formation (Fig. 4). However, since a paternal DNA sample was not available for genetic testing, we cannot exclude the possibility that this rearrangement was formed via other rare processes.

In conclusion, the results indicate that complex X-chromosomal rearrangements in the germline lead to ovarian dysfunction with and without other Turner syndrome-associated features. Clinical outcomes of such rearrangements likely reflect X-chromosomal mispairing, haploinsufficiency of genes escaping X inactivation, and/or perturbed DNA methylation. Most importantly, our findings imply that germline complex X-chromosomal rearrangements are created through both chromothripsis/chromoanasynthesis-dependent and -independent processes.

Acknowledgements

This study was supported by the Grants-in-Aid from the Japan Society for the Promotion of Science; and by the Grants from the Ministry of Health, Labor and Welfare, the Japan Agency for Medical Research and Development, the National Center for Child Health and Development, and the Takeda Foundation.

Statement of Ethics

This study was approved by the Institutional Review Board Committee at the National Center for Child Health and Development and performed after obtaining written informed consent.

Disclosure Statement

The authors have no competing interests to declare.

References

Auger J, Bonnet C, Valduga M, Philippe C, Bertolo-Houriez E, et al: De novo complex X chromosome rearrangement unmasking maternally inherited *CSF2RA* deletion in a girl with pulmonary alveolar proteinosis. Am J Med Genet A 161A:2594–2599 (2013).

Bione S, Toniolo D: X chromosome genes and premature ovarian failure. Semin Reprod Med 18:51–57 (2000).

Bione S, Sala C, Manzini C, Arrigo G, Zuffardi O, et al: A human homologue of the *Drosophila melanogaster diaphanous* gene is disrupted in a patient with premature ovarian failure: evidence for conserved function in oogenesis and implications for human sterility. Am J Hum Genet 62:533–541 (1998).

Chu X, Shen M, Xie F, Miao XJ, Shou WH, et al: An X chromosome-wide association analysis identifies variants in *GPR174* as a risk factor for Graves' disease. J Med Genet 50:479–485 (2013).

Cotton AM, Chen CY, Lam LL, Wasserman WW, Kobor MS, Brown CJ: Spread of X-chromosome inactivation into autosomal sequences: role for DNA elements, chromatin features and chromosomal domains. Hum Mol Genet 23:1211–1223 (2014).

Elsheikh M, Wass JA, Conway GS: Autoimmune thyroid syndrome in women with Turner's syndrome – the association with karyotype. Clin Endocrinol (Oxf) 55:223–226 (2001).

Hatch EM, Hetzer MW: Chromothripsis. Curr Biol 25:R397–399 (2015).

Heard E, Clerc P, Avner P: X-chromosome inactivation in mammals. Annu Rev Genet 31: 571–610 (1997).

Kloosterman WP, Cuppen E: Chromothripsis in congenital disorders and cancer: similarities and differences. Curr Opin Cell Biol 25:341–348 (2013).

Leibowitz ML, Zhang CZ, Pellman D: Chromothripsis: A new mechanism for rapid karyotype evolution. Annu Rev Genet 49: 183–211 (2015).

Liu P, Erez A, Nagamani SC, Dhar SU, Kołodziejska KE, et al: Chromosome catastrophes involve replication mechanisms generating complex genomic rearrangements. Cell 146:889–903 (2011).

Mansouri MR, Schuster J, Badhai J, Stattin EL, Lösel R, et al: Alterations in the expression, structure and function of progesterone receptor membrane component-1 (*PGRMC1*) in premature ovarian failure. Hum Mol Genet 17:3776–3783 (2008).

Muroya K, Kosho T, Ogata T, Matsuo M: Female carriers of Xp22.3 deletion including MRX locus. Am J Med Genet 84:384–385 (1999).

Ochalski ME, Engle N, Wakim A, Ravnan BJ, Hoffner L, et al: Complex X chromosome rearrangement delineated by array comparative genome hybridization in a woman with premature ovarian insufficiency. Fertil Steril 95: 2433.e9–e15 (2011).

Ogata T, Matsuo N: Turner syndrome and female sex chromosome aberrations: deduction of the principal factors involved in the development of clinical features. Hum Genet 95:607–629 (1995).

Ogata T, Muroya K, Matsuo N, Shinohara O, Yorifuji T, et al: Turner syndrome and Xp deletions: clinical and molecular studies in 47 patients. J Clin Endocrinol Metab 86:5498–508 (2001a).

Ogata T, Matsuo N, Nishimura G: *SHOX* haploinsufficiency and overdosage: impact of gonadal function status. J Med Genet 38:1–6 (2001b).

Pellestor F: Chromothripsis: how does such a catastrophic event impact human reproduction? Hum Reprod 29:388–393 (2014).

Plaisancié J, Kleinfinger P, Cances C, Bazin A, Julia S, et al: Constitutional chromoanasynthesis: description of a rare chromosomal event in a patient. Eur J Med Genet 57:567–570 (2014).

Rao E, Weiss B, Fukami M, Rump A, Niesler B, et al: Pseudoautosomal deletions encompassing a novel homeobox gene cause growth failure in idiopathic short stature and Turner syndrome. Nat Genet 16:54–63 (1997).

Uehara S, Hanew K, Harada N, Yamamori S, Nata M, et al: Isochromosome consisting of terminal short arm and proximal long arm X in a girl with short stature. Am J Med Genet 99: 196–199 (2001).

Zhang CZ, Spektor A, Cornils H, Francis JM, Jackson EK, et al: Chromothripsis from DNA damage in micronuclei. Nature 522:179–184 (2015).

Zhong Q, Layman LC: Genetic considerations in the patient with Turner syndrome – 45,X with or without mosaicism. Fertil Steril 98:775–779 (2012).

Intragenic *DOK7* deletion detected by whole-genome sequencing in congenital myasthenic syndromes

OPEN

Yoshiteru Azuma, MD, PhD
Ana Töpf, PhD
Teresinha Evangelista, MD
Paulo José Lorenzoni, MD, PhD
Andreas Roos, PhD
Pedro Viana, MD
Hidehito Inagaki, PhD
Hiroki Kurahashi, MD, PhD
Hanns Lochmüller, MD

Correspondence to Dr. Lochmüller: hanns.lochmuller@newcastle.ac.uk

ABSTRACT

Objective: To identify the genetic cause in a patient affected by ptosis and exercise-induced muscle weakness and diagnosed with congenital myasthenic syndromes (CMS) using whole-genome sequencing (WGS).

Methods: Candidate gene screening and WGS analysis were performed in the case. Allele-specific PCR was subsequently performed to confirm the copy number variation (CNV) that was suspected from the WGS results.

Results: In addition to the previously reported frameshift mutation c.1124_1127dup, an intragenic 6,261 bp deletion spanning from the 5′ untranslated region to intron 2 of the *DOK7* gene was identified by WGS in the patient with CMS. The heterozygous deletion was suspected based on reduced coverage on WGS and confirmed by allele-specific PCR. The breakpoints had microhomology and an inverted repeat, which may have led to the development of the deletion during DNA replication.

Conclusions: We report a CMS case with identification of the breakpoints of the intragenic *DOK7* deletion using WGS analysis. This case illustrates that CNVs undetected by Sanger sequencing may be identified by WGS and highlights their relevance in the molecular diagnosis of a treatable neurologic condition such as CMS. ***Neurol Genet* 2017;3:e152; doi: 10.1212/NXG.0000000000000152**

GLOSSARY

aCGH = array comparative genomic hybridization; **AChE** = acetylcholinesterase; **CMS** = congenital myasthenic syndromes; **CNV** = copy number variation; **MLPA** = multiplex ligation-dependent probe amplification; **MuSK** = muscle-specific tyrosine kinase; **NMJ** = neuromuscular junction; **WES** = whole-exome sequencing; **WGS** = whole-genome sequencing.

Congenital myasthenic syndromes (CMS) are inherited disorders characterized by fatigable muscle weakness with or without other associated signs or symptoms.[1] They are caused by mutations in genes expressed at the neuromuscular junction (NMJ). DOK7 is one of the components of the NMJ and an activator of the muscle-specific tyrosine kinase (MuSK).[2] Recessive mutations in *DOK7* cause approximately 10% of the genetically diagnosed CMS cases.[1]

CMS are heterogeneous diseases, and to date, more than 25 genes have been reported to be causative. Consecutive single-gene screening has been routinely used as a diagnostic tool; however, next-generation sequencing allows the analysis of all these genes simultaneously to identify the causative variant and obtain a genetic diagnosis. The efficacy of whole-exome sequencing (WES) for the diagnosis of CMS cases has been reported,[3,4] as well as its ability to identify new causal genes.[5,6] However, the limitation is that WES is designed to detect only protein-coding regions and exon-intron boundaries of the genome.

Supplemental data at Neurology.org/ng

From the Institute of Genetic Medicine (Y.A., A.T., T.E., P.J.L., A.R., H.L.), Newcastle University, UK; Division of Neurology (P.J.L.), Federal University of Parana, Brazil; Leibniz-Institut für Analytische Wissenschaften ISAS e.V. (A.R.), Germany; Department of Neurosciences and Mental Health (P.V.), University of Lisbon, Portugal; and Division of Molecular Genetics (H.I., H.K.), Fujita Health University, Japan.

Funding information and disclosures are provided at the end of the article. Go to Neurology.org/ng for full disclosure forms. The Article Processing Charge was funded by the Medical Research Council.

On the other hand, whole-genome sequencing (WGS) allows the analysis of deep intronic, intergenic, and other noncoding regions. Furthermore, WGS allows to detect copy number variations (CNVs), as coverage is more homogeneous than that of WES.[7]

We present a CMS case in which a large intragenic *DOK7* deletion was identified by WGS compound heterozygous to a known exonic mutation.

METHODS ***DOK7* screening.** DNA from the patient was extracted from whole blood by standard methods. Screening of hot-spot mutations was performed by Sanger sequencing, encompassing a region of ~600 bp covering the previously reported European founder mutation c.1124_1127dup.[2] Subsequently, full screening of coding regions and exon-intron boundaries of the *DOK7* gene was performed. Primer sequences are listed in table e-1 at Neurology.org/ng. Annotation of the human *DOK7* cDNA is according to the GenBank accession number NM_173660.

Mutation analysis by WGS. WGS was performed by the TruSeq PCR–free library preparation kit and HiSeqX v2 SBS kit (Illumina, San Diego, CA) for 30× mean coverage on a HiSeqX sequencer. Reads were mapped against hg19 reference genome using the Burrows-Wheeler transform,[8] and duplicates were removed using Picard tools.[9]

Sequence variants were called using the Genome Analysis Toolkit.[10] WGS data were then analyzed using deCODE's platform (Clinical Sequence Miner; WuXi NextCODE, Cambridge, MA). Rare variants were filtered by threshold of coverage (≥8), variant call (≥2), and ratio of variant (≥0.2) and allele frequency of 1% in 1000 Genomes database.[11]

Sanger sequencing of large deletion. We amplified DNA samples to identify the suspected intragenic deletion with primers 5′-CCCAGATGGTGCGCTTGCTCC-3′and 5′-GCCCACCCCCTCACGCTCAG-3′. The PCR protocol comprised 35 cycles and annealing temperature of 68°C using HotStarTaq DNA polymerase with Q-Solution for the GC rich region (QIAGEN, Düsseldorf, Germany).

Standard protocol approvals, registrations, and patient consents. All human studies including genetic analysis were approved by institutional review boards, and appropriate written informed consent was obtained from all the patients and family members.

RESULTS **Clinical findings.** The patient is a 39-year-old Portuguese man who presented with bilateral ptosis and exercise-induced muscle weakness. He had no family history of muscle disease, and his motor milestones in childhood were normal. He showed mild ptosis from infancy and noticed mild lower limb weakness at 13 years of age. He was admitted to hospital for a month because of sudden severe generalized muscle weakness and worsening ptosis at 15 years of age. He has bilateral facial weakness and winged scapula, and the clinical diagnosis of a neuromuscular transmission defect was confirmed by neurophysiologic studies. EMG showed myopathic changes on facial muscles. Repetitive nerve stimulation showed a remarkable decremental response of 76% in proximal muscles. Both antiacetylcholine-receptor and anti-MuSK antibodies were negative, and immunosuppressive treatment was unsuccessful. Acetylcholinesterase (AChE) inhibitor of pyridostigmine up to 360 mg/d for 10 years had little effect and was discontinued without clinical deterioration after the trial of oral administration of salbutamol which effected significantly. He has not experienced severe muscle weakness for 5 years since salbutamol was started.

***DOK7* screening.** Based on the limb-girdle clinical presentation of the patient, a hot-spot region of *DOK7* was investigated as a first screening step. Sanger sequencing revealed that the patient carried the heterozygous c.1124_1127dup reported as a founder mutation in European CMS patients.[2] This mutation was not present in the mother (DNA from the father was unavailable). However, this single heterozygous mutation does not explain *DOK7*-CMS, which invariably shows autosomal recessive inheritance. To identify a second heteroallelic *DOK7* variant, the whole coding region and exon-intron boundaries of the *DOK7* gene were Sanger sequenced, but no potentially pathogenic exonic or splice site variants were found. The sample was therefore subjected to WGS to try to identify other mutations within the *DOK7* gene or elsewhere in the genome.

WGS analysis. As expected, applying a standard pipeline for variant filtering (minor allele frequency 1% in coding region), the heterozygous c.1124_1127dup in *DOK7* was detected in the WGS data. This filtering did not identify any other coding variants in known CMS causal genes.

However, visual inspection of the sequencing reads of the *DOK7* gene for this patient revealed that the read depth for exons 1 and 2 was lower than that of neighboring regions and other control samples (figure 1A). Furthermore, there were no heterozygous variants within this region, indicating a run of homozygosity or hemizygosity suggesting a single copy region. Close inspection of the boundaries of this region showed that in some instances, sections of the sequencing reads did not match the reference sequence. These reads were considered chimeric or split reads, as the unmatched sequences did align to a different region of the genome. Split reads are indicative of structural variation. In fact, the 3′ section of the split reads of the proximal boundary aligns to the 3′end of the distal boundary, and vice versa (figure 1B, red underline and red box). The proximal and distal breakpoints lie approximately 6 kb away. These findings suggested that this patient

Figure 1 **Whole-genome sequencing analysis and allele-specific PCR**

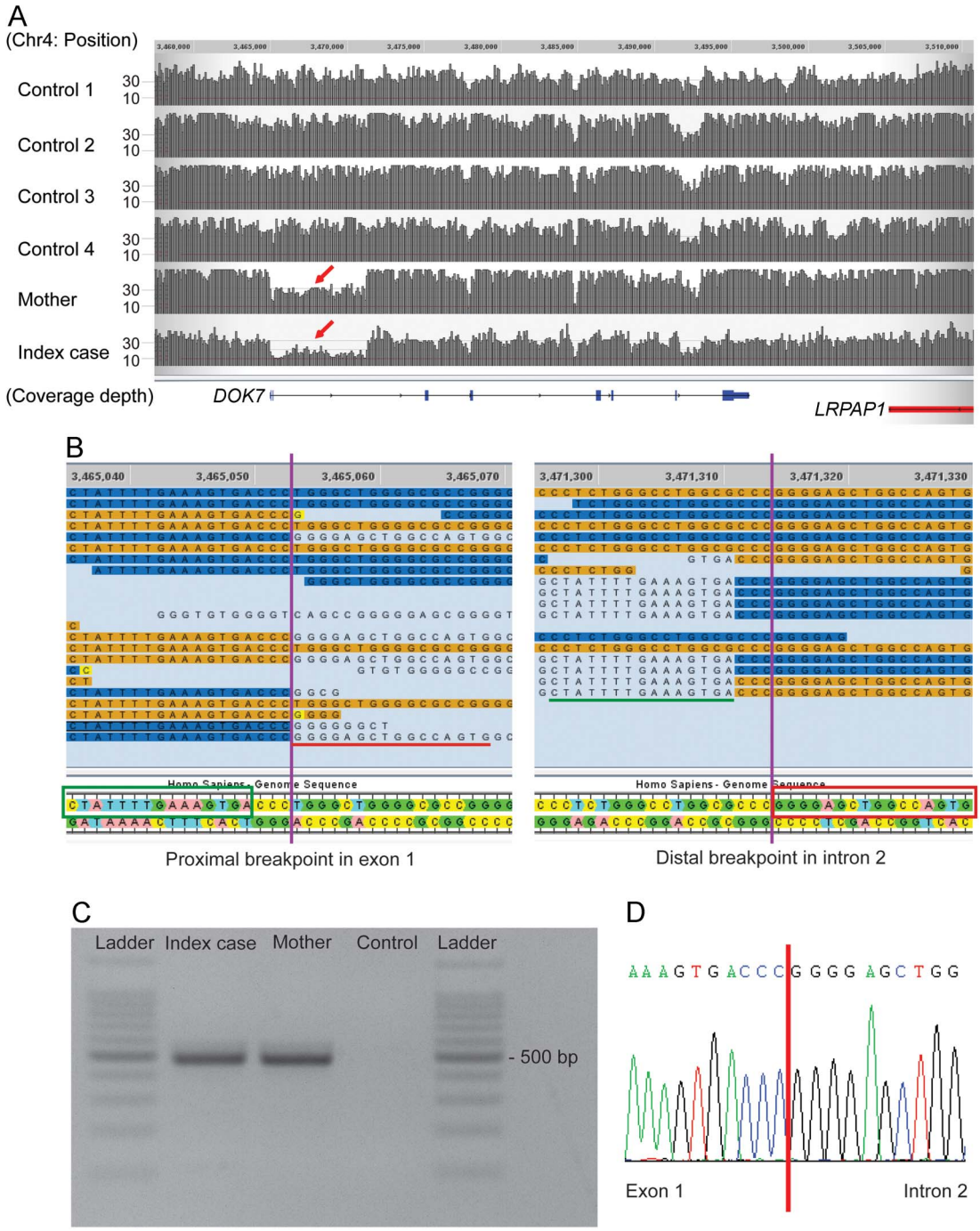

(A) Both index case and his mother show reduced read depth (coverage) from exon 1 to deep intron 2 of the *DOK7* gene (red arrow). Controls 1–4 correspond to samples sequenced and analyzed through the same pipeline and without the diagnosis of congenital myasthenic syndromes. (B) Split reads were observed at both presumed breakpoints. Nucleotides matching the reference sequence of *DOK7* are highlighted in orange/blue. Single unmatched nucleotides are highlighted in yellow, and further unmatched sequences are not highlighted. The unmatched sequence (indicated with red/green underline) of the split reads of the proximal breakpoint aligns to the reference sequence (indicated in green/red boxes) at the distal breakpoint, and vice versa. (C) The expected products amplified by allele-specific PCR were identified in the index case and the mother. (D) The junction of the breakpoint in the allele with the intragenic deletion was confirmed by Sanger sequencing of the PCR product. Coverage and reads were drawn by the graphical user interface of Sequence Miner 5.21.1 (WuXi NextCODE).

has a heterozygous 6-kb deletion in *DOK7* encompassing exons 1 and 2.

Identification and analysis of the intragenic *DOK7* deletion. We performed PCR using a pair of primers designed around 250 bp away from the presumed breakpoints of the deletion, between the 5′ untranslated region and intron 2. The expected product of 488 bp was amplified in the DNA samples of the patient, but not in control DNA

(figure 1C). The junction of the 2 breakpoints was identified by Sanger sequencing of the PCR product (figure 1D). The exact size of the deletion is 6,261 bp. The deletion was also detected by PCR in the mother, who did not carry the c.1124_1127dup mutation. We therefore concluded that the CMS in the patient is caused by the compound heterozygous mutations in *DOK7*.

Figure 2 **Analysis of the breakpoints of the intragenic 6-kb deletion**

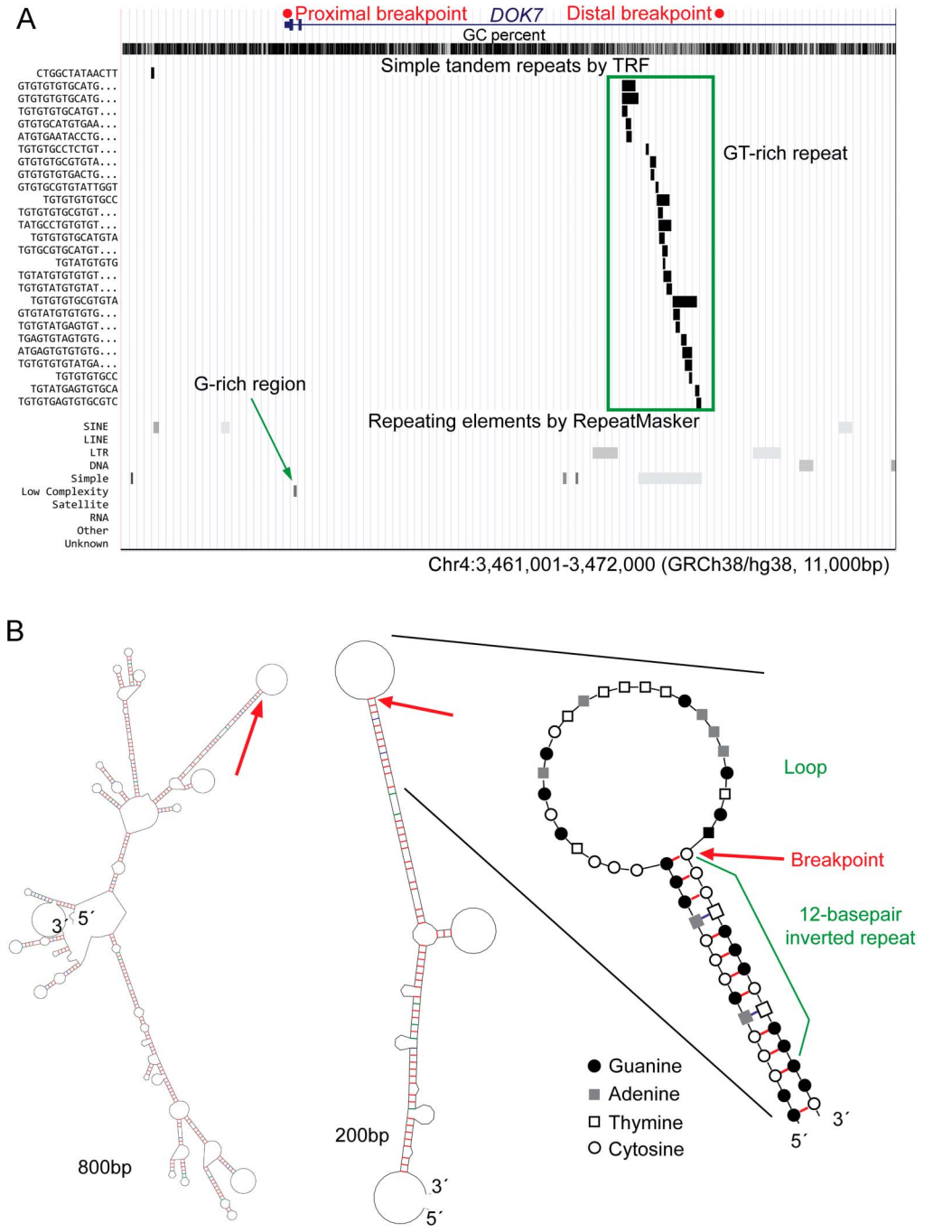

(A) University of California Santa Cruz genome browser (genome.ucsc.edu/) view of the deleted region showing the Simple Tandem Repeats track (based on Tandem Repeats Finder, TRF[18]) and the Repeating Elements track (based on RepeatMasker[19]). GT-rich repeat regions (green box) are seen around the distal breakpoint, and a G-rich region (green arrow) is located near the proximal breakpoint. (B) The secondary DNA structure with the lowest delta G value was predicted by the mfold tool (unafold.rna.albany.edu/?q=mfold) for the 800 and 200 bp regions around the proximal breakpoint. An enlarged view of the breakpoint area highlighting the complementary nucleotides is also shown. The proximal breakpoint (indicated by the red arrows) is at the boundary of a loop and a 12-bp inverted repeat that may cause stalling of DNA replication. It is possible that deletion/duplication can occur if stalled replication resumes using an alternate location on the same chromosome. Red/blue/green bars represent hydrogen bonds between G-C/T-A/G-T.

The 2 breakpoints of the deletion have a C-triplet homology region, and the deleted region contains a G-rich region and GT-rich repeat region (figure 2A). In silico secondary structure analysis using the prediction program mfold[12] showed that the proximal breakpoint is at the boundary of a loop and a 12-bp inverted repeat (figure 2B). This may cause stalling of DNA replication and subsequently result in chromosomal structural changes including deletions, if replication resumes using an alternate chromosomal location.

Screening of the intragenic deletion in a CMS cohort. To identify carriers of single heterozygous mutations in *DOK7* (i.e., without a second rare variant within coding regions and exon-intron boundaries), we interrogated our database of clinically diagnosed CMS cases referred to us in the years 1996–2015. The total number of patients with CMS was 577, of which 7 genetically unsolved cases had single frameshift mutations in *DOK7* (c.1124_1127dup in 6 cases and c.1378dup in 1 case). These samples were amplified using the deletion-specific pair of primers used to detect the 6-kb deletion of the index family. All 7 samples were negative using this PCR method. This does not exclude that they carry CNVs in *DOK7* different from the one described in this study.

DISCUSSION We identified an intragenic *DOK7* deletion in a patient with clinically diagnosed CMS. Patients lacking a second heteroallelic mutation in *DOK7* were reported in a previous study.[2] Moreover, multiexon genomic deletions of *RAPSN*[13] and *COLQ*[14] have also been identified as causative of CMS. It is therefore conceivable that CNVs in *DOK7* may explain a proportion of cases assessed as negative or inconclusive by conventional sequencing analysis.

Our study shows the advantage of WGS analysis and detailed interrogation for detecting CNVs, using coverage and visual analysis of split reads. Traditionally, multiplex ligation–dependent probe amplification (MLPA) is considered the method of choice to detect previously described CNVs, where kits are available commercially. To identify new CNVs, however, specific MLPA primers for each gene need to be designed, rendering it expensive and time consuming for testing a genetically heterogeneous syndrome such as CMS. Array comparative genomic hybridization (aCGH) is also a valuable method for CNVs analysis; nevertheless, deletions/duplications are not detectable by aCGH if they are shorter than the spacing of the hybridization probes. In addition, neither MLPA nor aCGH can detect single nucleotide variants. Despite WES being widely used for clinical sequencing, the library preparation step results in uneven coverage, which makes the estimation of CNVs by read depth less reliable. This can be overcome by the homogenous coverage of WGS, allowing both the detection of single nucleotide as well as CNV.

WGS analysis is still more expensive than WES and Sanger sequencing. In addition, computational tools need further improvement in sensitivity and specificity to detect CNVs exhaustively.[15] Taken together, we believe that WGS is advantageous and will become the method of choice for genetic diagnosis in rare, heterogeneous conditions such as CMS. We suggest that previously unsolved cases or the carriers of a single mutation in a causal gene are especially suitable cases of CMS for WGS analysis. The 6-kb deletion was not identified in other cases tested by PCR, although it is inherited from the mother, suggesting this is likely a private mutation. However, it is possible that other CNVs in *DOK7* underlie in CMS cases.

We also determined the breakpoints of the 6-kb deletion, and analysis of the sequence and secondary structure suggested that long inverted repeats might cause the development of the deletion due to a stall of replication, and microhomology might have played a role in the repair process.[16] Further documentation of breakpoints and sequences would help understand the mechanism for the development of CNVs.

Obtaining genetic diagnosis of CMS is very important because the therapy varies depending on the affected gene. Poor response to AChE inhibitors is often observed in patients affected by limb-girdle CMS due to *DOK7* mutations. Salbutamol therapy has now been started for the patient described in this study, which has been reported of good response in *DOK7*-CMS.[17]

AUTHOR CONTRIBUTIONS

Yoshiteru Azuma: drafting the manuscript, acquisition of data, and analysis and interpretation. Ana Töpf: analysis and interpretation and critical revision of the manuscript. Teresinha Evangelista and Paulo José Lorenzoni: acquisition of data. Andreas Roos: analysis and interpretation and study supervision. Pedro Viana: acquisition of data. Hidehito Inagaki and Hiroki Kurahashi: analysis and interpretation. Hanns Lochmüller: study concept and design and study supervision.

STUDY FUNDING

Study funded by European Commission's Seventh Framework Programme (FP7/2007-2013) under grant agreement no. 2012-305121 (NEUROMICS). Hanns Lochmüller—funding from the Medical Research Council as part of the MRC Centre for Neuromuscular Diseases (reference G1002274, grant ID 98482) and by the European Union Seventh Framework Programme (FP7/2007-2013) under grant agreement no. 305444 (RD-Connect).

DISCLOSURE

Yoshiteru Azuma, Ana Töpf, and Teresinha Evangelista report no disclosures. Paulo José Lorenzoni has received research support from CNPq (Brazil). Andreas Roos, Pedro Viana, Hidehito Inagaki, and Hiroki Kurahashi report no disclosures. Hanns Lochmüller has served on the scientific advisory boards of German Duchenne parents project, IRDiRC Interdisciplinary Scientific Committee, German Muscular Dystrophy

Network, Myotubular Trust Patient Registry, Action Duchenne Patient Registry, German Patient Registries on DMD, and SMA; has received travel funding/speaker honoraria from PTC Therapeutics Inc. and Ultragenyx Pharmaceuticals Inc.; serves on the editorial boards of the *Journal of Neuromuscular Diseases* and the *Journal of Neurology*; has been a consultant for Roche Pharmaceuticals, ASD Therapeutics Partners LLC, IOS Press, Alexion Pharmaceuticals Inc., Ultragenyx Pharmaceutical Inc., and Fondazione Cariplo (funding from each paid to Newcastle University); and has received research support from Marigold Foundation Ltd., Ultragenyx Pharmaceutical Inc., PTC Therapeutics Inc., Eli Lilly and Co., Action Benni & Co., GSK (GlaxoSmithKline), Trophos SA, European Commission (RD-Connect), European Commission (OPTIMISTIC), European Commission (NeurOmics), Medical Research Council (MRC), National Institute for Health Research (NIHR), Action Duchenne, Association Francaise Contre les Myopathies, British Heart Foundation, Muscular Dystrophy UK, National Cancer Institute, Spinal Muscular Atrophy Support UK, Wellcome Trust, Jennifer Trust, and Duchenne Parent Project. Go to Neurology.org/ng for full disclosure forms.

Received January 19, 2017. Accepted in final form March 14, 2017.

REFERENCES

1. Engel AG, Shen XM, Selcen D, Sine SM. Congenital myasthenic syndromes: pathogenesis, diagnosis, and treatment. Lancet Neurol 2015;14:420–434.
2. Beeson D, Higuchi O, Palace J, et al. Dok-7 mutations underlie a neuromuscular junction synaptopathy. Science 2006;313:1975–1978.
3. Das AS, Agamanolis DP, Cohen BH. Use of next-generation sequencing as a diagnostic tool for congenital myasthenic syndrome. Pediatr Neurol 2014;51:717–720.
4. Garg N, Yiannikas C, Hardy TA, et al. Late presentations of congenital myasthenic syndromes: how many do we miss? Muscle Nerve 2016;54:721–727.
5. Bauche S, O'Regan S, Azuma Y, et al. Impaired presynaptic high-affinity choline transporter causes a congenital myasthenic syndrome with episodic apnea. Am J Hum Genet 2016;99:753–761.
6. O'Connor E, Topf A, Muller JS, et al. Identification of mutations in the MYO9A gene in patients with congenital myasthenic syndrome. Brain 2016;139:2143–2153.
7. Lelieveld SH, Spielmann M, Mundlos S, Veltman JA, Gilissen C. Comparison of exome and genome sequencing technologies for the complete capture of protein-coding regions. Hum Mutat 2015;36:815–822.
8. Li H, Durbin R. Fast and accurate long-read alignment with Burrows-Wheeler transform. Bioinformatics 2010; 26:589–595.
9. Picard. Available at: broadinstitute.github.io/picard/. Accessed March 23, 2017.
10. McKenna A, Hanna M, Banks E, et al. The Genome Analysis Toolkit: a MapReduce framework for analyzing next-generation DNA sequencing data. Genome Res 2010;20:1297–1303.
11. Auton A, Brooks LD, Durbin RM, et al. A global reference for human genetic variation. Nature 2015; 526:68–74.
12. Zuker M. Mfold web server for nucleic acid folding and hybridization prediction. Nucleic Acids Res 2003;31: 3406–3415.
13. Gaudon K, Penisson-Besnier I, Chabrol B, et al. Multiexon deletions account for 15% of congenital myasthenic syndromes with RAPSN mutations after negative DNA sequencing. J Med Genet 2010;47: 795–796.
14. Wang W, Wu Y, Wang C, Jiao J, Klein CJ. Copy number analysis reveals a novel multiexon deletion of the *COLQ* gene in congenital myasthenia. Neurol Genet 2016;2: e117. doi: 10.1212/NXG.0000000000000117.
15. Pirooznia M, Goes FS, Zandi PP. Whole-genome CNV analysis: advances in computational approaches. Front Genet 2015;6:138.
16. Hastings PJ, Ira G, Lupski JR. A microhomology-mediated break-induced replication model for the origin of human copy number variation. PLoS Genet 2009;5: e1000327.
17. Lorenzoni PJ, Scola RH, Kay CS, et al. Salbutamol therapy in congenital myasthenic syndrome due to DOK7 mutation. J Neurol Sci 2013;331:155–157.
18. Benson G. Tandem repeats finder: a program to analyze DNA sequences. Nucleic Acids Res 1999;27: 573–580.
19. Smit A, Hubley R, Green P. RepeatMasker Open-3.0. 1996–2010. Available at: repeatmasker.org. Accessed March 23, 2017.

Kohmoto et al. Molecular Cytogenetics (2017) 10:15
DOI 10.1186/s13039-017-0316-6

Molecular Cytogenetics

CASE REPORT Open Access

A case with concurrent duplication, triplication, and uniparental isodisomy at 1q42.12-qter supporting microhomology-mediated break-induced replication model for replicative rearrangements

Tomohiro Kohmoto[1†], Nana Okamoto[2†], Takuya Naruto[1], Chie Murata[1], Yuya Ouchi[3], Naoko Fujita[3], Hidehito Inagaki[3], Shigeko Satomura[4], Nobuhiko Okamoto[5], Masako Saito[1], Kiyoshi Masuda[1], Hiroki Kurahashi[3] and Issei Imoto[1*]

Abstract

Background: Complex genomic rearrangements (CGRs) consisting of interstitial triplications in conjunction with uniparental isodisomy (isoUPD) have rarely been reported in patients with multiple congenital anomalies (MCA)/intellectual disability (ID). One-ended DNA break repair coupled with microhomology-mediated break-induced replication (MMBIR) has been recently proposed as a possible mechanism giving rise to interstitial copy number gains and distal isoUPD, although only a few cases providing supportive evidence in human congenital diseases with MCA have been documented.

Case presentation: Here, we report on the chromosomal microarray (CMA)-based identification of the first known case with concurrent interstitial duplication at 1q42.12-q42.2 and triplication at 1q42.2-q43 followed by isoUPD for the remainder of chromosome 1q (at 1q43-qter). In distal 1q duplication/triplication overlapping with 1q42.12-q43, variable clinical features have been reported, and our 25-year-old patient with MCA/ID presented with some of these frequently described features. Further analyses including the precise mapping of breakpoint junctions within the CGR in a sequence level suggested that the CGR found in association with isoUPD in our case is a triplication with flanking duplications, characterized as a triplication with a particularly long duplication-inverted triplication-duplication (DUP-TRP/INV-DUP) structure. Because microhomology was observed in both junctions between the triplicated region and the flanking duplicated regions, our case provides supportive evidence for recently proposed replication-based mechanisms, such as MMBIR, underlying the formation of CGRs + isoUPD implicated in chromosomal disorders.

Conclusions: To the best of our knowledge, this is the first case of CGRs + isoUPD observed in 1q and having DUP-TRP/INV-DUP structure with a long proximal duplication, which supports MMBIR-based model for genomic rearrangements. Molecular cytogenetic analyses using CMA containing single-nucleotide polymorphism probes with further analyses of the breakpoint junctions are recommended in cases suspected of having complex chromosomal abnormalities based on discrepancies between clinical and conventional cytogenetic findings.

Keywords: 1q, Complex genomic rearrangement, Uniparental isodisomy, DUP-TRP/INV-DUP structure, Microhomology-mediated break-induced replication model, Template switching, Chromosomal microarray, Breakpoint junction sequence

* Correspondence: issehgen@tokushima-u.ac.jp
†Equal contributors
[1]Department of Human Genetics, Graduate School of Biomedical Sciences, Tokushima University, 3-18-15 Kuramoto-cho, Tokushima 770-8503, Japan
Full list of author information is available at the end of the article

Background

Complex genomic rearrangements (CGRs) consisting of two or more breakpoint junctions have been frequently observed during the characterization of nonrecurrent microduplications associated with genomic disorders [1, 2]. The occurrence of CGRs, such as partial tetrasomy induced by an interstitial triplication, contiguous distally with an extended segment uniparental isodisomy (isoUPD), has recently been reported as a rare event [3–7]. The recent establishment of high-resolution chromosomal microarray (CMA) using probes designed to detect copy number variations (CNVs) and genotype single-nucleotide polymorphism (SNP) simultaneously in a genome-wide manner has accelerated the identification of cases with such CGRs + isoUPD observations [8]. Although the cause, mechanism, and phenotypic effect of such CGR + isoUPD remain unclear, Carvalho et al. [5] provided evidence that CGRs generated post-zygotically through microhomology-mediated break-induced replication (MMBIR) can lead to regional isoUPD. In this replication-based mechanism model, a triplicated segment inserted in an inverted orientation between two copies of the duplicated segments (duplication-inverted triplication-duplication, DUP-TRP/INV-DUP) followed by regional isoUPD is generated via template switches between homologs and sister chromatids using MMBIR [5].

Here, we report on a patient with the co-occurrence of interstitial trisomy at 1q42.12-q42.2 and tetrasomy at 1q42.2-q43, followed by a segmental isoUPD for 1q43-qter, as additional evidence for an MMBIR-based model generating DUP-TRP/INV-DUP rearrangement followed by isoUPD. Detailed molecular genetic analyses at the sequence level revealed the presence of microhomology at two breakpoint junctions of the CGR, probably underlying the formation of the complicated genomic alteration (CGR + isoUPD). Notably, this is the first case of CGR + isoUPD detected in the long arm of chromosome 1. In addition, the pattern of flanking duplications experimentally documented in the present case, namely, a long duplicated segment with a size on the order of megabases at the centromeric junction observed by CMA with a short duplication at the telomeric junction only identified by sequencing of the breakpoint, has not been reported previously.

Case presentation

The 25-year-old Japanese male reported on here was the first child of a non-consanguineous healthy mother (G0P0, 24 years of age) and father (details are unclear due to a divorce) with no notable family disease history. After an uncomplicated pregnancy, he had been born at 38 weeks of gestation by a normal delivery. His birth weight was 1958 g (−2.52 SD) and he was introduced into a neonatal incubator to treat intrauterine growth retardation (IUGR) and poor sucking by tube feeding for 20 days, although detailed medical records of his physique are not available. Physical examination at the age of 1 month showed height 46 cm (−3.4 SD), weight 2715 g (−2.6 SD), and head circumference 29.8 cm (−4.6 SD). The abilities to hold up his head, eat solid food, imitate the behaviors of others, and walk alone were recognized at 6 months, 18 months, 2 years and 6 months, and 3 years of age, respectively. The patient had never been able to speak until now, and his comprehension was limited to simple signs, but he recognized various sounds. At 3 years of age, he was diagnosed with the congenital heart defect of tetralogy of Fallot (TOF) but was not treated surgically, although he showed frequent squatting and cyanotic attacks. On physical examination at 24 years and 6 months of age, he showed growth retardation with height 136 cm (−6 SD), weight 28.1 kg (−3.3 SD), and severe mental retardation with a developmental quotient of 5. At 25 years of age, he had TOF, bilateral congenital inguinal hernia, bilateral cryptorchidism, club feet, scoliosis, Chilaiditi's syndrome, and several facial anomalies, such as thinning of the hair, strabismus, widely spaced eyes, a down-slanted palpebral fissure, low-set ears, a prominent forehead, and a coarse face. He has some missing teeth due to having suffered from periodontal disease. Serial complete blood counts showed thrombocytopenia, and magnetic resonance imaging showed cerebral atrophy especially of the frontal lobe, with enlargement of the ventricles. His karyotype at birth was reported to be normal, but repeatedly performed karyotyping revealed 46,XY,dup(1)(q32.1q42.1),inv(9)(p12q13).

Molecular cytogenetic studies

This research protocol for this study was approved by the local ethics committee of Tokushima University. Written informed consent for the participation of the patient in this study was obtained from the patient's mother DNA was extracted from a peripheral blood sample.

A high-resolution CMA using the CytoScan HD array (Affymetrix, Santa Clara, CA) with Chromosome Analysis Suite software (ChAS, Affymetrix) to process the raw data detected a 9.2-Mb trisomy at 1q42.12-q42.2, a 6.7-Mb tetrasomy consisting of the duplication of two haplotypes, each of which probably derives from either the father or the mother, at 1q42.2-q43, and a 8.2-Mb segment with the absence of heterozygosity at 1q43-qter consistent with isoUPD (arr[hg19]1q42.12q42.2(225,101,799_234,324,222)x3,1q42.2q43(234,330,738_240,992,219)x4,1q43qter(240,993,835_249,224,684)x2 hmz, Fig. 1a). Trisomic, tetrasomic, and iUPD regions contain 88, 38, and 94 Refseq genes, and 49, 21, and 24 OMIM genes, respectively. Neither copy number abnormalities nor iUPD around 1q42.2-qter was detected in the DNA of the patient's mother (data not shown). Since the genotyping

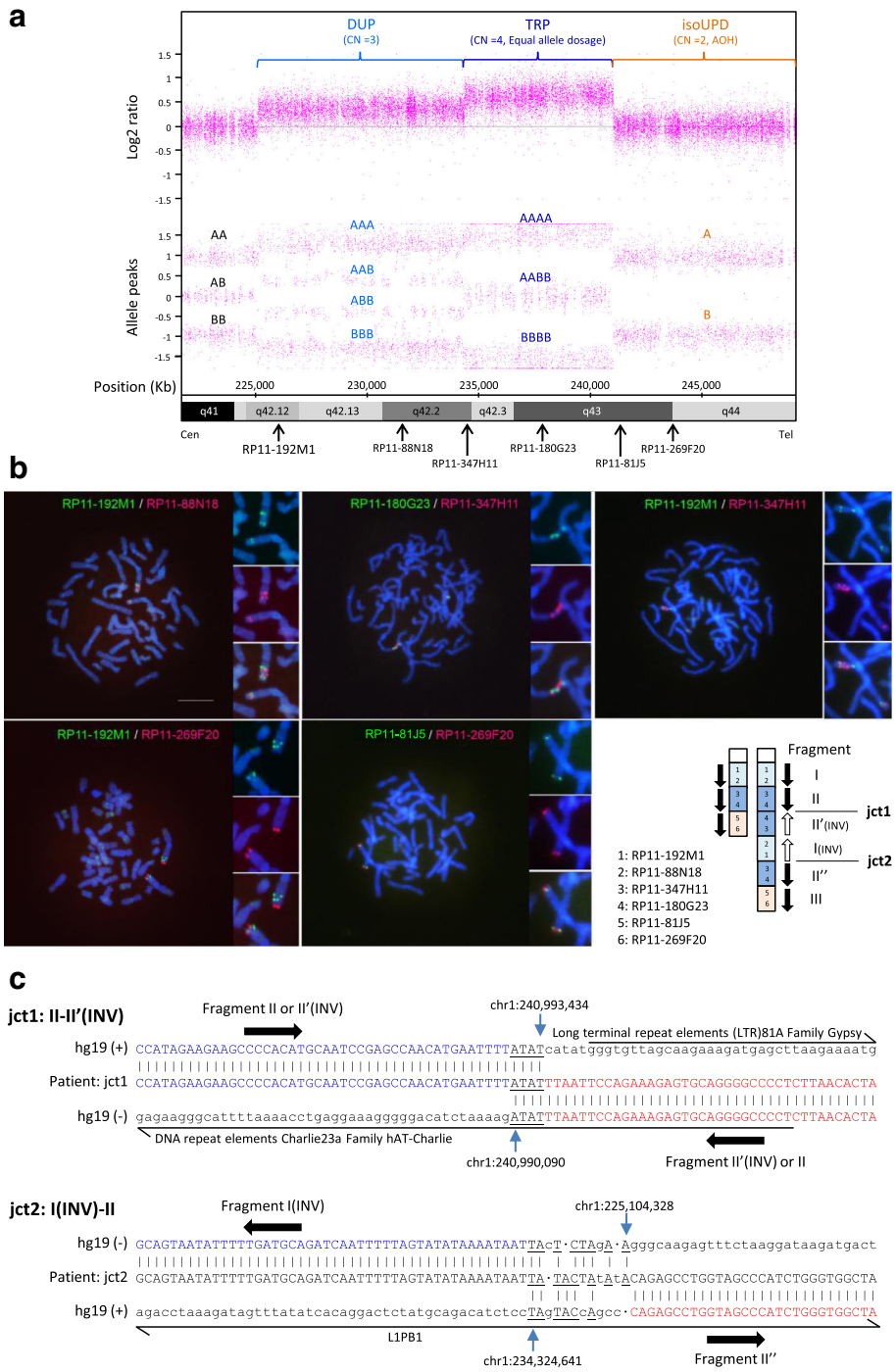

Fig. 1 (See legend on next page.)

(See figure on previous page.)
Fig. 1 a Chromosome Analysis Suite (ChAS) graphic results of Affymetrix CytoScan HD analysis for the 1q region that presented duplication (DUP), triplication (TRP), or isoUPD in the patient. Detection of CGR and isoUPD were performed using an Affymetrix CytoScan HD CMA platform (Affymetrix), which provides 906,600 polymorphic (SNP) and 946,000 non-polymorphic (CNV) markers, according to the manufacturer's recommendations. In addition, we used Chromosome Analysis Suite software (ChAS, Affymetrix) to process the raw data, and the output data were interpreted with the UCSC Genome Browser (http://genome.ucsc.edu; GRCh37/hg19 assembly). *Top*, copy number log2 ratio; bottom, allele peaks. CN, copy number. Possible genotype calls based on the allele dosage normalization algorithm are shown using A and B. The location of each BAC used for FISH analysis is shown. **b** Images of two-color FISH mapping using six BAC clones and the scheme of distal 1q CGR based on FISH data. Metaphase FISH images with high-magnification images of the distal 1q. BAC clones labeled with either FITC (*green*) or rhodamine (*red*) were hybridized to 4′,6-diamidino-2-phenylindole (DAPI)-stained chromosomes of the patient. The location and detailed information of each BAC are shown in Fig. 1a and Additional file 1: Table S1, respectively. In the scheme, arrows indicate the direction of chromosomal fragments I, II (II′, II″), and III, which presented duplication, triplication, and isoUPD, respectively, in CMA. Two junctions (jct 1 and jct2) between fragments II and II′ and between I and II″ are also shown. **c** Color-matched sequence alignment of breakpoint junctions in rearrangements. Top, jct1 (breakpoint junction 1 between segments II and II′); *bottom*, jct2 (breakpoint junction 2 between segments I and II″) (see Fig. 1b). Microhomology at the junctions is represented by underlined letters. Frequent mismatch sequences were only observed near jct2 within long-range PCR products (data not shown). Thick arrows indicate the possible orientation of chromosomal fragments. Various types of repeat elements observed around junctions are shown

results using SNP typing probe within the iUPD region of the patient matched at least one of the maternal alleles, the iUPD segment is likely to have been inherited from his mother (data not shown), although genomic DNA of his father was not available to confirm the inheritance of this region. On the other hand, genotyping results within the trisomic region suggest that the duplicated segment is unlikely to have been inherited from his mother (data not shown). In the tetrasomic region (the triplicated segment), three allele peaks (AA, AB, and BB) with unusually large spaces between them were observed (Fig. 1a), suggesting the presence of AA/AA, AA/BB, and BB/BB tracks, which is only possible if each parent contributed equally with two alleles (either AA or BB).

Next, the location and orientation of each segment within this structurally altered region were determined by a series of dual-color fluorescence *in situ* hybridization (FISH) studies using bacterial artificial chromosome (BAC) clones located around the region (Fig. 1a and b, Additional file 1: Table S1) performed as described elsewhere [9]. Two signals (duplication) with a direct-inverted orientation and three signals (triplication) with a direct-inverted-direct orientation were detected by probes on the trisomic and tetrasomic regions, respectively. The triplicated segment in an inverted orientation was observed between the proximal triplicated segment in a direct orientation (junction 1, jct1) and the distal duplicated segment in an inverse orientation. The distal triplicated segment in a direct orientation is joined with the inversely oriented distal duplicated segment (junction 2, jct2). The isoUPD segment is then joined with this triplicated segment and terminates the abnormal chromosome 1. Taking these findings together, the final karyotype was interpreted as 46,XY,der(1)dup trp(pter → q43::q43 → q42.12::q42.2 → qter).

Genomic investigation

For the precise mapping of breakpoint junctions in the CGR (jct 1 and 2), we first performed mate pair next-generation sequencing using the Nextera Mate Pair Sample Preparation Kit and Illumina HiSeq 1500 with 100 paired-end cycles according to the manufacturer instructions (Illumina, San Diego, CA). Reads were aligned to the human genome sequence using the Burrows-Wheeler Alignment tool 0.7.12. (http://bio-bwa.sourceforge.net). Two recurrent structural variations within 1q42.12-1qter were identified from the discordant read pairs around the estimated boundary areas by the expected number of reads per region and visual inspection using the Integrative Genomics Viewer. Long-range polymerase chain reaction (PCR) using primers designed around the estimated boundaries (Additional file 2: Table S2) and Takara LA Taq (Takara Bio, Otsu, Japan) with the two step protocol according to the manufacturer instructions. The direct sequencing of PCR products defined sequences around two breakpoint junctions, jct1 and jct2 (Fig. 1c). Based on these results, the duplication and the triplication start around chr1:225,104,328 and 234,324,641, respectively, and the triplication stops around 240,990,090. Interestingly, the small telomeric duplication, namely, of approximately 3 Kb, which evaded CMA detection, is located between 240,990,090 and 240,993,434, and isoUPD starts around 240,993,434, although the copy number of the distal flanking duplication was not experimentally validated. Therefore, the CGR observed in our case seems to involve triplication with flanking duplications, which has been characterized as a type II triplication proposed by Liu et al. [10] with a particular DUP-TRP/INV-DUP structure, and isoUPD was also reported to be associated with this type of CGR [5]. Notably, all reported cases with triplication with flanking duplications followed by isoUPD have small flanking duplications (<0.258 Mb and < 0.004 Mb in proximal and distal duplications, respectively) [5], indicating that our case is the first with a large proximal duplication (approximately 9.2 Mb) in this type of CGR. Microhomology (ATAT) was observed at the jct1 breakpoint interval, whereas a microhomologous sequence with some mismatch sequences including insertions, deletion,

and point mutations was observed at the jct2 breakpoint interval (Fig. 1c). Mismatch sequences only near jct2 of CGR, which might occur during the same event as the *de novo* CGR/isoUPD formation, have previously been reported [5]. These mismatch sequences near to the breakpoint junctions of CGR are proposed to be one of the potential signature features of highly error prone replication-based mechanisms using DNA polymerase(s) of low fidelity or a replisome with reduced fidelity [2], although it remains unclear why mismatch sequences have been observed only in jct2 of CGR/isoUPD cases.

Within the isoUPD region, three genes were associated with four autosomal recessive diseases, as determined by a search of the Online Mendelian Inheritance in Man database (OMIM, http://www.omim.org, accessed 1 December, 2016; Additional file 3: Table S3). No phenotypes matching these four diseases were observed in the patient described here, and no pathogenic mutation was found in the three genes by Sanger sequencing. In addition, databases of imprinted genes, such as Geneimprint (http://www.geneimprint.com/site/genes-by-species, accessed 1 December, 2016) and the Catalogue of Parent of Origin Effects (http://igc.otago.ac.nz/home.html, accessed 1 December, 2016), indicated that there are no known imprinting genes within this isoUPD region.

Discussion

In the case presented here, our comprehensive analyses of all of the cytogenetic, microarray, and sequencing data suggest that the MMBIR-based template-switching model (Fig. 2a) recently proposed by Carbalho et al. [5] is one of the most plausible mechanisms underlying the gain of interstitial copy number followed by distal isoUPD to the telomere, which has not previously been described in the long arm of chromosome 1. In this model, two-step template switches triggered by stalled or collapsed replication forks might have occurred. The first template switch is supposed to use a sister chromatid to resume replication. Microhomology at the annealing site (jct1, Fig. 1c) in the complementary strand close to breakpoint is used to prime DNA synthesis, although it is difficult to determine whether this template switching occurred between c and d_c or d and c_c in our sequencing method. Then, unidirectional replication resumes in an inverted orientation and forms an inverted partially duplicated segment. A new event of fork stalling or collapsing might occur and release a free 3' end, which can be resolved by a second template switch to the homologous chromosome using microhomology again, resulting in the formation of a jct2 (Figs. 1c and 2a). This second compensating inversion might contribute to result in a viable cell. A target annealing site was selected between alleles B and C in the present case, and the derivative chromosome results in a DUP-TRP/INV-DUP structure with a unique long proximal duplicated region (b and b_c, Fig. 2b). Because BIR cannot account for the observations of microhomology identified in both jct1 and jct2 (Fig. 1c), MMBIR is probably involved in resolving both the first and the second breaks. In our case and some previously reported cases [5], however, various mismatch sequences including insertions, deletions, and/or point mutations around breakpoint junction sequences were observed only in jct2 of CGR and the size of the proximal duplicated region containing jct2 was commonly larger than that of the distal duplicated region containing jct1. Therefore, the accomplishment of the resolution of the second break might need additional mechanisms. It also remains unknown whether those two events occurred either all at once in a post-zygotic mitotic cell or in two steps: the first step occurring in a pre-meiotic cell was resolved by the second step occurring in a post-zygotic cell. These alternatives cannot be distinguished using the current data. In addition, it also difficult to rule out tissue-specific mosaicism as a post-fertilization mitotic event in this case, although no finding of mosaicism was observed in all data obtained from the peripheral leukocytes/lymphocytes of the patient.

Recently, several cases along with our own with concurrent triplication (tetrasomy) and isoUPD, which may be explained by the MMBIR-based mechanism, detected by CMA containing SNP probes, have been reported [4–7]. However, detailed analyses of centromeric and telomeric junctions of triplicated regions in a tiling array or at the sequence level have only been performed on the cases reported by Carvalho et al. [5] and the present case. In most of those cases with detailed junctional analyses, relatively short flanking duplications were observed. These findings suggest that the small size of flanking duplications might have led to the evasion of array-based detection in three reported cases without detailed junction analyses [4, 6, 7]. Indeed, the concurrent triplication (tetrasomy) and isoUPD were detected by Affymetrix arrays including SNP probes in all cases, but a flanking duplication was observed in this analysis only at the centromeric junction in the present case. In addition, microhomology was observed in breakpoint junctions in most of the cases with the DUP-TRP/INV-DUP rearrangement followed by isoUPD reported by Carvalho et al. [5] and the present case, suggesting that an MMBIR-based mechanism might underline the formation of at least this type of genomic alteration implicated in constitutional disorders. Detailed junction analyses of additional cases showing CGRs + isoUPD will be needed to provide support for an MMBIR-based mechanism inducing complex copy number gains and segmental isoUPD in tandem in subjects with multiple congenital anomalies.

Because partial 1q trisomy is a rare disorder and unbalanced chromosomal translocations are often observed

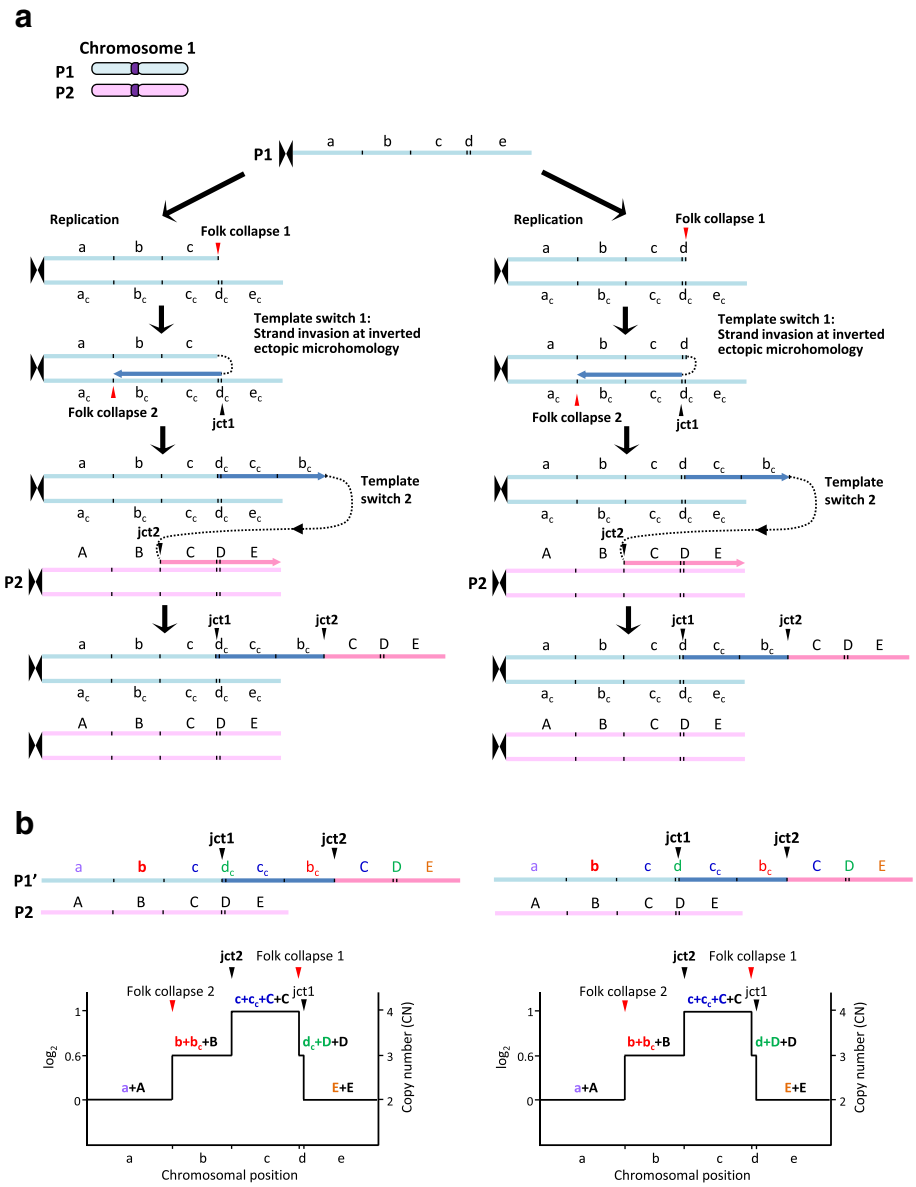

Fig. 2 Replication-based mechanism model for the generation of DUP-TRP/INV-DUP rearrangement followed by isoUPD detected in the present case. **a** The event probably occurred involving parental homolog chromosomes, P1 and P2. The first template switch (template switch 1) have been triggered by a stalled or collapsed replication fork (fork collapse 1), and used a complementary strand to resume replication through using microhomology in the complementary strand at the annealing site (jct1, Fig. 1c) to prime DNA synthesis, resulting in the production of a segment with the inverse orientation compared with the reference genome. Two putative jct1 sites, jct1 between c and d_c (*left*) and jct1 between d and c_c, (*right*) are predicted, because the same sequence result can be obtained in both cases (see Fig. 1c). Then, a new fork stalling or collapsing event (fork collapse 2) have released a free 3' end that can be resolved by the second template switching (template switch 2) through using the microhomology in the homologous chromosome at the annealing site (jct2, Fig. 1c) to prime and resume DNA synthesis, resulting in the generation of jct2 as well as isoUPD. a–d, representative chromosome alleles in P1 chromosome; a_c–e_c, complementary chromosome alleles in P1 chromosome; A–E: corresponding homologous chromosome alleles in the P2 chromosome. **b** *Top*: different genomic structures are predicted to be generated depending on the location of the selected annealing site (jct1) to prime DNA synthesis in the first template switch event. isoUPD will result if the unidirectional replication fork continues until the telomere. *Bottom*: predicted segmental CNV in a simulated CMA. Note that the small size of the telomeric duplication between fork collapse 1 and jct1 led to the evasion of CMA detection (Fig. 1a), because the region was too small to be detected by Affymetrix Cytoscan HD array

with this alteration [11–16], it is difficult to evaluate the contribution of 1q trisomy to the phenotype in cases involving another chromosome. Patients with pure partial distal trisomy 1q are known to demonstrate a wide range of manifestations of variable severity. However, distal 1q duplication syndrome is characterized by the

signs present in many of the previously reported cases [15, 16]. The present case showed some of the symptoms characteristic of distal 1q duplication syndrome, such as psychomotor developmental delay, cardiac defect, widely spaced eyes, a down-slanted palpebral fissure, low-set ear, a prominent forehead, club feet, and scoliosis, although psychomotor developmental delay and cardiac defect were very severe compared with those in previously reported cases and some features commonly found elsewhere were not observed [15, 16]. Because the present patient is the first known case of pure distal partial 1q tetrasomy and trisomy, it is possible that the copy number increase in some of the genes located between 1q42.12 and the middle of 1q43 (approximately 180 RefSeq genes) contributes to these symptoms, although no causal regions responsible for each symptom of distal trisomy/tetrasomy 1 syndrome have been clarified. In addition, the influence of isoUPD on the clinical features of the present case remains unknown because of a lack of reported cases with distal 1q UPD.

Conclusions

We report the first case with concurrent CGR (duplications and triplication) + isoUPD in 1q42.12-qter, from an initial diagnosis of interstitial trisomy 1q by conventional karyotyping. Comprehensive cytogenetic and molecular analyses provide additional evidence that DUP-TRP/INV-DUP rearrangement having a unique long proximal DUP structure followed by isoUPD may be generated by an MMBIR-based mechanism. Because it is almost impossible to quantify precise chromosomal copy numbers and detect UPD by conventional karyotyping, molecular cytogenetic analyses using CMA containing SNP probes with additional detailed analyses of the breakpoint junctions in a sequence level are recommended in cases suspected of having complex chromosomal abnormalities based on clinical and cytogenetic findings.

Additional files

Additional file 1: Table S1. BAC clones used in FISH experiments. (DOCX 14 kb)

Additional file 2: Table S2. List of primer sets used in PCR and sequencing for junctions of the CGR. (DOCX 14 kb)

Additional file 3: Table S3. Autosomal recessive diseases and causative genes aound the isoUPD region. (DOCX 14 kb)

Abbreviations

BAC: Bacterial artificial chromosome; CGR: Complex genomic rearrangements; CMA: Chromosomal microarray; CNV: Copy number variation; DUP-TRP/INV-DUP: Duplication-inverted triplication-duplication; FISH: Fluorescence *in situ* hybridization; isoUPD: Uniparental isodisomy; IUGR: Intrauterine growth retardation; MCA: Multiple congenital anomalie; MMBIR: Microhomology-mediated break-induced replication; PCR: Polymerase chain reaction; SNP: Single-nucleotide polymorphism; TOF: Tetralogy of Fallot

Acknowledgements

We thank the patient and his mother for their participation in this study and the Support Center for Advanced Medical Sciences, Graduate School of Biomedical Sciences, Tokushima University for technical assistances. This work was partly performed in the Cooperative Research Project Program of the Medical Institute of Bioregulation, Kyushu University.

Funding

This study was supported by JSPS KAKENHI Grant Numbers 26293304, 16K15618, and 15K19620 from the Ministry of Education, Culture, Sports, Science and Technology, Japan, and there is no role for funding agent in this study.

Availability of data and materials

The datasets supporting the conclusions of this article are included within the article and its additional file. More details are available on request.

Authors' contributions

TK, NO, and TN performed the genetic analysis and drafted the paper. CM performed the FISH experiments. YO, NF, and HI performed the genetic analysis. SS and NO collected the data of the patient. MS, KM, and HK contributed in writing the manuscript. Il performed CMA, contributed in writing the manuscript, and supervised the study. All the authors have read and approved the final manuscript.

Competing interests

The authors declare that they have no competing interests.

Consent for publication

Mother of the patient has given her informed written consent for publication of the present case report.

Ethics approval and consent to participate

The research protocol for this study was approved by the local ethics committee of Tokushima University. Written informed consent for the participation of the patient in this study was obtained from the patient's mother.

Publisher's Note

Author details

[1]Department of Human Genetics, Graduate School of Biomedical Sciences, Tokushima University, 3-18-15 Kuramoto-cho, Tokushima 770-8503, Japan. [2]Department of Oral and Maxillofacial Surgery, Kobe University Graduate School of Medicine, 7-5-1 Kusunoki-cho, Chuo-ku, Kobe, Hyogo 650-0017, Japan. [3]Division of Molecular Genetics, Institute for Comprehensive Medical Science, Fujita Health University, 1-98 Dengakugakubo Kutsukake-cho, Toyoake, Aichi 470-1192, Japan. [4]Japanese Red Cross Tokushima Hinomine Rehabilitation Center for People with Disabilities, 4-1 Shinkai Chuden-cho, Komatsushima, Tokushima 773-0015, Japan. [5]Department of Medical Genetics, Osaka Medical Center and Research Institute for Maternal and Child Health, 840 Murodo-cho, Izumi, Osaka 594-1101, Japan.

Received: 15 March 2017 Accepted: 21 April 2017
Published online: 28 April 2017

References

1. Zhang F, Carvalho CM, Lupski JR. Complex human chromosomal and genomic rearrangements. Trends Genet. 2009;25:298–307.
2. Carvalho CM, Pehlivan D, Ramocki MB, Fang P, Alleva B, Franco LM, et al. Replicative mechanisms for CNV formation are error prone. Nat Genet. 2013;45:1319–26.
3. Beneteau C, Landais E, Doco-Fenzy M, Gavazzi C, Philippe C, Béri-Dexheimer M, et al. Microtriplication of 11q24.1: a highly recognisable phenotype with short stature, distinctive facial features, keratoconus, overweight, and intellectual disability. J Med Genet. 2011;48:635–9.
4. Fujita A, Suzumura H, Nakashima M, Tsurusaki Y, Saitsu H, Harada N, et al. A unique case of de novo 5q33.3-q34 triplication with uniparental isodisomy of 5q34-qter. Am J Med Genet A. 2013;161A:1904–9.

5. Carvalho CM, Pfundt R, King DA, Lindsay SJ, Zuccherato LW, Macville MV, et al. Absence of heterozygosity due to template switching during replicative rearrangements. Am J Hum Genet. 2015;96:555–64.
6. Sahoo T, Wang JC, Elnaggar MM, Sanchez-Lara P, Ross LP, Mahon LW, et al. Concurrent triplication and uniparental isodisomy: evidence for microhomology-mediated break- induced replication model for genomic rearrangements. Eur J Hum Genet. 2015;23:61–6.
7. Xiao B, Xu H, Ye H, Hu Q, Chen Y, Qiu W. De novo 11q13.4q14.3 tetrasomy with uniparental isodisomy for 11q14.3qter. Am J Med Genet A. 2015;167A:2327–33.
8. Wiszniewska J, Bi W, Shaw C, Stankiewicz P, Kang SH, Pursley AN, et al. Combined array CGH plus SNP genome analyses in a single assay for optimized clinical testing. Eur J Hum Genet. 2014;22:79–87.
9. Murata C, Kuroki Y, Imoto I, Tsukahara M, Ikejiri N, Kuroiwa A. Initiation of recombination suppression and PAR formation during the early stages of neo-sex chromosome differentiation in the Okinawa spiny rat, Tokudaia muenninki. BMC Evol Biol. 2015;15:234.
10. Liu P, Carvalho CM, Hastings PJ, Lupski JR. Mechanisms for recurrent and complex human genomic rearrangements. Curr Opin Genet Dev. 2012;22:211–20.
11. Nowaczyk MJ, Bayani J, Freeman V, Watts J, Squire J, Xu J. De novo 1q32q44 duplication and distal 1q trisomy syndrome. Am J Med Genet A. 2003;120A:229–33.
12. Coccé MC, Villa O, Obregon MG, Salido M, Barreiro C, Solé F, Gallego MS. Duplication dup(1)(q41q44) defined by fluorescence in situ hybridization: delineation of the 'trisomy 1q42– > qter syndrome'. Cytogenet Genome Res. 2007;118:84–6.
13. Kulikowski LD, Bellucco FT, Nogueira SI, Christofolini DM, Smith Mde A, de Mello CB, et al. Pure duplication 1q41-qter: further delineation of trisomy 1q syndromes. Am J Med Genet A. 2008;146A:2663–7.
14. Balasubramanian M, Barber JC, Collinson MN, Huang S, Maloney VK, Bunyan D, Foulds N. Inverted duplication of 1q32.1 to 1q44 characterized by array CGH and review of distal 1q partial trisomy. Am J Med Genet A. 2009;149A:793–7.
15. Watanabe S, Shimizu K, Ohashi H, Kosaki R, Okamoto N, Shimojima K, et al. Detailed analysis of 26 cases of 1q partial duplication/triplication syndrome. Am J Med Genet A. 2016;170A:908–17.
16. Morris ML, Baroneza JE, Teixeira P, Medina CT, Cordoba MS, Versiani BR, Roese LL, Freitas EL, Fonseca AC, Dos Santos MC, Pic-Taylor A, Rosenberg C, Oliveira SF, Ferrari I, Mazzeu JF. Partial 1q duplications and associated phenotype. Mol Syndromol. 2016;6:297–303.

JIMD Reports
DOI 10.1007/8904_2018_108

RESEARCH REPORT

Disruption of the Responsible Gene in a Phosphoglucomutase 1 Deficiency Patient by Homozygous Chromosomal Inversion

Katsuyuki Yokoi • Yoko Nakajima • Tamae Ohye • Hidehito Inagaki • Yoshinao Wada • Tokiko Fukuda • Hideo Sugie • Isao Yuasa • Tetsuya Ito • Hiroki Kurahashi

Received: 13 February 2018 / Revised: 06 April 2018 / Accepted: 10 April 2018

Abstract Phosphoglucomutase 1 (PGM1) deficiency is a recently defined disease characterized by glycogenosis and a congenital glycosylation disorder caused by recessive mutations in the *PGM1* gene. We report a case of a 12-year-old boy with first-cousin parents who was diagnosed with a PGM1 deficiency due to significantly decreased PGM1 activity in his muscle. However, Sanger sequencing revealed no pathogenic mutation in the *PGM1* gene in this patient. As this case presented with a cleft palate in addition to hypoglycemia and elevated transaminases and creatine kinase, karyotyping was performed and identified homozygous inv(1)(p31.1p32.3). Based on the chromosomal location of the *PGM1* gene at 1p31, we analyzed the breakpoint of the inversion. Fluorescence in situ hybridization (FISH) combined with long PCR analysis revealed that the inversion disrupts the *PGM1* gene within intron 1. Since the initiation codon in the *PGM1* gene is located within exon 1, we speculated that this inversion inactivates the *PGM1* gene and was therefore responsible for the patient's phenotype. When standard molecular testing fails to reveal a mutation despite a positive clinical and biochemical diagnosis, the presence of a gross structural variant that requires karyotypic examination must be considered.

Communicated by: Eva Morava, MD PhD

K. Yokoi · Y. Nakajima · T. Ito
Department of Pediatrics, Fujita Health University School of Medicine, Toyoake, Japan

K. Yokoi · T. Ohye · H. Inagaki · H. Kurahashi (✉)
Division of Molecular Genetics, Institute for Comprehensive Medical Science, Fujita Health University, Toyoake, Japan
e-mail: kura@fujita-hu.ac.jp

Y. Wada
Department of Obstetric Medicine, Osaka Women's and Children's Hospital, Osaka, Japan

T. Fukuda
Department of Pediatrics, Hamamatsu University School of Medicine, Hamamatsu, Japan

H. Sugie
Faculty of Health and Medical Sciences, Tokoha University, Hamamatsu, Japan

I. Yuasa
Division of Legal Medicine, Tottori University Faculty of Medicine, Yonago, Japan

H. Kurahashi
Genome and Transcriptome Analysis Center, Fujita Health University, Toyoake, Japan

H. Kurahashi
Center for Collaboration in Research and Education, Fujita Health University, Toyoake, Japan

Introduction

Phosphoglucomutase 1 (PGM1) deficiency is a recently defined disease, characterized by glycogenosis and a congenital disorder of glycosylation (CDG) (Tagtmeyer et al. 2014). ς PGM1 deficiency is rare with only 38 patients from 29 families with different ethnic backgrounds described in the literature so far (Perez et al. 2013; Ondruskova et al. 2014; Tagtmeyer et al. 2014; Loewenthal et al. 2015; Zeevaert et al. 2016; Wong et al. 2016; Preisler et al. 2017; Nolting et al. 2017; Voermans et al. 2017). PGM1 is an essential enzyme in carbohydrate biosynthesis and metabolism and functions both in glycogen synthesis and breakdown through a reversible conversion of glucose

1-phosphate to glucose 6-phosphate (Morava 2014). Since glucose 1-phosphate is a precursor of the nucleotide sugars used for glycan biosynthesis, PGM1 activity is also required for protein *N*-glycosylation (Beamer 2015). Hence, PGM1 deficiency has considerably diverse phenotypes. Most of the affected patients develop a congenital anomaly syndrome showing a bifid uvula, cleft palate, and Pierre Robin sequence as clinical manifestations from the time of birth. Hepatopathy, dilated cardiomyopathy (DCM), hypoglycemia, muscle weakness, exercise intolerance, growth retardation, and endocrine abnormalities emerge in these cases over time (Scott et al. 2014). Many of these manifestations can be linked to the role of PGM1 in glucose metabolism and glycosylation (Beamer 2015).

PGM1 deficiency is caused by homozygous or compound heterozygous nucleotide alterations in the *PGM1* gene (Herbich et al. 1985). Several types of mutations have been reported to date including missense mutations, frameshifts, and splicing mutations (Tagtmeyer et al. 2014; Lee et al. 2014; Perez et al. 2013; Timal et al. 2012; Stojkovic et al. 2009; Ondruskova et al. 2014). In our current report, we describe a case of PGM1 deficiency caused by a homozygous chromosomal inversion that disrupts the *PGM1* gene at chromosome 1p31.

Materials and Methods

Cytogenetic Analysis

Fluorescence in situ hybridization (FISH) analysis of the patient and his parents was performed using standard methods to detect the breakpoint region at the chromosome level. Briefly, phytohemagglutinin-stimulated lymphocytes or Epstein-Barr virus-transformed lymphoblastoid cell lines derived from the subjects were arrested by exposure to colcemid. Metaphase preparations were then obtained by hypotonic treatment with 0.075 M KCl followed by methanol/acetate fixation. A bacterial artificial clone (BAC) containing 1p31.1, RP4-534K7 (chr1:63,525,021-63,677,603), was used as the test probe, and a chromosome 1 centromere probe (CEN1 SpectrumOrange Probe; Abbott Laboratories, Abbott Park, IL) was used as a reference. The probes were labeled by nick translation with digoxigenin-11-dUTP. After hybridization, the probes were detected with DyLight 488 Anti-Digoxigenin/Digoxin. Chromosomes were visualized by counterstaining with 4;6-diamino-2-phenylindole.

Sequence Analysis

To isolate the breakpoint, long-range PCR with several sets of primers for the *PGM1* gene was performed using LA Taq (TaKaRa, Shiga, Japan) (Fig. 3c). The PCR conditions were 35 cycles of 10 s at 98°C and 15 min at 60°C. PCR primers were designed using sequence data from the human genome database. PCR products were separated on 0.8% (w/v) agarose gels and visualized with ethidium bromide. The homology between the obtained sequence around the breakpoint within the *PGM1* gene and the 1p32.3 sequence obtained from the database was examined using the BLAT in UCSC genome browser (http://genome-asia.ucsc.edu/human GRCh38/hg38).

Patient

The current study patient was a 12-year-old boy from consanguineous parents who are first cousins without a family history of congenital metabolic disease (Fig. 1). The patient's height was 137 cm (*z*-score −2.3), and he had a normal body weight of 39 kg (*z*-score −0.6). He was born at term with a normal body weight and length. A cleft palate was noted at birth and closure surgery was performed at 12 months. Persistently elevated transaminases (AST 50–400 U/L [normal value <33 U/L] and ALT 40–300 U/L [normal value <30 U/L]) had been observed since that surgery. In addition, mild hypoglycemia after overnight fasting and an occasionally elevated serum creatine kinase (100–2,600 U/L [normal value <287 U/L]) were evident from 2 years of age. The echocardiogram and electrocardiogram readings showed no abnormalities, and his psychomotor development was normal. Oral administration of uncooked corn starch prior to bedtime was commenced to prevent morning hypoglycemia.

At 2 years of age, the patient was referred to our department for further examination. Intravenous glucose loading at 2 g/kg led to an elevated lactate level (from 7 to 37 mg/dL at 120 min) with a normal lactate/pyruvate ratio. Intramuscular glucagon loading at 0.03 mg/kg caused no increase of blood sugar either during fasting or at 2 h after a meal, indicating a deficiency in the generation of hepatic glucose from glycogen. However, the activity of the debrancher enzyme responsible for glycogen storage disease (GSD) type III, phosphorylase involved in GSD type VI, and phosphorylase kinase enzyme associated with GSD type IX in the peripheral blood was normal. A forearm nonischemic exercise test was performed when the patient was 8 years old. No increase in venous lactate with a large elevation in his ammonia levels (297 μg/dL) was observed, suggesting inadequate glycogen utilization in the muscle. A muscle biopsy was therefore performed, and a significant decrease in PGM activity was identified (62.1 nmol/min/mg [controls 351.1 ± 81.1]). Isoelectric focusing (IEF) of serum transferrin was performed as previously described (Okanishi et al. 2008) and revealed a mixed type I and type II pattern, typical features of CDG-I and CDG-II (Fig. 2) (Tagtmeyer et al. 2014).

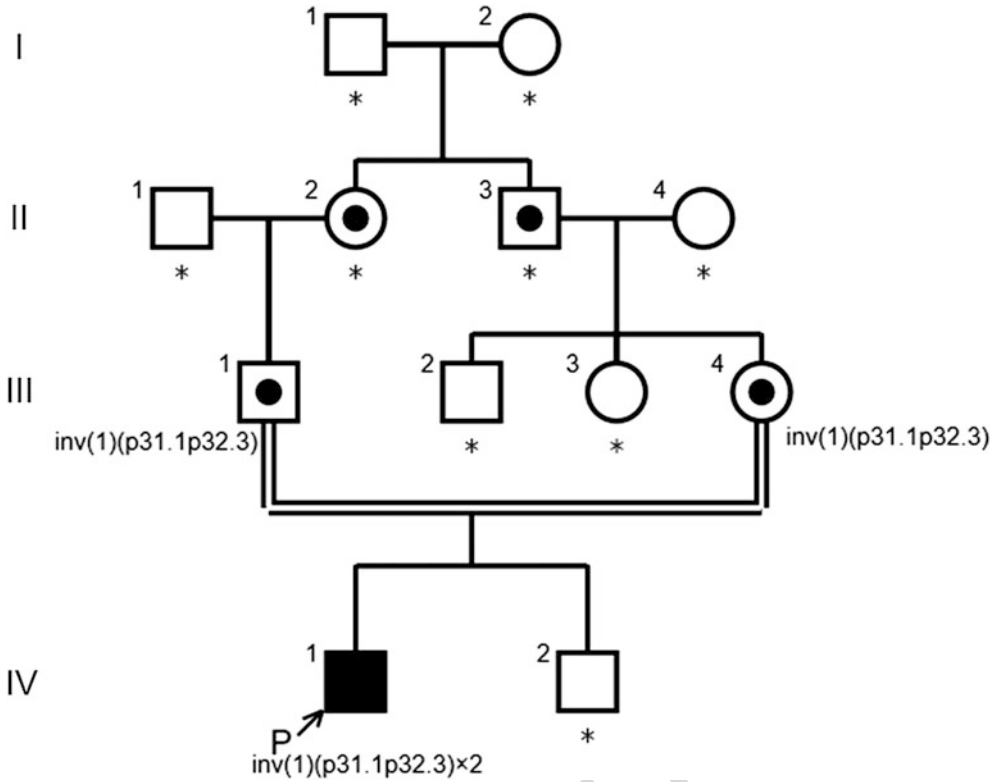

Fig. 1 Pedigree of the family. Arrow indicates proband. Carriers are represented by a dot in the middle of circles or squares. Asterisks indicate the family members who have not been tested AU4

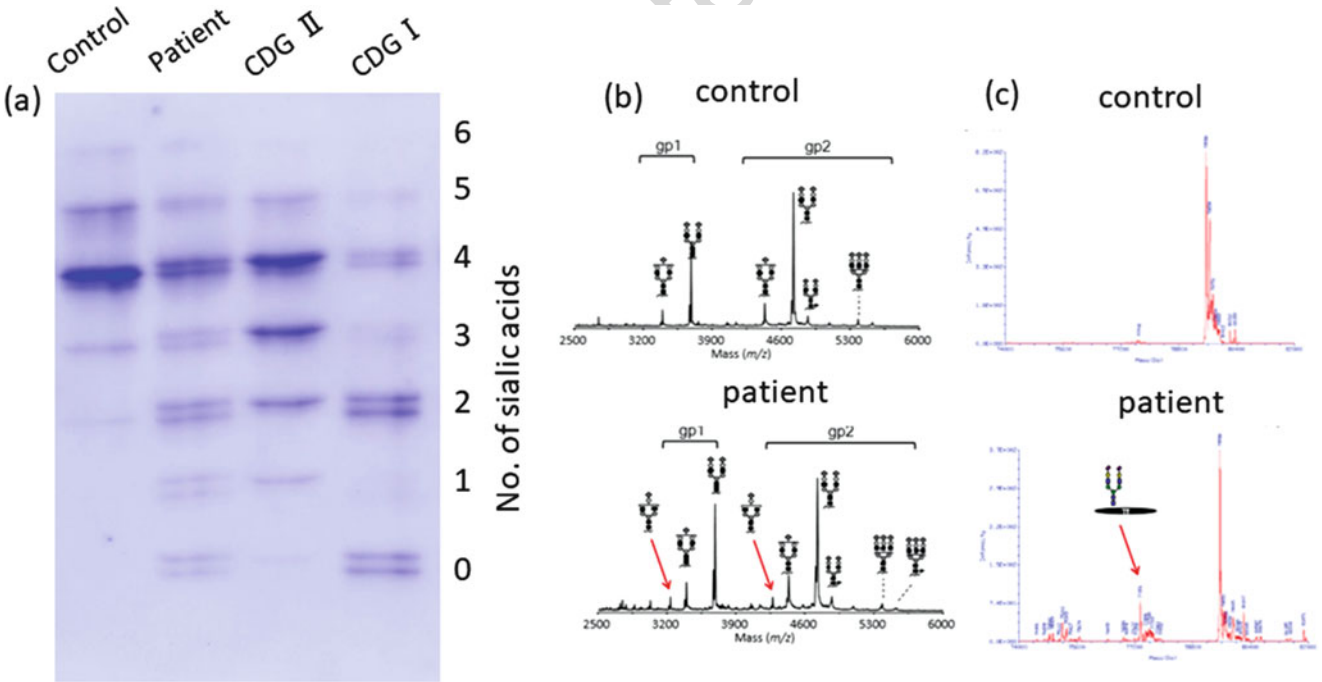

Fig. 2 Serum transferrin isoelectric focusing (IEF) and mass spectrometry (MS) of serum glycoproteins. (**a**) IEF patterns of serum transferrin. The number of negatively charged sialic acids of transferrin is indicated on the right. Reduced glycosylation of transferrin including an unusual mixture of CDG-I and CDG-II patterns (increased tri-, di-, mono-, and asialotransferrin) is shown. (**b**) Matrix-assisted laser desorption/ionization (MALDI) mass spectrum of (glycol) tryptic peptides of transferrin. A biantennary glycan lacking galactose and sialic acid are observed in patient's transferrin (arrows). (**c**) Electrospray ionization (ESI) mass spectrum of transferrin. An abnormal transferrin isoform having a single glycan is present in the patient (arrow)

Mass spectrometry to characterize the molecular abnormality of transferrin was performed as previously described (Wada 2016) and further revealed the presence of a variety of transferrin glycoforms, including forms lacking one or both glycans as well as forms with truncated glycan (Fig. 2). These findings were consistent with a PGM1 deficiency (Tagtmeyer et al. 2014), and genetic analysis was performed to confirm this. Sanger sequencing revealed only c.1258T>C, a common polymorphism in the database. The karyotype of the patient was determined to be 46,XY, inv(1)(p31.1p32.3)x2, of which inv(1) was homozygous (Fig. 3a). Since the *PGM1* gene is localized at 1p31, we hypothesized that the inversion disrupts this gene in our patient, and we thus analyzed its distal breakpoint.

Results

FISH signals for the BAC RP4-534K7 probe that incorporates the entire *PGM1* gene are observed on the short arm of chromosome 1 in an individual with a normal karyotype. In our current study patient however, two distinct signals were detected on the short arm of both chromosome 1 homologues (Fig. 3b). This result indicated that the inversion breakpoint in the patient had disrupted the *PGM1* genomic region. Karyotype analysis of both parents showed 46,XY,inv(1)(p31.1p32.3). Both parents carried the inv(1) in a heterozygous state, suggesting that the two inv(1) homologues of the patient had been transmitted from each parent, respectively (data not shown).

Long PCR revealed that one of the PCR primer pairs (4F-4R) within intron 1 failed to amplify the products in the patient DNA, indicating that the breakpoint of the inversion was located in intron 1 (Fig. 3d). To analyze the breakpoint region in more detail, we performed additional long PCR. The 4F4-4R but not the 4F3-4R primer pair successfully yielded a PCR product. This indicated that the breakpoint was located between primer 4F3 and 4F4. We did not obtain the sequence of the other breakpoint region at

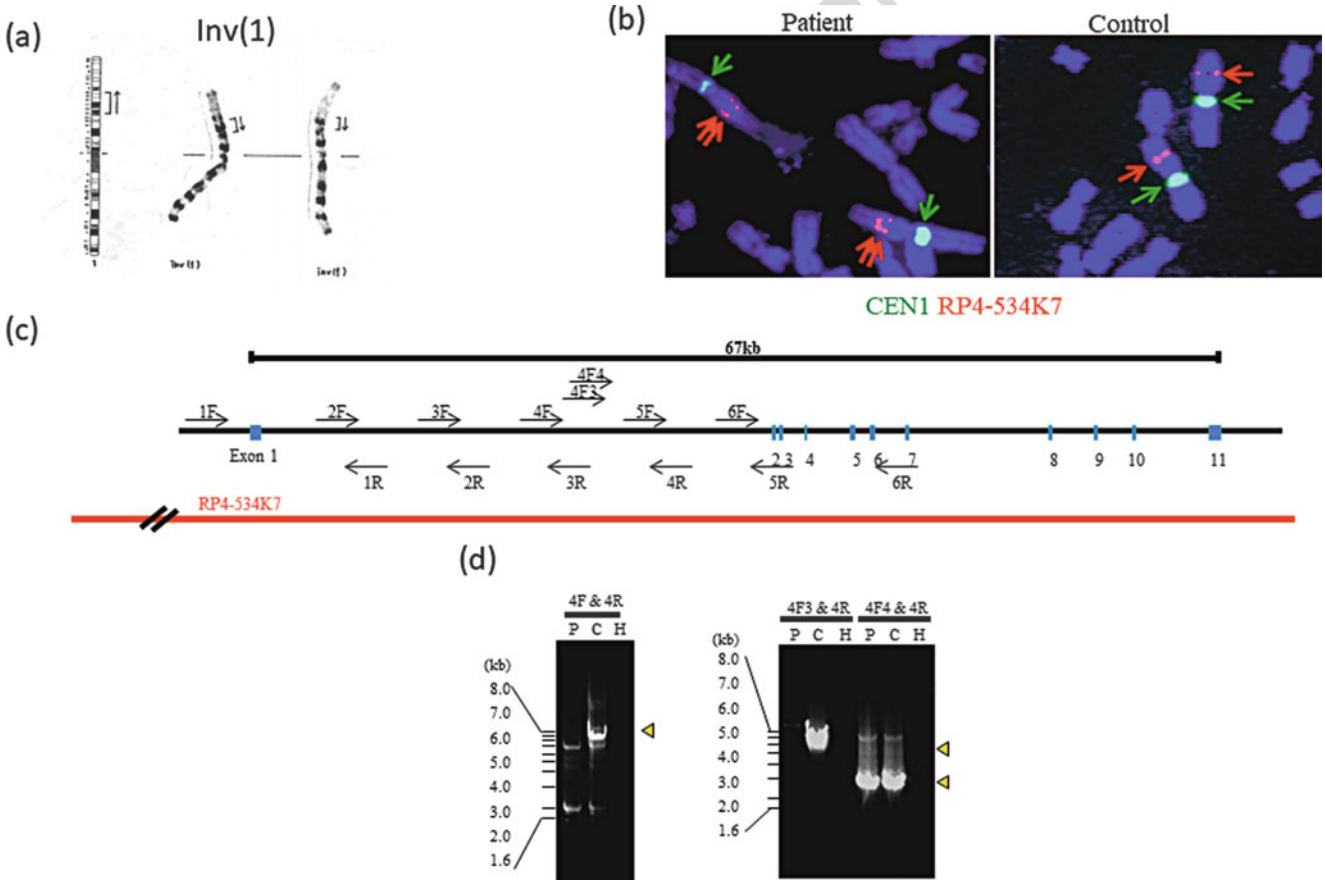

Fig. 3 Disruption of the *PGM1* gene in the study patient by a chromosomal inversion. (**a**) G-banding of the patient's karyotype which was determined to be 46,XY,inv(1)(p31.1p32.3)x2, in which inv(1) was homozygous. (**b**) FISH signals for *PGM1* (red arrow) are typically observed on the short arm of chromosome 1 in a normal karyotype. In contrast, the two distinctive signals were detected on the chromosome 1 arm in the study patient. (**c**) Schematic representation of the *PGM1* gene structure. The blue boxes denote exons. The positions of the PCR primers are indicated by arrows. The position of the BAC probe is also indicated. (**d**) Agarose gel electrophoresis of long PCR products. 4F-4R and 4F3-4R primer pairs failed to amplify the PCR products in the study patient. *P* patient, *C* control, *H* H_2O

1p32.3. To ascertain the mechanism leading to the inversion, we obtained the sequence information of the 1p32.3 from the database and analyzed the homology with the 4F3-4F4 sequence. However, we did not find any sequence similarity between the 4F3-4F4 sequence and the genomic sequence at 1p32.3.

Discussion

PGM1 deficiency is a newly identified metabolic disorder which manifests features of both CDG and glycogenosis (Tagtmeyer et al. 2014). Our present case report describes a young male patient with PGM1 deficiency caused by a homozygous inv(1) inherited from his first-cousin parents that disrupts each of the two *PGM1* alleles. To date, 38 PGM1 deficiency patients have been reported, and pathogenic mutations in the *PGM1* gene were identified and genetically confirmed in most of these cases (Perez et al. 2013; Ondruskova et al. 2014; Tagtmeyer et al. 2014; Loewenthal et al. 2015; Zeevaert et al. 2016; Wong et al. 2016; Preisler et al. 2017; Nolting et al. 2017; Voermans et al. 2017). However, a small subset of patients exists without mutations in the *PGM1* gene. In our present case, Sanger sequencing did not identify any pathogenic mutation in the *PGM1* gene initially. However, subsequent chromosome karyotyping of our patient detected the presence of multiple congenital malformations and led to the identification of the aforementioned chromosomal inversion as the responsible mutation for his condition. Hence, when standard molecular testing does not reveal any abnormalities in patients who have been clinically and biochemically diagnosed with a known congenital disorder, chromosome testing may be a fruitful approach for identifying the responsible mutation in the candidate gene.

In mutational screening for single-gene disorders involving an autosomal recessive inheritance of a known causative gene, it is often the case that only one of the recessive mutations is identified. If standard PCR and Sanger methods fail to identify two pathogenic mutations within the exons or flanking intronic regions of the responsible gene, a subsequent approach can be MLPA (multiplex ligation-dependent probe amplification) analysis of structural variant copy number variations or repeat PCR/Sanger analysis to identify possible mutations in noncoding regions such as the promoter or enhancer. In addition to these methods, standard chromosomal karyotyping is important for identifying large-scale chromosomal abnormalities that may disrupt the causative gene.

A possible mechanism of inversion formation is interspersed repeat sequences that may induce chromosomal aberrations. Direct repeats can induce deletions or duplications via recombination between them, whereas inverted repeats sometimes cause pericentric or paracentric inversion (Lakich et al. 1993). In our present case, we didn't find any specific segmental duplication sequences at the breakpoint region within the intron of the *PGM1* gene. Likewise, there was no evidence of segmental duplication sequences that were common to the proximal and distal breakpoint regions. Our patient harbored a rare homozygous pericentric inversion of chromosome 1 inherited from first-cousin parents. We assume therefore that the inversion chromosome in this patient is rare in the general population and is not a recurrent type variation.

Since the initiation codon in the *PGM1* gene is located within exon 1, the inversion in our patient that disrupts intron 1 produces a truncated protein containing only the amino acids encoded by exon 1 or no protein product at all due to nonsense-mediated mRNA decay. The crystal structure of human PGM1 has not been characterized, but the structure of the analogous PGM from rabbit has been described (Liu et al. 1997). Because of the high amino acid sequence identity (97%) between these two proteins, the rabbit PGM structure provides a highly accurate model for the human enzyme. PGM1 is a monomeric protein of 562 amino acids and 4 structural domains (Beamer 2015). The active site is located in a large, centrally located cleft and can be segregated into four highly conserved regions which are located behind exon 2. In our present case therefore, even if a truncated protein was produced, it would have no active site, and PGM1 deficiency would still arise. Further, we performed RT-PCR using the patient's peripheral blood. The exon 1 transcript was found to be present, but we did not find any transcripts distal to the exon 2 (data not shown). Some residual enzymatic activity might be possibly due to other members of phosphoglucomutase family, PGM2 and PGM3, that could compensate the PGM1 activity (Maliekal et al. 2007; Wong et al. 2016).

In conclusion, we have identified and analyzed an inverted chromosome from a PGM1 deficiency patient. Our present report also emphasizes the potential benefits of karyotype analysis in congenital cases in which molecular genetic testing fails to identify the responsible mutations.

Acknowledgments We thank the patient and his family for their participation in this study. We also thank past and present members of our laboratory. This research was partly supported by the intramural research grant (29-4) for Neurological and Psychiatric Disorders of NCNP (H. Sugie).

Synopsis Sentence

Karyotypic examination must be considered when standard molecular testing fails to reveal a mutation despite a positive clinical and biochemical diagnosis.

Conflict of Interest

Katsuyuki Yokoi, Yoko Nakajima, Ohye Tamae, Hidehito Inagaki, Yoshinao Wada, Tokiko Fukuda, Hideo Sugie, Isao Yuasa, Tetsuya Ito, and Hiroki Kurahashi declare that they have no conflict of interest.

Informed Consent

All procedures followed were in accordance with the ethical standards of the responsible committee on human experimentation (institutional and national) and with the Helsinki Declaration of 1975, as revised in 2005(5). Informed consent was obtained from all patients for inclusion in the study.

Author Contributions

Katsuyuki Yokoi retrieved the data and drafted and revised the manuscript.

Yoko Nakajima and Tetsuya Ito discovered the patients and provided many data.

Tamae Ohye did cytogenetic analysis and sequence analysis.

Hidehito Inagaki supported and supervised experiments.

Yoshinao Wada did mass spectrometry.

Tokiko Fukuda and Hideo Sugie estimated enzyme activity.

Isao Yuasa did IEF of serum transferrin.

Hiroki Kurahashi: conception and design, analysis and interpretation, and revising the article critically for important intellectual content.

All authors contributed to and reviewed the manuscript.

References

Beamer LJ (2015) Mutations in hereditary phosphoglucomutase 1 deficiency map to key regions of enzyme structure and function. J Inherit Metab Dis 38:243–256

Herbich J, Szilvassy J, Schnedl W (1985) Gene localisation of the PGM1 enzyme system and the Duffy blood groups on chromosome no. 1 by means of a new fragile site at 1p31. Hum Genet 70:178–180

Lakich D, Kazazian HH Jr, Antonarakis SE, Gitschier J (1993) Inversions disrupting the factor VII gene are a common cause of severe haemophilia A. Nat Genet 5:236–241

Lee Y, Stiers KM, Kain BN, Beamer LJ (2014) Compromised catalysis and potential folding defects in in vitro studies of missense mutants associated with hereditary phosphoglucomutase 1 deficiency. J Biol Chem 289:32010–32019

Liu Y, Ray W, Baranidharan S (1997) Structure of rabbit muscle phosphoglucomutase refined at 2.4A resolution. Acta Crystallogr D 53:392–405

Loewenthal N, Haim A, Parvari R, Hershkovitz E (2015) Phosphoglucomutase-1 deficiency: intrafamilial clinical variability and common secondary adrenal insufficiency. Am J Med Genet A 167A:3139–3143

Maliekal P, Sokolova T, Vertommen D, Veiga-da-Cunha M, Van Schaftingen E (2007) Molecular identification of mammalian phosphopentomutase and glucose-1,6-bisphosphate synthase, two members of the alpha-D-phosphohexomutase family. J Biol Chem 282:31844–31851

Morava E (2014) Galactose supplementation in phosphoglucomutase-1 deficiency; review and outlook for a novel treatable CDG. Mol Genet Metab 112:275–279

Nolting K, Park JH, Tegtmeyer LC et al (2017) Limitations of galactose therapy in phosphoglucomutase 1 deficiency. Mol Genet Metab Rep 13:33–40

Okanishi T, Saito Y, Yuasa I et al (2008) Cutis laxa with frontoparietal cortical malformation: a novel type of congenital disorder of glycosylation. Eur J Paediatr Neurol 12:262–265

Ondruskova N, Honzik T, Vondrackova A, Tesarova M, Zeman J, Hansikova H (2014) Glycogen storage disease-like phenotype with central nervous system involvement in a PGM1-CDG patient. Neuro Endocrinol Lett 35:137–141

Perez B, Medrano C, Ecay MJ et al (2013) A novel congenital disorder of glycosylation type without central nervous system involvement caused by mutations in the phosphoglucomutase 1 gene. J Inherit Metab Dis 36:535–542

Preisler N, Cohen J, Vissing CR et al (2017) Impaired glycogen breakdown and synthesis in phosphoglucomutase 1 deficiency. Mol Genet Metab 122:117–121

Scott K, Gadomski T, Kozicz T, Morava E (2014) Congenital disorders of glycosylation: new defects and still counting. J Inherit Metab Dis 37:609–617

Stojkovic T, Vissing J, Petit F et al (2009) Muscle glycogenosis due to phosphoglucomutase 1 deficiency. N Engl J Med 361:425–427

Tagtmeyer LC, Rust S, van Scherpenzeel M et al (2014) Multiple phenotypes in phosphoglucomutase 1 deficiency. N Engl J Med 370:533–542

Timal S, Hoischen A, Lehle L et al (2012) Gene identification in the congenital disorders of glycosylation type I by whole-exome sequencing. Hum Mol Genet 21:4151–4161

Voermans NC, Preisler N, Madsen KL et al (2017) PGM1 deficiency: substrate use during exercise and effect of treatment with galactose. Neuromuscul Disord 27:370–376

Wada Y (2016) Mass spectrometry of transferrin and apolipoprotein C-III for diagnosis and screening of congenital disorder of glycosylation. Glycoconj J 33:297–307

Wong SY, Beamer LJ, Gadomski T et al (2016) Defining the phenotype and assessing severity in phosphoglucomutase-1 deficiency. J Pediatr 175:130–136

Zeevaert R, Scalais E, Muino Mosquera L et al (2016) PGM1 deficiency diagnosed during an endocrine work-up of low IGF-1 mediated growth failure. Acta Clin Belg 71:435–437

The Journal of Obstetrics and Gynaecology

Taylor & Francis
Taylor & Francis Group

Journal of Obstetrics and Gynaecology

ISSN: 0144-3615 (Print) 1364-6893 (Online) Journal homepage: http://www.tandfonline.com/loi/ijog20

Twin pregnancy with chromosomal abnormalities mimicking a gestational trophoblastic disorder and coexistent foetus on ultrasound

Akiko Ohwaki, Haruki Nishizawa, Noriko Aida, Takema Kato, Asuka Kambayashi, Jun Miyazaki, Mayuko Ito, Makoto Urano, Yuka Kiriyama, Makoto Kuroda, Masahiro Nakayama, Shin-Ichi Sonta, Kaoru Suzumori, Takao Sekiya, Hiroki Kurahashi & Takuma Fujii

To cite this article: Akiko Ohwaki, Haruki Nishizawa, Noriko Aida, Takema Kato, Asuka Kambayashi, Jun Miyazaki, Mayuko Ito, Makoto Urano, Yuka Kiriyama, Makoto Kuroda, Masahiro Nakayama, Shin-Ichi Sonta, Kaoru Suzumori, Takao Sekiya, Hiroki Kurahashi & Takuma Fujii (2018): Twin pregnancy with chromosomal abnormalities mimicking a gestational trophoblastic disorder and coexistent foetus on ultrasound, Journal of Obstetrics and Gynaecology, DOI: 10.1080/01443615.2017.1401598

To link to this article: https://doi.org/10.1080/01443615.2017.1401598

JOURNAL OF OBSTETRICS AND GYNAECOLOGY, 2018
https://doi.org/10.1080/01443615.2017.1401598

Taylor & Francis
Taylor & Francis Group

CASE REPORT

Twin pregnancy with chromosomal abnormalities mimicking a gestational trophoblastic disorder and coexistent foetus on ultrasound

Akiko Ohwaki[a,b], Haruki Nishizawa[a], Noriko Aida[a], Takema Kato[b], Asuka Kambayashi[a], Jun Miyazaki[a,b], Mayuko Ito[a,b], Makoto Urano[c], Yuka Kiriyama[c], Makoto Kuroda[c], Masahiro Nakayama[d], Shin-Ichi Sonta[e], Kaoru Suzumori[e], Takao Sekiya[a], Hiroki Kurahashi[b] and Takuma Fujii[a]

[a]Department of Obstetrics and Gynecology, Fujita Health University School of Medicine, Toyoake, Japan; [b]Division of Molecular Genetics, Institute for Comprehensive Medical Science, Fujita Health University, Toyoake, Japan; [c]Department of Diagnostic Pathology, Fujita Health University School of Medicine, Toyoake, Japan; [d]Department of Pathology and Laboratory Medicine, Osaka Medical Center and Research Institute for Maternal and Child Health, Izumi, Japan; [e]Fetal Life Science Center, Ltd, Nagoya, Japan

Case report

Gestational trophoblastic disorder with a coexistent foetus occurs in 1 in 20,000–100,000 pregnancies (Wee and Jauniaux 2005) and mostly involves a partial hydatidiform mole with a live foetus and rarely a twin pregnancy with a complete hydatidiform mole and co-twin foetus (Gupta et al. 2015). Most cases of partial hydatidiform mole have triploidy with multiple structural anomalies and result in first trimester miscarriage (Toufaily et al. 2016). However, their management is complicated because the coexistent foetus is occasionally a normal healthy diploid foetus. Furthermore, this condition is often accompanied by severe complications such as hyperemesis, preeclampsia or thromboembolic disease (Matsui et al. 2000; Sebire et al. 2002). Thus, the diagnosis and management of gestational trophoblastic diseases with coexistent foetus are clinically important.

A gravid 33-year-old woman (gravid 4, para 3) was referred to our hospital with vaginal bleeding from 9 weeks of gestation. She was noted on prenatal ultrasound to have a normal foetus with an abnormally thickened space in the placental region. At 11 gestational weeks, a snowstorm pattern was observed on ultrasound examination, but it was slightly different from the typical pattern for hydatidiform mole. Multivesicular areas were prominent, but the other areas appeared relatively normal (Figure 1(A)). At 13 gestational weeks, the snowstorm pattern persisted with a foetal growth retardation of a biparietal diameter of 22.3 mm (−1.9 SD). The serum β-human chorionic gonadotropin (β-hCG) level was alarmingly elevated at 369,065 mIU/ml at 14 gestational weeks, whereas alpha-fetoprotein (AFP) showed a normal level of 109.5 ng/ml. β-hCG was persistently high at 207,336 mIU/ml at 16 gestational weeks, whereas AFP was 159.8 ng/ml.

The couple decided to terminate the pregnancy after considering the risks because the possibility of hydatidiform mole and coexistent foetus could not be excluded. After the curettage, the woman was in good condition and the β-hCG level decreased to 4 mIU/ml. The delivered foetus had a median cleft lip and palate (Figure 1(B)). The placenta appeared to have patchy villous hydropic changes (Figure 1(C)). Histological examination revealed focal villous oedema. Trophoblast hyperplasia was not observed (Figure 1(D)). After receiving approval from the Ethical Review Board and obtaining written informed consent from the couple, we obtained samples from the foetal skin and from the oedematous and normal-seeming areas of the placenta.

Initial cytogenetic analysis by Giemsa staining indicated a normal karyotype (data not shown). Cytogenetic microarray of the foetus revealed three copies of an 8-Mb region at the terminus of 9p, but monosomy 2q and trisomy 4q in the placenta (Figure 1(E–G)). Although hydatidiform moles generally result from dispermic triploidy or diandric diploidy with the paternal genome only, there was no evidence of triploidy or uniparental disomy. The foetus was found to carry arr[hg19] 9p24.3p24.1(326,927–8,441,863)x3, which appeared to be mosaic with normal cells because the copy number (CN) state was 2.80. On the other hand, the placental tissue was found to carry arr[hg19] 2q37.3(237,337,625–242,408,074)x1, 4q25q35.2(113,816,349–190,957,.473)x3. These appeared to be in mosaicism because the CN state was 1.35 and 2.67, respectively. Approximately 65–67% of cells showed monosomy 2q and trisomy 4q, and it is likely that the same cells had monosomy 2q and trisomy 4q simultaneously. The placental tissue also showed 9p trisomy at CN state 2.33, suggesting that 33% of cells carried the 9p trisomy identified in the foetus. On the other hand, we did not detect monosomy 2q and trisomy 4q in foetal tissue at all.

Microsatellite analysis of the DXS0767 locus revealed that there was only a small level of maternal tissue contamination in placental tissue (2–3%, data not shown) and none in foetal tissue. The pattern of whole-genome SNP genotyping also excluded the chimeric pattern but indicated a single zygote origin, suggesting that all of the foetus and placenta were derived from a monozygotic twin or somatic

CONTACT Haruki Nishizawa nharuki@fujita-hu.ac.jp Department of Obstetrics and Gynecology, Fujita Health University, 1-98 Dengakugakubo, Kutsukake, Toyoake, Aichi, 470-1192 Japan

Supplemental data for this article can be accessed here.

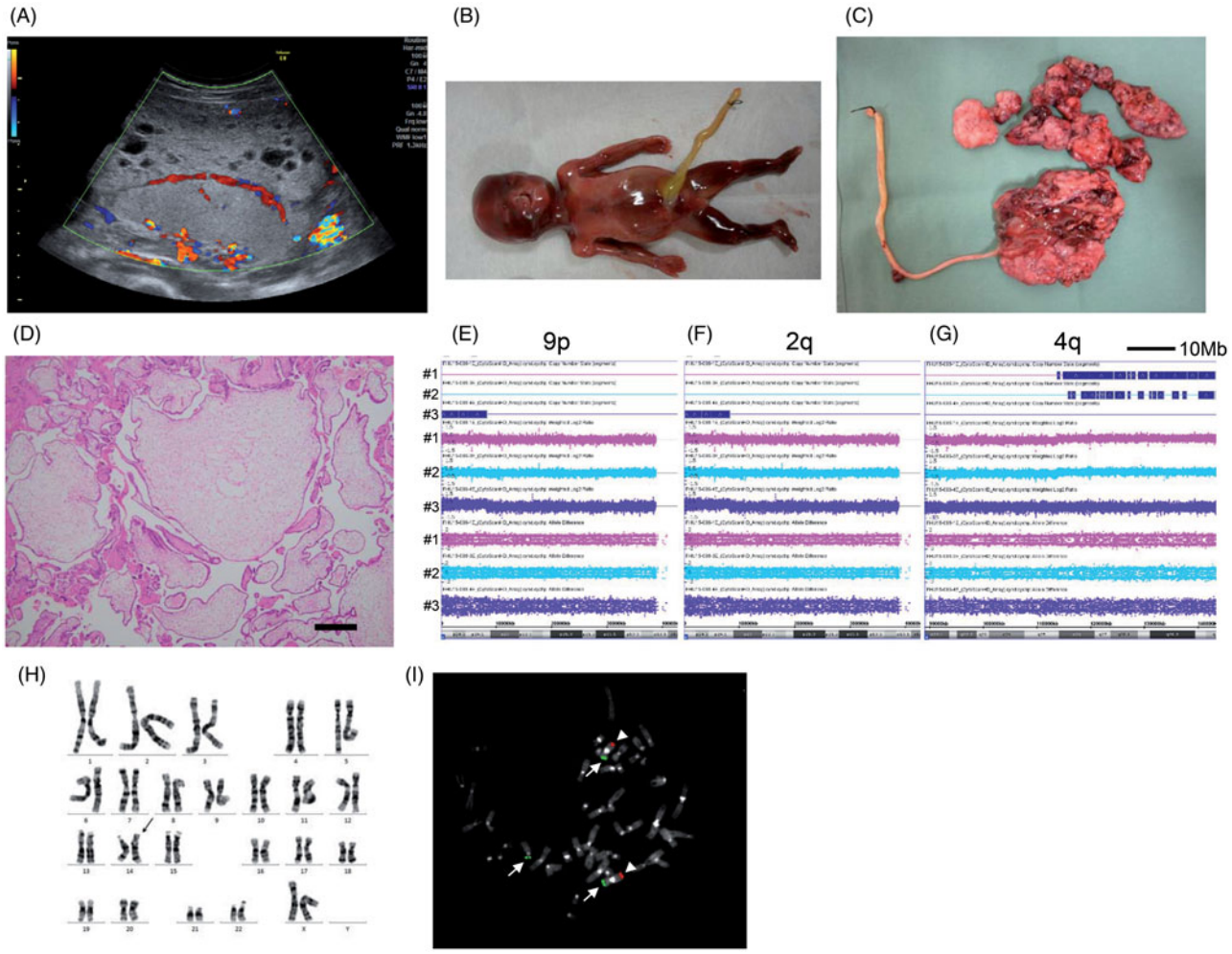

Figure 1. Clinical phenotypes and cytogenetic analysis of the foetus and placenta. Cytogenetic microarray was performed using CytoScan HD Array (Affymetrix). #1: placenta that appeared relatively normal; #2: placenta that included villous hydrops lesions; and #3: foetus. (A) Ultrasound examination at 11 weeks of gestation. Two separate areas – a vesicular area (upper area) and relatively normal area (lower area) – were observed, which are atypical for gestational trophoblastic disease. (B) Foetus. A median cleft lip and palate were observed. (C) Macroscopic analysis of the placenta. Patchy villous hydropic changes were observed. (D) Histological specimen for chorionic villi. Focal villous oedema was observed. Scale bars, 100 m. (E) 9p and 9q. (F), 2q. (G), 4q. Scale bars, 10 Mb. (H), Giemsa staining. Additional material was observed at the terminal region of 14p. (I) FISH. Subtelomeric probes (Vysis ToTelVision, Abbott Molecular) revealed the presence of der(14)t(9;14)(p24;p11.2) (arrow). White arrows: 9p; and white arrow heads: 9q.

mosaicism of a single zygote. As the CN state showed that the cell population with 9p and that with monosomy 2q and trisomy 4q were mutually exclusive, we concluded that they were likely from monozygotic twins (Supplementary Figure).

Reexamination of Giemsa staining of the foetal fibroblasts showed additional material at the terminal of 14p. Subtelomeric FISH was performed to further characterise the CN abnormalities. Trisomy 9p was found to originate from der(14)t(9;14)(p24; p11.2) in all of the 20 metaphases examined (Figure 1(H,I)). As the CN states of monosomy 2q and trisomy 4q are reciprocal, the monosomy 2q and trisomy 4q found in the placenta were likely to have originated from unbalanced t(2;4)(q37.3; q25) translocation. However, subtelomeric FISH did not detect the t(2;4) translocation in any of the foetal cells. We did not study the karyotype of the couple because they did not want to undergo the required examinations.

We recommend careful performance of the differential diagnosis of abnormal placenta with snowstorm pattern, particularly in cases with a coexistent foetus. A molecular cytogenetic study including zygosity test is necessary for differential diagnosis because it is possible that a chromosomal disorder might underlie placental abnormalities. The severities of the clinical symptoms in the foetus with such disorders vary widely. These disorders often result in lethality from multiple congenital anomalies, whereas cases with milder cytogenetic abnormalities can occasionally survive and live to a good age. Furthermore, confined placental mosaicism might affect the foetus to a lesser degree (Johnson and Wapner 1997; Lestou and Kalousek 1998). Thus, the results of the cytogenetic test might seriously affect the choice of treatment for the ultrasound findings.

Acknowledgements

We gratefully acknowledge the patients and their families for participating in this study.

Disclosure statement

The authors report no conflicts of interest.

Funding

This study was supported by the Ogyaa Donation Foundation from the Japan Association of Obstetricians & Gynecologists and by grants-in-aid for Scientific Research from the Ministry of Education, Culture, Sports, Science, and Technology and from the Ministry of Health, Labour and Welfare of Japan.

References

Gupta K, Venkatesan B, Kumaresan M, Chandra T. 2015. Early detection by ultrasound of partial hydatidiform mole with a coexistent live fetus. WMJ: Official Publication of the State Medical Society of Wisconsin 114:208–211.

Johnson A, Wapner RJ. 1997. Mosaicism: implications for postnatal outcome. Current Opinion in Obstetrics & Gynecology 9:126–135.

Lestou VS, Kalousek DK. 1998. Confined placental mosaicism and intrauterine fetal growth. archives of disease in childhood. Fetal and Neonatal Edition 79:F223–F226.

Matsui H, Sekiya S, Hando T, Wake N, Tomoda Y. 2000. Hydatidiform mole coexistent with a twin live fetus: a national collaborative study in Japan. Human Reproduction (Oxford, England) 15:608–611.

Sebire NJ, Foskett M, Paradinas FJ, Fisher RA, Francis RJ, Short D, et al. 2002. Outcome of twin pregnancies with complete hydatidiform mole and healthy co-twin. Lancet (London, England) 359:2165–2166.

Toufaily MH, Roberts DJ, Westgate MN, Holmes LB. 2016. Triploidy: variation of phenotype. American Journal of Clinical Pathology 145:86–95.

Wee L, Jauniaux E. 2005. Prenatal diagnosis and management of twin pregnancies complicated by a co-existing molar pregnancy. Prenatal Diagnosis 25:772–776.

JOURNAL OF GENERAL VIROLOGY

RESEARCH ARTICLE

Kawamura *et al.*, *Journal of General Virology* 2017;98:1823–1830

DOI 10.1099/jgv.0.000834

MICROBIOLOGY SOCIETY

Analysis of the origin of inherited chromosomally integrated human herpesvirus 6 in the Japanese population

Yoshiki Kawamura,[1,*†] Tamae Ohye,[2,3] Hiroki Miura,[1] Masaru Ihira,[4] Yuri Kato,[5] Hiroki Kurahashi[2] and Tetsushi Yoshikawa[1]

Abstract

Integration of the complete human herpesvirus 6 (HHV-6) genome into the telomere of a chromosome has been reported in some individuals (inherited chromosomally integrated HHV-6; iciHHV-6). Since the proportion of iciHHV-6-positive individuals with integration in chromosome 22 is high in Japan, we hypothesized a founder effect. In this study, we sought to elucidate the reason for the high proportion of viral integrations into chromosome 22. We analyzed six cases of iciHHV-6A and two cases of iciHHV-6B, including one iciHHV-6A case with a matched sample from a father and one iciHHV-6B case with a matched sample from a mother. In iciHHV-6A, the same copy numbers of viral telomeric repeat sequences (TRS) and the same five microsatellite markers were detected in both the index case and paternal sample. Moreover, the same five microsatellite markers were demonstrated in four cases and the same copy numbers of viral TRS were demonstrated in two pairs of two cases. The present microsatellite analysis suggested that the viral genomes detected in some iciHHV-6A patients were derived from a common ancestral integration.

INTRODUCTION

Human herpesvirus 6 (HHV-6) is categorized into two distinct species, HHV-6A and HHV-6B, which are closely related herpesviruses with an overall nucleotide sequence identity of 90 % [1, 2]. Although HHV-6B is a ubiquitous virus in developed countries, prevalence of HHV-6A infection is very low in those countries [3]. Primary HHV-6B infection generally occurs in infancy and causes a common febrile exanthematous disease, exanthem subitum [4, 5]. In contrast, the clinical features of primary HHV-6A infection remain unclear. Horizontal transmission of HHV-6 is considered to be the main route of viral infection from parents to children because HHV-6 is frequently excreted in saliva in seropositive individuals [6, 7].

In addition to horizontal viral transmission, HHV-6 is transmitted from parent to child as an inherited chromosomally integrated HHV-6 (iciHHV-6) [8]. The complete HHV-6 genome is integrated into the telomere of a chromosome in some individuals [9, 10]. The prevalence of iciHHV-6 in the USA [11] and UK [12] is approximately 0.8 % compared to only 0.2 % in Japan [13]. As iciHHV-6 patients have one viral copy per cell, the result of real-time polymerase chain reaction (PCR) analysis demonstrates extremely high copy numbers of viral DNA; generally, over 1 million copies ml^{-1} in whole blood and over 3000 copies ml^{-1} in serum [14]. Furthermore, an individual with a high viral load may be misdiagnosed with an active HHV-6 infection and unnecessarily prescribed antiviral drugs [15]. Although iciHHV-6 has been associated with several clinical manifestations such as encephalitis [16, 17], cognitive dysfunction and fatigue [18], and angina pectoris [19], the precise role of iciHHV-6 in these clinical manifestations is still under debate. Additionally, viral reactivation from integrated HHV-6 genomes has also been suggested in immunocompromised patients [20] and pregnant women [21, 22], as well as under *in vitro* experimental conditions [23].

Received 3 March 2017; Accepted 12 May 2017

Author affiliations: [1]Department of Pediatrics, Fujita Health University School of Medicine, 1-98 Dengakugakubo, Kutsukake-cho, Toyoake, Aichi 470-1192, Japan; [2]Division of Molecular Genetics, Institute for Comprehensive Medical Science, Fujita Health University, 1-98 Dengakugakubo, Kutsukake-cho, Toyoake, Aichi 470-1192, Japan; [3]Department of Molecular Laboratory Medicine, Faculty of Medical Technology, Fujita Health University, 1-98 Dengakugakubo, Kutsukake-cho, Toyoake, Aichi 470-1192, Japan; [4]Faculty of Clinical Engineering, Fujita Health University School of Health Sciences, 1-98 Dengakugakubo, Kutsukake-cho, Toyoake, Aichi 470-1192, Japan; [5]Department of Clinical Laboratory, Fujita Health University Hospital, 1-98 Dengakugakubo, Kutsukake-cho, Toyoake, Aichi 470-1192, Japan.

***Correspondence:** Yoshiki Kawamura, yoshiki19810830@gmail.com *or* kyoshiki3@hotmail.com

Keywords: inherited chromosomally integrated human herpesvirus 6; telomere repeat sequence; microsatellite; founder effect.

Abbreviations: FISH, fluorescence *in situ* hybridization; HHV-6, human herpesvirus 6; iciHHV-6, inherited chromosomally integrated HHV-6; TRS, telomeric repeat sequences; PBMC, peripheral blood mononuclear cell; PCR, polymerase chain reaction; PHA, phytohemagglutinin.

†Present address: Division of Viral Products, Office of Vaccines Research and Review, Center for Biologics Evaluation and Research, Food and Drug Administration, 1090340 New Hampshire Avenue, Silver Spring, MD 20993, USA.

The HHV-6 genome can be integrated into a host chromosome by homology-mediated integration between human telomere repeat sequences and viral telomere repeat-like sequences and the integrated viral genome is transmitted by Mendelian inheritance [24, 25]. Furthermore, a recent study has demonstrated that TRS, in particular the perfect TRS, is crucial for integration and maintenance of a viral genome in HHV-6A integration [26]. Several sites of viral integration have been reported to date based on fluorescence *in situ* hybridization (FISH) analysis [27, 28]. Although the HHV-6 genome is believed to be randomly integrated into the telomeric region of host chromosomes, we discovered several individuals and families with iciHHV-6 integration into chromosome 22. Additionally, although HHV-6A infection rarely occurs in developed countries, it has been demonstrated that frequency of ciHHV-6A was higher than that of ciHHV-6B [29]. These findings suggest that HHV-6A may have higher potency for integration into a host genome or chromosome 22 may be more susceptible to viral genome integration than other chromosomes. Another possible hypothesis for explaining the unique findings is the founder effect. Therefore, we sought to elucidate the mechanism of viral integration into chromosome 22, particularly the founder effect.

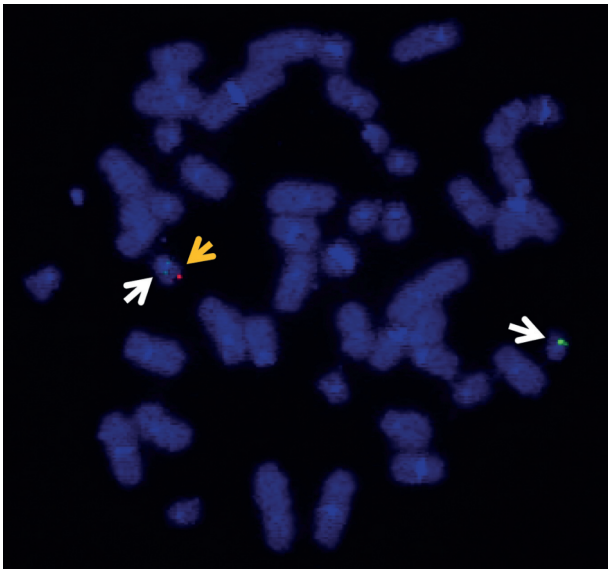

Fig. 1. FISH analyses of metaphase chromosomes derived from the iciHHV-6A study subjects. The red signal from HHV-6 is detectable (yellow arrowhead) at the end of chromosome 22q (family 5 index case). The green reference signals for chromosome 22q11.21 are indicated by white arrowheads.

RESULTS

Virological and microsatellite analyses of the two matched parent and index cases

FISH analysis confirmed that the virus genome was integrated into chromosome 22 in all of the analyzed subjects (one representative image is shown in Fig. 1). As an initial experiment, in order to evaluate the reliability of the analysis, microsatellite and TRS analyses were carried out in the matched parent and index cases. The data for virological and microsatellite analyses of two families (families 1 and 7) are shown in Fig. 2. In family 1, 16 HHV-6A TRS were detected in both the index case and paternal genomes. Additionally, the PCR products were exactly the same sizes for all five microsatellite markers on one of the alleles. The haplotypes for the integration of HHV-6A in chromosome 22 were estimated as follows: 242 bp for rs71772361; 102 bp for rs386395698; 273 bp for rs71810967; 215 bp for rs746349407; and 141 bp for rs762747991. Similarly, in family 7, 32 HHV-6B TRS were demonstrated in both the index case and maternal genomes. Moreover, the PCR products were exactly the same sizes for all of the microsatellite markers. Haplotypes of chromosome 22, in which HHV-6B might be integrated, were estimated to be 232 or 238 bp for rs71772361, 106 bp for rs386395698, 271 bp for rs71810967, 213 or 217 bp for rs746349407 and 141 bp for rs762747991. As expected, TRS and microsatellites were matched completely between each parent and index case suggesting the analysis is highly reliable.

Virological and microsatellite analyses of all cases of iciHHV-6A

Next, the TRS and microsatellite analysis were carried out in other unrelated families (index cases) to examine a founder effect. As assumed by the analysis of family 1, PCR product sizes of the microsatellite markers at rs71772361, rs386395698, rs71810967, rs746349407 and rs762747991, representing the integration of the HHV-6A genome, were 242, 102, 273, 215 and 141 bp, respectively. As shown in Table 1, the five haplotypes of one allele in families 2, 3 and 4 were exactly the same as family 1; however, these haplotypes were different in families 5 and 6. Additionally, 16 HHV-6A TRS were found to be identical in families 1 and 2, but not in families 3 and 4 that had 14 HHV-6A TRS. Families 5 and 6 contained 15 and 12 HHV-6A TRS, respectively.

Virological and microsatellite analyses of iciHHV-6B cases (Table 2)

In addition to iciHHV-6A, we compared the microsatellite markers of iciHHV-6B in families 7 and 8. PCR product sizes for microsatellite markers at rs71772361, rs386395698, rs71810967, rs746349407 and rs762747991 in family 8 were 232, 106, 255 or 277 bp, 215 or 211 bp, and 141 or 139 bp, respectively. Thus, distinct haplotypes of chromosome 22 were detected for family 8 relative to family 7. We detected 32 HHV-6B TRS in family 7 compared to 29 HHV-6B TRS in family 8.

DISCUSSION

A microsatellite is a tract of repetitive DNA ranging in length from two to five base pairs that is typically repeated 5–50 times [30]. Microsatellites have been identified in thousands of locations throughout the human genome, and are associated with a high mutation rate as well as high diversity in the population. Therefore, microsatellite marker

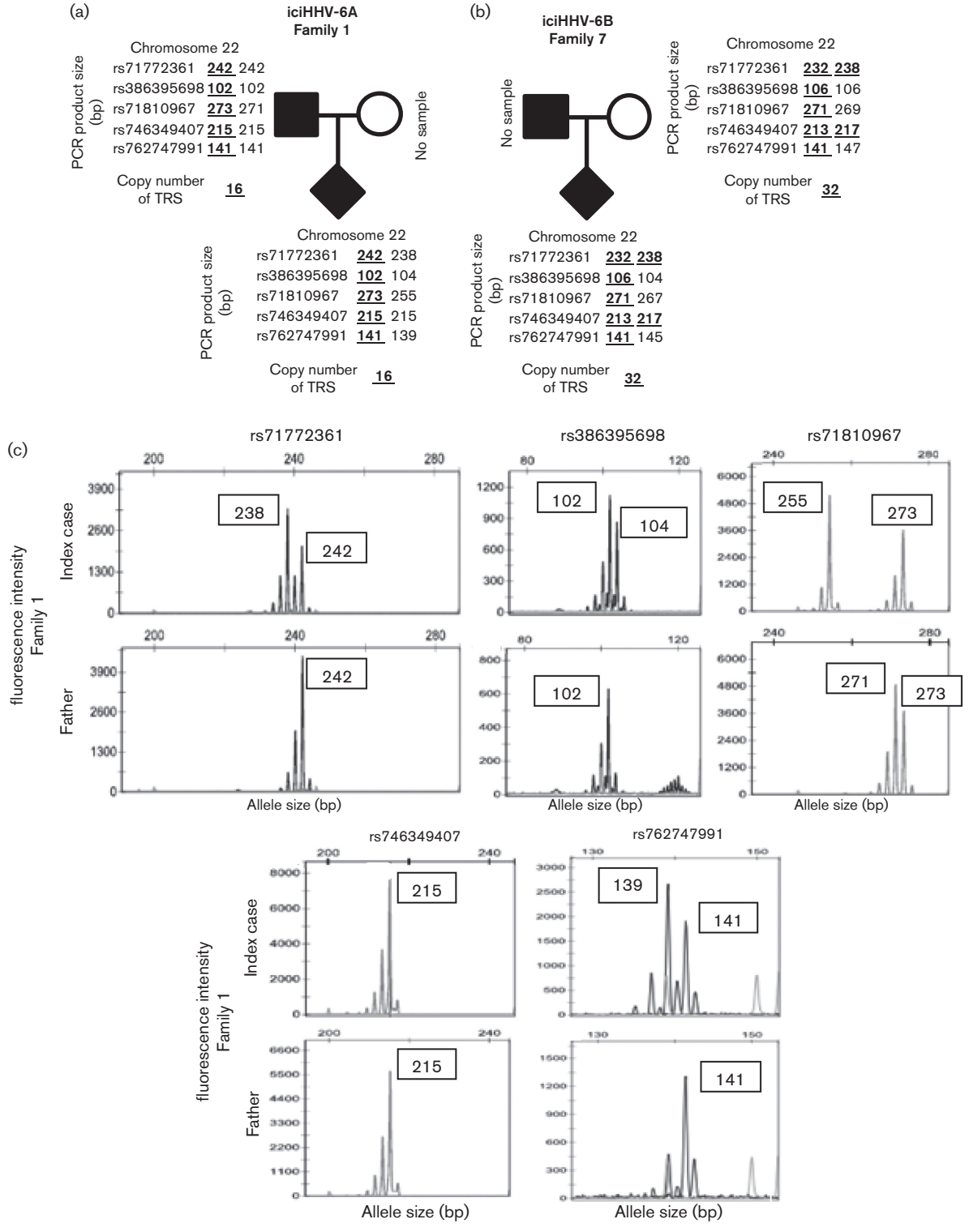

Fig. 2. Haplotypes of microsatellite markers and copy number of TRS for (a) the index case of iciHHV-6A and matched father and (b) the index case of iciHHV-6B and matched mother. (c) Genotyping microsatellite data. The dye labeled PCR amplicons of each microsatellite were separated by size using electrophoresis and were then identified by fluorescence detection. The data were genotyped detecting the peaks. The data of the index case and father from family 1 are shown here as a representative.

Table 1. PCR product size (bp) of microsatellite markers and copy number of TRS in iciHHV-6A patients and families

Family	1				2		3		4		5		6	
Case	Index		Father		Index		Index		Index		Index		Index	
rs71772361	**242**	238	**242**	242	**242**	242	**242**	236	**242**	236	**242**	242	**242**	232
rs386395698	**102**	104	**102**	102	**102**	102	**102**	102	**102**	102	110	110	**102**	102
rs71810967	**273**	255	**273**	271	**273**	271	**273**	255	**273**	271	**273**	269	**273**	269
rs746349407	**215**	215	**215**	215	**215**	213	**215**	209	**215**	217	**215**	213	219	227
rs762747991	**141**	139	**141**	141	**141**	143	**141**	141	**141**	139	**141**	143	143	139
Copy no. of TRS	**16**		**16**		**16**		14		14		15		12	

The bold underlined numbers indicate matched haplotypes among different families.

iciHHV-6, inherited chromosomally integrated human herpesvirus 6; no., number; TRS, telomeric repeat sequences.

analysis has been used to discover founder effects in several important genetic diseases [31–33]. In this study, the haplotypes of the microsatellites that are located close to the HHV-6 genome integration site in chromosome 22q were exactly the same between the index cases and matched parental samples for both HHV-6A and HHV-6B. Previous reports using FISH analysis [20, 23, 25, 34], revealed that if two generations had the same HHV-6 genome integration sites then the integrated viral genome was likely inherited from a parent. Our present data further support the hypothesis for hereditary transmission of iciHHV-6 from parent to child. Three of the five iciHHV-6A index cases (families 2, 3 and 4) from unrelated families had the same type of microsatellite markers as family 1. These results suggested that the HHV-6A genome was integrated into chromosome 22 of their ancestors and passed on to offspring in Japan. Although lack of basic data for the present microsatellites in the Japanese population is considered to be limitation of this study, as shown in Tables 1 and 2, the diversity of these microsatellites in iciHHV-6A patients was different from those of iciHHV-6B patients. Therefore, it is considered that the microsatellites measured in this study have sufficient diversity for evaluation of the founder effect.

Recently, Tweedy *et al.* demonstrated a founder HHV-6A integration in the telomere of chromosome 17p by phylogenetic analysis and Sanger sequencing of integration sites [35]. To the best of our knowledge, this is the first data that suggests the founder effect on iciHHV-6 in chromosome 22q, which is relatively common for the integration site in the Japanese population. Despite the fact that HHV-6A is not commonly detected in children in Japan [36], the USA and Europe [37–39], the HHV-6A genome was integrated into six of the eight iciHHV-6 cases in this study. Thus, this curious phenomenon further supports the notion of the founder effect of iciHHV-6A.

Two families of iciHHV-6B were analyzed in this study. The haplotypes of the microsatellites were the same in the index case and matched maternal sample (family 7). However, distinct haplotypes were identified for families 7 and 8. Thus, inherited transmission of iciHHV-6B genomes between generations was demonstrated, but it is unclear whether founder effects also play a role in iciHHV-6B. Future studies on a large number of cases are needed to elucidate the founder effect on iciHHV-6B in the Japanese population.

In order to determine whether integrated HHV-6 genomes were the same among the families, we examined the numbers of TRS located in the direct repeats of the HHV-6 genome. Previous studies determined that the number of TRS in the HHV-6 genome was highly variable among laboratory strains and clinical specimens [40]. In our previous study, the number of TRS was stable after at least 17 passages of cultured cells, and was useful for the differentiation of HHV-6 strains [41]. In contrast to our expectation, the number of HHV-6A TRS was different in some families with the same haplotype of microsatellites. For example, families 1 and 2 had 16 TRS and families 3 and 4 had 14 TRS. Although the number of TRS are stable after at least 17 passages of cultured cells [41], it is unclear whether the number of TRS is stable after more than 17 passages and is stable *in vivo*. It is possible that mutations may occur in a unique region of integrated HHV-6A causing the number of TRS to change over many generations after the initial integration of the viral genome in a Japanese ancestor. The

Table 2. PCR product size (bp) of microsatellite markers and copy numbers of TRS in iciHHV-6B patients and families

Family	7				8	
Case	Index		Mother		Index	
rs71772361	**232**	**238**	**232**	**238**	**232**	232
rs386395698	**106**	104	**106**	106	**106**	106
rs71810967	**271**	217	**271**	269	255	277
rs746349407	**213**	**217**	**213**	**217**	215	211
rs762747991	**141**	145	**141**	147	**141**	139
Copy no. of TRS	**32**		**32**		29	

The bold underlined numbers indicate matched haplotypes among different families.

iciHHV-6, inherited chromosomally integrated human herpesvirus 6; no., number; TRS, telomeric repeat sequences.

Table 3. Clinical characteristics of iciHHV-6 patients and families

Family	Cases	Trigger for the diagnosis of iciHHV-6
1	Index case and father	Examination for the causative agent of hemophagocytic lymphohistiocytosis
2	Index case	Virus monitoring in ALL patients after bone-marrow transplantation
3	Index case	Examination for the causative agent of uveitis
4	Index case	Examination for the causative agent of encephalitis
5	Index case	Examination for the causative agent of multiform exudative erythema
6	Index case	Virus monitoring in AML patients after bone-marrow transplantation
7	Index case and mother	Examination for the causative agent of meningitis
8	Index case	Virus monitoring in patients with aplastic anemia after bone-marrow transplantation

iciHHV-6, inherited chromosomally integrated human herpesvirus 6; ALL, acute lymphoblastic leukemia; AML, acute myeloid leukemia.

copy numbers of TRS were different between iciHHV-6A patients (from 12 to 16) and iciHHV-6B patients (from 29 to 32). These results were consistent with previous studies that demonstrated 15 to 25 TRS in HHV-6A strains and 22 to 90 TRS in HHV-6B strains [40, 41]. Although the underlying mechanism responsible for the variance in the copy number of TRS is unknown, these differences may depend on the HHV-6 species.

Most iciHHV-6 patients are diagnosed based on real-time PCR analysis. However, in transplant recipients, PCR monitoring may lead to the misdiagnosis of active HHV-6 infection and unnecessary administration of toxic antiviral drugs [15, 42]. FISH analysis is required for identification of the viral integration site, but it is a time-consuming method that requires informed consent from the patient. We understand that the small number of cases analyzed was a limitation of the current study. Therefore, we believe a longitudinal study enrolling a large number of cases is needed to confirm our hypothesis. Additionally, an international collaborative study is also important to elucidate the origin of the first integration of either the HHV-6A or HHV-6B genome into the human genome.

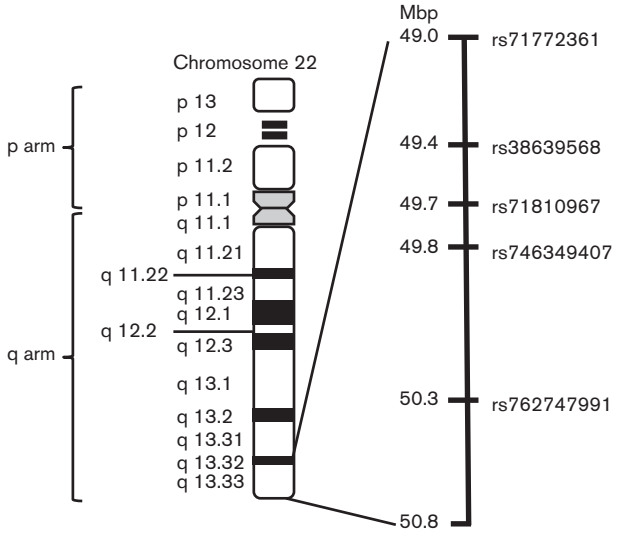

Fig. 3. Schematic of chromosome 22 including microsatellite markers at 22q13.33.

Based on our findings, the detection of iciHHV-6 in some patients is likely due to viral integration in their ancestors. Although previous reports have demonstrated the integration of HHV-6 into telomeres of naïve cells upon their infection *in vitro* [23], reports of this phenomenon has not yet been established *in vivo*. It is important to highlight the fact that iciHHV-6 represents a risk factor for the development of angina [19]. Therefore, we believe that it is critically important to elucidate the mechanism of viral integration into hosts to clarify the pathogenic relationship between reactivation and various diseases.

METHODS

Human subjects

Eight Japanese cases with iciHHV-6 integrated into chromosome 22, including two cases with matched parental samples, were analyzed in this study. All of the cases were from different regions in Japan, and there were no known blood relationships among them. iciHHV-6 was confirmed by real-time PCR analysis, which detected high copy numbers of viral DNA in peripheral blood mononuclear cells (PBMCs), hair follicle and nail samples [43], and by FISH of PBMCs [27]. Restriction digestion of PCR products was used to discriminate between integration of HHV-6A and HHV-6B viruses [44]. The clinical features of each case are summarized in Table 3.

FISH

FISH was conducted to identify the integration sites of HHV-6 on the human chromosome as previously described [27]. Briefly, phytohemagglutinin (PHA)-stimulated lymphocytes or Epstein Barr virus-transformed lymphoblasts were treated with colcemid to induce cell-cycle arrest. Metaphase preparations were obtained using 0.075 M KCl followed by methanol/acetate fixation. FISH probes were made from PCR products and a plasmid containing HHV-6 sequences that were labeled by nick-

Table 4. Position and primer sequences for the PCR of each microsatellite

Microsatellite			Primer sequence	
Name	Start position	End position	Forward	Reverse
rs71772361	49 006 333	49 006 366	5′-FAM-ACAACTTCCAGCAGACGTGGTG-3′	5′-CACACTCACTCACACAAAATCATG-3′
rs386395698	49 424 694	49 424 743	5′-FAM-TACCTCCTCCTCCTTGAGAC-3′	5′-GATCAGGGAGGAAGCAACAG-3′
rs71810967	49 706 585	49 706 632	5′-VIC-GCACAGATGGGATCCTAGAGTG-3′	5′-GATCCATTGACCAAAGATGACTTC-3′
rs746349407	49 832 718	49 832 765	5′-VIC-CAGACAGAGCTAGGAAATAAGTATG-3′	5′-AGCTACTAAGTGAAGGCATAGATAG-3′
rs762747991	50 296 194	50 296 230	5′-FAM-ATAGTGGTGAACTTTGGGAGCAAG-3′	5′-CGGTCTAGTTCAAGTTCCTTGAAC-3′

translation with biotin-16-dUTP or digoxigenin-11-dUTP. After hybridization, the probes were visualized using either Alexa Fluor 488-conjugated streptavidin or rhodamine-conjugated anti-digoxigenin in cells that were counter stained with 4′,6-diamino-2-phenylindole (DAPI). As reference standards, we used Bac clone RP11-186O8 (22q11.21) or TelVysion 22q SpectrumOrange (5J04-022, Abbott Molecular, Illinois, USA).

DNA extraction and PCR assay for the viral TRS of HHV-6

TRS analysis was conducted as previously described [41]. DNA was extracted from the stored PBMCs using a QIAamp DNA blood minikit (QIAGEN, Chatsworth, CA, USA) according to the manufacturer's instructions. Extracted DNA was eluted in 100 µl buffer and stored at −20 °C until ready to be assayed using PCR. TRS of HHV-6A and HHV-6B were amplified using primers that were specific to sequences containing the perfect telomere repeat known as TRS-2 in the direct repeat region (DR)-L of each virus as previously described [40, 41]. LA Taq (TaKaRa Bio, Otsu, Japan) and the following conditions were used for the PCRs: denaturation at 94 °C for 1 min, followed by 30 cycles at 94 °C for 30 s, 63 °C for 30 s and 72 °C for 1 min. The sizes of the amplified products were analyzed by electrophoresis on a 1 % agarose gel with ethidium bromide staining.

Sequence analysis of the TRS of HHV-6

PCR products were purified using a PCR purification kit (QIAGEN), and directly sequenced using a BigDye Terminator cycle sequencing kit and a Prism 3100 Avant analyzer (Applied Biosystems, Foster City, CA, USA). The purified PCR products were sequenced using H6 TRS F (5′-C TCGGACCCATGCTATCCT-3′) for HHV-6B cases and using HHVA (5′-CTACCACGGACGCGTACACACG-3′) for HHV-6A cases according to the manufacturer's instructions. The size of the TRS was enumerated by counting the copy number of TAACCC repeats.

PCR assay of microsatellites and microsatellite analysis using fragment analysis

Genotyping was performed by selecting five microsatellites using Tandem Repeats Finder on chromosome 22q13.33 (UCSC Genome Browser on Human Dec. 2013 (GRCh38/hg38) Assembly) [45] (Fig. 3). There were at least 15 perfect dinucleotide repeat sequences that were highly polymorphic in our population. These microsatellite loci were amplified by PCR using primer pairs consisting of a forward primer that was labeled at the 5′-end with either FAM or VIC and unlabeled reverse primers (Applied Biosystems). Since these microsatellites have not been submitted to GenBank, the rs number which includes each microsatellite region from the Single Nucleotide Polymorphism Database was used as the microsatellite name in this study, and the positions at chromosome 22 and primer sequences of each microsatellite are shown in Table 4. AmpliTaq Gold (Applied Biosystems, Foster City, CA, USA) and the following conditions were used for the PCRs: denaturation at 95 °C for 10 min, followed by 30 cycles at 94 °C for 1 min, 60 °C at rs71772361, rs71810967, and rs746349407, 65 °C at rs386395698, and 62 °C at rs762747991 for 1 min, and 72 °C for 1 min. The PCR products were separated by capillary electrophoresis, and were detected by the intensity of emitted fluorescence on an ABI Prism 3100-Avant Genetic analyzer (Applied Biosystems, Foster City, CA, USA). Raw data were analyzed with the GeneMapper Software v.3.7 (Applied Biosystems, Foster City, CA, USA). The sizes of these PCR products were determined based on the peak detection of fluorescence intensity, and this size was used to identify the haplotypes of each allele.

Funding information
This work was supported by the NEXT-Supported Program for the Strategic Research Foundation at Private Universities (HK) from the Ministry of Education, Culture, Sports, Science.

Acknowledgements
We would like to thank Mrs Akiko Yoshikawa, Mrs Chieko Mori, and Mrs Yoko Osakabe for their technical support and Dr Takema Kato and Dr Hidehito Inagaki for fruitful discussions about the names of the microsatellites.

Conflicts of interest
The authors declare that there are no conflicts of interest.

Ethical statement
This study was approved by the Ethical Review Board Human Genome Studies at Fujita Health University (Accession number 90, approved on 24 March 2010). Written informed consents were obtained from all of the participants or their guardians.

References
1. Dominguez G, Dambaugh TR, Stamey FR, Dewhurst S, Inoue N *et al.* Human herpesvirus 6B genome sequence: coding content

and comparison with human herpesvirus 6A. *J Virol* 1999;73: 8040–8052.

2. Isegawa Y, Mukai T, Nakano K, Kagawa M, Chen J *et al.* Comparison of the complete DNA sequences of human herpesvirus 6 variants A and B. *J Virol* 1999;73:8053–8063.
3. Dewhurst S, Mcintyre K, Schnabel K, Hall CB. Human herpesvirus 6 (HHV-6) variant B accounts for the majority of symptomatic primary HHV-6 infections in a population of US infants. *J Clin Microbiol* 1993;31:416–418.
4. Yamanishi K, Okuno T, Shiraki K, Takahashi M, Kondo T *et al.* Identification of human herpesvirus-6 as a causal agent for exanthem subitum. *Lancet* 1988;1:1065–1067.
5. Yoshikawa T, Suga S, Asano Y, Yazaki T, Kodama H *et al.* Distribution of antibodies to a causative agent of exanthem subitum (human herpesvirus-6) in healthy individuals. *Pediatrics* 1989;84: 675–677.
6. Collot S, Petit B, Bordessoule D, Alain S, Touati M *et al.* Real-time PCR for quantification of human herpesvirus 6 DNA from lymph nodes and saliva. *J Clin Microbiol* 2002;40:2445–2451.
7. Yoshikawa T, Ihira M, Taguchi H, Yoshida S, Asano Y. Analysis of shedding of 3 β-herpesviruses in saliva from patients with connective tissue diseases. *J Infect Dis* 2005;192:1530–1536.
8. Daibata M, Taguchi T, Nemoto Y, Taguchi H, Miyoshi I. Inheritance of chromosomally integrated human herpesvirus 6 DNA. *Blood* 1999;94:1545–1549.
9. Hall CB, Caserta MT, Schnabel K, Shelley LM, Marino AS *et al.* Chromosomal integration of human herpesvirus 6 is the major mode of congenital human herpesvirus 6 infection. *Pediatrics* 2008;122:513–520.
10. Morissette G, Flamand L. Herpesviruses and chromosomal integration. *J Virol* 2010;84:12100–12109.
11. Pellett PE, Ablashi DV, Ambros PF, Agut H, Caserta MT *et al.* Chromosomally integrated human herpesvirus 6: questions and answers. *Rev Med Virol* 2012;22:144–155.
12. Leong HN, Tuke PW, Tedder RS, Khanom AB, Eglin RP *et al.* The prevalence of chromosomally integrated human herpesvirus 6 genomes in the blood of UK blood donors. *J Med Virol* 2007;79: 45–51.
13. Tanaka-Taya K, Sashihara J, Kurahashi H, Amo K, Miyagawa H *et al.* Human herpesvirus 6 (HHV-6) is transmitted from parent to child in an integrated form and characterization of cases with chromosomally integrated HHV-6 DNA. *J Med Virol* 2004;73:465–473.
14. Ward KN, Leong HN, Nacheva EP, Howard J, Atkinson CE *et al.* Human herpesvirus 6 chromosomal integration in immunocompetent patients results in high levels of viral DNA in blood, sera, and hair follicles. *J Clin Microbiol* 2006;44:1571–1574.
15. Mori T, Tanaka-Taya K, Satoh H, Aisa Y, Yamazaki R *et al.* Transmission of chromosomally integrated human herpesvirsus 6 (HHV-6) variant A from a parent to children leading to misdiagnosis of active HHV-6 infection. *Transpl Infect Dis* 2009;11:503–506.
16. Troy SB, Blackburn BG, Yeom K, Caulfield AK, Bhangoo MS *et al.* Severe encephalomyelitis in an immunocompetent adult with chromosomally integrated human herpesvirus 6 and clinical response to treatment with foscarnet plus ganciclovir. *Clin Infect Dis* 2008;47:e93–e96.
17. Wittekindt B, Berger A, Porto L, Vlaho S, Grüttner HP *et al.* Human herpes virus-6 DNA in cerebrospinal fluid of children undergoing therapy for acute leukaemia. *Br J Haematol* 2009;145: 542–545.
18. Montoya JG, Neely MN, Gupta S, Lunn MR, Loomis KS *et al.* Antiviral therapy of two patients with chromosomally-integrated human herpesvirus-6A presenting with cognitive dysfunction. *J Clin Virol* 2012;55:40–45.
19. Gravel A, Dubuc I, Morissette G, Sedlak RH, Jerome KR *et al.* Inherited chromosomally integrated human herpesvirus 6 as a predisposing risk factor for the development of angina pectoris. *Proc Natl Acad Sci USA* 2015;112:8058–8063.
20. Endo A, Watanabe K, Ohye T, Suzuki K, Matsubara T *et al.* Molecular and virological evidence of viral activation from chromosomally integrated human herpesvirus 6A in a patient with X-linked severe combined immunodeficiency. *Clin Infect Dis* 2014;59:545–548.
21. Hall CB, Caserta MT, Schnabel KC, Shelley LM, Carnahan JA *et al.* Transplacental congenital human herpesvirus 6 infection caused by maternal chromosomally integrated virus. *J Infect Dis* 2010; 201:505–507.
22. Gravel A, Hall CB, Flamand L. Sequence analysis of transplacentally acquired human herpesvirus 6 DNA is consistent with transmission of a chromosomally integrated reactivated virus. *J Infect Dis* 2013;207:1585–1589.
23. Arbuckle JH, Medveczky MM, Luka J, Hadley SH, Luegmayr A *et al.* The latent human herpesvirus-6A genome specifically integrates in telomeres of human chromosomes *in vivo* and *in vitro*. *Proc Natl Acad Sci USA* 2010;107:5563–5568.
24. Arbuckle JH, Pantry SN, Medveczky MM, Prichett J, Loomis KS *et al.* Mapping the telomere integrated genome of human herpesvirus 6A and 6B. *Virology* 2013;442:3–11.
25. Ohye T, Inagaki H, Ihira M, Higashimoto Y, Kato K *et al.* Dual roles for the telomeric repeats in chromosomally integrated human herpesvirus-6. *Sci Rep* 2014;4:4559.
26. Wallaschek N, Sanyal A, Pirzer F, Gravel A, Mori Y *et al.* The telomeric repeats of human herpesvirus 6A (HHV-6A) are required for efficient virus integration. *PLoS Pathog* 2016;12:e1005666.
27. Ohye T, Kawamura Y, Inagaki H, Yoshikawa A, Ihira M *et al.* A simple cytogenetic method to detect chromosomally integrated human herpesvirus-6. *J Virol Methods* 2016;228:74–78.
28. Nacheva EP, Ward KN, Brazma D, Virgili A, Howard J *et al.* Human herpesvirus 6 integrates within telomeric regions as evidenced by five different chromosomal sites. *J Med Virol* 2008;80: 1952–1958.
29. Tweedy J, Spyrou MA, Hubacek P, Kuhl U, Lassner D *et al.* Analyses of germline, chromosomally integrated human herpesvirus 6A and B genomes indicate emergent infection and new inflammatory mediators. *J Gen Virol* 2015;96:370–389.
30. Queller DC, Strassmann JE, Hughes CR. Microsatellites and kinship. *Trends Ecol Evol* 1993;8:285–288.
31. Liu K, Martini M, Rocca B, Amos CI, Teofili L *et al.* Evidence for a founder effect of the MPL-S505N mutation in eight Italian pedigrees with hereditary thrombocythemia. *Haematologica* 2009;94: 1368–1374.
32. Haataja R, Väisänen ML, Li M, Ryynänen M, Leisti J. The fragile X syndrome in Finland: demonstration of a founder effect by analysis of microsatellite haplotypes. *Hum Genet* 1994;94:479–483.
33. Van Schil K, Klevering BJ, Leroy BP, Pott JWR, Bandah-Rozenfeld D *et al.* A nonsense mutation in FAM161A is a recurrent founder allele in Dutch and Belgian individuals with autosomal recessive retinitis pigmentosa. *Investigative Ophthalmol Vis Sci* 2015;56: 7418–7426.
34. Oikawa J, Tanaka J, Yoshikawa T, Morita Y, Hishiki H *et al.* An immunocompetent child with chromosomally integrated human herpesvirus 6B accidentally identified during the care of *Mycoplasma pneumoniae* infection. *J Infect Chemother* 2014;20:65–67.
35. Tweedy J, Spyrou MA, Pearson M, Lassner D, Kuhl U *et al.* Complete genome sequence of germline chromosomally integrated human herpesvirus 6A and analyses integration sites define a new human endogenous virus with potential to reactivate as an emerging infection. *Viruses* 2016;8:19.
36. Tanaka-Taya K, Kondo T, Mukai T, Miyoshi H, Yamamoto Y *et al.* Seroepidemiological study of human herpesvirus-6 and -7 in children of different ages and detection of these two viruses in throat swabs by polymerase chain reaction. *J Med Virol* 1996;48: 88–94.
37. Ward KN, Thiruchelvam AD, Couto-Parada X. Unexpected occasional persistence of high levels of HHV-6 DNA in sera: detection of variants A and B. *J Med Virol* 2005;76:563–570.

38. **Zerr DM, Meier AS, Selke SS, Frenkel LM, Huang ML *et al.*** A population-based study of primary human herpesvirus 6 infection. *N Engl J Med* 2005;352:768–776.
39. **Hall CB, Caserta MT, Schnabel KC, Mcdermott MP, Lofthus GK *et al.*** Characteristics and acquisition of human herpesvirus (HHV) 7 infections in relation to infection with HHV-6. *J Infect Dis* 2006; 193:1063–1069.
40. **Achour A, Malet I, Deback C, Bonnafous P, Boutolleau D *et al.*** Length variability of telomeric repeat sequences of human herpesvirus 6 DNA. *J Virol Methods* 2009;159:127–130.
41. **Kato Y, Ihira M, Umeda M, Higashimoto Y, Kawamura Y *et al.*** Copy numbers of telomeric repeat sequences of human herpesvirus 6B in clinical isolates: possibility of mixed infections. *J Clin Microbiol* 2014;52:419–424.
42. **Hubacek P, Maalouf J, Zajickova M, Kouba M, Cinek O *et al.*** Failure of multiple antivirals to affect high HHV-6 DNAaemia resulting from viral chromosomal integration in case of severe aplastic anaemia. *Haematologica* 2007;92:e98–e100.
43. **Tanaka N, Kimura H, Hoshino Y, Kato K, Yoshikawa T *et al.*** Monitoring four herpesviruses in unrelated cord blood transplantation. *Bone Marrow Transplant* 2000;26:1193–1197.
44. **Ablashi DV, Balachandran N, Josephs SF, Hung CL, Krueger GR *et al.*** Genomic polymorphism, growth properties, and immunologic variations in human herpesvirus-6 isolates. *Virology* 1991; 184:545–552.
45. **Benson G.** Tandem repeats finder: a program to analyze DNA sequences. *Nucleic Acids Res* 1999;27:573–580.